Piloted Assessment of the Lateral-Directional Handling Qualities of the Flying-V

Thesis Report

Sjoerd Joosten

Delft Univrsity of Technology

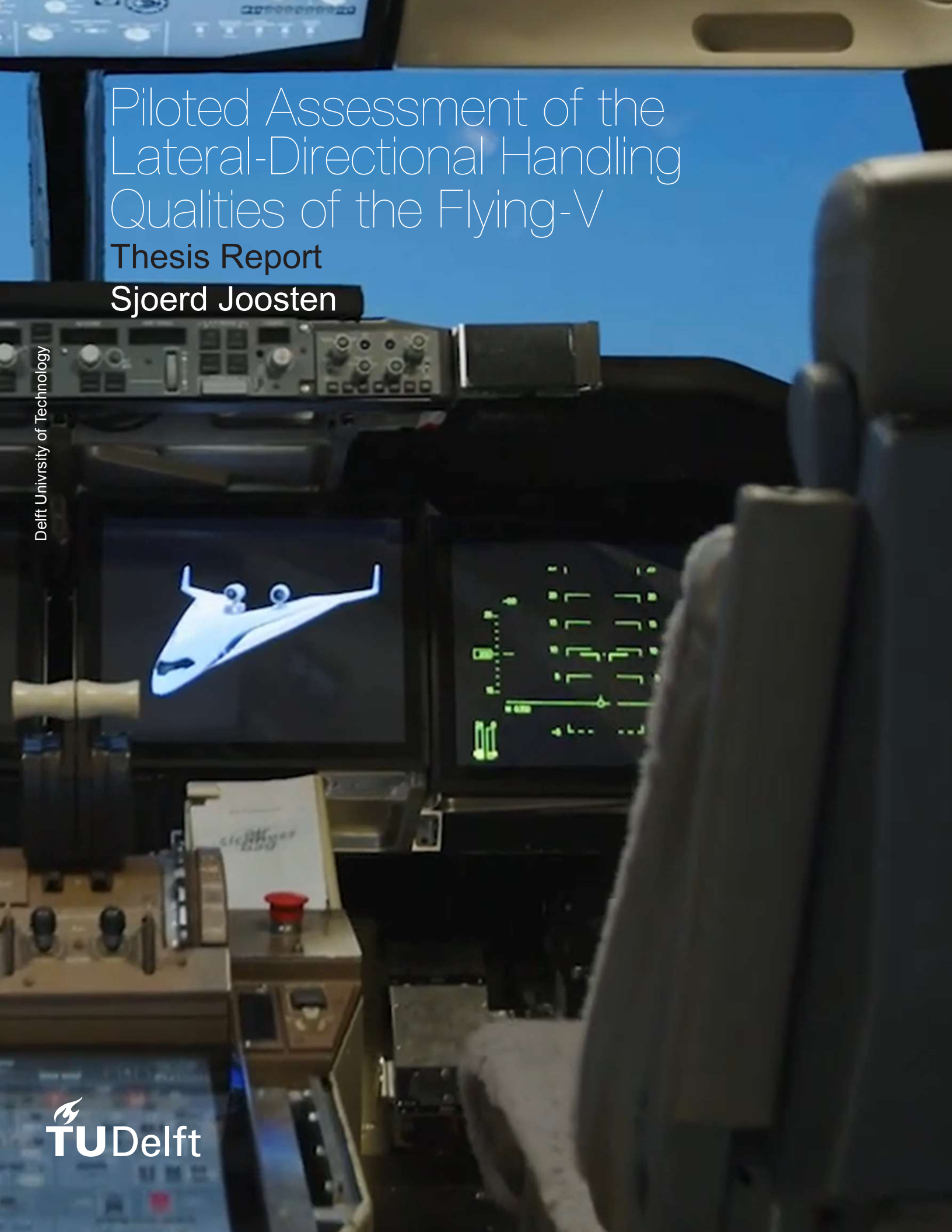

TU Delft

Thesis Report

Piloted Assessment of the Lateral-Directional Handling Qualities of the Flying-V

by

Sjoerd Joosten

To obtain the degree of Master of Science,
at Delft University of Technology,
to be defended publicly on Thursday April 21, 2022 at 13:00.

Student number:	4486048	
Project duration:	March 1, 2021 - April 21, 2022	
Thesis committee:	Prof. dr. ir. M. Mulder,	TU Delft, Chair
	Ir. O. Stroosma,	TU Delft, Supervisor
	Dr. ir. R. Vos,	TU Delft, Examiner
	Dr. X. Wang,	TU Delft, Examiner

Cover image source: KLM, copyright Joep van Oppen

TU Delft

This report contains confidential information, thus may only be shared after approval by the author.

Preface

Dear reader,

In this report, my thesis work regarding the lateral-directional handling qualities of the Flying-V is discussed in three parts. First, the paper discussing the study is presented in Part I. Second, a book of appendices supplementary to the paper is shown in Part II. Finally, the (**previously graded**) preliminary thesis report is attached in Part III.

Sjoerd Joosten

Part I: Thesis Paper

Piloted Assessment of the Lateral-Directional Handling Qualities of the Flying-V

Sjoerd Joosten
MSc Student, section Control & Simulation, Aerospace Engineering Delft University of Technology

Flying wings are known for their limited lateral-directional stability and handling qualities. This study aims at assessing the lateral-directional handling qualities of a conceptual flying wing aircraft currently in development at TU Delft, the Flying-V. It focuses on two aspects: First assess the lateral-directional handling qualities of the bare-airframe Flying-V, and the compliance to quantitative requirements. Second, improve these handling qualities through a prototype flight control system, and assess its effect on the handling qualities and the requirement compliance. These assessments were performed both analytically and with a pilot-in-the-loop experiment, in order to experimentally validate analytical findings and obtain new pilot-subjective insights. The analytical and experimental assessment both show the lateral-directional handling qualities of the Flying-V to be insufficient for requirement compliance, due to a lack of pitch, roll and yaw control authority in low-speed flight conditions and an insufficiently stable Dutch Roll eigenmode. The prototype flight control system, consisting of an adapted control allocation and a stability augmentation system, showed both analytically as experimentally to improve the control authority, stability, and handling qualities of the Flying-V. While the effect on the lateral-directional stability was sufficient for stability requirement compliance, the control authority was not sufficiently increased for manoeuvrability requirement compliance. Thus, a challenge remains to improve the handling qualities of the Flying-V. An approximation of the control authority required for full requirement compliance in the flight conditions tested showed a control authority increase of over a factor four to be required for future control surface design.

I. Introduction

The conventional wing-body-tail aircraft layout has been dominant in commercial aviation for over 50 years. It seems, however, that this configuration is converging to an asymptote of maximum performance and efficiency [1]. Therefore, new interest arises in unconventional aircraft layouts, such as the flying wing. This tail-less configuration was and is investigated by numerous companies and institutes, which led amongst others to designs of a blended-wing-body aircraft [2, 3]. Recently, TU Delft has researched the opportunities regarding a different flying wing design called the Flying-V, following a design by Benad [4]. A next design iteration was made at TU Delft by Faggiano [5]. Both show a promising performance, with a drag reduction of 10% compared to conventional aircraft with comparable performance requirements.

From a control perspective, flying wings are known for their limited lateral-directional stability [6] and their limited handling qualities [7], caused by the absence of a vertical tail surface, and a smaller moment arm from the control surfaces to the center of gravity than conventional aircraft. From this perspective followed a first handling quality assessment of the Flying-V by Cappuyns [8]. The study focused on developing the required aerodynamic model and simulation tools, with a brief analytical assessment of the handling quality performance of this model. It was found that, similar to earlier research, the lateral-directional stability and handling qualities were limited. It was recommended to further study this stability and these handling qualities.

Handling qualities can be assessed analytically and experimentally. The analytical assessment can be performed by simulating the aircraft and using this simulation to check against regulatory qualitative and quantitative requirements [9]. These analytical results, however, can differ from (experimental) pilot-perceived handling qualities, since these are a subjective measure [10]. Hence, to perform a complete handling quality assessment, both the analytical and experimental handling qualities have to be assessed. Obtaining the pilot perceived handling qualities requires a pilot-in-the-loop experiment, and although previous research exists on the lateral-directional handling qualities of the Flying-V, no pilot-in-the-loop experiment has been performed yet.

This study aims at bringing the insights in the lateral-directional handling qualities of the Flying-V a step further, by not only performing further analytical assessment, but by also performing the first piloted assessment. It focuses on two aspects: First, assess the handling qualities of the bare-airframe Flying-V, and the compliance to quantitative requirements selected from EASA CS-25 [11] and US Department of Defence military handbook MIL-HDBK-1797 [12]. Second, improve the handling qualities through designing a prototype flight control system, and assess its effect on the handling qualities and requirement compliance.

II. Background

A. The Flying-V

1. Flying-V development

The Flying-V initial design was performed by Benad, who predicted a performance increase with a drag reduction of 10% compared to conventional aircraft with comparable performance requirements [4]. A further design iteration was performed at TU Delft by Faggiano, who performed an aerodynamic design optimization for the Flying-V [5]. The design iteration consisted of designing the wing planform and airfoil based on aerodynamic optimization, and sizing the winglet fins with integrated rudders based on static stability requirements. This new design was used for further analyses in several TU Delft theses [13–16]. Following this research, Cappuyns performed a preliminary handling quality analysis by developing a full-scale aerodynamic simulation of the Flying-V [8], including the control surfaces as designed by Faggiano and Palermo [5, 16]. The Flying-V geometry and properties used for this study were obtained from Cappuyns [8], with the engine location obtained from Pascual [17].

2. Flying-V properties

The geometry properties of the Flying-V used in this study are shown in Table 18 in the appendix of this paper. The Maximum Take-Off Weight (MTOW) and Maximum Landing Weight (MLW) of the Flying-V were directly available from Cappuyns [8], as well as the moments of inertia for the MTOW. The moments of inertia for the MLW, however, were not directly available, thus were determined [18] based on the weight difference between the MTOW and MLW and the weight distribution as used by Cappuyns [8]. Figures 1(a) and 1(b) give an impression of, respectively, the top- and side-view of the Flying-V with associated dimensions and control surfaces indicated.

The control surfaces of the Flying-V are located at the outboard trailing edges. Both aircraft sides possess 2 elevons (i.e., elevator-aileron combinations) and a rudder embedded in the winglet. The control surface dimensions were obtained from the Airbus aerodynamic model of the Flying-V, as initially developed by Cappuyns [8]. It should be noted that Cappuyns developed the control surfaces based on simplicity and recommended further research to optimize them. The dimensions of the right elevons are indicated in Figure 1(a), the dimension of the left winglet rudder is indicated in Figure 1(b). The control surfaces are indicated by C1, C2, C3, C4, C5 and C6. These, respectively, indicate the left winglet rudder, left outboard elevon, left inboard elevon, right inboard elevon, right outboard elevon, and right winglet rudder, as seen when standing behind the aircraft.

[1]Flying-V impressions obtained from `https://www.tudelft.nl/lr/flying-v`, combined with geometry properties obtained from Cappuyns [8] and Pascual [17].

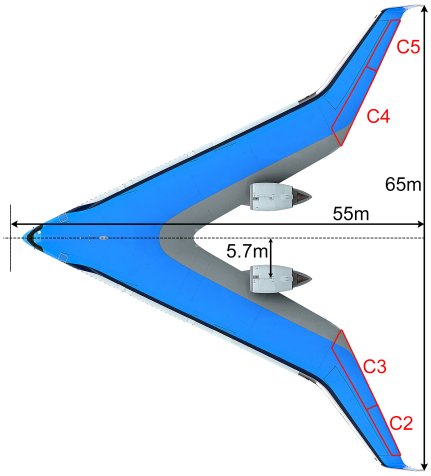

(a) Top view of the Flying-V

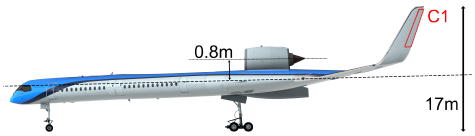

(b) Side view of the Flying-V

Figure 1. Flying-V impressions and dimensions[1].

3. Aerodynamic model implementation and simulation

Cappuyns developed a full-scale aerodynamic simulation-model of the Flying-V in collaboration with Airbus, based on the Vortex Lattice Method (VLM) [8]. This VLM model was provided by Airbus, and one iteration was collaboratively made to expand the VLM model to contain multiple center of gravity locations, more flight conditions and separately controllable control surfaces. This yielded a model with the following variables as inputs: Center of gravity in %MAC (CG), aircraft velocity in Mach (M), angle of attack in degrees (α), sideslip angle in degrees (β), normalized roll rate in radians (p^*), normalized pitch rate in radians (q^*), normalized yaw rate in radians (r^*), and the deflection of all six control surfaces in degrees (δ_{c1} to δ_{c6}). The range of input variables available for inter- and extrapolation is shown in Table 19 in the appendix of this paper.

The output of the VLM model is given in terms of contributions of the input variables to (non-dimensional) force and moment coefficients. The force coefficients are, in the aerodynamic reference frame, the backward force coefficient C_X, the side (right) force coefficient C_Y, and the upward force coefficient C_Z. The moment coefficients are, in the body reference frame, the roll moment coefficient C_L, the pitch moment coefficient C_M, and the yaw moment coefficient C_N. The force and moment coefficients are obtained by inter- or extrapolating the contribution of all input states to the corresponding coefficients and summing those. Illustrating the determination of a force or moment coefficient for a given Center of Gravity and velocity in Mach, the following equation shows the determination of force coefficient C_X, based on the VLM model output coefficients:

$$
\begin{aligned}
C_X = C_{X_0}(\alpha) + C_{X_\beta}(\alpha,\beta) + .. \\
C_{X_{p^*}}(\alpha,p^*) + C_{X_{q^*}}(\alpha,q^*) + C_{X_{r^*}}(\alpha,r^*) + .. \\
C_{X_{\delta_{c1}}}(\alpha,\delta_{c1}) + C_{X_{\delta_{c2}}}(\alpha,\delta_{c2}) + C_{X_{\delta_{c3}}}(\alpha,\delta_{c3}) + .. \\
C_{X_{\delta_{c4}}}(\alpha,\delta_{c4}) + C_{X_{\delta_{c5}}}(\alpha,\delta_{c5}) + C_{X_{\delta_{c6}}}(\alpha,\delta_{c6})
\end{aligned} \tag{1}
$$

The force and moment coefficients are dimensionalized using the air density, velocity, and for the moment coefficients also the mean aerodynamic chord. Using the mean aerodynamic chord for (non-)dimensionalizing the moment coefficients regardless of the axis of the coefficient is an Airbus convention. Next to these aerodynamic forces, two thrust vectors were added to the model: $T1$ for the left engine and $T2$ for the right engine, when seen from behind the aircraft. For each engine, a thrust vector was modeled as being aligned with the aircraft body-frame X-axis (nose forward direction). Thus, the additional force was added to the existing X-axis body-frame force component, and the additional body-frame moments around the Y and Z body-axes were calculated based on each engine's location with respect to these axes.

The aircraft state vector used consists of 12 states: the earth-fixed positions X_e, Y_e and Z_e, the body velocities U_b, V_b and W_b, the angular velocities p, q and r and the attitude angles φ, θ and ψ. With the aerodynamic forces X, Y, Z and the moments M_x, M_y, M_z obtained as previously discussed, equations of motion were used to simulate the aircraft response to inputs [19]. For the analytical assessment, Euler integration was used to simulate the aircraft over time. For the experimental assessment, this was adapted to Runge-Kutta integration to allow higher integration accuracy with a smaller time-step for calculation.

A linearized model of the aircraft was obtained by trimming the aircraft numerically at a set flight condition, following the same procedure of determining state derivatives as the non-linear simulation discussed above, and linearizing the aircraft around the trimmed state. The linear state-space model provided an uncomplicated way of assessing the eigenmode damping and frequency responses of the aircraft by assessing the eigenvalues of the state matrix (A), rapidly showing the aircraft eigenmode stability [18, 20].

4. Flying-V handling qualities

Flying wings are known for their limited lateral-directional stability [6] and limited handling qualities [7], due to the absence of a vertical tail surface. The preliminary winglet and rudder designs by Faggiano [5] and Palermo [16] took this stability into account, but were primarily based on the static stability of the Flying-V. Further analysis by Cappuyns [8] showed the dynamic lateral-directional stability of the Flying-V to be insufficient. Amongst others because of this, the lateral-directional handling qualities were found limited on two aspects. First on the lateral-directional eigenmodes, which showed an unstable Dutch Roll. Second, on the lateral-directional manoeuvrability, for which the control authority was shown to be insufficient for multiple handling quality requirements. Cappuyns recommended further research to focus on a more elaborate investigation into the handling qualities of the Flying-V. Recommended solutions for the limited lateral-directional handling qualities were, amongst others, a redesign of the control surfaces, the use of unconventional control surfaces, optimizing the control allocation and imposing a stability augmentation system. Of these, the control allocation and stability augmentation system are assessed further in this study.

It should be noted that the analysis by Cappuyns [8] was performed analytically, and no piloted experiment was performed. Hence, the obtained results were not validated as pilot-perceived, yielding a research-opportunity for this study.

B. Lateral-Directional Handling Qualities and Requirements

Both Cooper and Harper [21] as well as Roskam [22] describe handling qualities in a qualitative sense. Although they provide general requirements on aircraft performance, no quantitative requirements are set on aircraft attitudes or manoeuvres. Hence, in order to objectively assess whether the handling quality requirements were met, quantitative handling quality requirements were used. In line with Cappuyns [8], the US Department of Defence military handbook MIL-HDBK-1797 [12] and the EASA aircraft regulations of CS-25 [11] were used as this quantitative benchmark. The military handbook specifies quantitative stability requirements on frequency and damping parameters of aircraft eigenmodes, and associated handling quality classification. The EASA regulations specify airworthiness (manoeuvrability) requirements, with quantitative constraints on amongst others the control deflections used and time to perform a set manoeuvre. Since this study focuses on the lateral-directional handling qualities, only the requirements set on these were taken into account.

To further limit the scope of the handling quality assessment, literature was used to select the requirements and regulations to be tested. Research by Perez and Wahler [23, 24] discussed the design-constraining conditions selected from EASA CS-25 and the MIL-HDBK-1797 of the US Department of Defence for, respectively, conventional and unconventional aircraft configurations. In being the design-constraining conditions, these were chosen as the most relevant conditions to test the Flying-V design on. Finally, requirements were selected which allow for both an analytical and an experimental analysis. Table 1 shows an overview of the requirements and regulations tested.

Table 1. Selection of handling quality requirements for evaluation.

Requirement	Book	Article
Dutch Roll Stability (DR)	MIL-.	4.6.1.1
Coordinated Turn Capability (CTC)	CS-25	143(h)
Time to Bank, Roll Capability (TTB)	CS-25	147(f)
One Engine Inoperative Trim (OEI-T)	CS-25	161(d)
Steady Heading Sideslip (SHS)	CS-25	177(c)

C. Flight Control Systems and Handling Qualities

In order to take a first step in improving the lateral-directional handling qualities of the Flying-V, a prototype flight control system was designed. A flight control system can improve the handling qualities of the aircraft without the need to re-design the aircraft's planform or control surfaces. In a fly-by-wire controlled aircraft, the flight control system converts the pilot inputs to control surface actuation. Due to the flight control system being in between the pilot and the control surfaces, indirect control surface control is possible. This yields opportunities for unconventional (i.e., not direct, mechanically linked) control. In this study, two of those opportunities are focused on: an adapted (unconventional) control allocation and stability augmentation.

1. Control allocation and handling qualities

The control allocation determines which control surface contributes to the generation of which angular moments and by how much. Due to the lack of a conventional tail, the Flying-V control surfaces have a less clear predetermined allocation than those of a conventional wing-body-tail aircraft. Thus, a study into this control allocation can contribute to increasing the overall control-effectiveness and controllability of the Flying-V. Previous research on the control allocation of other flying wings, such as a blended-wing-body, showed the control allocation to have a large impact on the aircraft's command responses [25] and trim-drag [26].

When the handling qualities prove to be limiting in the control surface sizing and design, control allocation can increase the control-effectiveness such that smaller control surfaces are required [27]. Alternatively, for a given control surface design the increase of control-effectiveness due to adapting the control allocation can improve the handling qualities at (previously) limiting aircraft manoeuvres during the handling quality assessment. Only a limited increase in control authority is available with this method, however. The control allocation can be optimized to increase control effectiveness, but the overall control authority will still be limited by the maximum deflections available of the control surfaces.

2. Stability augmentation and handling qualities

Stability augmentation uses the aircraft state to change the commanded deflection of control surfaces. In this way, an aircraft can respond to state or condition changes without the pilot intervening. Stability augmentation is commonly used when the bare-airframe stability is found insufficient. As stated earlier, flying wings are known for their limited lateral-directional stability. Research has shown stability augmentation to be suitable to improve this lateral-directional stability of flying wings by the use of roll damping, yaw damping and sideslip angle feedback [7, 9, 28].

When increasing the lateral-directional stability with the use of stability augmentation, the handling qualities of an aircraft can inherently be improved. Specifically the eigenmodes of an aircraft can be largely influenced by stability augmentation, by either altering an eigenmode's damping, frequency or both [9, 29]. Since the damping and frequency parameters of eigenmodes are part of the Dutch Roll Stability handling quality requirement, implementing a stability augmentation system can improve compliance with this requirement.

III. Method

A. Flight Control System Design

1. Control allocation design

The aerodynamic model of the Flying-V contains six control surfaces, while three pilot inputs are assumed: two of the sidestick and one of the rudder pedals. A control allocation between these pilot inputs and the six control surfaces is required. The bare-airframe Flying-V uses a conventional elevator-aileron-rudder control allocation, analogous to previous research [8]. The control allocation method is called explicit ganging in literature [30], which assigns each control surface to a specific moment direction based on the designer choice. The inboard elevons were allocated to respond to a longitudinal stick input, providing a pitch moment by symmetric deflection. The outboard elevons were allocated to respond to a side-way stick input, providing a roll moment by asymmetric deflection. The rudders were allocated to respond to the rudder pedal input, providing a yaw moment by asymmetric (but in the same body Y-direction) deflection. Eq. 2 represents this control allocation by K_{alloc}, and shows how the pilot inputs (pitch input δ_e, roll input δ_a and yaw input δ_r) were allocated to the control surface deflections (δ_{C1}, δ_{C2}, δ_{C3}, δ_{C4}, δ_{C5}, δ_{C6}) with the bare-airframe Flying-V.

$$\begin{bmatrix} \delta_{C1} \\ \delta_{C2} \\ \delta_{C3} \\ \delta_{C4} \\ \delta_{C5} \\ \delta_{C6} \end{bmatrix} = K_{alloc} \cdot \begin{bmatrix} \delta_e \\ \delta_a \\ \delta_r \end{bmatrix} = \begin{bmatrix} 0 & 0 & 1 \\ 0 & 1 & 0 \\ -1 & 0 & 0 \\ -1 & 0 & 0 \\ 0 & -1 & 0 \\ 0 & 0 & -1 \end{bmatrix} \cdot \begin{bmatrix} \delta_e \\ \delta_a \\ \delta_r \end{bmatrix} \quad (2)$$

Due to the unconventional control surfaces of the tailless Flying-V, an opportunity exists to improve the control effectiveness with an unconventional control allocation. Numerous control allocation methods can be found in literature [25, 31], from which the generalized inverse was chosen. Amongst others Denieul [27] used the generalized inverse to design the control allocation of a blended-wing-body and Oppenheimer [32] used the generalized inverse for the control allocation of over-actuated systems.

The generalized inverse method uses the control effectiveness of each control surface around each moment axis to distribute the roles of controlling these moments between the control surfaces. The control effectiveness matrix, as shown in Eq. 3, is a 3 by 6 matrix holding the derivatives of the moments around the Y, X and Z body axes, respectively, m, l and n, with respect to deflection of each of the six control surfaces. This matrix can be obtained by linearizing the aircraft including the control surfaces around a trimmed state. Next, the coefficients

of Eq. 3 are obtained from the B matrix of the state-space system. Second, the control effectiveness matrix is used to determine the adapted control allocation matrix $K_{alloc_{new}}$ using the unweighted pseudo-inverse of the control allocation as shown in Eq. 4.

$$B = \begin{bmatrix} \frac{dm}{d\delta_{c1}} & \frac{dm}{d\delta_{c2}} & \frac{dm}{d\delta_{c3}} & \frac{dm}{d\delta_{c4}} & \frac{dm}{d\delta_{c5}} & \frac{dm}{d\delta_{c6}} \\ \frac{dl}{d\delta_{c1}} & \frac{dl}{d\delta_{c2}} & \frac{dl}{d\delta_{c3}} & \frac{dl}{d\delta_{c4}} & \frac{dl}{d\delta_{c5}} & \frac{dl}{d\delta_{c6}} \\ \frac{dn}{d\delta_{c1}} & \frac{dn}{d\delta_{c2}} & \frac{dn}{d\delta_{c3}} & \frac{dn}{d\delta_{c4}} & \frac{dn}{d\delta_{c5}} & \frac{dn}{d\delta_{c6}} \end{bmatrix} \tag{3}$$

$$K_{alloc_{new}} = B^T(BB^T)^{-1} \tag{4}$$

To obtain the control effectiveness matrix, the aircraft was linearized in cruise flight conditions with the aft CG position. This condition is expected to be occurring most during the aircraft mission, thus optimizing for this condition is expected to yield the least overall drag. Moreover, linearizing the aircraft in this condition yielded the most intuitive control allocation. To limit the complexity of the adapted control allocation, it was decided not to alter the control allocation for each flight condition. Eq. 5 shows the obtained control allocation matrix $K_{alloc_{new}}$. Using the equivalent moments $\delta_{m_{equi}}, \delta_{l_{equi}}$ and $\delta_{n_{equi}}$, each column of the control allocation matrix was scaled such that the largest magnitude equals 1, to make the relative control allocation more apparent. This does not limit the use of the controls, since the scaling and limiting of the pilot inputs was performed separately in the piloted experiment preparation.

$$\begin{aligned} \begin{bmatrix} \delta_{C1} \\ \delta_{C2} \\ \delta_{C3} \\ \delta_{C4} \\ \delta_{C5} \\ \delta_{C6} \end{bmatrix} &= K_{alloc_{new}} \cdot \begin{bmatrix} \delta_e \cdot \delta_{m_{equi}} \\ \delta_a \cdot \delta_{l_{equi}} \\ \delta_r \cdot \delta_{n_{equi}} \end{bmatrix} \\ &= \begin{bmatrix} -0.046 & -0.439 & 1.000 \\ -0.601 & 0.496 & 0.150 \\ -1.000 & 1.000 & -0.179 \\ -1.000 & -1.000 & 0.179 \\ -0.601 & -0.496 & -0.150 \\ -0.046 & 0.439 & -1.000 \end{bmatrix} \cdot \begin{bmatrix} \delta_e \\ \delta_a \\ \delta_r \end{bmatrix} \end{aligned} \tag{5}$$

2. Stability augmentation system design

The stability augmentation system design was based on the research of Castro [9], where a stability augmentation system was designed for a blended-wing-body aircraft. For lateral-directional stability augmentation, a combination of sideslip feedback with a reference command, a yaw damper with washout filter, and roll rate feedback with reference command was used. For longitudinal control, pitch rate feedback with a reference command was used. Since the sideslip angle β was not directly available as aircraft state, the body-frame side velocity V_b is used, since β converges to zero when V_b converges to zero.

Earlier research into the design and assessment of a flight control system for an unconventional (blended-wing-body) aircraft showed the effect of including or excluding roll damping in the stability augmentation system to be pilot-subjective [9]. Hence, the stability augmentation system will be tested both with, and without roll rate feedback. Without roll rate feedback, direct roll control was available, where full lateral stick deflection yields maximum roll input to the lateral control allocation input channel δ_a. The stability augmentation system (SAS) without roll rate feedback is labeled SAS-1, the stability augmentation system with roll rate feedback is labeled SAS-2. Figure 2 shows an overview of the stability augmentation system by means of a system diagram, with the lateral control of both SAS-1 and SAS-2 shown. Gain tuning was performed per SAS and flight condition based on the Dutch Roll Stability requirement, time-responses to inputs, and preliminary piloted simulation. An overview of the gain tuning is shown in Table 20 in the appendix of this paper.

B. Analytical Handling Quality Assessment

1. Analytical simulation of requirements

Analytical simulation of the bare-airframe Flying-V dynamics and trim states was used to assess the CS-25 [11] requirements specified in Table 1. The Coordinated Turn Capability, One Engine Inoperative Trim Condition, and Steady Heading Sideslip requirements specify trim states the aircraft should be able to attain and maintain. For the assessment of these requirements the aircraft was numerically trimmed. The requirements set on the aircraft states as stated in CS-25 were used as constraints, while the aircraft states without constraints and the control surface deflections were numerically optimized to trim the aircraft. The constraints used for the different manoeuvres are shown in Table 2. For the Time to Bank manoeuvre, the initial trim state is shown, from which the rolling manoeuvre started.

Table 2. State constraints for analytical assessment of handling quality requirements.

Requirement	Condition	β *deg*	ϕ *deg*	γ *deg*
CTC	ALL	0	40	0
TTB (init.)	ALL	0	30	0
OEI-T	ALL	n/a	< 5	0
	APP	13.1	n/a	0
SHS	TO	8.69	n/a	0
	CR	3.56	n/a	0

A requirement was complied with if the required control surface deflections for the trim state were within set control surface deflection limits: *37 degrees* for rudder deflection and *30 degrees* for elevon deflection, based on Cappuyns [8] and Castro [9]. For the Time to Bank requirement, assessing the roll capability of the aircraft, a non-linear simulation of the Flying-V dynamics was used. By iteratively simulating the roll manoeuvre as specified in CS-25, the minimum (constant)

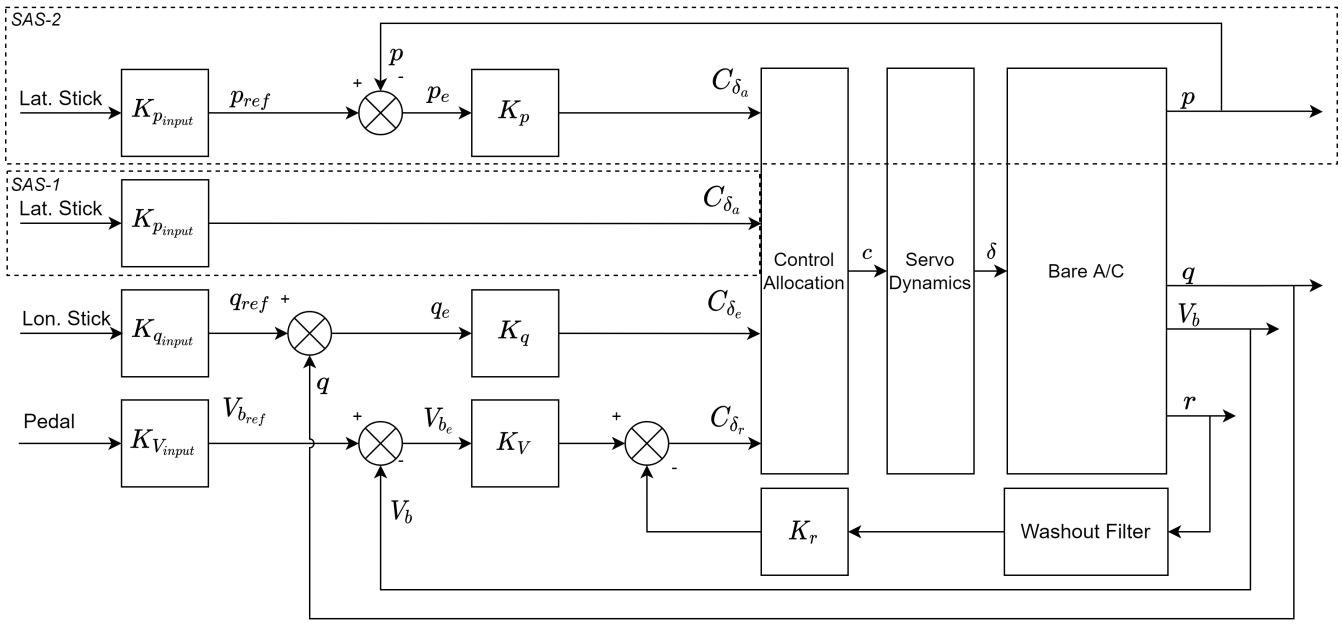

Figure 2. Stability augmentation system design, with SAS-1 and SAS-2 lateral input indicated.

lateral control surface deflections were found to perform the manoeuvre within the required time. Here, the lateral input δ_a was iterated to perform the roll manoeuvre. For the bare-airframe assessment the rudder input δ_r was also used, in order to reduce sideslip during this manoeuvre. For the assessment with stability augmentation system zero pedal input was assumed, since no pilot input should be required to reduce sideslip. Again, a requirement was complied with if the required control surface deflections for the manoeuvre were within the set control surface deflection limits.

The Dutch Roll Stability requirement, as stated in MIL-HDBK-1797 [12], requires the eigenvalues of the aircraft to obtain the Dutch Roll damping and frequency parameter. To obtain these eigenvalues, the linearisation procedure as discussed in Section II.A.3 was used. The eigenvalues were appointed to each eigenmode based on their eigenvectors [20]. Each eigenvalue then yielded the damping and frequency parameter of an eigenmode, amongst which the Dutch Roll. The Dutch Roll was assessed in trimmed, straight, horizontal flight, for each flight condition tested.

2. Flight control system influence on analytical assessment

The flight control system influence on the analytical handling quality assessment differed for the two flight control system elements, the adapted control allocation and the stability augmentation system. The increase in control effectiveness by adapting the control allocation can improve the requirement compliance for edge-of-the-envelope trim states and manoeuvres, by increasing the overall control effectiveness. Adapting the control allocation however does not influence the stability of the eigenmodes of the aircraft. Control allocation only takes effect in translating desired angular control inputs to control surface deflections, while the eigenmode stability is determined without a pilot input. Thus, only the CS-25 requirements had to be reassessed when implementing the adapted control allocation, since the MIL-HDBK-1797 Dutch Roll Stability was not influenced.

Stability augmentation can positively influence the eigenmodes of an aircraft, by either improving an eigenmode its damping, frequency or both [9, 29]. Hence, of the handling quality requirements listed in Table 1, primarily the Dutch Roll Stability requirement is influenced. The stability augmentation system was developed such that most EASA CS-25 requirements do not require re-assessment: the same trim control deflections as without the stability augmentation system are still attainable. However, the stability augmentation system does influence the aircraft's response on pilot inputs. Thus of the EASA CS-25 requirements, only the Time to Bank requirement is influenced, since this requirement does not only involve a trim condition but also performing a manoeuvre within a set time.

3. Flight condition and aircraft configuration selection

The flight conditions tested were chosen to be in line with earlier research, and were based on the flight conditions available in the aerodynamic aircraft model. Three different air speeds in Mach were used: Mach 0.2, 0.3 and 0.85, which were assumed to be applicable for, respectively, Approach, Take-Off and Cruise flight conditions. Table 3 shows an overview of these flight conditions, with their corresponding True Air Speed (TAS), altitude, air density, assumed aircraft weight (Maximum Take-Off or Maximum Landing Weight) and aircraft mass.

Next to these flight conditions, two Center of Gravity (CG) locations and two engine settings were tested. The CG locations tested were the forward and aft limit, respectively on 45 %MAC and 57.5 %MAC, as determined in earlier research [8]. The engine settings tested were an All Engines Operative (AEO) condition with both engines providing equal thrust, and an One Engine Inoperative (OEI) condition, in which the right engine

Table 3. Flight condition assumptions.

Condition	TAS	TAS	Altitude	Air Density	A/C Weight
	$Mach$	m/s	m	kg/m^3	–
Approach (APP)	0.2	68.6	0	1.225	MLW
Take-Off (TO)	0.3	102.9	0	1.225	MTOW
Cruise (CR)	0.85	250.8	13000	0.2655	MTOW

was killed. The engine settings assessed differed per manoeuvre, as specified in the requirements tested.

C. Experimental Handling Quality Assessment

1. Piloted simulation of the Flying-V

Real-time piloted simulation of the Flying-V was set-up using the *Delft University Environment for Communication and Activation* (DUECA) middleware. DUECA simplifies the composition of a simulation or experiment using new or existing models and facilitates data access and timing of activation [33]. The aerodynamic model, as discussed in Section II.A.3, was used as the basis to develop a non-linear simulation. The aircraft dynamics were implemented in a real-time simulation to respond to pilot inputs on stick, pedal, and thrust. Control surface and engine dynamics were modeled using a first-order lag approximation, with a time constant of 0.05 seconds for control surface dynamics [18] and a time constant of 1.0 seconds for engine dynamics [34]. Moreover, based on discussion with the representative from Airbus providing the aerodynamic model for this study, a control surface deflection rate-limit was set on 40 degrees per second. Finally, the different control allocations, stability augmentation systems, flight conditions, aircraft properties and experiment manoeuvres were made available to be selected externally by the researchers.

2. Piloted simulation of handling quality requirements

To simulate the different stability and manoeuvrability requirements, the manoeuvre to be performed in the simulator was determined for each. For this, a US Federal Aviation Administration flight test guide for certification of transport category airplanes, Advisory Circular (AC) 25-7D [35], was used. It includes flight test methods and procedures to show compliance with regulations as presented in EASA CS-25. For each of the CS-25 requirements tested, AC 25-7D discusses a manoeuvre which can be performed in flight (or flight simulation) and the allowed state limits to prove requirement compliance.

Since the Dutch Roll Stability requirement is set on a damping and frequency parameter, no corresponding flight manoeuvre with target state is present. To still obtain pilot feedback on the Dutch Roll stability of the aircraft, the pilot was asked to excite the Dutch Roll by means of a rudder doublet input, and when the eigenmode was in a sustained oscillation to counteract it. This yielded pilot-subjective feedback on the severity of the Dutch Roll eigenmode compared to conventional aircraft, and on the ease of counteracting it.

The Dutch Roll was expected to not only act when actively excited, but to also have an influence on other manoeuvres. Specifically manoeuvres where a roll angle, roll rate or sideslip angle is demanded were expected to be influenced by the Dutch Roll eigenmode. To assess whether and by how much the Dutch Roll eigenmode had increased or decreased throughout an experiment manoeuvre, the Mode Participation Factor of the Dutch Roll throughout each experiment manoeuvre was determined. The state-vector of the logged experiment data was transformed to modal coordinates. First, the trim state was subtracted from the state vector in the original coordinates $x(t)$. Second, the eigenvector-matrix V was used to transform the state vector to a vector in modal coordinates, $r(t)$, as shown in Eq. 6 [36]. Next, the columns representing the Dutch Roll eigenmode in the eigenvector-matrix were determined, and used to obtain the corresponding rows in the state vector in modal coordinates $r(t)$. By taking the absolute value of one of the two rows representing the Dutch Roll at every time-step, the Mode Participation Factor was obtained throughout each manoeuvre. An increasing Dutch Roll Mode Participation Factor represents an increase in the dominance of this eigenmode in the aircraft dynamics. The Dutch Roll Mode Participation Factor next was used to validate pilot comments on both the difficulty of counteracting the Dutch Roll eigenmode, as well as the Dutch Roll eigenmode interfering with other manoeuvres.

$$r(t) = V^{-1}x(t) \tag{6}$$

For the CS-25 requirements, state targets with associated limits for each manoeuvre were set. All attitude (lower-)margins were based on those in the analytical assessment, such that requirement compliance was met when the piloted manoeuvre was performed within margins from the target state. To set adequate outer margins from the target state, preliminary piloted simulation was used. Next to the analytically prescribed constraints, a maximum speed deviation from the target speed of 5% was set, and the target state had to be kept for 10 seconds to assure the maintainability of the state. For the Time to Bank manoeuvre, a time limit of 7 seconds to complete the manoeuvre was set, analogous to the analytical assessment of this CS-25 requirement. Besides, the positive Flight Path Angle was only required while starting the roll manoeuvre. An overview of the resulting limits as used in the experimental assessment is given in Table 4.

Many of the manoeuvres selected for the experiment were by analytical assessment hypothesized impossible to be performed successfully in a piloted simulation. To limit the time spent per manoeuvre, a procedure was developed to determine when a manoeuvre was passed or failed. A manoeuvre was passed when the aircraft was kept within the target state for 10 seconds or when, in case of the Time to Bank manoeuvre, the roll

Table 4. State targets and adequate- and desired-margins for experimental requirement assessment.

Req.	Cond.	β			ϕ			γ			ψ		
		Targ. deg	$\Delta_{Ade.}$ deg	$\Delta_{Des.}$ deg	Targ. deg	$\Delta_{Ade.}$ deg	$\Delta_{Des.}$ deg	Targ. deg	$\Delta_{Ade.}$ deg	$\Delta_{Des.}$ deg	Targ. deg	$\Delta_{Ade.}$ deg	$\Delta_{Des.}$ deg
CTC	ALL	0	±2	±1	42.5	±2.5	±1.5	2.5	±2.5	±1.5	n/a	n/a	n/a
TTB	ALL	n/a	n/a	n/a	33.5	±3.5	±2.5	2.5	±2.5	±1.5	n/a	n/a	n/a
OEI-T	ALL	n/a	n/a	n/a	0	±5	±4	2.5	±2.5	±1.5	0	±5	±10
	APP	15.1	±2	±1	n/a	n/a	n/a	2.5	±2.5	±1.5	-15.1	±7.5	±5
SHS	TO	10.7	±2	±1	n/a	n/a	n/a	2.5	±2.5	±1.5	-10.7	±7.5	±5
	CR	5.56	±2	±1	n/a	n/a	n/a	2.5	±2.5	±1.5	-5.56	±7.5	±5

manoeuvre was performed within 7 seconds or less. When a pilot was not able to attain, or sufficiently maintain, the target state for longer than several minutes, the simulation was paused. Next, in collaboration with the pilot, it was determined whether a further, in due time, try had a chance of success. If not, the manoeuvre was assessed to be failed, else the simulation was reset and another try was performed. The maximum tries allowed per manoeuvre was set on five, the maximum total time spent per manoeuvre on 7 minutes, both based on preliminary piloted simulations.

3. Experiment design

Use of flight control systems

The main focus of this study is assessing the bare-airframe handling qualities, and the influence of a prototype flight control system on these handling qualities. The flight control system design yielded SAS-1 without, and SAS-2 with roll damping. Based on analytical assessment of these, insufficient control authority was expected to be available in approach and take-off flight conditions. In order to assess whether increasing the control authority would yield sufficient handling qualities for experimental requirement compliance in these flight conditions, a flight control system with augmented increased control authority was set up. The maximum allowed control surface deflections were increased with a factor 5, allowing the deflections analytically predicted to be required while also providing excess deflection for attaining the target states. This configuration is labeled SAS-2 extended, or *SAS-2 ext.*.

Adding the flight control system with augmented extra control authority, *SAS-2 ext.*, to the main focus of the study, yielded three aircraft flight control system configurations to be tested in the main experiment: the bare-airframe, *SAS-2*, and *SAS-2 ext.*.

Selection of manoeuvres

Due to limited pilot availability, not all combinations of flight conditions, aircraft center of gravity locations, flight control system implementations, engine settings and requirements tested in the analytical assessment were feasible to test in a pilot-in-the-loop experiment. Hence, a selection of test conditions and requirements was made, focusing on assessing the worst and best cases from the analytical assessment. These were, respectively, the approach condition with forward limit center of gravity and cruise condition with aft limit center of gravity. Moreover, it was decided that a thorough validation of the flight control system implementation required the conditions on which the flight control system effect was found largest in preliminary simulation to also be tested: the forward center of gravity conditions of the Dutch Roll Stability and Steady Heading Sideslip requirement. This yielded 14 selected combinations of requirement, flight condition, engine setting and center of gravity, as shown in Table 5. Since these 14 manoeuvres needed to be flown with the bare-airframe, with *SAS-2,* and with *SAS-2 ext.*, a total of 42 manoeuvres were selected to be tested in the main experiment.

Table 5. Selected test conditions for experimental assessment of different manoeuvres.

	CG Forward	CG Aft
DR	APP, TO, CR (AEO)	CR (AEO)
CTC	APP (AEO)	CR (OEI)
TTB	APP (AEO)	CR (AEO)
OEI-T	APP (OEI)	CR (OEI)
SHS	APP, TO, CR (OEI)	CR (AEO)

Next to the selected combinations of conditions and requirements for the main experiment,, extra tests were included to assess the pilot-subjective difference between a stability augmentation system with and without roll damping. For this, the Dutch Roll Stability, Steady Heading Sideslip and Time to Bank requirement for the forward center of gravity and all three flight conditions are selected, as preliminary simulations showed these to require the largest lateral inputs, thus are expected to be influenced most by the roll damper. This yielded 9 manoeuvres, as shown in Table 6, to be tested with both *SAS-1* and *SAS-2*. Of these 18 tests, 7 were already present in the selection of the main experiment. Hence, when including 9 extra experiment runs, a total of 53 manoeuvres had to be tested.

Test pilots and experiment matrices

The pilot-in-the-loop experiment was performed by four pilots, denominated as Pilot 1 to 4. Table 7 shows an overview of the credentials of these pilots. Due to limited availability, Pilots 3 and 4 only performed the main experiment of 42 manoeuvres. Pilots 1 and 2 also performed the extra experiment runs, thus 53

Table 6. Selected test conditions for experimental assessment of the roll damper effect.

	CG Forward
DR	APP, TO, CR (AEO)
TTB	APP, CR (AEO), TO (OEI)
SHS	APP, TO, CR (OEI)

manoeuvres. In order to eliminate bias from the results, for the experiment design matrix initially a Latin-square distribution was used. Unfortunately, pilot availability limitations led to a less structured experiment design matrix. Table 8(a) shows the initial experiment design, Table 8(b) shows the final experiment design, altered due to pilot availability. It can be noted that the experiment runs of *SAS-2 ext.* were split in two parts, p1 and p2. This was done to at least allow the manoeuvres in approach and take-off flight conditions to be tested with *SAS-2 ext.*, since *SAS-2 ext.* was expected to yield the largest differences in requirement compliance with *SAS-2* in those conditions. The manoeuvres in cruise flight conditions were only tested with *SAS-2 ext.* when sufficient time was available.

Table 7. Test pilot credentials.

Pilot	Credentials
P1	Technical pilot (airliner)
P2	Flight Test Engineer, National Test Pilot School US
P3	Research pilot (airliner/business jet)
P4	Technical pilot (airliner)

Simulator

The pilot-in-the-loop experiment was performed in the SIMONA Research Simulator (SRS) of the TU Delft Aerospace Engineering faculty, shown in Figure 3. The SRS is a high fidelity, six-degree of freedom ground-based research simulator, initially developed for advanced research into simulation techniques, motion system control and navigation systems technologies [37]. Ever since, it has been used for a broad range of research such as piloted handling quality assessments [38] and pilot control behavior research [39]. The SRS was shown to have correlated results to simulators leading in fidelity such as the Calspan Total In-Flight Simulator (TIFS) and the NASA Ames Vertical Motion Simulator (VMS) [40]. The SRS thus was assumed to be of sufficiently high fidelity for the current development phase of the Flying-V to perform pilot-in-the-loop handling quality experiments.

In-flight display

The primary flight display of the simulator cockpit was used to present the pilot with available aircraft information in a head-up display (HUD) alike, green on black, layout. This included velocity, Mach number, thrust lever setting and output, roll angle, pitch angle, flight path angle, sideslip angle and altitude. For the different manoeuvres, different indicators with targets and limits were used. To de-clutter the HUD, only relevant indicators were shown when simulating

(a) Experiment setup inside SIMONA Research Simulator.

(b) Outside impression of SIMONA.

Figure 3. SIMONA Research Simulator, experiment setup.

a manoeuvre. Figure 4 shows a black and white example of the HUD with all indicators, with arbitrary targets and limits. Yellow inner margins were used as warning, while red outer margins were used to show the pilot the aircraft's state was out of the target bounds. Margins colored green when they were met.

Motion Cueing

The SRS allows for six-degree of freedom motion cueing to the pilot, using the hexapod hydraulic actuators. In order to allow for this motion cueing, filtering between the aircraft states and simulator motion was performed. For this, high pass filters were used to translate the aircraft simulation specific forces in surge (x), sway (y) and heave (z) to analogous simulator motion, and to translate aircraft simulation roll (ϕ), pitch (θ) and yaw (ψ) to analogous simulator motion. Moreover, low pass filters were used to translate aircraft low frequency surge and sway to simulator rotations, using tilt coordination in pitch and roll to replace the low frequency surge and sway. Gain tuning was performed to allow for (desired) maximal cueing, while

Table 8. Experiment designs.

(a) Initial experiment design matrix.

P1	SAS 2 ext	Bare-AC	SAS 2	SAS 1
P2	Bare-AC	SAS 2 ext	SAS 1	SAS 2
P3	SAS 2	SAS 1	SAS 2 ext	Bare-AC
P4	SAS 1	SAS 2	Bare-AC	SAS 2 ext

(b) Final experiment design matrix.

SAS 2 ext	Bare-AC	SAS 2	SAS 1	
Bare-AC	SAS 2 ext p1	SAS 1	SAS 2	SAS 2 ext p2
SAS 2 ext p1	SAS 2	Bare-AC		
SAS 2	Bare-AC	SAS 2 ext p1		

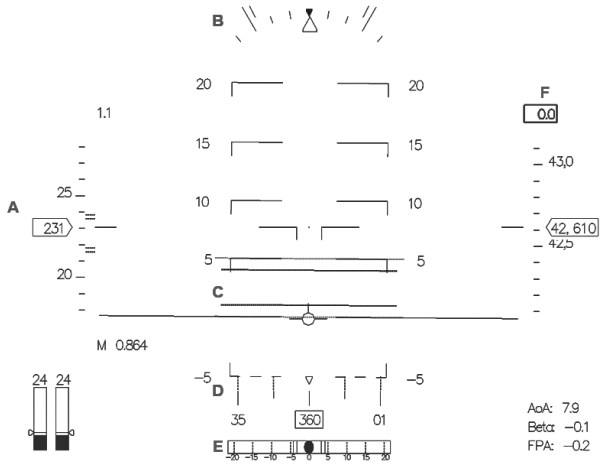

Figure 4. Primary flight display HUD view, with at A: Velocity indicator with (stippled) target margins; B: Roll angle indicator with target margins; C: Flight Path Marker with (stippled) target margins; D: Sideslip angle indicator with target margins; E: Heading indicator with (stippled) target margins; F: Manoeuvre timer.

keeping the simulator within its motion space. For this, the Gouverneur Tuning Approach was adopted [41], by identifying where motion limits were breached for different tuning settings and expected aircraft simulation manoeuvres. This yielded the gain tuning as shown in Table 9, showing an overview of the high- and low-pass filter parameters used for each aircraft simulation degree of freedom.

Table 9. SRS motion tuning settings used in experiment, filter settings for aircraft degrees of freedom (DOF); *indicating filter order, gain K, 2^{nd} order natural frequency ω_n, damping ζ, 1^{st} order break frequency ω_b.*

		High-pass filter				Low-pass filter		
DOF	Ord.	K	ω_n	ζ	ω_b	Ord.	ω_n	ζ
x	2^{nd}	0.4	1.0	0.7	-	2^{nd}	2.0	0.7
y	2^{nd}	0.4	1.0	0.7	-	2^{nd}	2.0	0.7
z	3^{rd}	0.4	2.0	0.7	1.5			
ϕ	1^{st}	0.4	1.0	0.7	-			
θ	1^{st}	0.4	1.0	0.7	-			
ψ	1^{st}	0.4	1.0	0.7	-			

Control Loading

The sidestick and pedal pilot controls in the SRS make use of a control loading mechanism to simulate sidestick spring stiffness and pedal force feel, which had to be set for the experiment. First, an estimation of conventional aircraft sidestick spring stiffness and pedal forces was made based on CS-25 regulations. Second, preliminary piloted simulation was used to further increase the fidelity compared to conventional aircraft. This yielded the sidestick spring stiffness and pedal force as shown in Table 10.

Table 10. Experiment control loading settings.

Pilot input	Stiffness		Motion space	
Longitudinal stick	5	N/deg	± 18	deg
Lateral stick	2	N/deg	± 18	deg
Pedal deflection	2100	N/m	$\pm$ 8	cm

Dependent measures

From the pilot-in-the-loop experiment runs, different types of output were obtained. Each experiment run yielded a pass or fail on whether the requirements of the manoeuvre were met. These were used to validate the analytical research, from which hypotheses on the success of each manoeuvre were set. For the manoeuvres used to compare the flight control system with and without roll damping, the pilots were asked to assign a Cooper-Harper rating to the manoeuvre [21, page 12]. These were used next to assess whether a significant difference in (subjective) handling qualities was present between the systems. The pilot was asked for his opinion on the handling qualities and controllability of the aircraft after every manoeuvre, yielding (subjective) feedback. Finally, the simulation variables such as the aircraft state vector, control surface deflections and pilot control inputs were logged throughout the entire experiment. These data were later used to assess mismatches between analytical and experimental findings and to validate pilot comments on the aircraft dynamics.

Processing pilot feedback

The pilot feedback after every tested manoeuvre provided a large set of comments. To aggregate the comments of over 200 manoeuvres, a set of defined keywords was used to comprise each comment into one or multiple keywords. By reducing the amount of describing keywords to eventually 26, a trend analysis could be performed. The keyword occurrence was set out against the different independent variables of the simulations. This yielded the opportunity to obtain between-pilot trends for distinct flight conditions, flight control systems, manoeuvres or combinations of these.

IV. Results

A. Bare-Airframe Handling Quality Analysis Results

1. Analytical assessment results

The analytical assessment of the handling qualities of the bare-airframe Flying-V yielded requirement compliance for tested combinations of flight conditions, aircraft center of gravity locations, flight control system implementations and engine settings with the five different handling quality requirements. Table 11 shows an overview of this requirement compliance, with the manoeuvres which failed to comply with the requirements shown as critical conditions with critical center of gravity locations. For the Dutch Roll Stability requirement, Figure 5 shows the obtained Dutch Roll damping and frequency parameters plotted against the MIL-HDBK-1797 handling quality requirement levels. Level III is required for compliance, Level I is desired. It should be noted that all tested conditions failed requirement compliance, except the cruise flight condition with aft center of gravity. Furthermore, Table 21 in the appendix of this paper shows the required control surface deflections for the critical requirement conditions. The control surface deflections larger than the set limits are indicated in red.

Table 11. Overview of the analytically assessed requirement compliance of the bare-airframe Flying-V.

Req.	Compl.	Critical Condition(s)	Critical CG
DR	Failed	APP, TO, CR	Forward, Aft
CTC	Failed	APP AEO	Forward
TTB	Failed	APP AEO	Forward, Aft
OEI-T	Failed	APP	Forward
SHS	Failed	APP AEO & OEI	Forward, Aft
		TO AEO & OEI	Forward, Aft

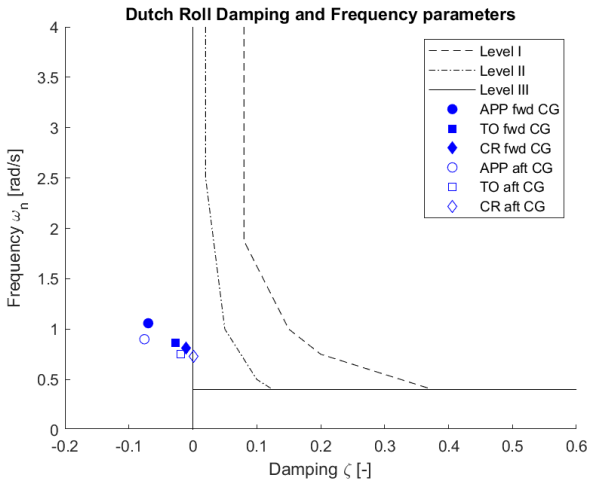

Figure 5. Dutch Roll parameters of bare-airframe analytical handling quality analysis.

2. Piloted assessment results

From the piloted assessment, the requirement compliance with each tested manoeuvre was obtained. As a validation of the analytical assessment, the experimental requirement compliance was compared to the analytically hypothesized requirement compliance. 52 out of the 56 manoeuvres were validated positively, which can be stated the vast majority. The manoeuvres with a mismatch to the hypothesized outcome are shown in Table 12.

Table 12. Bare-airframe experimental analysis, mismatches with analytical assessment.

Req.	Compliance	Cond.	CG	Pilot(s)
CTC	Failed	CR	aft	P3, P4
TTB	Failed	CR	aft	P3
SHS	Failed	CR	aft	P3

From the feedback retrieved from the pilots after each experiment run, several trends were obtained regarding the bare-airframe aircraft:

1) Control of the bare-airframe Flying-V was found difficult and inadequate.
2) Insufficient pitch control authority was found available in approach conditions.
3) The Dutch Roll Stability was found unstable in approach flight conditions, but controllable in take-off and cruise flight conditions.
4) Using the rudder pedals to counteract the Dutch Roll eigenmode was found difficult and counter-intuitive.
5) Inadvertent excitation of the Dutch Roll eigenmode interfered with performing other manoeuvres.
6) The roll control authority was at times found insufficient, mainly during the Time to Bank and Steady Heading Sideslip manoeuvres.
7) With the Steady Heading Sideslip manoeuvre, the roll control authority was found insufficient to keep the aircraft wings level.
8) The thrust effect was found unconventional, specifically the low thrust value required in trim and high value required for acceleration of the aircraft.

The manoeuvres with a mismatch between the analytically hypothesized result and experimental result, shown in Table 12, were further assessed. Whereas requirement compliance was expected, all failed to comply. The logged simulation data of each of these runs were assessed: comparing (between-pilots) passed versus failed experiment runs showed the failed runs to have larger oscillations in aircraft attitude, preventing target-state margin maintainability. Next, due to the pilot comments on the Dutch Roll eigenmode interference with other manoeuvres, the Dutch Roll Mode Participation Factor was assessed and compared between the passed and (unexpectedly) failed runs. For the failed runs, the Dutch Roll showed to build up (more) throughout the run, which is expected to cause the increase in attitude oscillation and to prevent target state maintainability.

B. Prototype Flight Control System *SAS-2* Implementation Results

1. Analytical assessment results

The analytical assessment of the handling quality requirements was repeated with the prototype flight control system *SAS-2* implemented. This yielded the requirement compliance as shown in Table 13. Figure 6 shows the Dutch Roll damping and frequency parameters with the flight control system implemented. Table 22 in the appendix of this paper shows the new required control surface deflections and thrust vectors to complete the manoeuvres, for the same conditions as (previously) critical in the bare-airframe analysis, as were shown in Table 21. Additionally, a new critical condition is present in the Time to Bank (TTB) manoeuvre in take-off flight conditions. Again, the control surface deflections larger than the set limits are indicated in red.

Table 13. Overview of the analytically assessed requirement compliance with SAS-2 implemented.

Req.	Compl.	Critical Condition(s)	Critical CG
DR	Passed	-	-
CTC	Failed	APP AEO	Forward
TTB	Failed	APP, TO	Forward, Aft
OEI-T	Failed	APP AEO	Forward
SHS	Failed	APP AEO, APP OEI	Forward, Aft

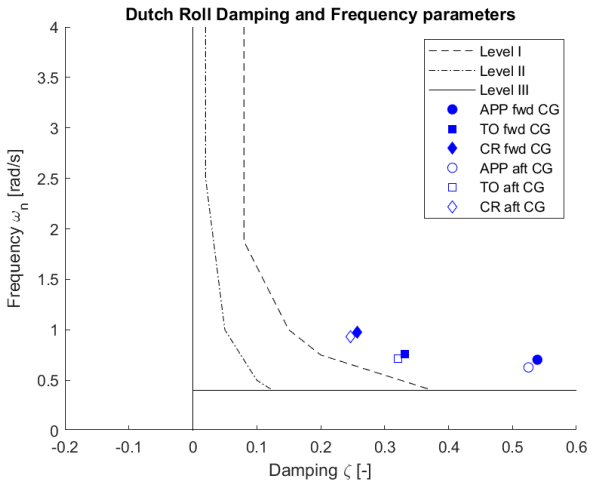

Figure 6. Dutch Roll parameters of analytical handling quality assessment with SAS-2 implemented.

2. Piloted assessment results

The piloted assessment also was repeated with the prototype flight control system implemented, and the requirement compliance with each tested manoeuvre was obtained. Analogous to the bare-airframe analysis, the experimental requirement compliance was compared to the analytically hypothesized requirement compliance. The manoeuvres with a mismatch to the hypothesized outcome are shown in Table 14.

Table 14. Flight control system SAS-2 experimental analysis, mismatches with analytical assessment.

Req.	Compl.	Cond.	CG	Pilot
TTB	Passed	APP	fwd	P2, P3
TTB	Passed	TO	fwd	P1, P2
OEI-T	Passed	APP	fwd	P2, P3, P4

From the feedback retrieved from the pilots after each experiment run, several trends were obtained regarding the aircraft with flight control system *SAS-2* implemented:

1) The implementation of the flight control system considerably improved the experienced handling qualities.
2) The Dutch Roll was positively damped and pleasant to fly, no pilot-compensation was required.
3) Insufficient pitch control authority was found available in approach conditions.
4) When control surfaces saturated, the control allocation yielded adverse axis-coupling.
5) Lateral Pilot Induced Oscillations occurred when ending the Time to Bank roll manoeuvre.
6) The lack of cross control required during a Steady Heading Sideslip manoeuvre was found unconventional.
7) The flight control system was found excessive in an engine failure situation, by keeping the pilot out of the loop.
8) Similar to the bare-airframe, the thrust effect was found unconventional, specifically the low thrust value required in trim and high value required for acceleration of the aircraft.

The manoeuvres with a mismatch between the analytically hypothesized result and experimental result, shown in Table 14, required further assessment. All showed requirement compliance, whereas analytically no requirement compliance was hypothesized. Hence, the logged experiment data was further assessed.

The pilot inputs of the (unexpectedly) passed Time to Bank manoeuvres showed use of the rudder pedals to roll the aircraft, both for the approach and take-off flight conditions. Since pedal use was not included in the analytical assessment of the roll manoeuvre, an increased roll capability was available to the pilots when using these rudder pedals. This is attributed to having caused the requirement compliance where non-compliance was hypothesized.

The One Engine Inoperative Trim manoeuvre in approach flight conditions was unexpectedly passed by multiple pilots. The logged aircraft state data showed the margins around the velocity and attitude targets were used to dynamically reach the 10 seconds required for manoeuvre requirement compliance. It is expected that further maintainability was not attainable with the set margins.

Of the pilot comments, the tendency for pilot induced oscillations while ending the Time to Bank roll manoeuvre was assessed further. The logged experiment data showed roll oscillations and lateral sidestick-input oscillations at the end of these manoeuvres. Further assessment showed these oscillations to

occur during control surface deflection-rate saturation. Since deflection-rate saturation is a known cause for (Category 2) pilot induced oscillations [42], it is attributed to have caused this tendency, and confirmed the trend in pilot comments.

C. Prototype Flight Control Systems *SAS-1* and *SAS-2 ext.* Implementation Results

Next to the results presented in the previous sections, two extra research directions were further explored. First, the effect of excluding the roll damping from the prototype flight control system, yielding *SAS-1*. Second, augmenting the control authority by extending the maximum allowed control surface deflections linearly, yielding *SAS-2 ext.*. The analytical assessment of these was of limited interest: the analysis with *SAS-1* yielded similar results to *SAS-2*, and no analytical assessment with *SAS-2 ext.* was performed. The extended control authority was expected to yield full requirement compliance, hence only required further piloted assessment. Table 15 shows the manoeuvres with a mismatch to the hypothesized outcome for the piloted assessment with *SAS-1* and *SAS-2 ext.*. The unexpected pass of the Time to Bank manoeuvre is again likely to be caused by rudder-pedal use; the unexpected failed compliance with the Coordinated Turn Capability requirement is discussed later in this section.

Table 15. Flight control systems *SAS-1* & *SAS-2 Ext.* mismatches experimental with analytical assessment.

Req.	Compl.	Cond.	CG	SAS	Pilot
TTB	Passed	TO	fwd	SAS-1	P1, P2
CTC	Failed	CR	aft	SAS-2 ext.	P3

The Cooper-Harper rating scale was used to assess the pilot-subjective handling qualities of using *SAS-1* and *SAS-2* to attain the adequate and desired performance as previously shown in Table 4. Table 16 shows the obtained Cooper-Harper ratings by Pilots 1 and 2 for the manoeuvres chosen to compare *SAS-1* and *SAS-2* on.

Table 16. Cooper-Harper rating results for *SAS-1* and *SAS-2* comparison.

Pilot	Condition	Engine	Req.	SAS 1	SAS 2
P1	APP	OEI	SHS	8	10
P1	APP	AEO	TTB	8	10
P1	TO	OEI	SHS	1	5
P1	TO	OEI	TTB	2	3
P1	CR	OEI	SHS	1	1
P1	CR	AEO	TTB	2	1
P2	APP	OEI	SHS	7	10
P2	APP	AEO	TTB	10	9
P2	TO	OEI	SHS	2	2
P2	TO	OEI	TTB	5	5
P2	CR	OEI	SHS	3	2
P2	CR	AEO	TTB	5	5

Pilot feedback on the comparison of the aircraft with flight control system *SAS-1* and *SAS-2* yielded multiple distinctive comments. Amongst others, Pilot 2 commented that *SAS-1* required logical inputs, and had a pleasant cross-control mix of pedal and lateral stick control. Besides, the pilot noted the use of *SAS-2* to be unconventional and peculiar, since the roll damping reduces the lateral stick input required during, e.g., a sideslip manoeuvre. Pilot 1 commented similarly, by stating *SAS-1* was more predictable than *SAS-2*. To assess if the pilot comments favoring *SAS-1* can be confirmed statistically significant from the obtained Cooper-Harper ratings, a Related-Samples Wilcoxon Signed Rank Test was used. A difference in median of the Cooper-Harper ratings given to SAS-1 and SAS-2 was tested, yielding a statistic significance of a difference in median of 0.090, larger than the set significance level of 0.050 thus not statistically significant.

In order to assure that sufficient control authority was available for full requirement compliance with *SAS-2 ext.*, the new control surface deflection limits allowed for excess deflection with respect to the analytically obtained surface deflections required. Next, the actual deflections used by the pilots were obtained, to be used as an approximate figure for future control surface design. Table 17 shows the (pilot-averaged) maximum control surface deflections used per control surface, for each manoeuvre separately. All maximum control surface deflections occurred while performing the manoeuvres in approach flight conditions.

Table 17. (Pilot-averaged) Maximum control surface deflections used with *SAS-2 ext.*.

	CTC	TTB	OEI-T	SHS
C1 [deg]	44.2	121.8	26.2	85.1
C2 [deg]	38.4	84.5	27.8	68.9
C3 [deg]	67.8	130.9	53.0	97.2
C4 [deg]	87.2	91.0	43.2	42.4
C5 [deg]	54.1	51.3	29.3	35.4
C6 [deg]	45.5	124.5	28.7	82.4

From the pilot feedback on flying the aircraft with *SAS-2 ext.*, it was obtained that the controls were found sufficient most often when compared to other configurations. Still, the pitch control authority in the Coordinated Turn Capability manoeuvre was found insufficient. Further research showed this to have occurred due to the gain tuning of the aircraft. While the control authority was extended by allowing increased maximum control servo deflections, the gain tuning was not altered to make full use of this new limit. Hence, the pitch control authority was found to be limited by the (input) gain tuning, and requirement compliance was found difficult to attain in approach flight conditions. This lack of pitch control authority is expected to have caused the failed requirement compliance of the Coordinated Turn Capability manoeuvre, shown in Table 15. Further pilot comments on *SAS-2 ext.* were analogous to those given on the stability and (unconventional) control of *SAS-2*.

V. Discussion

A. Bare-Airframe Handling Qualities

The bare-airframe handling quality analysis as presented in Section IV.A yields several results. First, the analytical assessment shows the control authority in pitch, roll, and yaw to be insufficient in approach flight conditions, and the control authority in roll to be insufficient in take-off flight conditions. The control deflections analytically found required to perform the critical manoeuvres violate the set limits, to the largest extent in the approach flight conditions. In take-off flight conditions the control surface deflection limits were also violated, but only during the Steady Heading Sideslip manoeuvre, and only around the roll axis.

The analytically found lack of control authority was validated by the piloted-experiment results: the runs hypothesized as not possible due to a lack of control authority were not passed by the pilots. Moreover, the pilot feedback shows a trend regarding a lack of pitch control authority, and at times a lack of roll control authority. Similar as analytically found, the pitch control authority was mainly pilot-declared insufficient in the approach flight conditions. The at times stated insufficient roll control authority of the bare-airframe Flying-V did not distinct for a single flight condition. It stood out most for the Steady Heading Sideslip manoeuvre in approach and take-off flight conditions, where the roll control authority was insufficient to keep the aircraft wings level at larger angles of sideslip. Contributing to this effect is the large sweep angle of the Flying-V, which yields a large roll moment when a sideslip angle occurs, i.e., possesses a large C_{l_β} [19]. This roll moment in sideslip was found too large to be compensated by the roll control surfaces.

Next to the limited control authority, the analytical assessment showed mainly an unstable (and once, marginally stable) Dutch Roll in the different flight conditions. Pilot feedback shows this to be of considerable influence on the experienced handling qualities of the aircraft. The Dutch Roll was stated to be unstable in approach, and although stated controllable in take-off and cruise, it was found to interfere with the performance in numerous manoeuvres throughout the different flight conditions. The Dutch Roll was found to be difficult to compensate with the rudder pedals and frequently showed a build-up throughout a manoeuvre, leading to lateral-directional oscillations preventing state maintainability.

The combination of lack of control authority at low speeds, and unstable, difficult to compensate Dutch Roll is expected to yield the pilot-declared difficult and inadequate flight characteristics of the bare-airframe Flying-V.

B. Flight Control System implementation effect

The implementation of the prototype flight control system, consisting of the adapted control allocation and stability augmentation system *SAS-2*, considerably improved the handling qualities.

The adapted control allocation showed by analytical assessment to increase overall control effectiveness, and decreased the required maximum control surface deflection in most manoeuvres. This decrease was sufficient to eliminate the take-off flight conditions as critical. The increase in control effectiveness however was insufficient for requirement compliance in approach flight conditions. The analytical findings were validated with the results of the experimental analysis and were confirmed by trends in the pilot feedback. Pilot feedback confirmed the increase in overall control effectiveness, but also confirmed the (longitudinal-) pitch axis control authority to still be insufficient in approach flight conditions. The latter to the extent of negatively influencing the lateral-directional requirement compliance in these flight conditions.

Despite the positive effect on overall control effectiveness, the adapted control allocation yielded adverse axis-coupling when control surfaces saturated. When pitch control surfaces saturated and a roll input was given simultaneously, the control allocation cannibalized the pitching moment to obtain a rolling moment. This yielded nose-down behavior when rolling while in pitch saturation, which occurred most in approach flight conditions. Pilot feedback showed this to severely influence the experienced handling qualities of the aircraft in approach flight conditions.

The Dutch Roll damping was increased by the implementation of the stability augmentation system, which can be seen when comparing Figure 5 and Figure 6. This analytically found improvement was validated in the piloted experiment. The pilots confirmed the Dutch Roll to be positively damped and pleasant to fly. Moreover, no Dutch Roll eigenmode interference with other manoeuvres was noted.

The implementation of the stability augmentation system showed to not only influence the Dutch Roll characteristics of the aircraft. Pilot feedback yielded multiple trends on unconventional behavior of the aircraft with flight control system *SAS-2*. First, Pilot Induced Oscillations occurred when the roll manoeuvre of the Time to Bank was stopped, and were determined to be caused by servo rate-limit saturation. Second, the stability augmentation led to only small deviations in attitude where pilots expected larger compensation to be necessary. Mainly during a Steady Heading Sideslip, where lateral stick deflection is expected to be necessary to compensate for the rudder induced roll moment. Similarly, during an engine failure situation, tested in the One Engine Inoperative Trim manoeuvre, only very limited lateral-directional attitude changes occurred due to compensation of the stability augmentation system. This yielded a trend in feedback on the pilot feeling kept out of the loop in an engine failure situation, which was deemed unsafe.

The positive effects of the control allocation and stability augmentation system are expected to have caused the trend in pilot feedback of the flight control system considerably improving the handling qualities compared to the bare-airframe. This despite the flight control system introducing side-effects, such as the adverse axis-coupling when control surfaces saturated, a tendency for pilot induced oscillations and unconventional controls required.

C. Roll Damping Experiment

As discussed in Section IV.C, pilot feedback favored *SAS-1* (without roll damping) over *SAS-2*. Since the effect on the

handling qualities of including roll-damping was found pilot subjective in previous research [9], it was decided a difference should be proven statistically significant instead of only be based on pilot feedback. SAS-1 was expected to yield better (i.e., lower) Cooper-Harper ratings. Since the Cooper-Harper rating scale yields ordinal data, a difference in median should be proven significant. The Related-Samples Wilcoxon Signed Rank Test was used to compare the medians of the Cooper-Harper ratings given to SAS-1 and SAS-2. The test statistic significance was found to be larger than the set significance level. Hence, for this experiment no statistically significant difference in median could be used to confirm the pilot comments, and no conclusion on the use of roll-damping is drawn.

D. Extended Control Authority Experiment

An experimental analysis with (augmented) extended control authority was performed, as introduced in Section III.C.3. It was expected that by extending the control authority sufficiently, full requirement compliance would be attained by each pilot. As shown in Table 15, it was not attained by one pilot out of four. The pitch control authority was found to be limited by the (input) gain tuning, and requirement compliance was found difficult to be attained in approach flight conditions.

Generally, augmenting the increased control authority allowed for requirement compliance where previous configurations did not. As introduced in Section IV.C, the new control surface deflection limits allowed for excess deflection with respect to the analytically obtained surface deflections required. The deflections used by the pilots can be interpreted as approximation for future control surface design, when assuming the pilots used approximately the amount of control surface deflection required for favorable handling qualities. As shown in Table 17, the maximum rudder deflection was up to 124.5 degrees, more than three times the current limit set. The maximum elevon deflection was up to 130.9 degrees, more than four times the current limit set. This shows a large challenge for future control surface design of the Flying-V, since the control effectiveness, maximum control surface deflections or both have to be drastically increased for requirement compliance at the tested flight conditions.

E. Remaining Challenges in Handling Qualities for the Flying-V

As discussed in Section V.A and Section V.B, implementing the prototype flight control system with the adapted control allocation and stability augmentation system showed to be a first improvement of the handling qualities of the Flying-V. Nevertheless, a challenge remains in improving the handling qualities of the Flying-V further, in order to obtain compliance with the handling quality requirements for conventional aircraft.

The analytical and experimental assessment of the Flying-V with the prototype flight control system implemented showed the handling qualities to still be insufficient. Foremost, even after adapting the control allocation, the control authority in pitch was insufficient for requirement compliance. Although the study focused on the lateral-directional handling qualities of the Flying-V, the lack of pitch authority at low speeds severely influenced the lateral-directional requirement compliance. Hence, if the approach velocity tested will be part of the Flying-V flight envelope, it is recommended to redesign the control surfaces to allow for more control authority in pitch.

Next to the pitch control authority, the roll control authority showed to, mainly, be insufficient for requirement compliance in sideslip manoeuvres in approach flight conditions. Analogous to the pitch control authority, servo saturation severely influenced the pilot-experienced handling qualities, and it is recommended to assess redesigning the control surfaces to allow for more control authority in roll and yaw.

The control authority around all axes could benefit from introducing new control surfaces, or from adapting the six control surfaces of the current design. New control surfaces could, e.g., consist of spoilers asymmetrically dumping lift for roll control [43]. The control surfaces of the current design could be adapted to unconventional control surface designs, such as split flaps or split rudders for roll or yaw control [44].

Next to the control surface design changes, it is recommended to re-assess the low speed handling qualities at velocities between the tested 0.2 and 0.3 Mach. Since the analysis showed increasing speed to be beneficial to the handling qualities, an approach speed with sufficient control authority could be found. If this speed is a feasible landing speed, none or less design changes are required if the flight envelope of the Flying-V is altered.

Finally, it is recommended to further develop the prototype flight control system. Amongst others, the effect of including or excluding a roll damper requires further research before the implementation can be decided on. Moreover, the simple feedback systems currently tested should be enhanced further before being able to comply with current fly-by-wire system standards. Amongst others, attitude hold, auto-throttle and turn coordination were noted to be missing by multiple pilots performing the experiment. Besides, the gain tuning of a stability augmentation system can yield pilot subjective results, such as for the (highly) augmented prototype flight control system, *SAS-2*, being at times stated to be excessive.

F. Reflection on Analytical and Experimental Analysis

Reflecting on the analytical and experimental analysis yields remarks on modeling the aircraft, and remarks on the difference between the analytical and experimental analysis. Two remarks can be made on the aerodynamic model used for the analysis. First, the control deflection force and moment contributions had to be linearly extrapolated based on only one deflection to force or moment output slope. A higher fidelity control deflection model would be preferred for future research, since non-linear force and moment outputs are expected from a linearly increasing control surface deflection. Second, the VLM method only simulated lift-induced drag, thus no parasitic (i.e., skin friction) drag was modeled. This yields a low drag in trim, and reduces the fidelity of engine-modeling.

Next to the modeling remarks, remarks can be made on differences between the analytical and experimental analysis. First, it was found that the analytical state-attainability did not

always correctly predict the experimental outcome: reaching and maintaining a state in a piloted experiment can differ from the analytical state-attainability. Although the vast majority of the analytically found hypotheses were experimentally validated, factors such as interfering Dutch Roll eigenmotion and operating at the edge of the aircraft control authority did at times result in insufficient handling qualities for requirement compliance. Second, differences in analytically hypothesized and experimentally obtained requirement compliance occurred due to the set state-limit margins on the flight conditions in the experiment. Whereas the analytical assessment uses exact flight conditions to assess state-attainability, the piloted experiment allowed for deviations around the flight conditions to increase the feasibility of performing the manoeuvres. This led to pilots using the margin around the target state to dynamically comply with a trim-state requirement.

VI. Conclusion

Analytical and experimental assessment showed the lateral-directional handling qualities of the bare-airframe Flying-V to be insufficient for compliance with set requirements, due to a lack of pitch, roll and yaw control authority in low-speed flight conditions, and an insufficiently stable Dutch Roll eigenmode. The Dutch Roll eigenmode not only failed to comply with the Dutch Roll Stability requirement assessed, but also interfered with piloted requirement compliance of other manoeuvres tested. The prototype flight control system, consisting of an adapted control allocation and stability augmentation system, showed to both analytically and experimentally improve the control authority, stability, and handling qualities of the Flying-V. While the effect on the lateral-directional stability was sufficient for compliance with the Dutch Roll Stability requirement, the control authority was not sufficiently increased for compliance with all manoeuvrability requirements. Thus, a challenge remains in improving the handling qualities of the Flying-V. Augmenting increased control authority yielded an approximation of the control authority required for full requirement compliance in the flight conditions tested, and showed a control authority increase of over a factor four to be required for future control surface design.

Acknowledgments

Hereby, I'd like to thank all involved in this research. Amongst others the five pilots contributing to the experiment, but especially my thesis supervisors. Olaf, you have been an incredibly supportive and involved supervisor. Especially during the piloted experiments, you spent a very large amount of time and effort in- and outside of the control room of SIMONA. Moreover, you were always available for a discussion or to help with issues, and I think the average response time to my emails was less than ten minutes. Max, you are a very inspiring mentor, and a very supportive professor. Thank you both for supporting me in finishing my Masters degree in Aerospace Engineering.

References

[1] Martinez-Val, R., "Flying Wings. A New Paradigm for Civil Aviation?" *Acta Polytechnica*, Vol. 47, 2007. https://doi.org/10.14311/914.

[2] Liebeck, R. H., "Design of the Blended Wing Body Subsonic Transport," *Journal of Aircraft*, Vol. 41, 2004, pp. 10–25. https://doi.org/10.2514/1.9084.

[3] Brown, M., and Vos, R., "Conceptual design and evaluation of blended-wing-body aircraft," *AIAA Aerospace Sciences Meeting, 2018*, 2018. https://doi.org/10.2514/6.2018-0522.

[4] Benad, J., "The Flying V-A new Aircraft Configuration for Commercial Passenger Transport," *Deutscher Luft- und Raumfahrtkongress 2015, Rostock*, 2015. https://doi.org/10.25967/370094.

[5] Faggiano, F., "Aerodynamic Design Optimization of a Flying V Aircraft," Master's Thesis, TU Delft, 2016. URL http://resolver.tudelft.nl/uuid:0b1472a5-3aad-433c-9a64-242c84b114fd.

[6] Bolsunovsky, A. L., Buzoverya, N. P., Gurevich, B. I., Denisov, V. E., Dunaevsky, A. I., Shkadov, L. M., Sonin, O. V., Udzhuhu, A. J., and Zhurihin, J. P., "Flying wing - Problems and decisions," *Aircraft Design*, Vol. 4, 2001, pp. 193–219. https://doi.org/10.1016/S1369-8869(01)00005-2.

[7] Pan, Y., and Huang, J., "Research on lateral-directional stability augmentation system of flying wing aircraft based on reliability model," *Proceedings of the Institution of Mechanical Engineers, Part G: Journal of Aerospace Engineering*, Vol. 233, 2019, pp. 4214–4221. https://doi.org/10.1177/0954410018817449.

[8] Cappuyns, T., "Handling Qualities of a Flying-V configuration," Master's Thesis, TU Delft, 2019. URL http://resolver.tudelft.nl/uuid:69b56494-0731-487a-8e57-cec397452002.

[9] Castro, H. V. D., "Flying and handling Qualities of a Fly-by-Wire Blended-Wing-Body Civil Transport Aircraft," Ph.D. Thesis, Cranfield University, 2003. URL https://dspace.lib.cranfield.ac.uk/handle/1826/119.

[10] Ehlers, J., Niedermeier, D., and Leißling, D., "Verification of a flying wing handling qualities analysis by means of in-flight simulation," *AIAA Atmospheric Flight Mechanics Conference 2011*, 2011. https://doi.org/10.2514/6.2011-6540.

[11] EASA, *Certification Specifications for Large Aeroplanes CS-25 - Amendment 23*, European Union Aviation Safety Agency, 2019. URL https://www.easa.europa.eu/document-library/certification-specifications/cs-25-amendment-23.

[12] US Department Of Defence, *Handbook MIL-HDBK-1797a Flying Qualities of Piloted Aircraft*, 1997. URL http://everyspec.com/MIL-HDBK/MIL-HDBK-1500-1799/MIL-HDBK-1797_NOTICE-1_39380/.

[13] Claeys, M., "Flying V and Reference Aircraft Structural Analysis and Mass Comparison," Master's Thesis, TU Delft, 2018. URL http://resolver.tudelft.nl/uuid:ee7f2ecb-cdb6-46de-8b57-d55b89f8c7e6.

[14] Viet, R. A., "Analysis of the flight characteristics of a highly swept cranked flying wing by means of an experimental test," Master's Thesis, TU Delft, 2019. URL http://resolver.tudelft.nl/uuid:90de4d9e-70ae-4efc-bd0a-7426a0a669c3.

[15] Garcia, A. R., "Aerodynamic Model Identification of the Flying V Using Wind Tunnel Data," Master's Thesis, TU Delft, 2019. URL http://resolver.tudelft.nl/uuid:79e01f29-1789-4501-8556-ca2bcf06f3ab.

[16] Palermo, M., and Vos, R., "Experimental aerodynamic analysis of a 4.6%-scale flying-v subsonic transport," *AIAA Scitech 2020 Forum*, Vol. 1 PartF, 2020. https://doi.org/10.2514/6.2020-2228.

[17] Pascual, B. R., "Engine-Airframe Integration for the Flying," Master's Thesis, TU Delft, 2018. URL http://resolver.tudelft.nl/uuid:75be27a7-6fd4-4112-a600-45df2999758f.

[18] Joosten, S., "Piloted assessment of the lateral-directional handling qualities of the Flying-V, Preliminary Thesis," , 2021. Unpublished.

[19] Mulder, J. A., van Staveren, W. H. J. J., van der Vaart, J. C., de Weerdt, E., de Visser, C. C., in 't Veld, A. C., and Mooij, E., *Flight Dynamics Lecture Notes*, Delft University of Technology, 2013.

[20] Etkin, B., and Reid, L. D., "Dynamics of Flight Stability and Control," , John Wiley & Sons, inc, 1996. URL https://www.worldcat.org/title/dynamics-of-flight-stability-and-control/oclc/849073275.

[21] Cooper, G. E., and Harper, R. P., "The Use of Pilot Rating in the Evaluation of Aircraft Handling Qualities," , NASA, 1969. URL https://ntrs.nasa.gov/citations/19690013177.

[22] Roskam, J., *Airplane design. Pt. 7. Determination of stability, control and performance characteristics : far and military requirements.*, Roskam Aviation and Engineering, 1988.

[23] Perez, R. E., Liu, H. H., and Behdinan, K., "Multidisciplinary optimization framework for control-configuration integration in aircraft conceptual design," *Journal of Aircraft*, Vol. 43, 2006, pp. 1937–1948. https://doi.org/10.2514/1.22263.

[24] Wahler, N. F. M., "The Impact of Control Allocation on Optimal Control Surface Positioning and Sizing A comparative study for a PrandtlPlane," Master's Thesis, TU Delft, 2021. URL http://resolver.tudelft.nl/uuid:5e9baf63-8a8f-4c1b-98cd-5aa993938027.

[25] Zhang, N., Li, F., and Wang, L., "Control allocation approach study for BWB aircraft," *The Proceedings of the 2018 Asia-Pacific International Symposim on Aerospace Technology*, Vol. 459, Springer Verlag, 2019, pp. 2099–2115. https://doi.org/10.1007/978-981-13-3305-7_168.

[26] Huijts, C., and Voskuijl, M., "The impact of control allocation on trim drag of blended wing body aircraft," *Aerospace Science and Technology*, Vol. 46, 2015, pp. 72–81. https://doi.org/10.1016/j.ast.2015.07.001.

[27] Denieul, Y., Bordeneuve, J., Alazard, D., Toussaint, C., and Taquin, G., "Multicontrol surface optimization for blended wing-body under handling quality constraints," *Journal of Aircraft*, Vol. 55, 2018, pp. 638–651. https://doi.org/10.2514/1.C034268.

[28] Rahman, N. U., and Whidborne, J. F., "A Lateral Directional Flight Control System for the MOB Blended Wing Body Planform," , 2008. URL https://www.researchgate.net/publication/237087377.

[29] Denieul, Y., Bordeneuve-Guibé, J., Alazard, D., Toussaint, C., and Taquin, G., "Integrated design of flight control surfaces and laws for new aircraft configurations," *IFAC-PapersOnLine*, Vol. 50, 2017, pp. 14180–14187. https://doi.org/10.1016/j.ifacol.2017.08.2085.

[30] Johansen, T. A., and Fossen, T. I., "Control allocation - A survey," *Automatica*, Vol. 49, 2013, pp. 1087–1103. https://doi.org/10.1016/j.automatica.2013.01.035.

[31] Oppenheimer, M. W., Doman, D. B., and Bolender, M. A., *Control Allocation*, Vol. 2, William S. Levine, 2010. URL https://nl1lib.org/book/899141/e56e71?id=899141&secret=e56e71&dsource=recommend.

[32] Oppenheimer, M. W., Doman, D. B., and Bolender, M. A., "Control allocation for over-actuated systems," *2006 14th Mediterranean Conference on Control and Automation*, 2006, pp. 1–6. https://doi.org/10.1109/MED.2006.328750.

[33] van Paassen, M., Stroosma, O., and Delatour, J., "DUECA - Data-driven activation in distributed real-time computation," *Modeling and Simulation Technologies Conference*, American Institute of Aeronautics and Astronautics Inc., 2000. https://doi.org/10.2514/6.2000-4503, cited By 36.

[34] Stevens, B. L., Lewis, F. L., and Johnson, E. N., *Aircraft Control and Simulation - Dynamics, Controls Design, and Autonomous Systems (3rd Edition)*, John Wiley & Sons, 2016. URL https://app.knovel.com/hotlink/toc/id:kpACSDCDAU/aircraft-control-simulation/aircraft-control-simulation.

[35] Johnson, M., and Romanowski, M. C., "Advisory Circular Subject: Flight Test Guide for Certification of Transport Category Airplanes," , 2018. URL https://www.faa.gov/documentLibrary/media/Advisory_Circular/AC_25-7D.pdf.

[36] Tillema, G. H., Stroosma, O., Miletović, I., and Mulder, M., "Perceptual eigenmode distortion analysis for motion cueing evaluation in fixed-wing aircraft simulators," *AIAA Scitech 2021 Forum*, American Institute of Aeronautics and Astronautics Inc, AIAA, 2021, pp. 1–22. https://doi.org/10.2514/6.2021-1012.

[37] Advani, S. K., "The development of SIMONA: A simulator facility for advanced research into simulation techniques, motion system control and navigation systems technologies," *Flight Simulation and Technologies*, American Institute of Aeronautics and Astronautics Inc, AIAA, 1993, pp. 156–166. https://doi.org/10.2514/6.1993-3574.

[38] Stroosma, O., Damveld, H. J., Mulder, J. A., Choe, R., Xargay, E., and Hovakimyan, N., "A handling qualities assessment of a business jet augmented with an L1 adaptive controller," 2011. URL https://www.scopus.com/record/display.uri?eid=2-s2.0-84880597033&origin=inward.

[39] Pieters, M., Zaal, P., Pool, D., Stroosma, O., and Mulder, M., "A simulator comparison study into the effects of motion filter order on pilot control behavior," *AIAA Scitech 2019 Forum*, American Institute of Aeronautics and Astronautics Inc, AIAA, 2019. https://doi.org/10.2514/6.2019-0712, cited By 2.

[40] Field, E. J., Paassen, M. M. V., Stroosma, O., and Salchak, P. W., "Validation of simulation models for piloted handling qualities evaluations," *Collection of Technical Papers - AIAA Modeling and Simulation Technologies Conference*, Vol. 2, 2004, pp. 815–828. https://doi.org/10.2514/6.2004-5268.

[41] Gouverneur, B., Mulder, J. B., van Paassen, M. R., Stroosma, O., and Field, E., *Optimisation of the SIMONA Research Simulator's Motion Filter Settings for Handling Qualities Experiments*, 2003. https://doi.org/10.2514/6.2003-5679, URL https://arc.aiaa.org/doi/abs/10.2514/6.2003-5679.

[42] Mcruer, D. T., "Pilot-Induced Oscillations and Human Dynamic Behavior," , 1995. URL https://ntrs.nasa.gov/citations/19960020960.

[43] Geisbauer, S., "Numerical simulation and validation of the aerodynamics of static and dynamic spoilers," *AIAA AVIATION 2020 FORUM*, Vol. 1 Part F, 2020, p. 1 – 23. https://doi.org/10.2514/6.2020-2776.

[44] Stenfelt, G., and Ringertz, U., "Yaw control of a tailless aircraft configuration," *Journal of Aircraft*, Vol. 47, 2010, pp. 1807–1810. https://doi.org/10.2514/1.C031017.

Appendix

Table 18. Flying-V geometry properties [8][17][13].

Property	Description	Value	Unit
T_{dy}	Engine (thrust vector) y location w.r.t. centre line	± 5.7	m
T_{dz}	Engine (thrust vector) z location w.r.t. centre line	0.8	m
S	Wing area	883.3	m^2
c / MAC	Wing Mean Aerodynamic Chord	18.7385	m
b	Wing span	65	m
L	Aircraft length	55	m
$CG_{forward}$	Centre of gravity forward stability limit	45	%MAC
CG_{aft}	Centre of gravity aft stability limit	57.5	%MAC

Table 19. Input variables and ranges of the Airbus Flying-V VLM model.

Variable	Description	Range	Unit
CG	Centre of Gravity	[45, 51.5, 57.5]	%MAC
M	A/C velocity in Mach	[0.2, 0.225, 0.25, 0.275, 0.3, 0.85]	-
α	Angle of Attack	[-5, 0, 5, 10, 12.5, 15, 16.5, 18, 20]	Degrees
β	Sideslip Angle	[-1, 0, 1]	Degrees
p^*	Normalized roll rate	[-1, 0, 1]	Radians
q^*	Normalized pitch rate	[-1, 0, 1]	Radians
r^*	Normalized yaw rate	[-1, 0, 1]	Radians
δ_{c1}	Deflection of left rudder	[-1, 0, 1]	Degrees
δ_{c2}	Deflection of left outboard elevon	[-1, 0, 1]	Degrees
δ_{c3}	Deflection of left inboard elevon	[-1, 0, 1]	Degrees
δ_{c4}	Deflection of right inboard elevon	[-1, 0, 1]	Degrees
δ_{c5}	Deflection of right outboard elevon	[-1, 0, 1]	Degrees
δ_{c6}	Deflection of right rudder	[-1, 0, 1]	Degrees

Table 20. Gain tuning of stability augmentation systems SAS-1 and SAS-2.

	SAS-1			SAS-2		
	Approach	Take-Off	Cruise	Approach	Take-Off	Cruise
K_r	-1000	-400	-200	-700	-200	-150
K_V	10	2	1	5	2	1
$K_{V_{input}}$	40	31.2	31.2	40	31.2	31.2
K_p	n/a	n/a	n/a	2000	900	400
$K_{p_{input}}$	30	30	30	0.3	0.3	0.3
K_q	-100	-55	-65	-100	-55	-65
$K_{q_{input}}$	0.2	0.2	0.2	0.2	0.2	0.2

Table 21. Trimmed control outputs of analytically critical requirements of bare-airframe Flying-V. [18]

Manoeuvre	CTC	TTB		OEI-T	SHS						
Condition	APP	APP		APP	APP				TO		
Engine	AEO	AEO		OEI	AEO		OEI		AEO	OEI	
CG	fwd	fwd	aft	fwd	fwd	aft	fwd	aft	fwd	fwd	aft
C1 [deg]	7.0	23.1	**90.6**	26.7	**-66.7**	**-41.5**	**-51.7**	-24.8	-10.9	-7.8	-5.8
C2 [deg]	-17.3	**-90.4**	**-99.5**	5.0	**-78.5**	**-71.3**	**-80.9**	**-74.0**	**-33.2**	**-33.7**	**-30.1**
C3 [deg]	**-52.9**	**-51.6**	-15.1	**-41.8**	**-36.5**	-7.5	**-36.6**	-7.5	-15.4	-15.4	-1.4
C4 [deg]	**-52.9**	**-51.6**	-15.1	**-41.8**	**-36.5**	-7.5	**-36.6**	-7.5	-15.4	-15.4	-1.4
C5 [deg]	17.3	**90.4**	**99.5**	-5.0	**78.5**	**71.3**	**80.9**	**74.0**	**33.2**	**33.7**	**30.1**
C6 [deg]	-7.0	-23.1	**-90.6**	-26.7	**66.7**	**41.5**	**51.7**	24.8	10.9	7.8	5.8
T1 [kN]	108.2	64.1	79.7	113.0	50.0	53.1	98.1	105.8	27.8	55.6	60.9
T2 [kN]	108.2	64.1	79.7	0.0	50.0	53.1	0.0	0.0	27.8	0.0	0.0

Table 22. Trimmed control outputs of previous and new critical manoeuvres, SAS-2 analytical handling quality assessment. [18]

Manoeuvre	CTC	TTB		OEI-T	SHS						
Condition	APP	APP	TO	APP	APP				TO		
Engine	AEO	AEO	OEI	OEI	AEO		OEI		AEO	OEI	
CG	fwd	fwd	aft	fwd	fwd	fwd	aft	fwd	aft	fwd	fwd	aft
C1 [deg]	4.0	**79.6**	**81.0**	19.8	4.9	**-68.3**	**-45.2**	**-52.8**	-28.7	-14.3	-11.1	-8.5
C2 [deg]	-26.2	**-62.6**	**-41.7**	-24.0	-20.8	**-50.0**	**-31.7**	**-47.9**	-29.4	-18.3	-17.9	-10.5
C3 [deg]	**-46.0**	**-101**	**-72.1**	**-33.1**	**-37.2**	**-54.0**	**-32.9**	**-57.1**	**-36.1**	-24.3	-24.9	-13.6
C4 [deg]	-28.4	**41.5**	**58.8**	-13.3	-21.8	2.4	22.3	5.4	25.5	2.2	2.8	11.6
C5 [deg]	-18.5	26.2	**32.4**	-11.8	-14.6	19.0	25.3	16.9	23.0	5.0	4.6	9.3
C6 [deg]	-7.4	**-82.4**	**-81.6**	-20.4	-7.6	**65.9**	**44.7**	**50.5**	28.2	13.3	10.1	8.4
T1 [kN]	113	61.0	67.0	74.9	122	52.3	53.9	105	107	29.6	59.1	61.8
T2 [kN]	113	61.0	67.0	0.0	0.0	52.3	53.9	0.0	0.0	29.6	0.0	0.0

Part II: Book of Appendices

Book of Appendices

Sjoerd Joosten

Supplementary to MSc Thesis Paper, Piloted Assessment of the Lateral-Directional Handling Qualities of the Flying-V

Contents

I. Pilot Briefing

On the following pages, the pilot briefing as was supplied to the test pilots before performing the experiment is shown.

Flying-V Lateral-Directional Handling Quality Assessment

Experiment Briefing

Sjoerd Joosten, January 2022, TU Delft

Research introduction

The lateral-directional stability and handling qualities of flying wings have been shown to differ from those of conventional aircraft due to the absence of a vertical tail surface. Earlier theoretical assessment of these handling qualities confirmed this for the Flying-V, making further research necessary. Handling qualities of an aircraft however can be assessed both theoretically and experimentally. Experimental, pilot-perceived handling qualities are a subjective measure; hence its results can differ from a theoretical assessment. For a complete evaluation of the (lateral-directional) handling qualities of the Flying-V, both a theoretical and an experimental assessment should be performed. This experimental assessment is the focus of the current study.

The study aims at bringing new insights in the lateral-directional handling qualities of the Flying-V by performing the first pilot-in-the-loop assessment of the asymmetric handling qualities. First the lateral-directional handling qualities of the Flying-V were theoretically (re-)assessed based on an aerodynamic model of the full-scale Flying-V. Next, a prototype flight control system was developed as an alternative to the original bare-airframe control structure. The next step in this study is performing a pilot-in-the-loop experiment in the full-motion SIMONA Research Simulator to validate the theoretical findings and to perform a qualitative, pilot-perceived assessment.

Flying-V Properties and Simulation Model

The Flying-V design as presented in earlier research by Cappuyns is used, which originated from a design by Benad and a design iteration by Faggiano. Table 1 below shows an overview of the Flying-V geometry properties.

Table 1: Flying-V geometry properties.

Property	Description	Value	Unit
T_{dy}	Engine (thrust vector) y location w.r.t. centre line	$\pm$ 5.6	m
T_{dz}	Engine (thrust vector) z location w.r.t. centre line	0.8	m
S	Wing area	883.3	m^2
c / MAC	Wing Mean Aerodynamic Chord	18.7385	m
b	Wing span	65	m
L	Aircraft length	55	m
$CG_{forward}$	Centre of gravity forward stability limit	45	%MAC
CG_{aft}	Centre of gravity aft stability limit	57.5	%MAC

As impression, a side and top view of the Flying-V are shown in, respectively, Figure 1 and Figure 2.

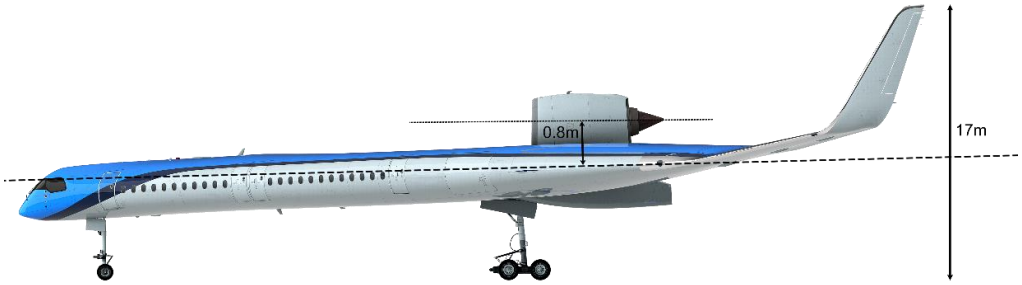

Figure 1: Flying-V impression, side view and dimensions.

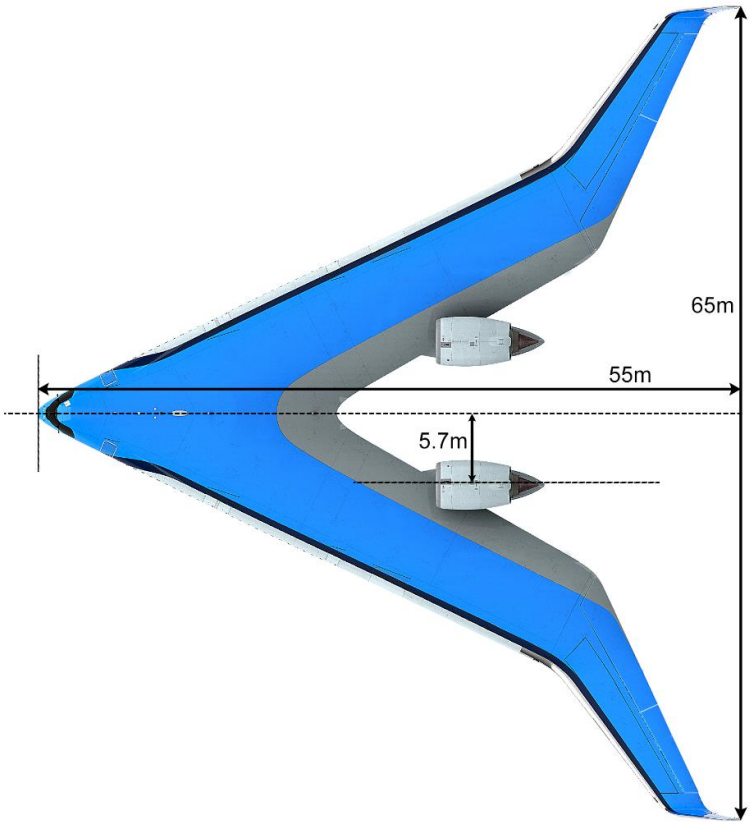

Figure 2: Flying-V impression, top view and dimensions

The Flying-V design contains six control surfaces, located at the outboard trailing edges. Both aircraft sides possess 2 elevons (i.e., elevator-aileron combinations) and a rudder embedded in the winglet. The control surfaces are indicated with variables C1 to C6, as shown in Table 2.

Table 2: Variables used to indicate control surfaces.

Variable	Control surface
C1	Left winglet rudder
C2	Left outboard elevon
C3	Left inboard elevon
C4	Right inboard elevon
C5	Right outboard elevon
C6	Right winglet rudder

As stated in the research introduction, the Flying-V simulation is based on an aerodynamic (Computational Flow Dynamics) model of the full-scale aircraft. This model was developed using the Vortex Lattice Method in a collaboration between Airbus and Cappuyns. For the research in the current experiment, it is the most recent aerodynamic model of the full-scale Flying-V available. It has to be noted however, that the Vortex Lattice Method only determines lift and lift-induced drag. Hence, no parasitic (e.g., skin friction) drag is present in the aerodynamic model. This yields an underestimation of the aircraft drag, and an underestimation of the engine thrust required. It was theoretically assessed to be of limited influence on the handling quality experiments but remains a topic of interest during the simulations.

Flying-V Configurations and Flight Conditions

Next to the bare-aircraft Flying-V, different flight control system prototypes will be tested. The flight control systems introduce different types of Stability Augmentation Systems (SAS), and an adapted control allocation. The stability augmentation systems each use a different set of aircraft states in different types of feedback loops to augment aircraft stability. The adapted control allocation increases the overall control efficiency. It no longer uses a classical elevator – aileron - rudder allocation for pitch, roll and yaw control. For control around each of these axes, it uses a combination of multiple control surfaces based on their control effectiveness around each axis. Table 3 shows an overview of the different configurations of the Flying-V to be tested.

Table 3: Flying-V configurations.

Configuration	Description
Bare-airframe	Bare-aircraft configuration: - Direct control of control surfaces - Conventional control allocation
SAS 1	Configuration with a stability augmentation system using: - **Sideslip command control through pedals & yaw damper** - Classical roll control through elevons - **Pitch rate command control** - **Control allocation based on control effectiveness**
SAS 2	Configuration with a stability augmentation system using: - Sideslip command control & yaw damper - **Roll rate command control** - Pitch rate command control - Control allocation based on control effectiveness
SAS 2 ext.	Configuration with a stability augmentation system using: - Sideslip command control & yaw damper - Roll rate command control - Pitch rate command control - Control allocation based on control effectiveness - **(Augmented) increased servo control authority**

The different aircraft configurations are to be tested in three defined flight conditions: Approach, Take-Off and Cruise. These flight conditions were chosen to be in line with earlier research, and with velocity points available in the aerodynamic model. Table 4 shows an overview of the properties of these flight conditions. In order to increase the simulation fidelity, the altitude for Approach and Take-Off condition was set to 305 m (1000 ft) in the simulation. To keep the assessment valid for lower altitudes, the air density and speed of sound were kept at the original, sea-level, values. The simplified engine characteristics do not take altitude into account.

Table 4: Flight condition assumptions.

Condition	TAS [Mach]	TAS [m/s]	Altitude [m]	Air Density [kg/m3]	Aircraft Weight
Approach	0.2	68.6	0	1.225	MLW
Take-Off	0.3	102.9	0	1.225	MTOW
Cruise	0.85	250.8	13000	0.2655	MTOW

Experiment Overview

Experiment Goals

The experiment aims at the following:

- To experimentally assess the lateral-directional handling qualities and stability of the bare-airframe Flying-V.
- To experimentally assess the influence of the prototype flight control systems on these handling qualities.
- To obtain qualitative feedback on the handling qualities of the tested configurations, to be used as guidance for further research.
- To show differences in the theoretically found and experimentally experienced handling qualities of the Flying-V.

Experiment Tasks

The handling qualities are quantified using current conventional aircraft regulations as a benchmark. EASA aircraft regulations CS-25 is used. In order to translate these regulations to flight manoeuvres for simulation, FAA flight test guide AC 25-7D was used. This flight test guide presents test procedures for CS-25 paragraphs and was used to develop flight simulation tasks.

The aircraft regulations selected primarily focus on attaining edge-of-the-envelope aircraft attitudes, and secondarily on performing edge-of-the-envelope time-constraint manoeuvres. Hence, also the simulation tasks have a focus on the attainability of attitudes under set conditions, and on manoeuvrability within a set time. The different tasks to be performed will separately be discussed below. Note that in each task the pilot is assisted by different visual indicators, targets and a timer, which are shown in the next chapter of this briefing.

MIL-HDBK-1797 - Dutch Roll

The Dutch Roll is excited by a rudder doublet input in phase with the aircrafts oscillatory response Next, the pilot is asked to counteract the oscillatory response in, respectively, three ways. First by using only the sidestick, second by using only the rudder pedals, and third by using both. Finally, the pilot is asked for qualitative feedback on the Dutch Roll magnitude and damping, and on the difficulty of counteracting the Dutch Roll mode. Since requirements on the Dutch Roll of an aircraft are based on the damping and frequency parameter of this eigenmode, it is further assessed in post-processing of the oscillatory response of the aircraft. Finally, it should be noted that a small rudder input is sufficient to obtain the oscillatory response. **Excessively large rudder inputs may cause the simulator to move out of its motion bounds, yielding an observable "bump". For experimental reasons the simulation will be paused and reset if this should occur.**

CS25.143(h) - Coordinated Turn Capability

In order to test the Coordinated Turn Capability of the aircraft, the pilot is asked to fly a turn with minimal sideslip while keeping a positive flight path angle.

A minimum bank angle of 40 degrees, maximum sideslip angle of 2 degrees and minimum flight path angle of zero are necessary for requirement compliance. To ensure a constant turn, the pilot is asked to keep the aircraft within the target margins for 10 seconds.

CS25.147(f) - Time to Bank, Roll Capability

The Roll Capability of the aircraft is tested by a time-constrained manoeuvre. The pilot is asked to fly a turn with at least a 30 degree roll angle and positive flight path angle, and next rotate 60 degrees to a 30 degree roll angle in the opposite direction.

The 60 degree roll manoeuvre has to be performed within 7 seconds for requirement compliance.

CS25.177(c) - Steady Heading Sideslip

The cross-wind capabilities of the aircraft are tested in the Steady Heading Sideslip manoeuvre. The pilot is asked to use the rudder pedals to attain a constant sideslip angle, while maintaining a constant heading and positive flight path angle. The minimum sideslip angle needed for requirement compliance differs per flight condition but corresponds with a 16 m/s cross-wind. To ensure a steady sideslip, the pilot is asked to keep the aircraft within the target margins for 10 seconds. Note that the heading target is set equal to the sideslip target, such that no heading change is required before initiating the sideslip.

CS25.161(d) - One Engine Inoperative Trim Condition

The One Engine Inoperative response of the aircraft is tested by cutting power to one engine while in straight, horizontal flight. Next, the pilot is allowed to intervene after 2 seconds, and is asked to return the aircraft to the original heading. A flight path angle larger than zero is required and a roll angle smaller than 5 degrees is required in the target state. To ensure a trimmed aircraft condition, the pilot again is asked to keep the aircraft within the target margins for 10 seconds.

Experiment task pass / fail procedure

For all tasks the experiment run result depends on pilot performance, which can improve over time. Some of the experiment runs however are expected to be impossible to complete successfully based on theoretical analysis. To limit the total experiment duration, a procedure was developed to be used during each experiment run. The procedure determines whether the experiment run passed or failed requirement compliance, and when to continue to the next experiment run or to retry the current one. Figure 3 shows the procedure in a diagram. It is shown that when the target state is attained (as was discussed in the previous section), the experiment run has passed. Next, it depends on the flight conditions and current experiment run duration whether the experiment is continued. When it is not, it depends on the pilot's opinion of the attainability of the state, on the maximum experiment duration, and on the amount of tries whether the experiment run is restarted. If not, the experiment run is considered failed. The following variables influence these decisions:

- Maximum flight condition deviation from trim +- 5% Mach
- Maximum time per run 2 minutes
- Maximum experiment run time 5 minutes
- Maximum amount of tries per experiment run 5

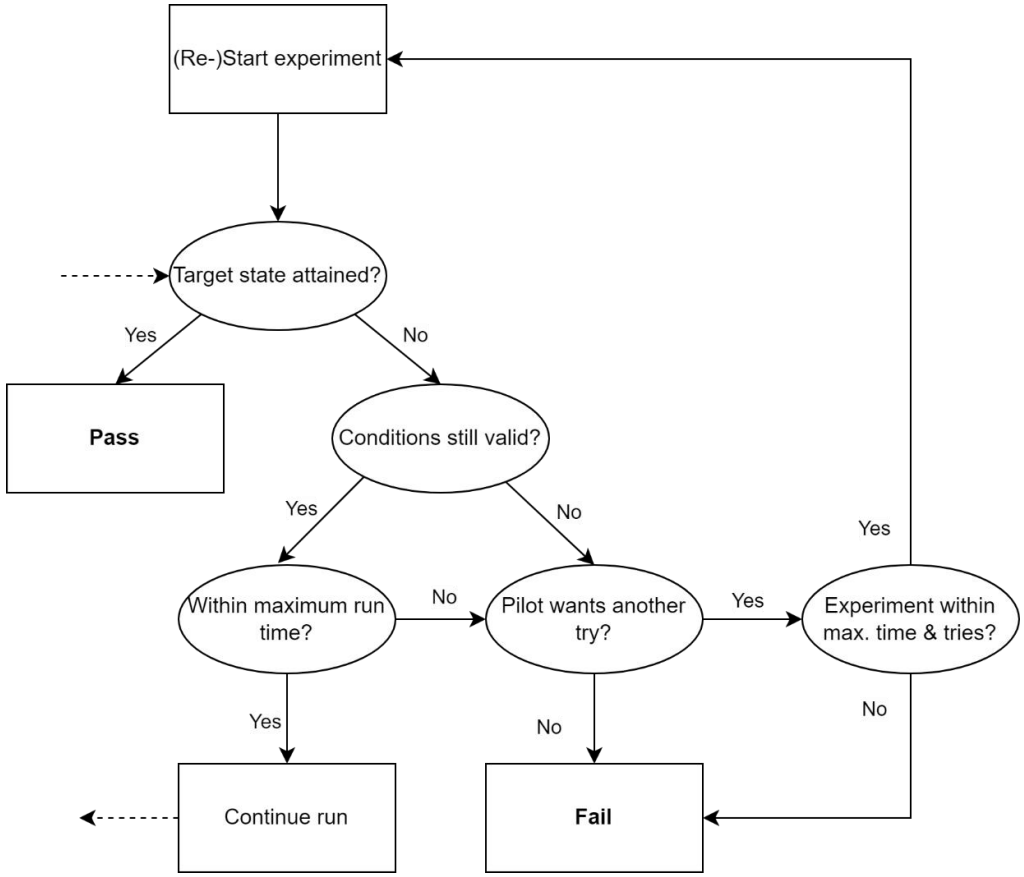

Figure 3: Experiment run pass / fail procedure.

Experiment condition selection

The theoretical analysis of the handling qualities of the Flying-V featured over 150 combinations of centre of gravity location, flight condition, engine setting, aircraft configuration and flight manoeuvre. Since testing all these in a pilot-in-the-loop simulation is deemed unfeasible with respect to time, a selection of these combinations was made for piloted simulation. This selection focused both on the best and worst case scenarios, as on special combinations of interest. This yields **53** flight manoeuvres to be tested. Next to these flight manoeuvres, each change of configuration or flight condition will be started by a familiarisation run. In this run, the pilot is asked to briefly test the stick on pitch and roll response, the pedals on yaw response and a change in thrust.

It has to be noted that of these selected flight manoeuvres, several are expected to be impossible to be achieved by the pilot. Thus, after failure of an experiment, the pilot is asked to discuss with the researchers whether the target state in a flight manoeuvre is attainable and another try is warranted: **does the pilot expect a further try to increase the performance sufficiently for requirement compliance?**

Cooper-Harper Rating Scale for flight control system comparison

To evaluate the pilot-experienced effect of implementing different flight control system prototypes, the Cooper-Harper Handling Qualities Rating Scale is used for mutual comparison. In a selection of manoeuvres with a selection of configurations, the pilot is asked to rate the task performed using this scale. The scale is shown below and will be available in the simulator during the experiment.

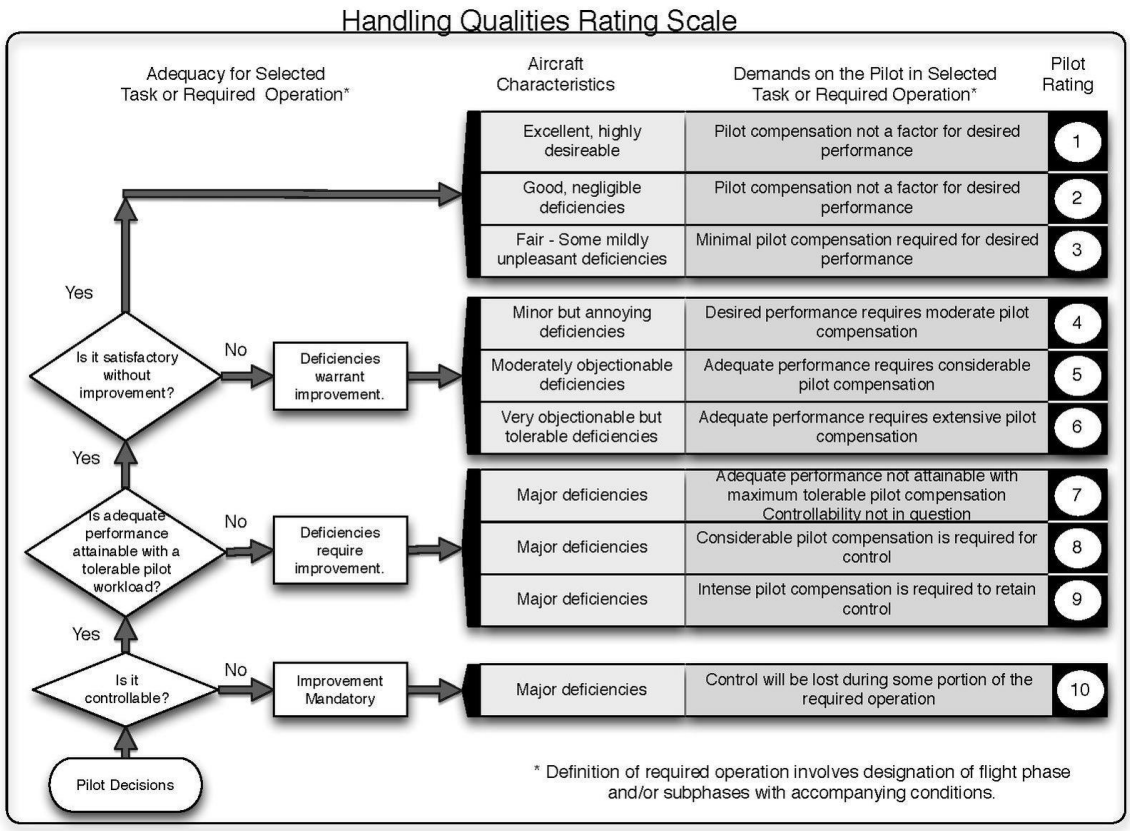

Figure 4: Cooper-Harper Handling Qualities Rating Scale

Simulation in SIMONA

The experiment will be performed in the SIMONA Research Simulator. Both visual as motion cueing will be used. For first-time pilots in the SIMONA Research Simulator, please watch the safety instruction video beforehand: https://youtu.be/PXijsyJ3hro

Figure 5 shows the simulator set-up during this particular experiment, with the following elements indicated:

1: Outside view

2: Throttle levers

3: Emergency button (shuts down the motion and flight controls in case of emergency)

4: Primary flight display showing the experiment HUD interface

5: Rudder pedals

6: Side-stick

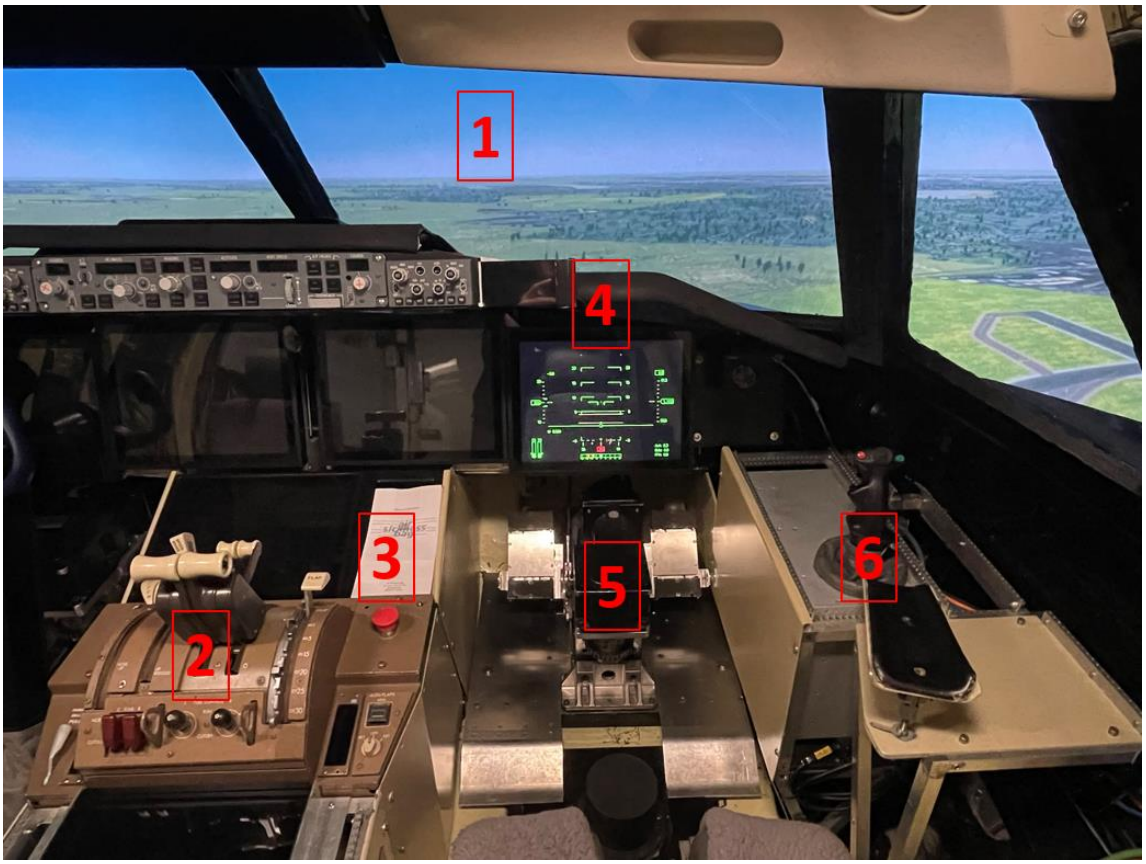

Figure 5: Experiment simulation set-up.

The experiment focuses on the use of green on black Head-Up Display (HUD) symbology, showing e.g., the aircraft's velocity, height, and attitude on the main instrument panel. Different indicators are used in combination with state targets and margins. The HUD and different indicators are further elaborated upon next.

Figure 6 shows the default HUD view. The following is indicated:

A: Load factor indication [g]

B: Indicated airspeed [kts] (with margins while in experiment run)

C: Airspeed in Mach [-]

D: Throttle-lever setting (line and arrows) and current thrust (green bar) [% of max.]

E: Pitch angle indication [deg]

F: Aircraft attitude indicator (w.r.t. pitch angle ladder) [deg]

G: Flight path marker (w.r.t. pitch angle ladder) [deg]

H: Altitude [ft]

I: Angle of attack [deg], sideslip angle [deg], flight path angle [deg]

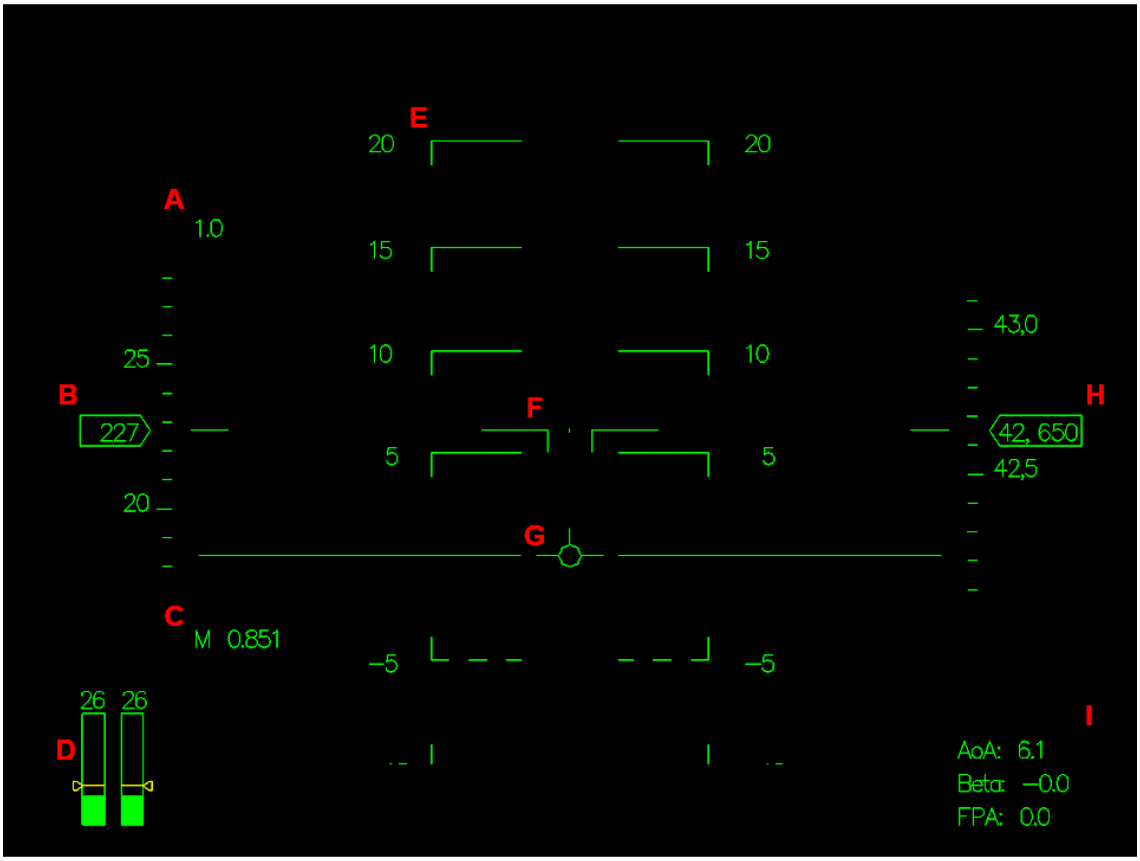

Figure 6: Default HUD view.

Next to the default HUD view, each experiment involves associated indicators, targets, and margins. Below, the HUD view for the Dutch Roll experiment is shown. It consists of the general HUD view, with a sideslip indicator added (indicated with J). Since the Dutch Roll experiment does not involve a target state, no target and margins are present in the sideslip indicator. The sideslip indicator follows the “Step on the ball” principle: when an undesired sideslip occurs, a pilot can counteract this sideslip by stepping on the rudder pedal on the side where the ball in the indicator is located. It should be noted that despite the visual resemblance with the ‘turn and slip indicator’ of conventional aircraft, a different measure is presented. The turn and slip indicator presents side-force, while the sideslip indicator in this HUD shows the sideslip angle, thus side-velocity.

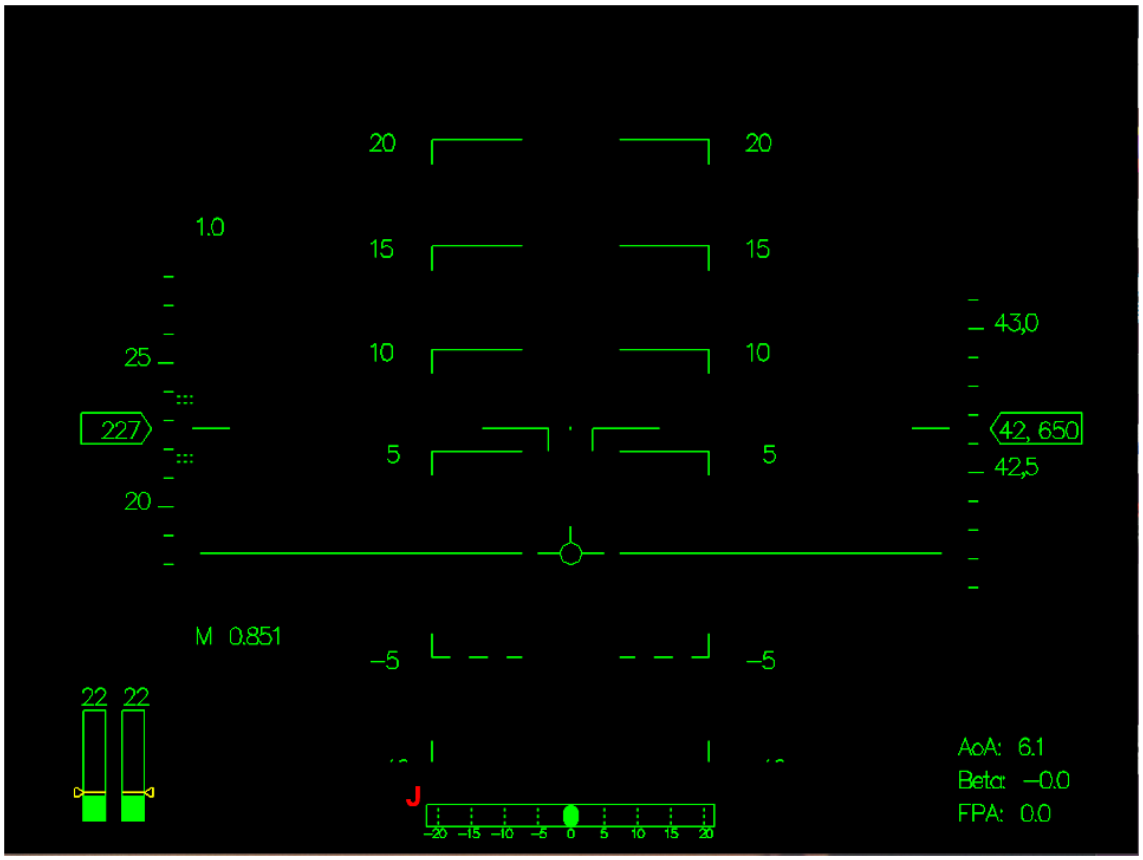

Figure 7: Dutch Roll experiment HUD view.

Below, the HUD view for the Coordinated Turn manoeuvre is shown. Again, a sideslip indicator is present, as indicated with J. For the Coordinated Turn however, the desired sideslip is zero, and margins around this target are indicated in the sideslip indicator. The ball has to be kept within the outer margins to comply with the requirement tested. Next, a roll indicator is present and indicated with K. The open-arrow moves with the rolling of the aircraft (i.e., a sky pointer) and needs to be put within the roll target margins indicated. Finally, stippled lines are shown near the flight path marker (indicated with L). These indicate the target of a positive flight path angle; thus, the flight path marker has to be put within these stippled margins. Finally, a timer is shown at M. This timer guides the pilot to stay for 10 seconds within the required margins.

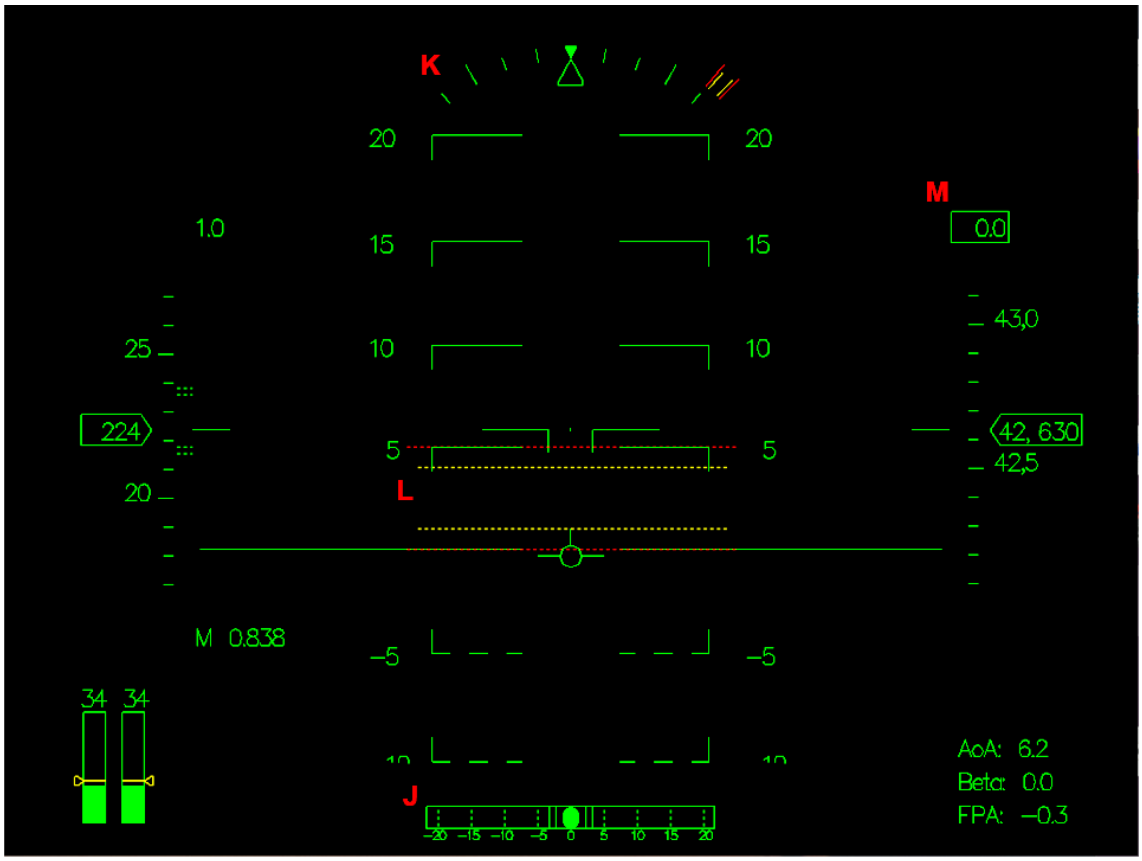

Figure 8: Coordinated Turn experiment HUD view.

Below, the HUD view for the Time to Bank manoeuvre is shown. A roll indicator with roll angle margins is shown, and the flight path angle margins are shown next to the flight path marker. When the bank manoeuvre is initiated by the pilot, starting from a 30 degree roll angle on one side, the roll target will move to the other side, indicating the new attitude target. Moreover, the timer (indicated with M) will start, to aid the pilot in achieving the 7 second time requirement for the manoeuvre. Note that the pilot determines the start of the manoeuvre by initiating the roll, but that the timer only runs when this start is performed from a flight condition complying with all bounds.

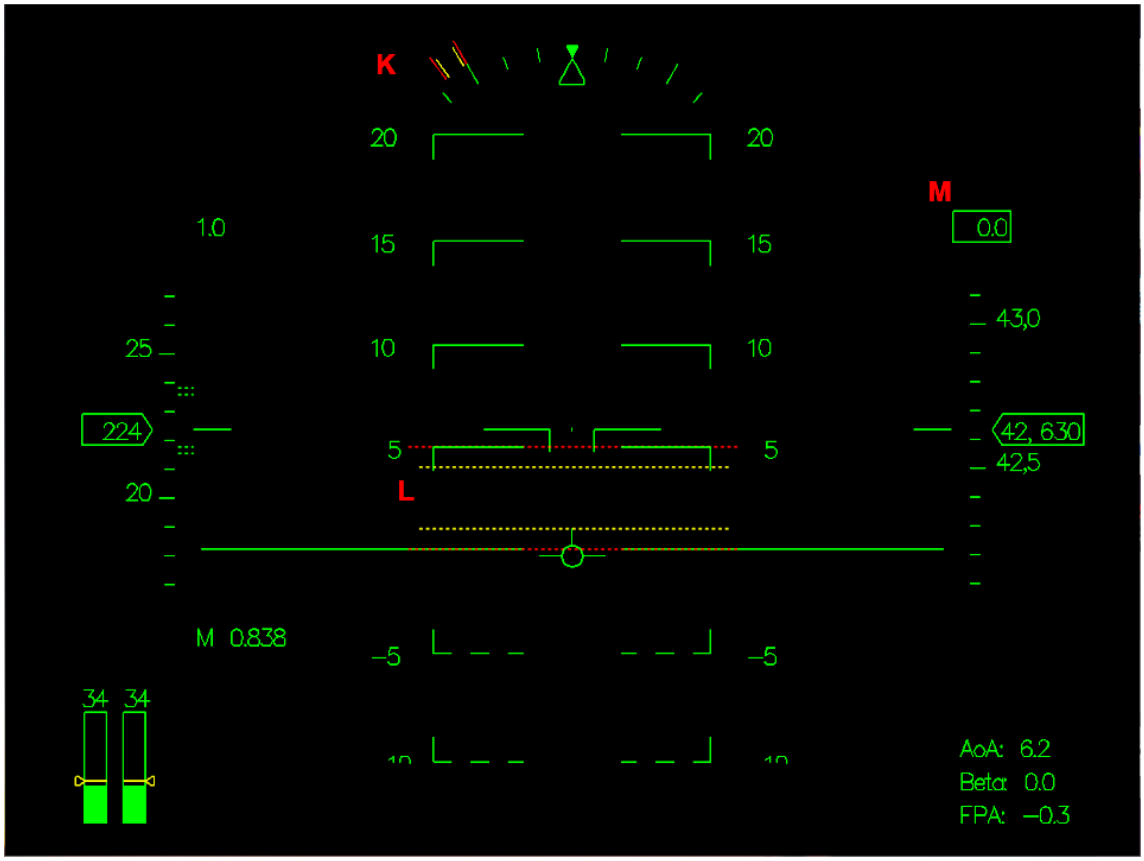

Figure 9: Time to Bank manoeuvre HUD view.

Below, the HUD view for the Steady Heading Sideslip manoeuvre is shown. Flight path angle margins are presented at L, near the flight path marker. A sideslip indicator with target margins is shown at J, and a heading indicator is shown at N. The heading indicator shows the current heading and heading target margins to ensure a steady heading during the sideslip manoeuvre. The heading target is set such that the sideslip indicator can be focused on: when the aircraft is flown at the target sideslip, the heading target was set to be complied with. However, further movement away from the heading target has to be compensated for. Finally, the target state needs to be kept for a duration of 10 seconds, which can be monitored with the timer shown at M. Note that since the sideslip indicator follows the “step on the ball” principle for minimising sideslip, a step opposite to the non-zero target is required (“step away from the target”).

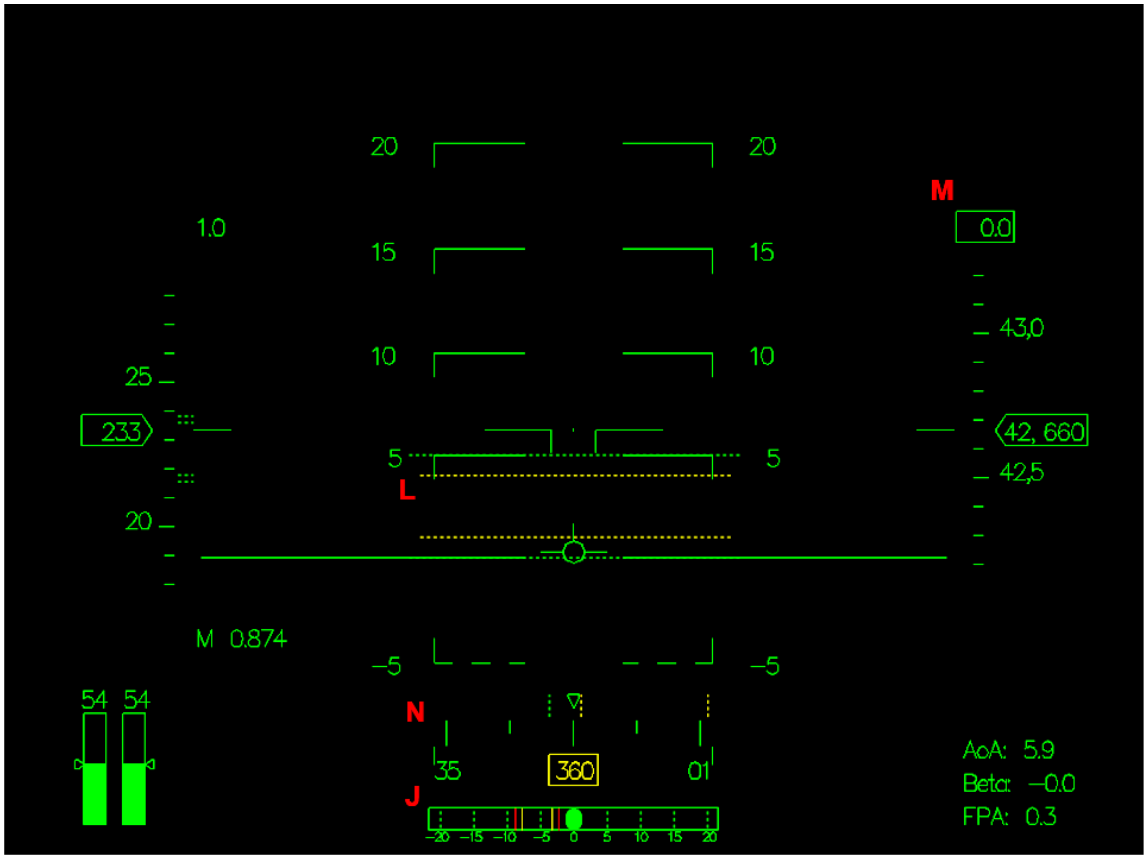

Figure 10: Steady Heading Sideslip manoeuvre HUD view.

Below, the HUD view for the One Engine Inoperative Trim manoeuvre is shown. A roll indicator with roll angle margins is shown at K, which is used to keep a small bank angle in the target state. Flight path angle margins are shown at L, next to the flight path marker. A heading indicator with target margins is shown at N, which is used to obtain the original heading after engine failure. Finally, the target state needs to be kept for a duration of 10 seconds, which can be monitored with the timer shown at M.

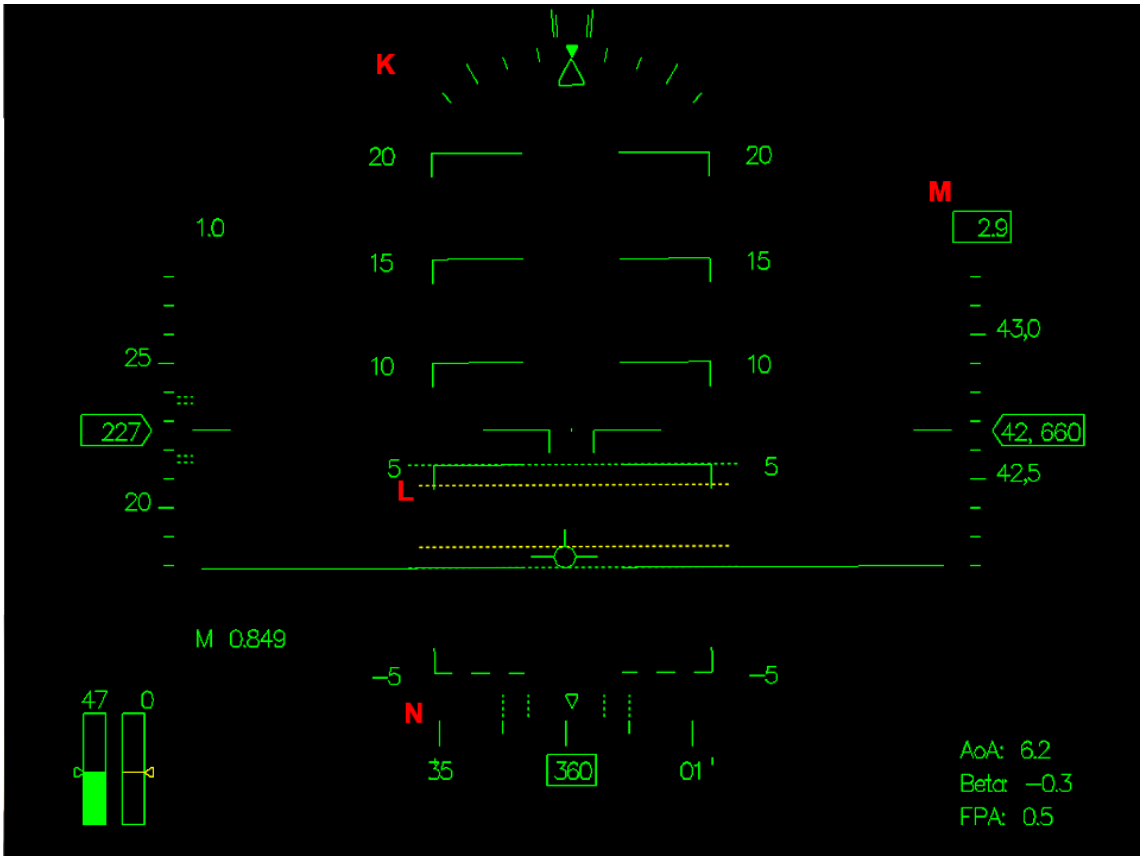

Figure 11: One Engine Inoperative manoeuvre HUD view.

Experiment Planning

As stated earlier in this briefing, 53 experiment conditions will be tested. A total simulation time of 4 hrs is estimated. The total simulation time however depends on pilot performance and opinion, thus can take less or more time. The experiment is aimed to be performed in 4 simulation blocks, using the 4 different aircraft configurations shown in Table 3 as guide. The breaks between simulation blocks however are open for the pilot to be moved, thus the pilot is asked to indicate if a break is expected to be required soon. The planning aimed at is shown in Table 5.

Table 5: Experiment planning (Start 8:00).

Experiment phase	Duration	Planning
Reception and briefing	1 hr	08:00 – 09:00
Simulation block 1	1 hr	09:00 – 10:00
Break 1	15 min	10:00 – 10:15
Simulation block 2	1 hr 15 min	10:15 – 11:30
Break 2	15 min	11:30 – 11:45
Simulation block 3	1 hr 15 min	11:45 – 13:00
Break 3 (Lunch)	1 hr	13:00 – 14:00
Simulation block 4	45 min	14:00 – 14:45
Break 4	15 min	14:45 – 15:00
Buffer	15 min	15:00 – 15:15
Debriefing	30 min	15:15 – 15:45

II. Experiment Matrices and Experimental Results

The following pages show the experiment matrices for Pilots 1 to 4, with both the analytically hypothesized as experimental outcome shown.

Experiment Matrix Pilot 1

Run	Configuration	CG location	Condition	Engine	Manoeuvre	CH	Hyp	Outcome	Match
1	SAS 2 ext.	Front	APP	AEO	Training				
2	SAS 2 ext.	Front	APP	AEO	DR		pass	pass	TRUE
3	SAS 2 ext.	Front	APP	AEO	CTC		pass	pass	TRUE
4	SAS 2 ext.	Front	APP	AEO	TTB		pass	pass	TRUE
5	SAS 2 ext.	Front	APP	AEO	OEI		pass	pass	TRUE
6	SAS 2 ext.	Front	APP	OEI	SHS		pass	pass	TRUE
7	SAS 2 ext.	Front	TO	AEO	Training				
8	SAS 2 ext.	Front	TO	AEO	DR		pass	pass	TRUE
9	SAS 2 ext.	Front	TO	OEI	SHS		pass	pass	TRUE
10	SAS 2 ext.	Front	CR	AEO	Training				
11	SAS 2 ext.	Front	CR	AEO	DR		pass	pass	TRUE
12	SAS 2 ext.	Front	CR	OEI	SHS		pass	pass	TRUE
13	SAS 2 ext.	Aft	CR	AEO	DR		pass	pass	TRUE
14	SAS 2 ext.	Aft	CR	OEI	CTC		pass	pass	TRUE
15	SAS 2 ext.	Aft	CR	AEO	TTB		pass	pass	TRUE
16	SAS 2 ext.	Aft	CR	AEO	OEI		pass	pass	TRUE
17	SAS 2 ext.	Aft	CR	AEO	SHS		pass	pass	TRUE
Run	Configuration	CG location	Condition	Engine	Manoeuvre	CH	Hyp	Outcome	Match
18	Bare A/C	Front	APP	AEO	Training				
19	Bare A/C	Front	APP	AEO	DR		fail	fail	TRUE
20	Bare A/C	Front	APP	AEO	CTC		fail	fail	TRUE
21	Bare A/C	Front	APP	AEO	TTB		fail	fail	TRUE
22	Bare A/C	Front	APP	AEO	OEI		fail	fail	TRUE
23	Bare A/C	Front	APP	OEI	SHS		fail	fail	TRUE
24	Bare A/C	Front	TO	AEO	Training				
25	Bare A/C	Front	TO	AEO	DR		fail	fail	TRUE
26	Bare A/C	Front	TO	OEI	SHS		fail	fail	TRUE
27	Bare A/C	Front	CR	AEO	Training				
28	Bare A/C	Front	CR	AEO	DR		fail	fail	TRUE
29	Bare A/C	Front	CR	OEI	SHS		pass	pass	TRUE
30	Bare A/C	Aft	CR	AEO	DR		fail	fail	TRUE
31	Bare A/C	Aft	CR	OEI	CTC		pass	pass	TRUE
32	Bare A/C	Aft	CR	AEO	TTB		pass	pass	TRUE
33	Bare A/C	Aft	CR	AEO	OEI		pass	pass	TRUE
34	Bare A/C	Aft	CR	AEO	SHS		pass	pass	TRUE
Run	Configuration	CG location	Condition	Engine	Manoeuvre	CH	Hyp	Outcome	Match
35	SAS 2	Front	APP	AEO	Training				
36	SAS 2	Front	APP	AEO	DR		pass	pass	TRUE
37	SAS 2	Front	APP	AEO	CTC		fail	fail	TRUE
38	SAS 2	Front	APP	AEO	TTB	10	fail	fail	TRUE
39	SAS 2	Front	APP	AEO	OEI		fail	fail	TRUE
40	SAS 2	Front	APP	OEI	SHS	10	fail	fail	TRUE
41	SAS 2	Front	TO	AEO	Training				
42	SAS 2	Front	TO	AEO	DR		pass	pass	TRUE
43	SAS 2	Front	TO	OEI	SHS	5	pass	pass	TRUE
44	SAS 2	Front	TO	OEI	TTB	3	fail	pass	FALSE
45	SAS 2	Front	CR	AEO	Training				
46	SAS 2	Front	CR	AEO	DR		pass	pass	TRUE
47	SAS 2	Front	CR	OEI	SHS	1	pass	pass	TRUE
48	SAS 2	Front	CR	AEO	TTB	1	pass	pass	TRUE
49	SAS 2	Aft	CR	AEO	DR		pass	pass	TRUE
50	SAS 2	Aft	CR	OEI	CTC		pass	pass	TRUE
51	SAS 2	Aft	CR	AEO	TTB		pass	pass	TRUE
52	SAS 2	Aft	CR	AEO	OEI		pass	pass	TRUE
53	SAS 2	Aft	CR	AEO	SHS		pass	pass	TRUE
Run	Configuration	CG location	Condition	Engine	Manoeuvre	CH	Hyp	Outcome	Match
54	SAS 1	Front	APP	AEO	Training				
55	SAS 1	Front	APP	AEO	DR		pass	pass	TRUE
56	SAS 1	Front	APP	OEI	SHS	8	fail	fail	TRUE
57	SAS 1	Front	APP	AEO	TTB	8	fail	fail	TRUE

58	SAS 1	Front	TO	AEO	Training				
59	SAS 1	Front	TO	AEO	DR		pass	pass	TRUE
60	SAS 1	Front	TO	OEI	SHS	1	pass	pass	TRUE
61	SAS 1	Front	TO	OEI	TTB	2	fail	pass	FALSE
62	SAS 1	Front	CR	AEO	Training				
63	SAS 1	Front	CR	AEO	DR		pass	pass	TRUE
64	SAS 1	Front	CR	OEI	SHS	1	pass	pass	TRUE
65	SAS 1	Front	CR	AEO	TTB	2	pass	pass	TRUE

Experiment Matrix Pilot 2

Run	Configuration	CG location	Condition	Engine	Manoeuvre	CH	Hyp	Outcome	Match
1	Bare A/C	Front	APP	AEO	Training				
2	Bare A/C	Front	APP	AEO	DR		fail	fail	TRUE
3	Bare A/C	Front	APP	AEO	CTC		fail	fail	TRUE
4	Bare A/C	Front	APP	AEO	TTB		fail	fail	TRUE
5	Bare A/C	Front	APP	AEO	OEI		fail	fail	TRUE
6	Bare A/C	Front	APP	OEI	SHS		fail	fail	TRUE
7	Bare A/C	Front	TO	AEO	Training				
8	Bare A/C	Front	TO	AEO	DR		fail	fail	TRUE
9	Bare A/C	Front	TO	OEI	SHS		fail	fail	TRUE
10	Bare A/C	Front	CR	AEO	Training				
11	Bare A/C	Front	CR	AEO	DR		fail	fail	TRUE
12	Bare A/C	Front	CR	OEI	SHS		pass	pass	TRUE
13	Bare A/C	Aft	CR	AEO	DR		fail	fail	TRUE
14	Bare A/C	Aft	CR	OEI	CTC		pass	pass	TRUE
15	Bare A/C	Aft	CR	AEO	TTB		pass	pass	TRUE
16	Bare A/C	Aft	CR	AEO	OEI		pass	pass	TRUE
17	Bare A/C	Aft	CR	AEO	SHS		pass	pass	TRUE
Run	Configuration	CG location	Condition	Engine	Manoeuvre	CH	Hyp	Outcome	Match
18	SAS 2 ext.	Front	APP	AEO	Training				
19	SAS 2 ext.	Front	APP	AEO	DR		pass	pass	TRUE
20	SAS 2 ext.	Front	APP	AEO	CTC		pass	pass	TRUE
21	SAS 2 ext.	Front	APP	AEO	TTB		pass	pass	TRUE
22	SAS 2 ext.	Front	APP	AEO	OEI		pass	pass	TRUE
23	SAS 2 ext.	Front	APP	OEI	SHS		pass	pass	TRUE
24	SAS 2 ext.	Front	TO	AEO	Training				
25	SAS 2 ext.	Front	TO	AEO	DR		pass	pass	TRUE
26	SAS 2 ext.	Front	TO	OEI	SHS		pass	pass	TRUE
Run	Configuration	CG location	Condition	Engine	Manoeuvre	CH	Hyp	Outcome	Match
27	SAS 1	Front	APP	AEO	Training				
28	SAS 1	Front	APP	AEO	DR		pass	pass	TRUE
29	SAS 1	Front	APP	OEI	SHS	7	fail	fail	TRUE
30	SAS 1	Front	APP	AEO	TTB	10	fail	fail	TRUE
31	SAS 1	Front	TO	AEO	Training				
32	SAS 1	Front	TO	AEO	DR		pass	pass	TRUE
33	SAS 1	Front	TO	OEI	SHS	2	pass	pass	TRUE
34	SAS 1	Front	TO	OEI	TTB	5	fail	pass	FALSE
35	SAS 1	Front	CR	AEO	Training				
36	SAS 1	Front	CR	AEO	DR		pass	pass	TRUE
37	SAS 1	Front	CR	OEI	SHS	3	pass	pass	TRUE
38	SAS 1	Front	CR	AEO	TTB	5	pass	pass	TRUE
Run	Configuration	CG location	Condition	Engine	Manoeuvre	CH	Hyp	Outcome	Match
39	SAS 2	Front	APP	AEO	Training				
40	SAS 2	Front	APP	AEO	DR		pass	pass	TRUE
41	SAS 2	Front	APP	AEO	CTC		fail	fail	TRUE
42	SAS 2	Front	APP	AEO	TTB	9	fail	pass	FALSE
43	SAS 2	Front	APP	AEO	OEI		fail	pass	FALSE
44	SAS 2	Front	APP	OEI	SHS	10	fail	fail	TRUE
45	SAS 2	Front	TO	AEO	Training				
46	SAS 2	Front	TO	AEO	DR		pass	pass	TRUE
47	SAS 2	Front	TO	OEI	SHS	2	pass	pass	TRUE
48	SAS 2	Front	TO	OEI	TTB	5	fail	pass	FALSE

49	SAS 2	Front	CR	AEO	Training				
50	SAS 2	Front	CR	AEO	DR		pass	pass	TRUE
51	SAS 2	Front	CR	OEI	SHS	2	pass	pass	TRUE
52	SAS 2	Front	CR	AEO	TTB	5	pass	pass	TRUE
53	SAS 2	Aft	CR	AEO	DR		pass	pass	TRUE
54	SAS 2	Aft	CR	OEI	CTC		pass	pass	TRUE
55	SAS 2	Aft	CR	AEO	TTB		pass	pass	TRUE
56	SAS 2	Aft	CR	AEO	OEI		pass	pass	TRUE
57	SAS 2	Aft	CR	AEO	SHS		pass	pass	TRUE
Run	Configuration	CG location	Condition	Engine	Manoeuvre	CH	Hyp	Outcome	Match
58	SAS 2 ext.	Front	CR	AEO	Training				
59	SAS 2 ext.	Front	CR	AEO	DR		pass	pass	TRUE
60	SAS 2 ext.	Front	CR	OEI	SHS		pass	pass	TRUE
61	SAS 2 ext.	Aft	CR	AEO	DR		pass	pass	TRUE
62	SAS 2 ext.	Aft	CR	OEI	CTC		pass	pass	TRUE
63	SAS 2 ext.	Aft	CR	AEO	TTB		pass	pass	TRUE
64	SAS 2 ext.	Aft	CR	AEO	OEI		pass	pass	TRUE
65	SAS 2 ext.	Aft	CR	AEO	SHS		pass	pass	TRUE

Experiment Matrix Pilot 3

Run	Configuration	CG location	Condition	Engine	Manoeuvre	Hyp	Outcome	Match
1	SAS 2 ext.	Front	APP	AEO	Training			
2	SAS 2 ext.	Front	APP	AEO	DR	pass	pass	TRUE
3	SAS 2 ext.	Front	APP	AEO	CTC	pass	fail	FALSE
4	SAS 2 ext.	Front	APP	AEO	TTB	pass	pass	TRUE
5	SAS 2 ext.	Front	APP	AEO	OEI	pass	pass	TRUE
6	SAS 2 ext.	Front	APP	OEI	SHS	pass	pass	TRUE
7	SAS 2 ext.	Front	TO	AEO	Training			
8	SAS 2 ext.	Front	TO	AEO	DR	pass	pass	TRUE
9	SAS 2 ext.	Front	TO	OEI	SHS	pass	pass	TRUE
Run	Configuration	CG location	Condition	Engine	Manoeuvre	Hyp	Outcome	Match
10	SAS 2	Front	APP	AEO	Training			
11	SAS 2	Front	APP	AEO	DR	pass	pass	TRUE
12	SAS 2	Front	APP	AEO	CTC	fail	fail	TRUE
13	SAS 2	Front	APP	AEO	TTB	fail	pass	FALSE
14	SAS 2	Front	APP	AEO	OEI	fail	pass	FALSE
15	SAS 2	Front	APP	OEI	SHS	fail	fail	TRUE
16	SAS 2	Front	TO	AEO	Training			
17	SAS 2	Front	TO	AEO	DR	pass	pass	TRUE
18	SAS 2	Front	TO	OEI	SHS	pass	pass	TRUE
19	SAS 2	Front	CR	AEO	Training			
20	SAS 2	Front	CR	AEO	DR	pass	pass	TRUE
21	SAS 2	Front	CR	OEI	SHS	pass	pass	TRUE
22	SAS 2	Aft	CR	AEO	DR	pass	pass	TRUE
23	SAS 2	Aft	CR	OEI	CTC	pass	pass	TRUE
24	SAS 2	Aft	CR	AEO	TTB	pass	pass	TRUE
25	SAS 2	Aft	CR	AEO	OEI	pass	pass	TRUE
26	SAS 2	Aft	CR	AEO	SHS	pass	pass	TRUE
Run	Configuration	CG location	Condition	Engine	Manoeuvre	Hyp	Outcome	Match
27	Bare A/C	Front	APP	AEO	Training			
28	Bare A/C	Front	APP	AEO	DR	fail	fail	TRUE
29	Bare A/C	Front	APP	AEO	CTC	fail	fail	TRUE
30	Bare A/C	Front	APP	AEO	TTB	fail	fail	TRUE
31	Bare A/C	Front	APP	AEO	OEI	fail	fail	TRUE
32	Bare A/C	Front	APP	OEI	SHS	fail	fail	TRUE
33	Bare A/C	Front	TO	AEO	Training			
34	Bare A/C	Front	TO	AEO	DR	fail	fail	TRUE
35	Bare A/C	Front	TO	OEI	SHS	fail	fail	TRUE
36	Bare A/C	Front	CR	AEO	Training			
37	Bare A/C	Front	CR	AEO	DR	fail	fail	TRUE
38	Bare A/C	Front	CR	OEI	SHS	pass		
39	Bare A/C	Aft	CR	AEO	DR	fail	fail	TRUE
40	Bare A/C	Aft	CR	OEI	CTC	pass	fail	FALSE
41	Bare A/C	Aft	CR	AEO	TTB	pass	fail	FALSE
42	Bare A/C	Aft	CR	AEO	OEI	pass	pass	TRUE
43	Bare A/C	Aft	CR	AEO	SHS	pass	fail	FALSE

Experiment Matrix Pilot 4

Run	Configuration	CG location	Condition	Engine	Manoeuvre	Hyp	Outcome	Match
1	SAS 2	Front	APP	AEO	Training			
2	SAS 2	Front	APP	AEO	DR	pass	pass	TRUE
3	SAS 2	Front	APP	AEO	CTC	fail	fail	TRUE
4	SAS 2	Front	APP	AEO	TTB	fail	fail	TRUE
5	SAS 2	Front	APP	AEO	OEI	fail	pass	FALSE
6	SAS 2	Front	APP	OEI	SHS	fail	fail	TRUE
7	SAS 2	Front	TO	AEO	Training			
8	SAS 2	Front	TO	AEO	DR	pass	pass	TRUE
9	SAS 2	Front	TO	OEI	SHS	pass	pass	TRUE
10	SAS 2	Front	CR	AEO	Training			
11	SAS 2	Front	CR	AEO	DR	pass	pass	TRUE
12	SAS 2	Front	CR	OEI	SHS	pass	pass	TRUE
13	SAS 2	Aft	CR	AEO	DR	pass	pass	TRUE
14	SAS 2	Aft	CR	OEI	CTC	pass	pass	TRUE
15	SAS 2	Aft	CR	AEO	TTB	pass	pass	TRUE
16	SAS 2	Aft	CR	AEO	OEI	pass	pass	TRUE
17	SAS 2	Aft	CR	AEO	SHS	pass	pass	TRUE
Run	Configuration	CG location	Condition	Engine	Manoeuvre	Hyp	Outcome	Match
18	Bare A/C	Front	APP	AEO	Training			
19	Bare A/C	Front	APP	AEO	DR	fail	fail	TRUE
20	Bare A/C	Front	APP	AEO	CTC	fail	fail	TRUE
21	Bare A/C	Front	APP	AEO	TTB	fail	fail	TRUE
22	Bare A/C	Front	APP	AEO	OEI	fail	fail	TRUE
23	Bare A/C	Front	APP	OEI	SHS	fail	fail	TRUE
24	Bare A/C	Front	TO	AEO	Training			
25	Bare A/C	Front	TO	AEO	DR	fail	fail	TRUE
26	Bare A/C	Front	TO	OEI	SHS	fail	fail	TRUE
27	Bare A/C	Front	CR	AEO	Training			
28	Bare A/C	Front	CR	AEO	DR	fail	fail	TRUE
29	Bare A/C	Front	CR	OEI	SHS	pass	pass	TRUE
30	Bare A/C	Aft	CR	AEO	DR	fail	fail	TRUE
31	Bare A/C	Aft	CR	OEI	CTC	pass	fail	FALSE
32	Bare A/C	Aft	CR	AEO	TTB	pass	pass	TRUE
33	Bare A/C	Aft	CR	AEO	OEI	pass	pass	TRUE
34	Bare A/C	Aft	CR	AEO	SHS	pass	pass	TRUE
Run	Configuration	CG location	Condition	Engine	Manoeuvre	Hyp	Outcome	Match
35	SAS 2 ext.	Front	APP	AEO	Training			
36	SAS 2 ext.	Front	APP	AEO	DR	pass	pass	TRUE
37	SAS 2 ext.	Front	APP	AEO	CTC	pass	pass	TRUE
38	SAS 2 ext.	Front	APP	AEO	TTB	pass	pass	TRUE
39	SAS 2 ext.	Front	APP	AEO	OEI	pass	pass	TRUE
40	SAS 2 ext.	Front	APP	OEI	SHS	pass	pass	TRUE
41	SAS 2 ext.	Front	TO	AEO	Training			TRUE
42	SAS 2 ext.	Front	TO	AEO	DR	pass	pass	TRUE
43	SAS 2 ext.	Front	TO	OEI	SHS	pass	pass	TRUE

III. Dutch Roll Mode Participation Factor - Pilot Compensation of Dutch Roll

The following figures show the pilot inputs, aircraft attitudes, angle of attack and sideslip angle, and Dutch Roll Mode Participation Factor of two Dutch Roll manoeuvres in the piloted experiment. Figures 1(a) to (d) show an experiment run in which the pilot failed to (with the rudder pedals) compensate the Dutch Roll after exciting it, illustrating the pilot comment of counter-intuitive rudder use and difficult to compensate Dutch Roll. Second, Figures 2(a) to (d) show an experiment run in which the pilot successfully decreases the Dutch Roll eigenmode dominance after exciting it, first with lateral sidestick deflection and second with the rudder pedals, illustrating the pilot comment of a controllable Dutch Roll eigenmode.

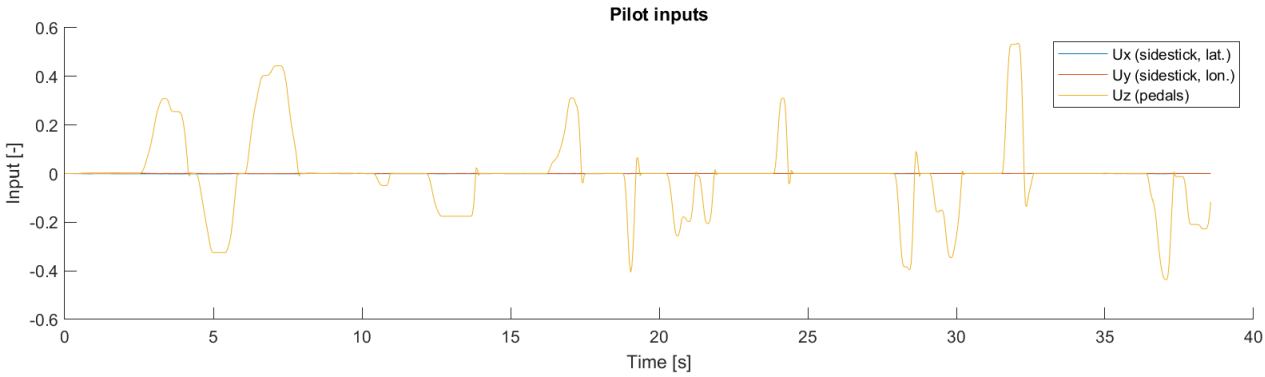

(a) Pilot inputs

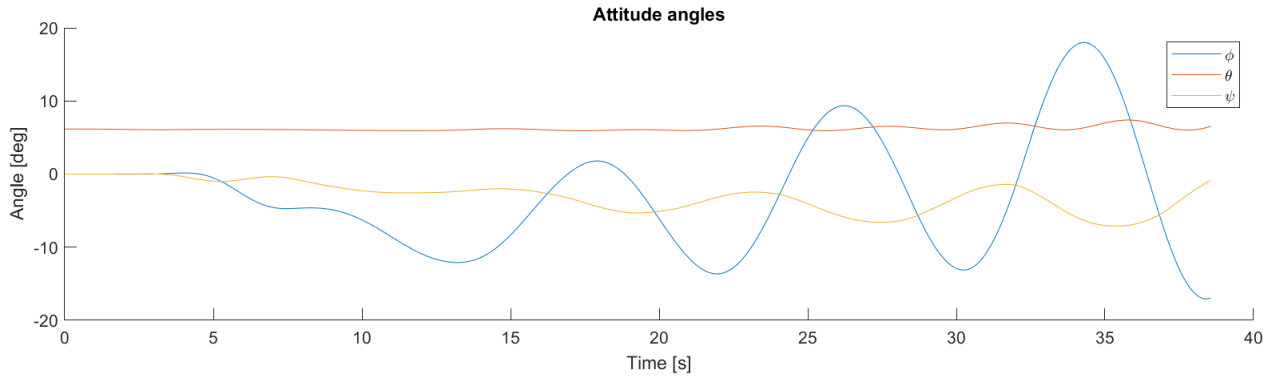

(b) Attitude angles

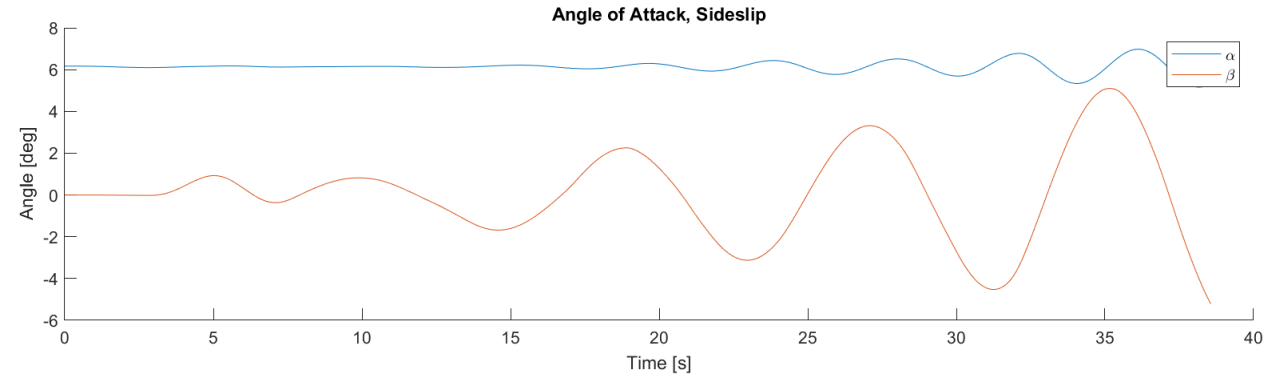

(c) Angle of Attack and Sideslip

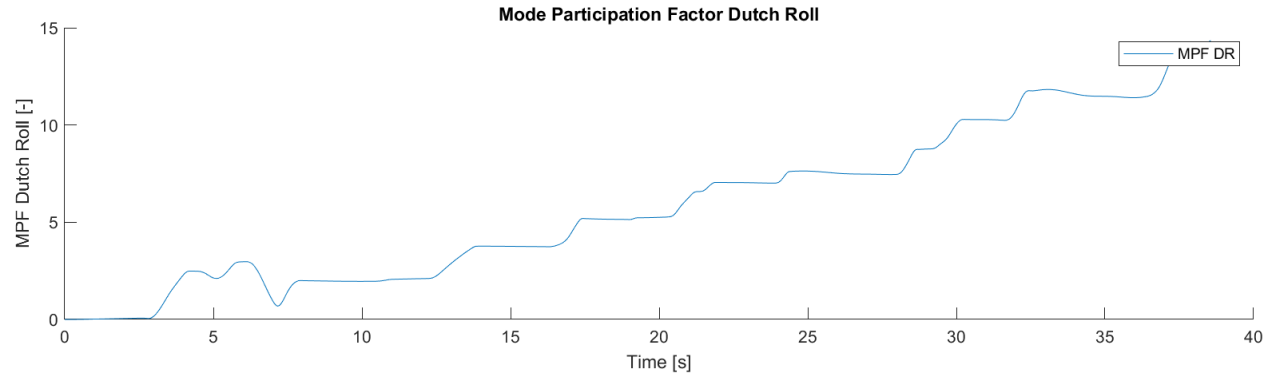

(d) Mode participation Factor Dutch Roll

Figure 1. Pilot input, Aircraft attitude, angle of attack, sideslip and Mode Participation Factor Dutch Roll for Dutch Roll manoeuvre (Pilot 3, Bare-Airframe, Aft CG, Cruise flight conditions, AEO, Dutch Roll, Try 2).

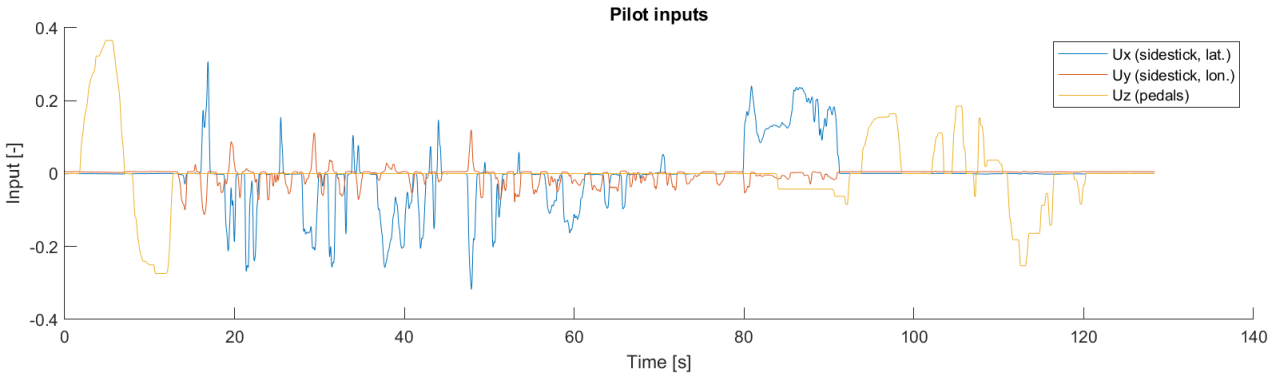

(a) Pilot inputs

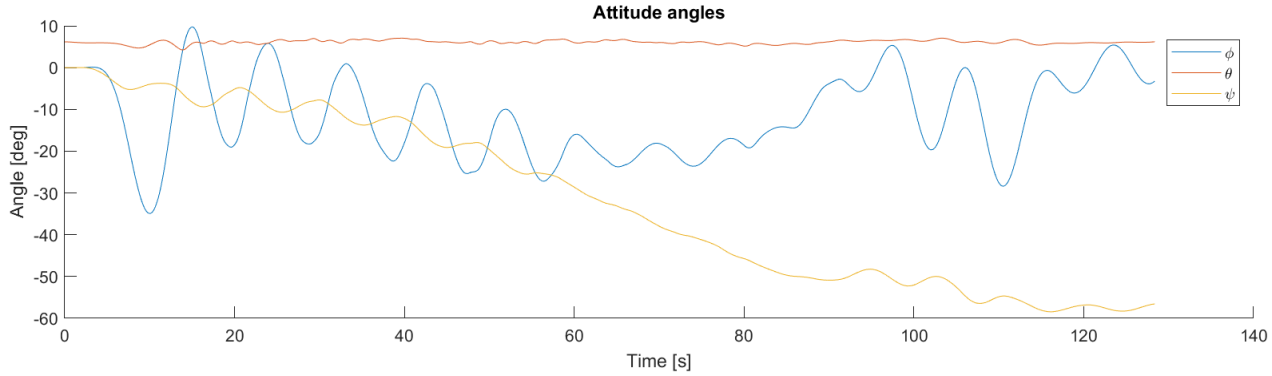

(b) Attitude angles

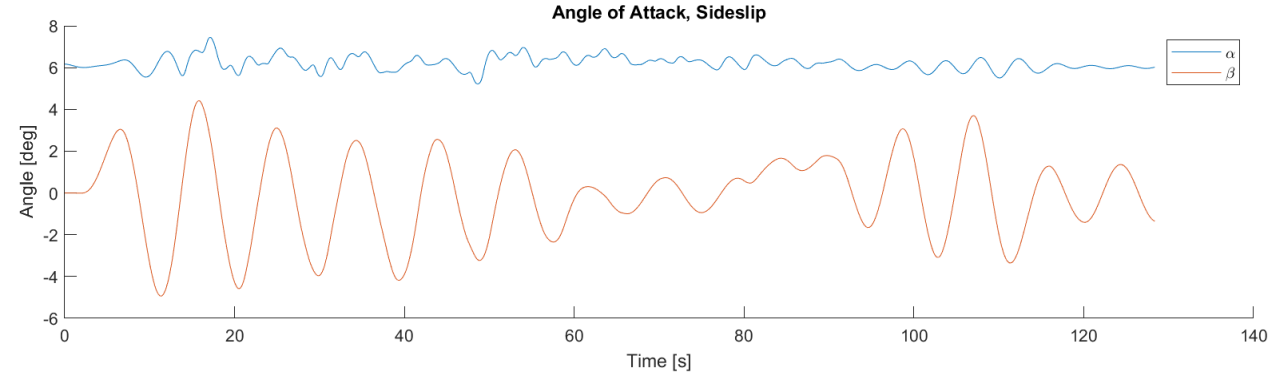

(c) Angle of Attack and Sideslip

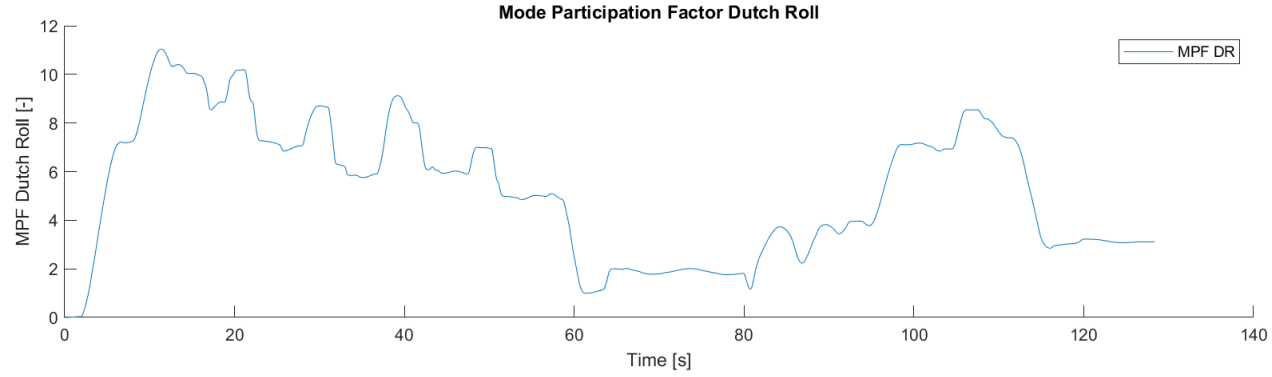

(d) Mode participation Factor Dutch Roll

Figure 2. Pilot input, aircraft attitude, angle of attack, sideslip and Mode Participation Factor Dutch Roll for Dutch Roll manoeuvre (Pilot 1, Bare-Airframe, Aft CG, Cruise flight conditions, AEO, Dutch Roll, Try 1).

IV. Dutch Roll Mode Participation Factor - Dutch Roll Interference with other Manoeuvres

The following figures show the pilot inputs, aircraft attitudes, angle of attack and sideslip angle, and Dutch Roll Mode Participation Factor of two Coordinated Turn Capability manoeuvres in the piloted experiment. First, Figures 3(a) to (d) show an experiment run in which the target state was not maintained for 10 seconds due to increasing sideslip, attitude oscillation, and Dutch Roll eigenmode dominance, illustrating the interference of the Dutch Roll eigenmode in other manoeuvres. An increase in Mode Participation Factor of the Dutch Roll is seen while within the target state, eventually yielding the aircraft attitude to move out of the target margins. Second, Figures 4(a) to (d) show an equivalent experiment run, in which the target state was only maintained for 10 seconds when the Dutch Roll Mode Participation Factor was kept at a lower magnitude than earlier in the run. This also illustrates the Dutch Roll eigenmode interference in this manoeuvre, and the need to counteract the Dutch Roll before the manoeuvre was passed.

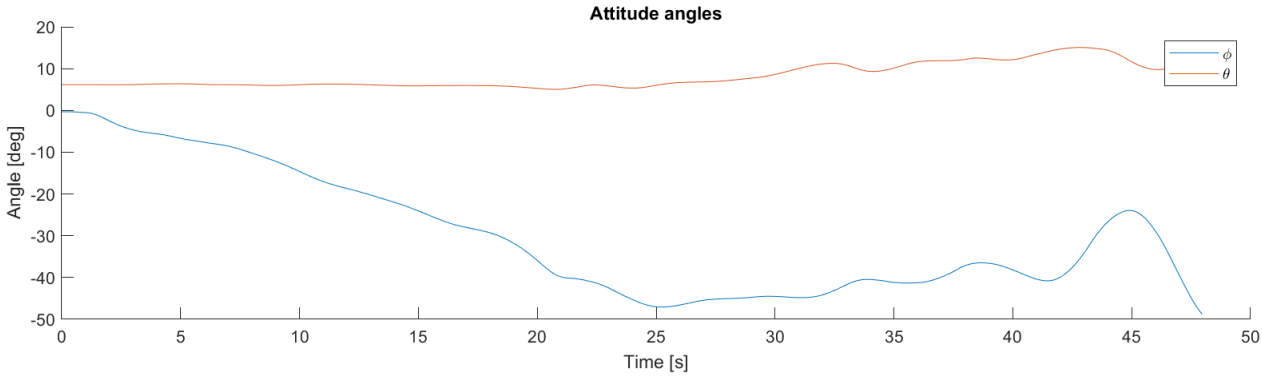

(a) Attitude angles

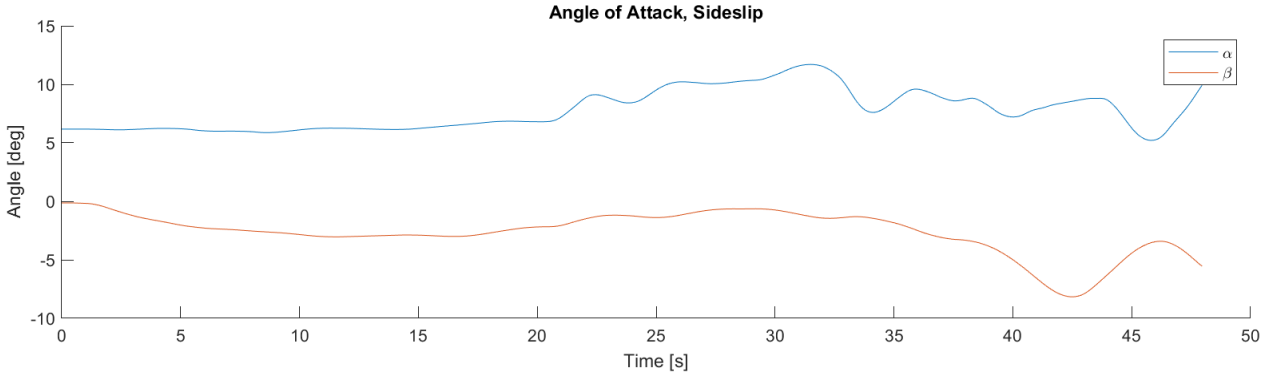

(b) Angle of Attack and Sideslip

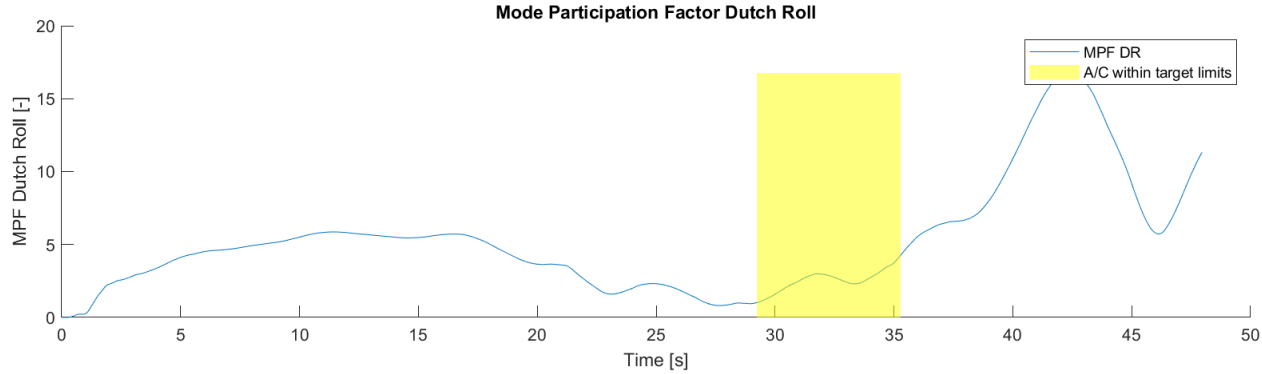

(c) Mode participation Factor Dutch Roll

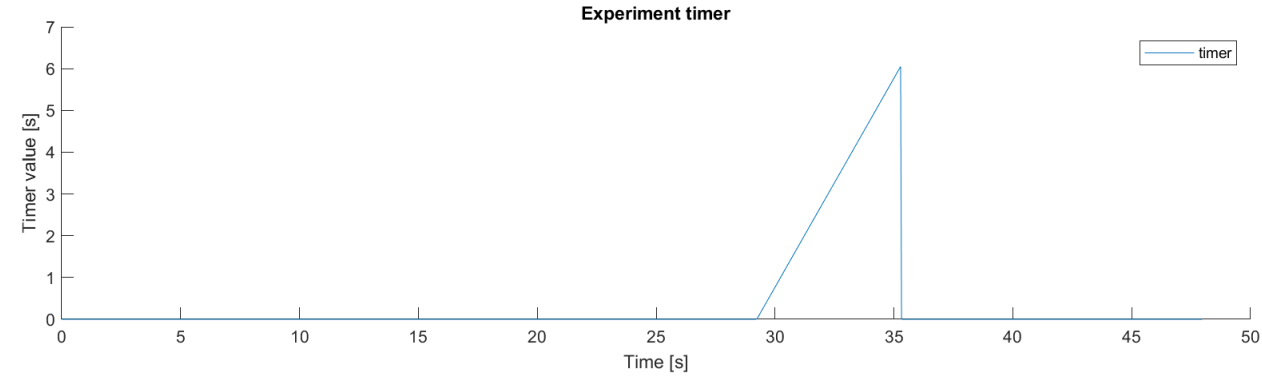

(d) Experiment Timer

Figure 3. Aircraft attitude, angle of attack, sideslip, Mode Participation Factor Dutch Roll and experiment timer for Coordinated Turn Capability manoeuvre (Pilot 3, Bare-Airframe, Aft CG, Cruise flight conditions, OEI, Coordinated Turn Capability, Try 1).

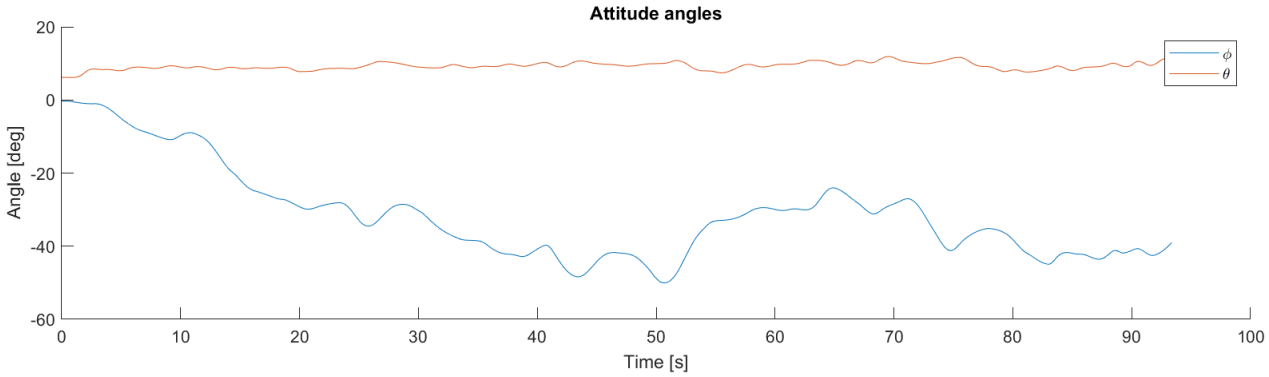

(a) Attitude angles

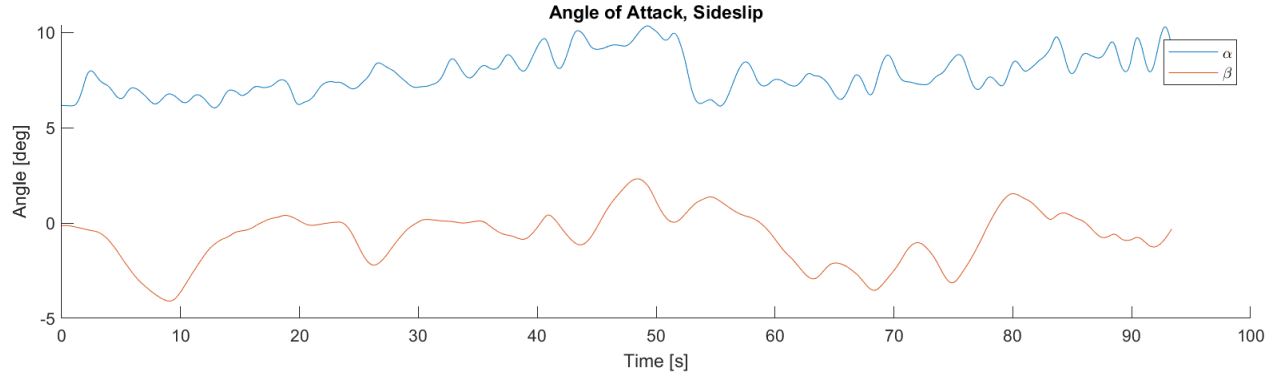

(b) Angle of Attack and Sideslip

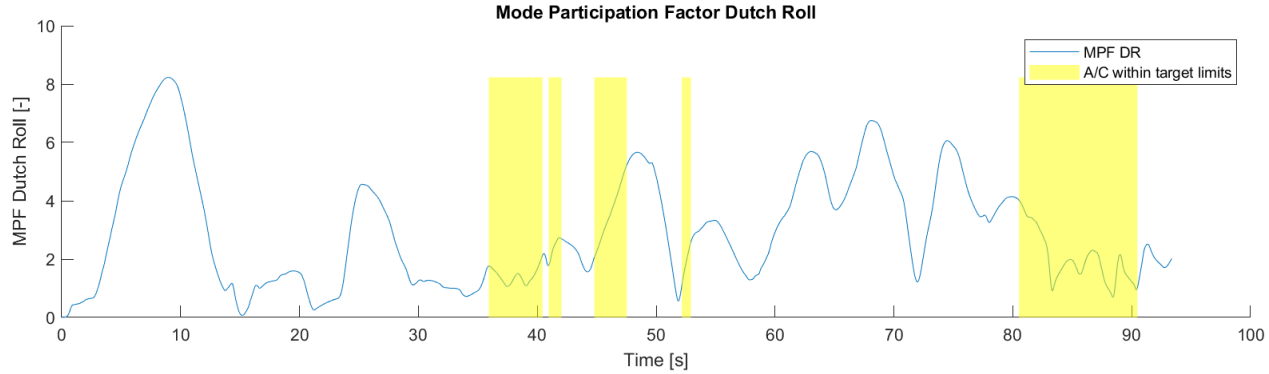

(c) Mode participation Factor Dutch Roll

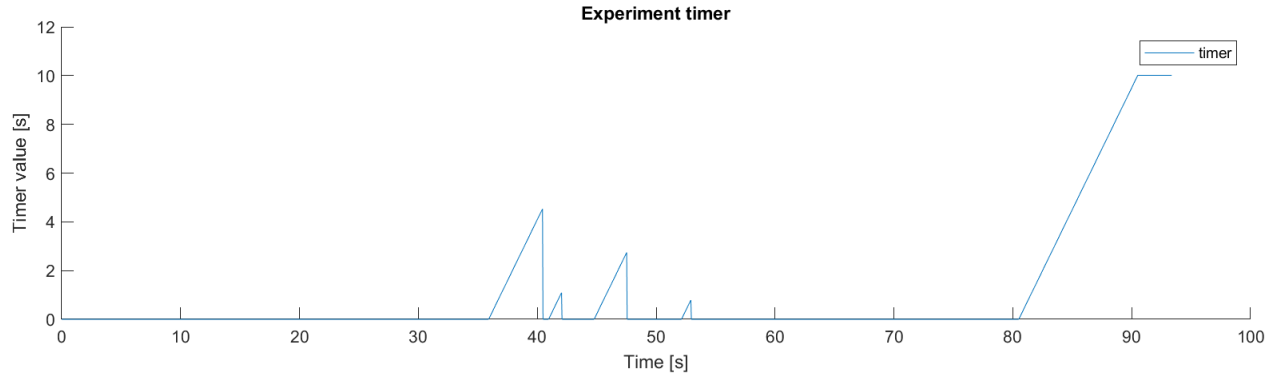

(d) Experiment Timer

Figure 4. Aircraft attitude, angle of attack, sideslip, Mode Participation Factor Dutch Roll and experiment timer for Coordinated Turn Capability manoeuvre (Pilot 1, Bare-Airframe, Aft CG, Cruise flight conditions, OEI, Coordinated Turn Capability, Try 2).

V. Adverse Axis-Coupling with SAS-2 at Control Surface Saturation

To illustrate the adverse axis-coupling, which occurred during control surface saturation with SAS-2, two experiment runs are used as example. First, Figures 5(a) to (d) show a Time to Bank manoeuvre, with at the end of the run a large nose-down attitude change. This attitude change occurred due to the demanded roll-rate by the pilot, which by means of the control allocation cannibalizes the available pitch control authority. This can be seen in the control surface deflection plots, where during the roll manoeuvre from around, 35 seconds, C2 and C3 were saturated and C4 and C5 deflected opposite to provide the rolling moment. Due to C2 and C3 not being able to sufficiently compensate the now opposing pitching moment of C4 and C5, a nose-down attitude change occurred. Second, Figures 6(a) to (d) show a Steady Heading Sideslip manoeuvre, with two nose-down attitude changes within the experiment run between 10 and 50 seconds. Here, the demanded sideslip angle by means of the rudder pedals yields a rudder- and sideslip-induced rolling moment, which is compensated by means of a roll-channel input of the stability augmentation system. This yields control surfaces C4 and C5 to generate this rolling moment, while generating less pitching moment. Since control surfaces C2 and C3 are saturated, the decrease in pitching moment can not be compensated and the nose-down attitude changes occurred.

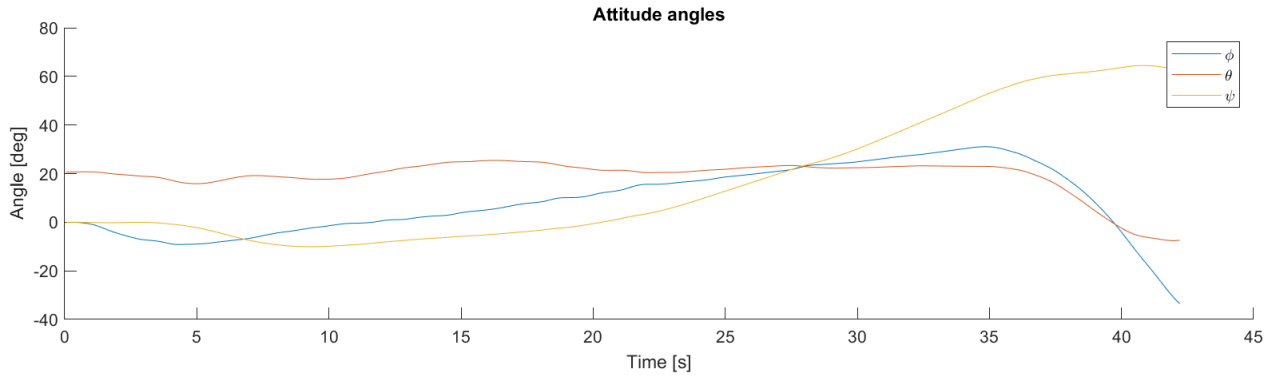

(a) Attitude angles

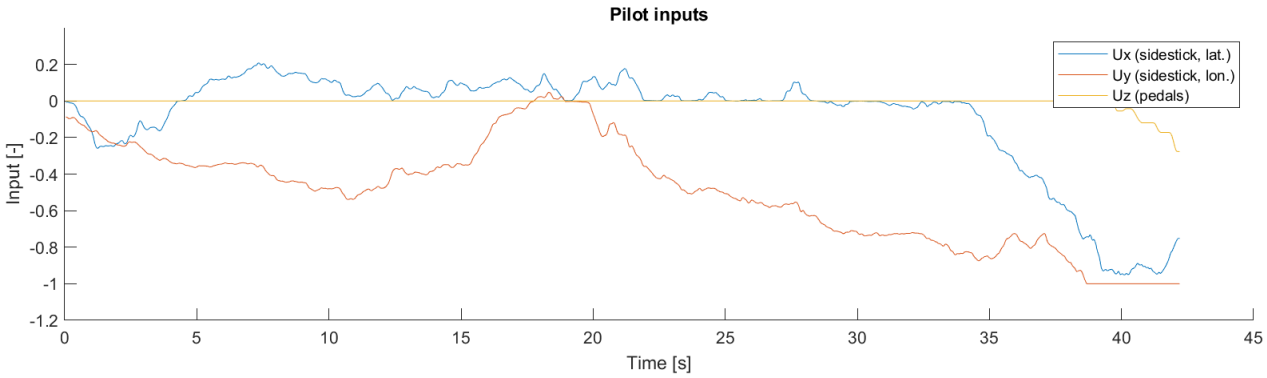

(b) Pilot inputs

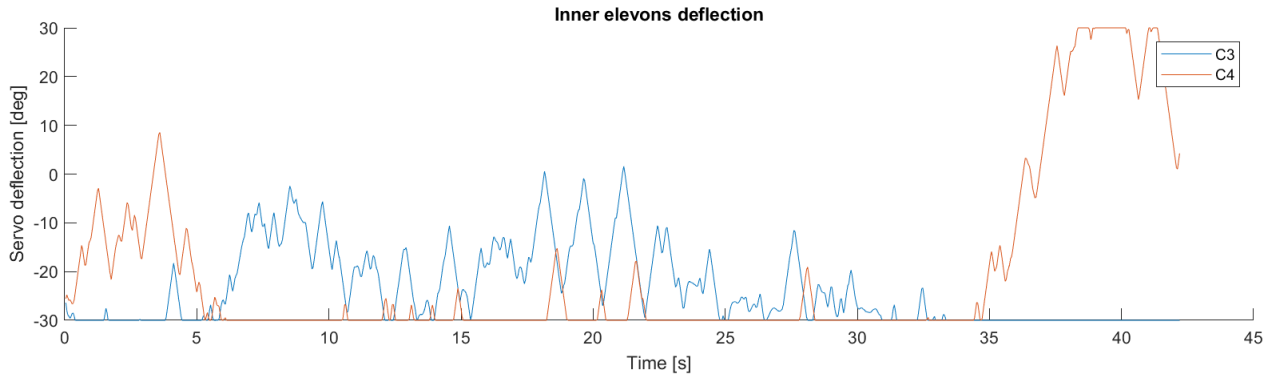

(c) Inner elevon control surface deflections

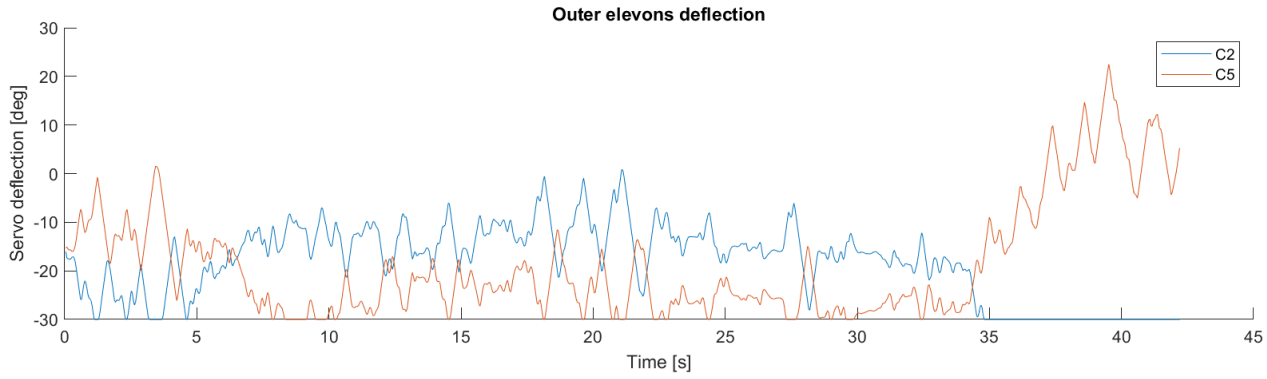

(d) Outer elevon control surface deflections

Figure 5. Aircraft attitude, pilot inputs, inner elevon control surface deflections, outer elevon control surface deflections in a Time to Bank manoeuvre (Pilot 3, SAS-2, Forward CG, Approach flight conditions, AEO, Time to Bank, Try 2).

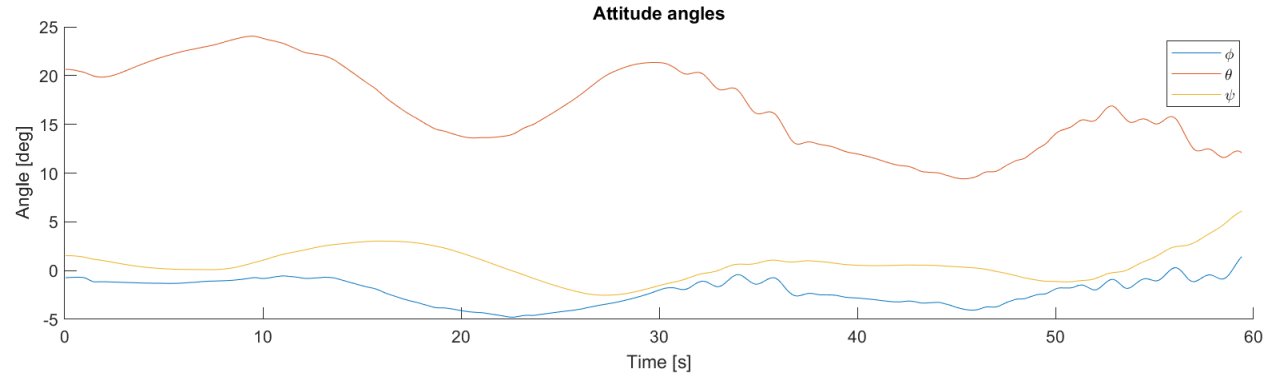

(a) Attitude angles

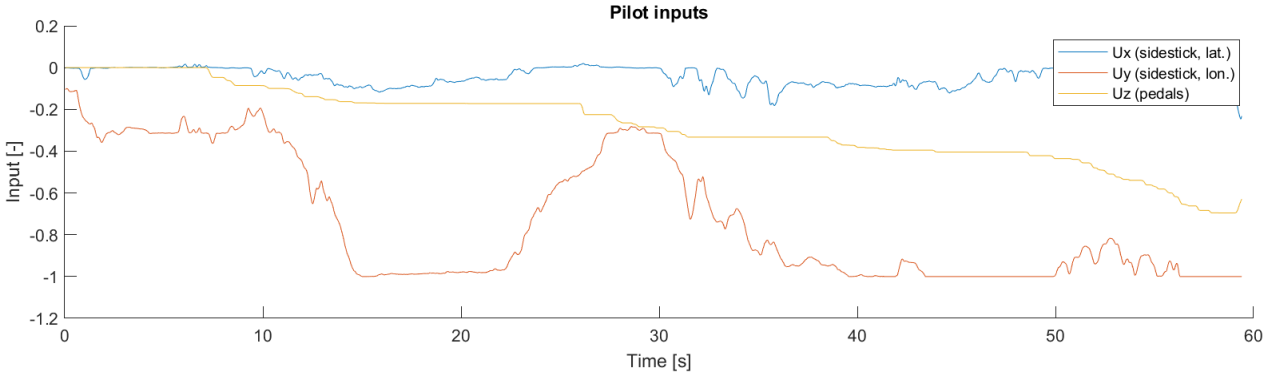

(b) Pilot inputs

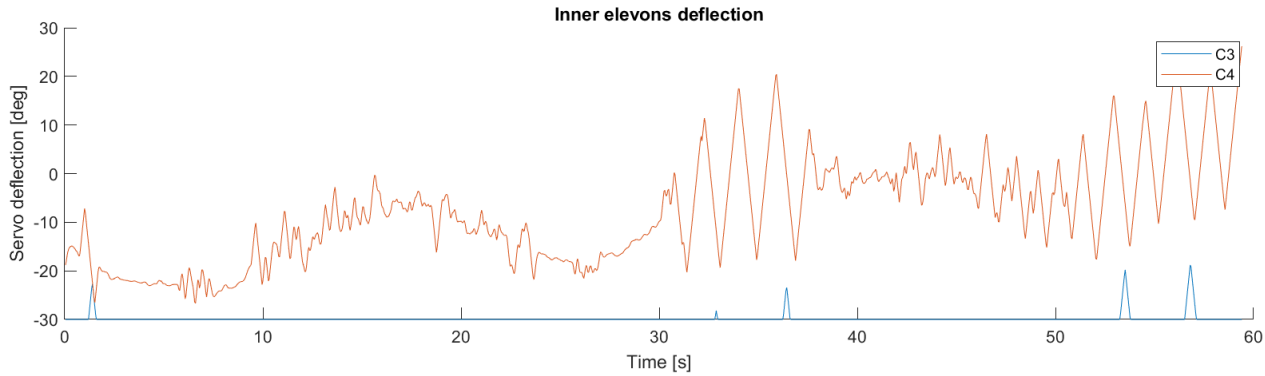

(c) Inner elevon control surface deflections

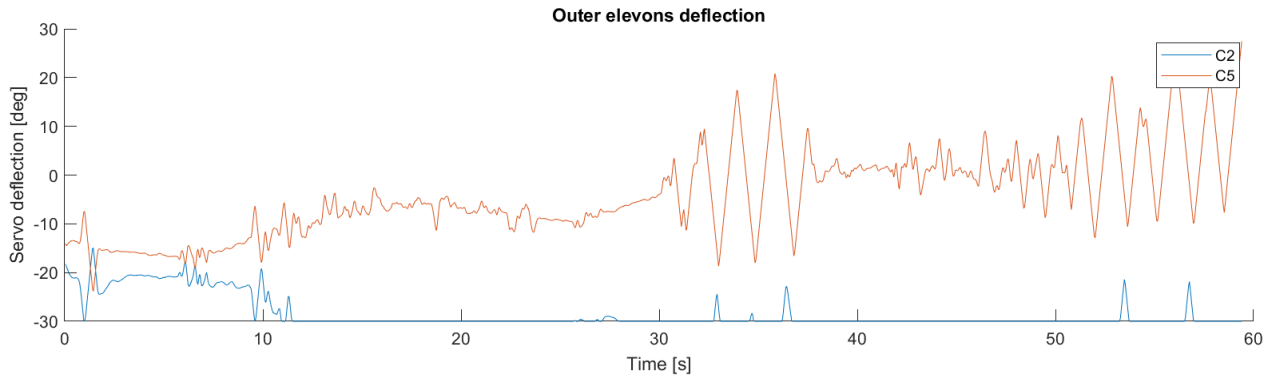

(d) Outer elevon control surface deflections

Figure 6. Aircraft attitude, pilot inputs, inner elevon control surface deflections, outer elevon control surface deflections in a Steady Heading Sideslip manoeuvre (Pilot 2, SAS-2, Forward CG, Approach flight conditions, OEI, Steady Heading Sideslip, Try 1).

VI. Pilot Induced Oscillations with SAS-2 in Time to Bank Manoeuvre

To illustrate the PIO tendency with SAS-2 while stopping the roll motion of the Time to Bank manoeuvre, two experiment runs are used as example. First, Figures 7(a) to (e) show a Time to Bank manoeuvre, with the (pilot induced) roll oscillation at the end of the manoeuvre (starting at 19 seconds). The oscillation in pilot input and roll output occurred while all control surfaces were at their deflection-rate limits, indicating a Category 2 Pilot Induced Oscillation. Second, 8(a) to (e) show a Time to Bank manoeuvre, with the (pilot induced) roll oscillation again at the end of the manoeuvre (starting at 26 seconds). Again, the oscillation in pilot input and roll output occurred while all control surfaces were at their deflection-rate limits, indicating a Category 2 Pilot Induced Oscillation.

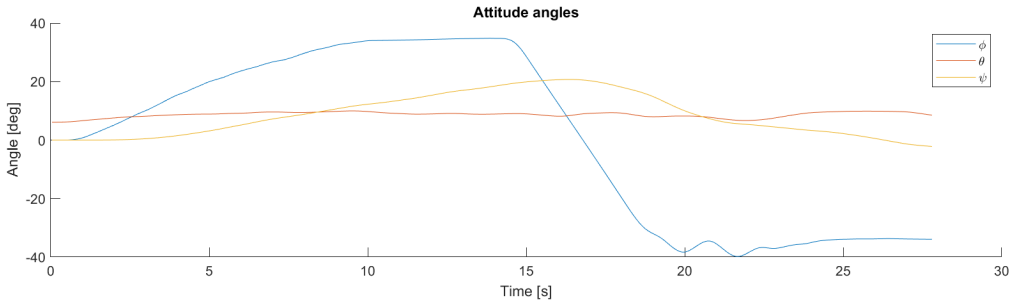

(a) Attitude angles

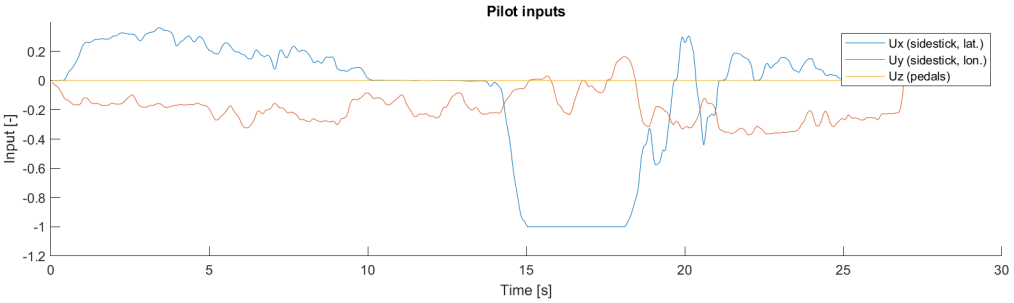

(b) Pilot inputs

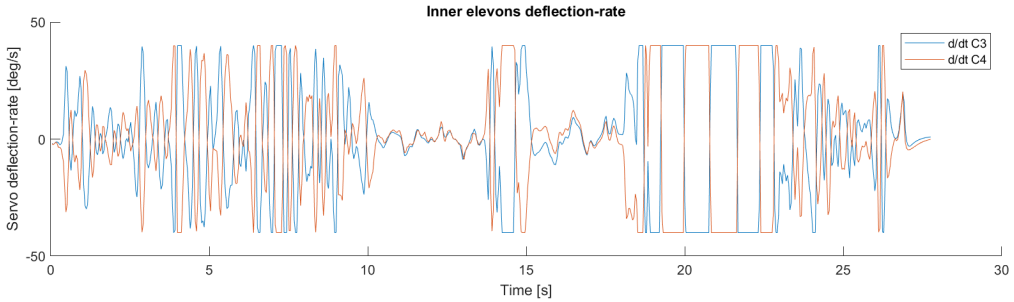

(c) Inner elevon control surface deflection-rates

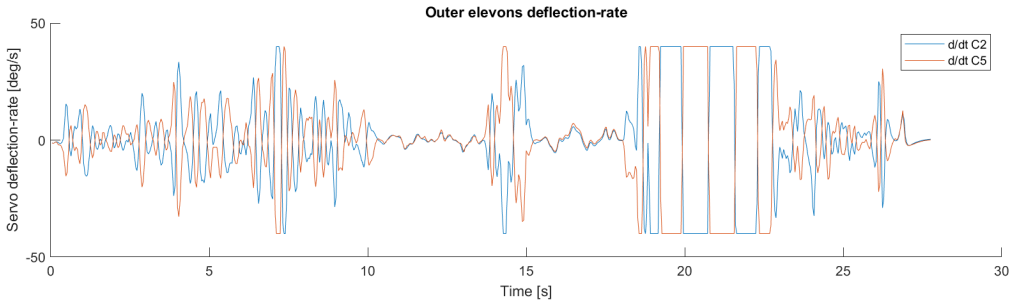

(d) Outer elevon control surface deflection-rates

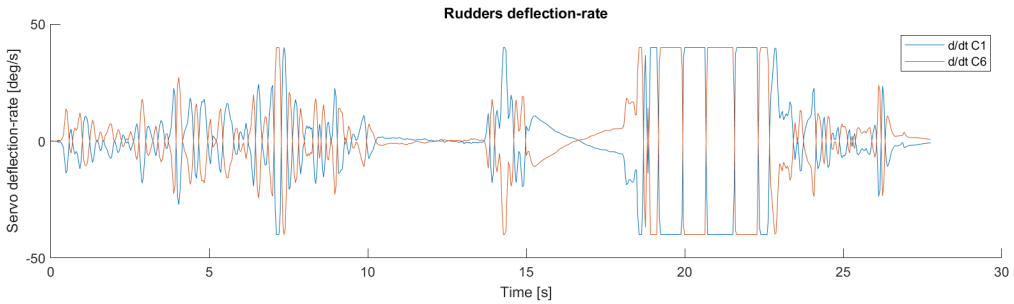

(e) Rudder control surface deflection-rates

Figure 7. Aircraft Attitude, pilot inputs, and control surface deflection-rates in a Time to Bank manoeuvre (Pilot 1, SAS-2, Aft CG, Cruise flight conditions, AEO, Time to Bank, Try 1).

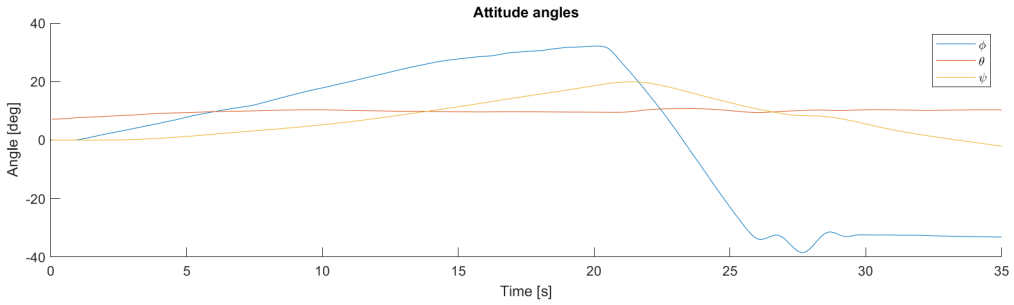

(a) Attitude angles

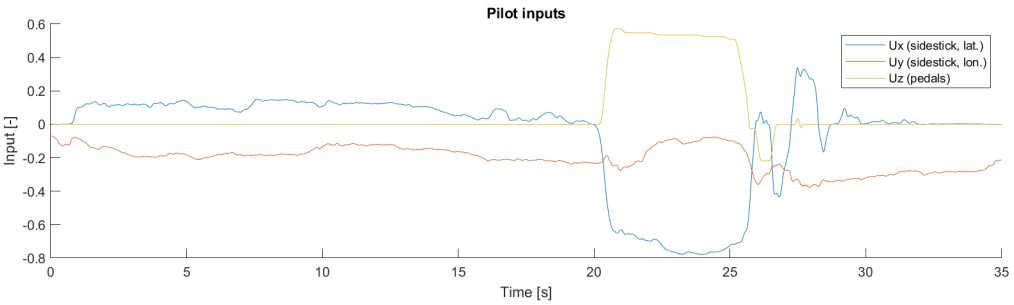

(b) Pilot inputs

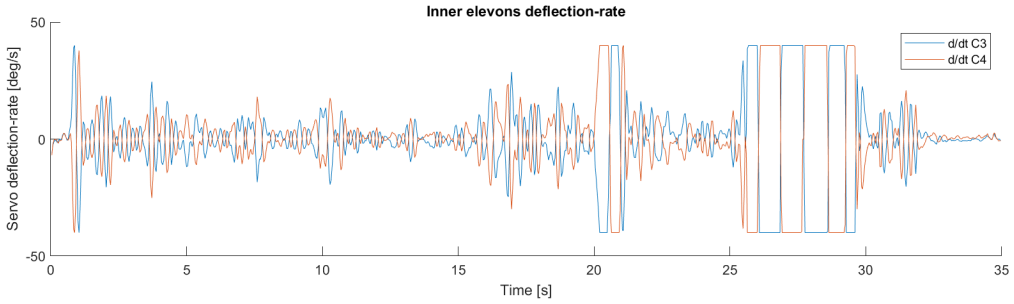

(c) Inner elevon control surface deflection-rates

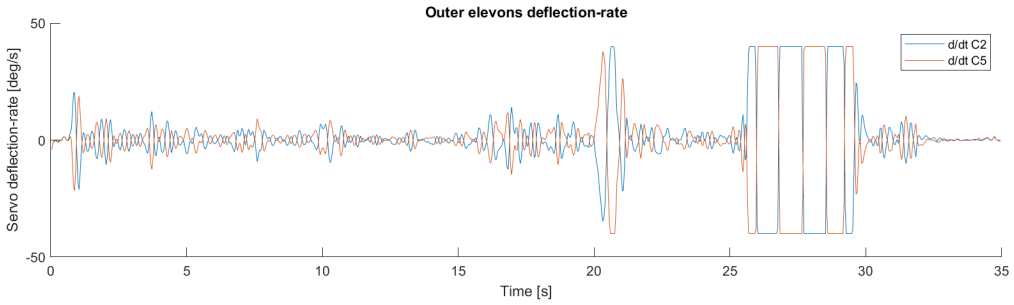

(d) Outer elevon control surface deflection-rates

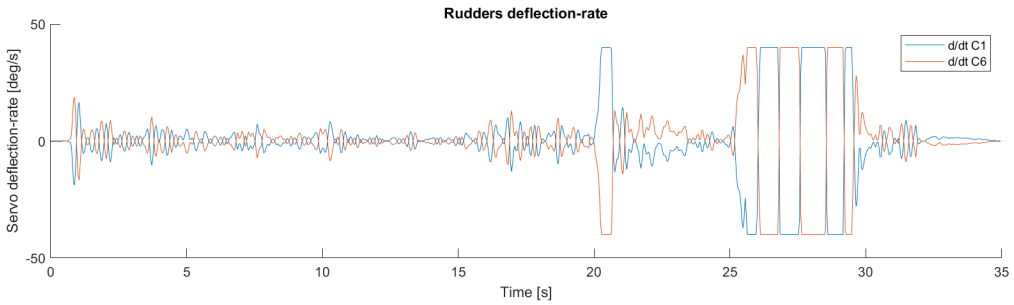

(e) Rudder control surface deflection-rates

Figure 8. Aircraft attitude, pilot inputs, and control surface deflection-rates in a Time to Bank manoeuvre (Pilot 2, SAS-2, Forward CG, Cruise flight conditions, AEO, Time to Bank, Try 1).

VII. Pilot Comments, Keyword Trend Analysis

For the assessment of trends in pilot comments, keywords were assigned to each comment. These keywords next were used to find trends within the pilot comments, distinct per flight condition, flight control system, manoeuvre or a combination of these. The following tables were used to find these trends. First, Table 1 shows the keyword occurrence summed per flight condition. Second, Table 2 shows the keyword occurrence summed per flight control system. Third, Table 3 shows the keyword occurrence summed per manoeuvre tested. Finally, Table 4 shows the keyword occurrence per pilot to assess pilot bias.

Table 1. Pilot comment keywords, summed by flight conditions.

Keyword	Conditions		
total runs tested	*80*	*46*	*88*
	APP	TO	CR
Requires training	1	1	2
Difficult	7	3	5
Inadequate	4	1	3
DR interfering	4	1	6
Unstable DR	9	1	3
Pitch authority insufficient	40	2	1
Roll authority Insufficient	9	5	4
Lateral PIO	1	2	4
Pedal control sensitive	0	0	0
Rudder misuse	2	3	7
Large pedal input	0	2	6
Non-balanced cross controls	5	5	3
Adverse axis-coupling	12	1	2
Lack of turn coordination	1	2	0
Excessive SAS	2	0	1
Large sideslip in roll	3	2	3
Small OEI effect	3	0	6
Small thrust effect	3	0	5
Moderately controllable	2	4	5
Sufficient control	8	15	35
Predictable	1	1	5
Sufficient pitch authority	0	2	1
Sufficient roll authority	10	3	6
Sufficient lat-dir control	4	0	1
DR controllable	3	6	10
DR stable	8	10	12

Table 2. Pilot comment keywords, summed by flight control system.

Keyword	Flight Control System			
total runs tested	*68*	*24*	*72*	*50*
	Bare A/C	SAS 1	SAS 2	SAS 2 ext.
Requires training	1	1	1	1
Difficult	10	1	2	2
Inadequate	6	1	1	0
DR interfering	10	0	1	0
Unstable DR	12	1	0	0
Pitch authority insufficient	18	5	14	6
Roll authority Insufficient	14	3	1	0
Lateral PIO	2	0	4	1
Pedal control sensitive	0	0	0	0
Rudder misuse	12	0	0	0
Large pedal input	0	2	2	4
Non-balanced cross controls	7	3	3	0
Adverse axis-coupling	2	3	9	1
Lack of turn coordination	0	0	1	2
Excessive SAS	0	0	1	2
Large sideslip in roll	4	1	2	1
Small OEI effect	2	0	5	2
Small thrust effect	2	0	5	1
Moderately controllable	7	1	3	0
Sufficient control	5	8	23	22
Predictable	0	4	3	0
Sufficient pitch authority	3	0	0	0
Sufficient roll authority	1	2	11	5
Sufficient lat-dir control	1	0	4	0
DR controllable	17	1	1	0
DR stable	0	4	16	10

Table 3. Pilot comment keywords, summed by flight manoeuvre.

Keyword	Manoeuvre					
total runs tested	*50*	*22*	*32*	*21*	*49*	*40*
	DR	CTC	TTB	OEI	SHS	Training
Requires training	0	1	0	0	3	0
Difficult	4	1	1	0	5	4
Inadequate	3	1	0	1	2	1
DR interfering	1	3	2	0	3	2
Unstable DR	5	1	0	1	3	3
Pitch authority insufficient	2	12	12	6	4	7
Roll authority Insufficient	2	0	4	2	9	1
Lateral PIO	1	0	6	0	0	0
Pedal control sensitive	0	0	0	0	0	0
Rudder misuse	12	0	0	0	0	0
Large pedal input	0	0	2	0	6	0
Non-balanced cross controls	0	0	1	0	11	1
Adverse axis-coupling	3	1	5	2	4	0
Lack of turn coordination	0	1	0	0	0	2
Excessive SAS	0	0	0	2	1	0
Large sideslip in roll	0	1	4	0	0	3
Small OEI effect	0	0	0	9	0	0
Small thrust effect	0	4	1	1	0	2
Moderately controllable	0	1	3	2	3	2
Sufficient control	2	4	5	7	25	15
Predictable	1	0	0	0	6	0
Sufficient pitch authority	0	0	0	0	0	3
Sufficient roll authority	0	3	10	1	1	4
Sufficient lat-dir control	0	4	0	1	0	0
DR controllable	14	0	1	0	2	2
DR stable	30	0	0	0	0	0

Table 4. Pilot comment keywords, summed by pilot.

Keyword	Pilot			
total runs tested	*65*	*63*	*43*	*43*
	P1	P2	P3	P4
Requires training	1	2	0	1
Difficult	3	3	5	4
Inadequate	2	0	3	3
DR interfering	4	1	5	1
Unstable DR	3	1	6	3
Pitch authority insufficient	12	10	9	12
Roll authority Insufficient	5	5	2	6
Lateral PIO	0	3	0	4
Pedal control sensitive	0	0	0	0
Rudder misuse	3	3	3	3
Large pedal input	2	4	1	1
Non-balanced cross controls	3	8	1	1
Adverse axis-coupling	6	5	2	2
Lack of turn coordination	3	0	0	0
Excessive SAS	0	3	0	0
Large sideslip in roll	1	4	2	1
Small OEI effect	1	2	4	2
Small thrust effect	5	1	1	1
Moderately controllable	6	4	1	0
Sufficient control	22	17	7	12
Predictable	1	3	2	1
Sufficient pitch authority	0	1	0	2
Sufficient roll authority	4	7	1	7
Sufficient lat-dir control	1	4	0	0
DR controllable	3	6	3	7
DR stable	10	8	6	6

VIII. Extended Control Authority Augmentation, Control Surface Deflection Assessment.

The control surface deflections used during manoeuvres with the flight control system *SAS-2 Ext.* were used to approximate the control authority required for full requirement compliance. To show the between-pilot differences not available from the averaged results shown in the paper, the (absolute) maximum control surface deflections used by each pilot for the successful manoeuvres with SAS-2 ext are shown in this appendix. First, the maximum control surface deflections used for the Coordinated Turn Capability manoeuvre are shown in Table 5. Second, the maximum control surface deflections used for the Time to Bank manoeuvre are shown in Table 6. Third, the maximum control surface deflections used for the One Engine Inoperative Trim manoeuvre are shown in Table 7. Finally, the maximum control surface deflections used for the Steady Heading Sideslip manoeuvre are shown in Table 8. All maximum deflections occurred with the approach flight conditions, at the forward center of gravity.

Table 5. Maximum control surface deflections (absolute) used for successful Coordinated Turn Capability manoeuvres with *SAS-2 Ext.*.

Pilot	1	2	4	
FCS	SAS-2 Ext.	SAS-2 Ext.	SAS-2 Ext.	
CG	forward	forward	forward	
Condition	APP	APP	APP	
Engine	AEO	AEO	AEO	
Manoeuvre	CTC	CTC	CTC	
Try	2	1	1	*Average*
C1 max (*deg*)	67.8	28.3	36.7	*44.2*
C2 max (*deg*)	37.8	36.4	41.0	*38.4*
C3 max (*deg*)	75.8	65.0	62.5	*67.8*
C4 max (*deg*)	107.3	68.1	86.3	*87.2*
C5 max (*deg*)	59.6	45.6	57.0	*54.1*
C6 max (*deg*)	70.4	31.7	34.4	*45.5*
timer (*s*)	10.01	10.01	10.01	

Table 6. Maximum control surface deflections (absolute) used for successful Time to Bank manoeuvres with *SAS-2 Ext.*.

Pilot	1	2	3	4	
FCS	SAS-2 Ext.	SAS-2 Ext.	SAS-2 Ext.	SAS-2 Ext.	
CG	forward	forward	forward	forward	
Condition	APP	APP	APP	APP	
Engine	AEO	AEO	AEO	AEO	
Manoeuvre	TTB	TTB	TTB	TTB	
Try	1	1	4	2	*Average*
C1 max (*deg*)	148.7	152.5	95.5	90.6	*121.8*
C2 max (*deg*)	110.4	81.4	69.8	76.2	*84.5*
C3 max (*deg*)	150.0	128.4	122.7	122.4	*130.9*
C4 max (*deg*)	113.4	95.1	69.8	85.7	*91.0*
C5 max (*deg*)	71.9	46.9	38.0	48.4	*51.3*
C6 max (*deg*)	151.7	155.3	98.0	93.0	*124.5*
timer (*s*)	5.02	4.15	6.66	6.19	

Table 7. Maximum control surface deflections (absolute) used for successful One Engine Inoperative Trim manoeuvres with *SAS-2 Ext.*.

Pilot	1	2	3	4	
FCS	SAS-2 Ext.	SAS-2 Ext.	SAS-2 Ext.	SAS-2 Ext.	
CG	forward	forward	forward	forward	
Condition	APP	APP	APP	APP	
Engine	AEO	AEO	AEO	AEO	
Manoeuvre	OEI-T	OEI-T	OEI-T	OEI-T	
Try	2	2	2	1	*Average*
C1 max (*deg*)	33.8	38.3	18.9	13.8	*26.2*
C2 max (*deg*)	19.9	40.8	27.5	23.0	*27.8*
C3 max (*deg*)	43.9	70.5	53.1	44.3	*53.0*
C4 max (*deg*)	35.4	57.0	43.9	36.3	*43.2*
C5 max (*deg*)	25.3	36.0	34.3	21.6	*29.3*
C6 max (*deg*)	36.3	40.9	21.4	16.3	*28.7*
timer (*s*)	10.01	10.01	10.01	10.01	

Table 8. Maximum control surface deflections (absolute) used for successful Steady Heading Sideslip manoeuvres with *SAS-2 Ext.*.

Pilot	1	2	4	
FCS	SAS-2 Ext.	SAS-2 Ext.	SAS-2 Ext.	
CG	forward	forward	forward	
Condition	APP	APP	APP	
Engine	OEI	OEI	OEI	
Manoeuvre	SHS	SHS	SHS	
Try	2	1	2	*Average*
C1 max (*deg*)	89.5	90.6	75.1	*85.1*
C2 max (*deg*)	74.3	66.8	65.7	*68.9*
C3 max (*deg*)	98.9	91.0	101.6	*97.2*
C4 max (*deg*)	44.2	36.2	46.8	*42.4*
C5 max (*deg*)	40.3	33.2	32.8	*35.4*
C6 max (*deg*)	86.9	88.0	72.3	*82.4*
timer (*s*)	10.01	10.01	10.01	

IX. DUECA Simulation Verification

The correct implementation of the Flying-V aerodynamic model in the DUECA simulation for the piloted experiment was verified using the MATLAB analytical simulation. Test simulations with the bare-airframe and with SAS-2 implemented were flown, both in cruise flight conditions to assure a stable aircraft. The logged pilot input of the DUECA simulation next was used as input for the MATLAB simulation. Finally, different aircraft states were compared graphically to verify the match.

Figure 9(a) to (d) shows the test simulation with the bare-airframe, comparing the states of the DUECA and MATLAB simulation. The differences in aircraft states are assumed sufficiently small for positive verification. Moreover, the difference in integration method (Euler for the MATLAB simulation, Runge-Kutta for the DUECA simulation) is expected to cause the mismatch occurring.

Figure 10(a) to (d) shows the test simulation with SAS-2, comparing the states of the DUECA and MATLAB simulation. Again, the differences in aircraft states are assumed sufficiently small for positive verification, and the difference in integration method is expected to cause the mismatch occurring.

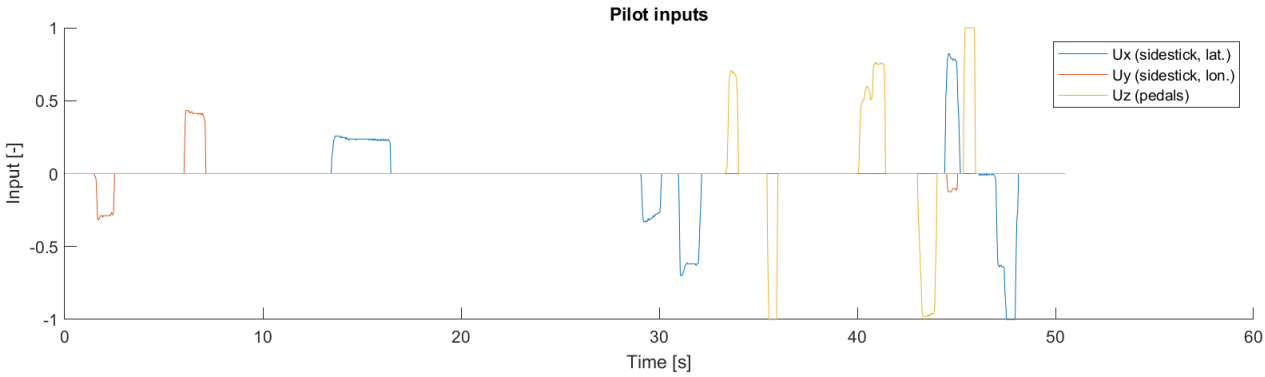

(a) Pilot Inputs

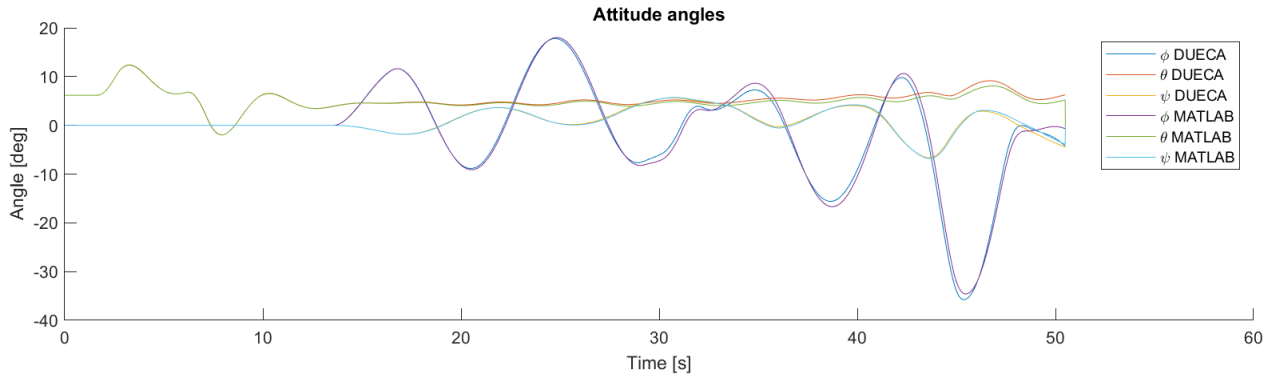

(b) Attitude angles

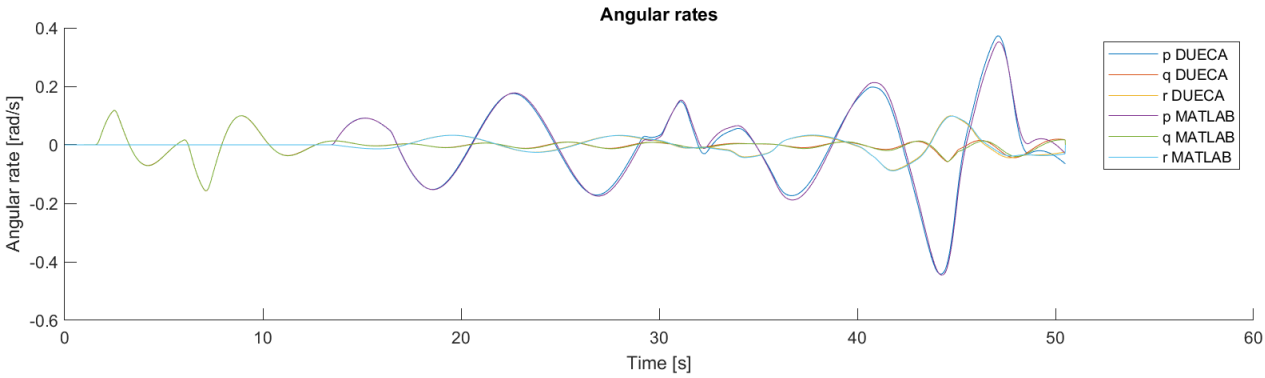

(c) Angular rates

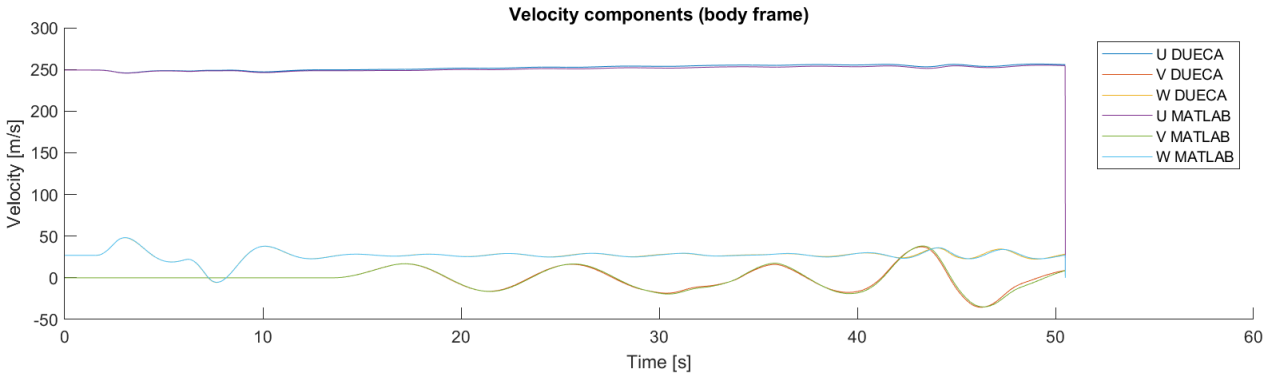

(d) Velocity components

Figure 9. Pilot inputs, aircraft attitude, angular rates, and velocity components in body frame, for a simulation test with Bare-Airframe in cruise flight conditions.

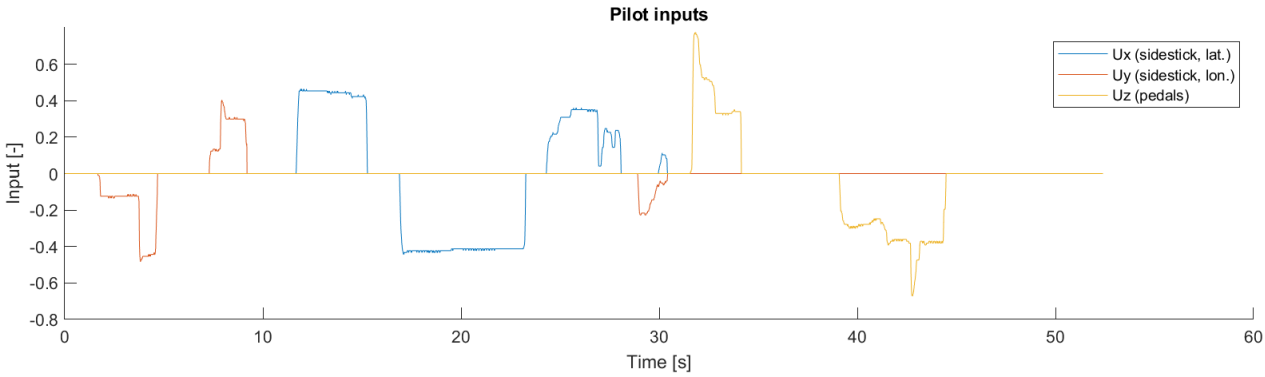

(a) Pilot Inputs

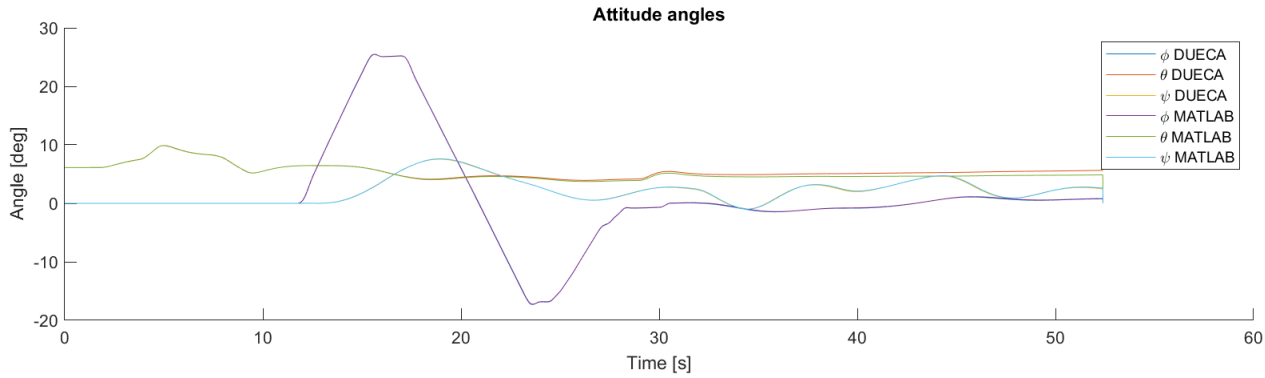

(b) Attitude angles

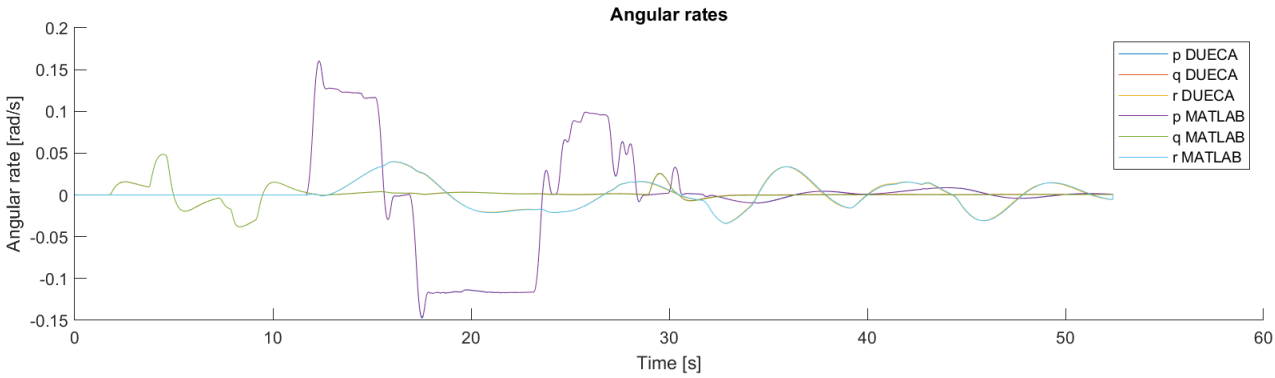

(c) Angular rates

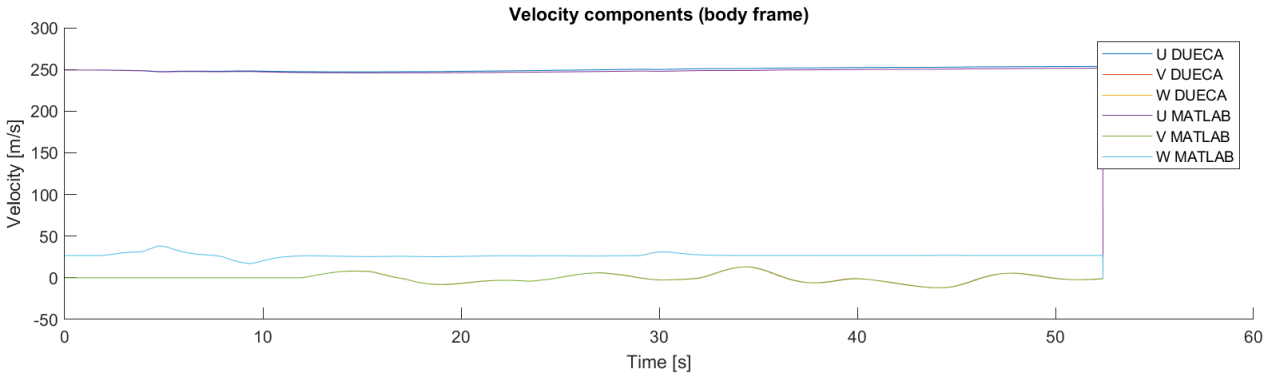

(d) Velocity components

Figure 10. Pilot inputs, aircraft attitude, angular rates, and velocity components in body frame, for a simulation test with SAS-2 in cruise flight conditions.

Part III: Preliminary Thesis Report

Previously graded for course AE4020

,

Preliminary Thesis Report

Piloted assessment of the lateral-directional handling qualities of the Flying-V

Sjoerd Joosten

TU Delft

Preliminary Thesis Report

Piloted assessment of the lateral-directional handling qualities of the Flying-V

by

Sjoerd Joosten

Student number: 4486048
Thesis committee: Ir. O. Stroosma, TU Delft, daily supervisor
Prof. dr. ir. M. Mulder, TU Delft, supervisor

Cover mage source: https://www.tudelft.nl/lr/flying-v, copyright Edwin Wallet

TU Delft

This report contains confidential information, thus may only be shared after approval by the author.

Contents

1 Introduction

The conventional wing-body-tail aircraft layout has been dominant in commercial aviation for over 50 years. It seems, however, that this configuration is converging to an asymptote of maximum performance and efficiency [1]. Therefore, new interest arises in unconventional aircraft layouts, such as the flying wing. This tail-less configuration was and is investigated by numerous companies and institutes, which led amongst others to designs of a blended-wing-body aircraft [2] [3]. Recently, the TU Delft has researched the opportunities regarding a different flying wing design, called the Flying-V. It followed from a design by Benad at the TU Berlin in collaboration with Airbus [4]. A next design iteration was made at the TU Delft by Faggiano [5]. Both show a promising performance, with a drag reduction of 10% compared to conventional aircraft with comparable performance requirements.

From a control perspective, flying wings are known for their limited lateral-directional stability [6] and their limited handling qualities [7], both due to the absence of a vertical tail surface and a smaller moment arm from the control surfaces to the centre of gravity than conventional aircraft. From this perspective followed a first handling quality assessment of the Flying-V design in a TU Delft thesis, performed by Cappuyns in collaboration with Airbus [8]. This research focused on developing the required aerodynamic model and simulation tools, with a brief analytical assessment of the handling quality performance of this model. It was found that, similar to earlier research, the lateral-directional stability and handling qualities were limited. It was recommended to further study this stability and these handling qualities.

Handling qualities can be assessed both theoretically and experimentally. The theoretical assessment can be performed by simulating the aircraft and using this simulation to check against regulatory qualitative and quantitative requirements [9]. These theoretical results, however, can differ from (experimental) pilot-perceived handling qualities, since these are a subjective measure [10]. Hence, to perform a complete handling quality assessment, both the theoretical and experimental handling qualities have to be assessed. Obtaining the pilot perceived handling qualities requires a pilot-in-the-loop experiment, and although previous theoretical research exists on the handling qualities of the Flying-V, no pilot-in-the-loop experiment has been performed yet.

This research aims at bringing the insights in the lateral-directional handling qualities of the Flying-V a step further, by performing the first pilot-perceived assessment of these handling qualities. In order to find the challenges in the lateral-directional handling qualities of the Flying-V and to develop the hypotheses to be tested experimentally, first a theoretical analysis of these handling qualities is performed. Moreover, it is decided that a pilot-in-the-loop experiment is more relevant when the aircraft possesses a minimum level of handling qualities to provide for a successful experiment, i.e., the aircraft should be flyable. Hence, it is decided to design and implement a prototype flight control system using an unconventional control surface allocation and a stability augmentation system. A flight control system can improve the handling qualities and stability of an aircraft without the need to re-design the planform or control surfaces of the aircraft. This extends the scope of the research, by taking the first step in increasing the lateral-directional handling qualities of the Flying-V.

Next, the pilot-in-the-loop experiment is developed, which aims at both validating the theoretical handling-quality assessment as well as at providing new insights in the pilot-perceived handling qualities and

the implication of those results on future Flying-V design choices. A proposal for this experiment is discussed in the final part of this report, and marks the start of the second phase of the research. This report acts as predecessor for the main research of the author's MSc. thesis, covering all research and results up to, and including, the experiment proposal.

First, in Chapter 2, the Flying-V is introduced and its properties, method of simulation and earlier research are discussed. Second, Chapter 3 discusses the simulation, evaluation and requirements of aircraft handling qualities, and briefly discusses the influence of a flight control system on these aspects. Third, the thesis research objectives are presented in Chapter 4. Next, the methodology and results of the theoretical handling quality assessment of the bare-airframe Flying-V are discussed in Chapter 5. Fifth, the results of designing and implementing a prototype flight control system are discussed in Chapter 6. Next, the experiment proposal for the final phase of the thesis research is presented in Chapter 7. Finally, the conclusions of this preliminary thesis research are discussed in Chapter 8.

2
The Flying-V

In this chapter, the aircraft subject to the research is elaborated upon: the Flying-V. First, the development of the aircraft is discussed in Section 2.1. Second, the Flying-V geometry, mass and control surface properties are discussed in Section 2.2. Third, the implementation of the aerodynamic model used for the research is elaborated upon in Section 2.3. Next, earlier research on the handling qualities of the Flying-V is briefly discussed in Section 2.4. Finally, the key takeaways of the discussion of the Flying-V in this chapter are presented in Section 2.5.

2.1. Flying-V Development

The Flying-V initial design was performed by Benad, who predicted a promising performance increase with a drag reduction of 10% compared to conventional aircraft with comparable performance requirements [4]. A further design iteration was performed at the TU Delft by Faggiano, who performed an aerodynamic design optimisation for the Flying-V [5]. The design iteration consisted of designing the wing planform and airfoil based on aerodynamic optimisation, and sizing the winglet fins with integrated rudders based on static stability requirements. This led to a different design than initially developed by Benad, and this new design was used in further analyses in several TU Delft theses. Claeys performed a structural analysis on the Flying-V design, providing amongst others an estimation of the mass moments of inertia for further analysis [11]. Viet performed an experimental analysis of the flight characteristics of a sub-scale model of the Flying-V [12]. From this, Garcia identified an aerodynamic model of the Flying-V using wind tunnel data [13]. Palermo used the previous research to perform a longitudinal static stability and control analysis on a Flying-V scale model, while simultaneously designing the control surfaces for this scale model [14]. Following on this research, Cappuyns performed a preliminary handling quality analysis by developing a full-scale aerodynamic simulation of the Flying-V [8], including the control surfaces as designed by Faggiano and Palermo [5][14].

2.2. Properties

The properties of the Flying-V are discussed in two parts. First, the Flying-V geometry and mass assumptions are discussed in subsection 2.2.1. Second, the control surfaces are elaborated upon in subsection 2.2.2.

2.2.1. Flying-V geometry and mass

Table 2.1 shows an overview of the Flying-V geometry properties. All are obtained from Cappuyns [8] except the engine location, which is obtained from Pascual [15]. Next, Table 2.2 shows an overview of the Flying-V mass and moment of inertia properties for Maximum Take-Off Weight (MTOW) and Maximum Landing Weight (MLW). The MTOW and MLW were obtained from Cappuyns [8], as well as the moments of inertia for the MTOW. The moments of inertia for the MLW were not directly available, thus were determined based on the weight difference between the MTOW and MLW and the weight distribution as used by Cappuyns [8]. The determination of the moments of inertia for the MLW is further elaborated upon in Appendix A.

Figure 2.1 gives an impression of the top-view of the Flying-V with associated dimensions. Figure 2.2 gives an impression of the side-view of the Flying-V with associated dimensions.

Table 2.1: Flying-V geometry properties [8][15].

Property	Description	Value	Unit
T_{dy}	Engine (thrust vector) y location w.r.t. centre line	$\pm$ 5.7	m
T_{dz}	Engine (thrust vector) z location w.r.t. centre line	0.8	m
S	Wing area	883.3	m^2
c / MAC	Wing Mean Aerodynamic Chord	18.7385	m
b	Wing span	65	m
L	Aircraft length	55	m
$CG_{forward}$	Centre of gravity forward stability limit	45	%MAC
CG_{aft}	Centre of gravity aft stability limit	57.5	%MAC

Table 2.2: Flying-V mass and moments of inertia properties [8][11].

Property	Description	Value	Unit
MTOW	Maximum Take-Off Weight	X	$10^3 kg$
MLW	Maximum Landing Weight	X	$10^3 kg$
$I_{xx_{MTOW}}$	Mass Moment of Inertia around X axis MTOW	X	$10^7 kgm^2$
$I_{yy_{MTOW}}$	Mass Moment of Inertia around Y axis MTOW	X	$10^7 kgm^2$
$I_{zz_{MTOW}}$	Mass Moment of Inertia around Z axis MTOW	X	$10^7 kgm^2$
$I_{xz_{MTOW}}$	Mass Moment of Inertia Cross product of X and Z axes MTOW	X	$10^7 kgm^2$
$I_{xx_{MLW}}$	Mass Moment of Inertia around X axis MLW	X	$10^7 kgm^2$
$I_{yy_{MLW}}$	Mass Moment of Inertia around Y axis MLW	X	$10^7 kgm^2$
$I_{zz_{MLW}}$	Mass Moment of Inertia around Z axis MLW	X	$10^7 kgm^2$
$I_{xz_{MLW}}$	Mass Moment of Inertia Cross product of X and Z axes MLW	X	$10^7 kgm^2$

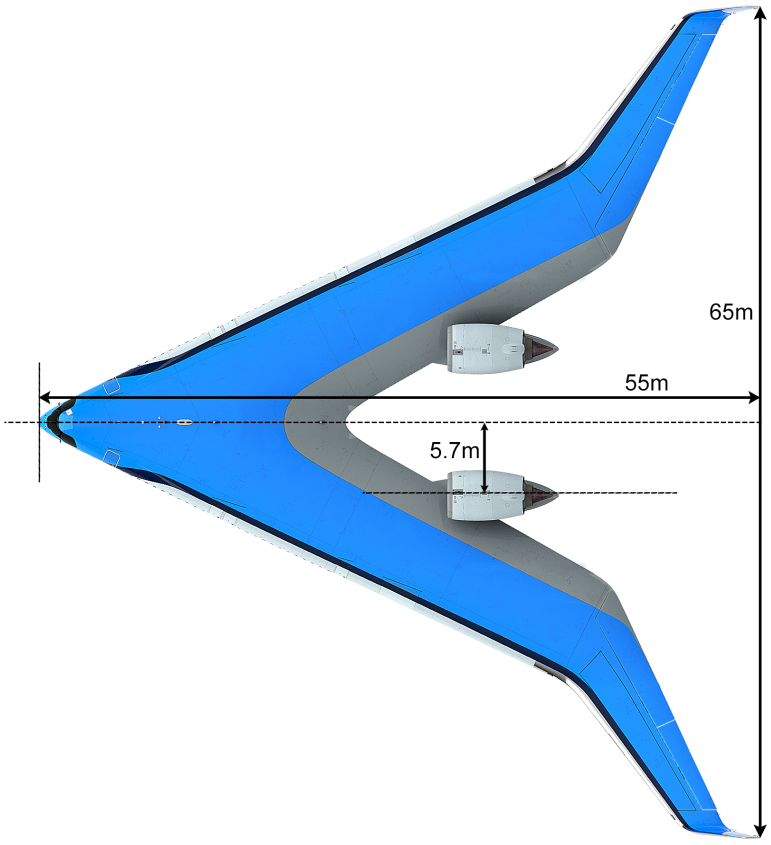

Figure 2.1: Flying-V impression, top view and dimensions[1].

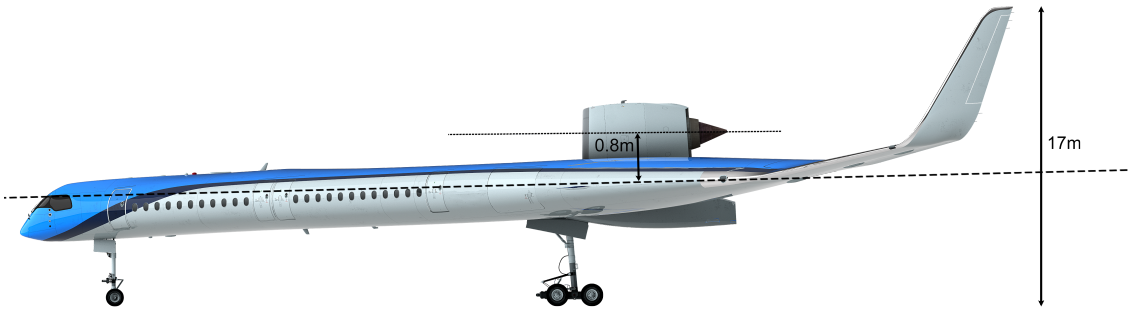

Figure 2.2: Flying-V impression, side view and dimensions[1].

2.2.2. Control surfaces

The control surfaces of the Flying-V are located at the outboard trailing edges. Both aircraft sides possess 2 elevons (i.e., elevator-aileron combinations) and a rudder embedded in the winglet. The control surface dimensions were obtained from the Airbus VLM model of the Flying-V, as initially developed by Cappuyns [8], of which the application will further be discussed in subsection 2.3.1. It should be noted that Cappuyns developed the control surfaces based on simplicity and recommended further research to optimise them. The control surfaces thus are expected to perform sub-optimally. The locations and dimensions of the right elevons are indicated in Figure 2.1, the location and dimension of the left winglet rudder is indicated in Figure 2.2. Finally, Table 2.3 shows the variables used to indicate each control surface further in this report, as seen when standing behind the aircraft.

Table 2.3: Variables used to indicate control surfaces.

Variable	Control surface
C1	Left winglet rudder
C2	Left outboard elevon
C3	Left inboard elevon
C4	Right inboard elevon
C5	Right outboard elevon
C6	Right winglet rudder

2.3. Aerodynamic Model Implementation and Simulation

In this section, the implementation of the aerodynamic model of the Flying-V used in this research is discussed. First, the application of the model is discussed in subsection 2.3.1. Second, using this application to simulate the aircraft over time is elaborated upon in subsection 2.3.2. Finally, trimming the aircraft to a constant state and linearising the aircraft around this state is discussed in subsection 2.3.3.

2.3.1. Airbus Flying-V VLM model application

As introduced in Section 2.1, Cappuyns developed a full-scale aerodynamic simulation-model of the Flying-V in collaboration with Airbus, which was based on the Vortex Lattice Method (VLM). This VLM model was obtained from Airbus, and one iteration was collaboratively made to expand the VLM model to contain multiple centre of gravity locations, more flight conditions and separately controllable control surfaces. This led to a model with as inputs the variables as shown in the first two columns of

[1] Flying-V impressions obtained from `https://www.tudelft.nl/lr/flying-v`, combined with geometry properties obtained from Cappuyns [8] and Pascual [15].

Table 2.4. For the roll, pitch and yaw rate the normalised rates are used, equal to the rate in radians per second multiplied by c/V, the mean aerodynamic chord divided by the airspeed. Simulation results of the model are available at all combinations of the input variables at the values shown in the third column of Table 2.4.

The output of the VLM model is given in terms of contributions of the input variables to force and moment coefficients. These force and moment coefficients and their corresponding reference frame are shown in Table 2.5. The force and moment coefficients are obtained by inter- or extrapolating all input states their contribution to the corresponding coefficients and summing those. Illustrating the determination of a force or moment coefficient, Equation 2.1 shows the determination of force coefficient C_X, based on the VLM model output coefficients.

As shown in Table 2.4, the simulation results of the angular rate and control surface deflection input variables are available only at -1, 0, and 1 radians or degrees. Hence, for a given Angle of Attack, linearly inter- or extrapolating these variables yields a linear contribution to the force or moment coefficient, with a slope dependent on the sign of the input variable. The Airbus representative confirmed this implementation to be in line with the linear modelling of these rates and deflections.

$$\begin{aligned} C_X = C_{X_0}(\alpha) + C_{X_\beta}(\alpha,\beta) + \dots \\ C_{X_{p^*}}(\alpha,p^*) + C_{X_{q^*}}(\alpha,q^*) + C_{X_{r^*}}(\alpha,r^*) + \dots \\ C_{X_{\delta_{c1}}}(\alpha,\delta_{c1}) + C_{X_{\delta_{c2}}}(\alpha,\delta_{c2}) + C_{X_{\delta_{c3}}}(\alpha,\delta_{c3}) + \dots \\ C_{X_{\delta_{c4}}}(\alpha,\delta_{c4}) + C_{X_{\delta_{c5}}}(\alpha,\delta_{c5}) + C_{X_{\delta_{c6}}}(\alpha,\delta_{c6}) \end{aligned} \tag{2.1}$$

Table 2.4: Input variables and ranges of the Airbus Flying-V VLM model.

Variable	Description	Range	Unit
CG	Centre of Gravity	[45, 51.5, 57.5]	%MAC
M	A/C velocity in Mach	[0.2, 0.225, 0.25, 0.275, 0.3, 0.85]	-
α	Angle of Attack	[-5, 0, 5, 10, 12.5, 15, 16.5, 18, 20]	Degrees
β	Sideslip Angle	[-1, 0, 1]	Degrees
p^*	Normalised roll rate	[-1, 0, 1]	Radians
q^*	Normalised pitch rate	[-1, 0, 1]	Radians
r^*	Normalised yaw rate	[-1, 0, 1]	Radians
δ_{c1}	Deflection of left rudder	[-1, 0, 1]	Degrees
δ_{c2}	Deflection of left outboard elevon	[-1, 0, 1]	Degrees
δ_{c3}	Deflection of left inboard elevon	[-1, 0, 1]	Degrees
δ_{c4}	Deflection of right inboard elevon	[-1, 0, 1]	Degrees
δ_{c5}	Deflection of right outboard elevon	[-1, 0, 1]	Degrees
δ_{c6}	Deflection of right rudder	[-1, 0, 1]	Degrees

Table 2.5: Force and moment coefficient, as resulting from implementation of the Airbus Flying-V VLM model.

Variable	Description	Unit	Reference Frame
C_X	Backward force coefficient	-	Aerodynamic
C_Y	Side (right) force coefficient	-	Aerodynamic
C_Z	Upward force coefficient	-	Aerodynamic
C_L	Roll moment coefficient	-	Body
C_M	Pitch moment coefficient	-	Body
C_N	Yaw moment coefficient	-	Body

From the (normalised) force and moment coefficients ($C_X, C_Y, C_Z, C_L, C_M, C_N$), the actual forces and moments acting on the aircraft can be obtained. By multiplying the force variables with C_X, C_Y, C_Z with a combination of the air density and velocity ($0.5 \cdot \rho \cdot V^2$) and the moment variables C_L, C_M, C_N with a combination of the air density, velocity and mean aerodynamic chord ($0.5 \cdot \rho \cdot V^2 \cdot c$), the forces and moments are de-normalised and can be used for further simulation. Using the mean aerodynamic chord for normalising and de-normalising the forces and moments is an Airbus convention.

2.3.2. Flying-V simulation

Using the de-normalised forces as elaborated in the previous subsection, equations of motion can be used to simulate the aircraft dynamics [16]. First, the aerodynamic forces (X, Y, Z) are transformed to the body reference frame for further use. This is done using the aerodynamic to body transformation matrix as shown in Equation 2.2 and 2.3. The moments L, M and N (i.e., M_x, M_y, M_z) do not require this transformation, since their coefficients are already expressed in the body reference frame in the aerodynamic model.

Next to the aerodynamic forces as obtained from the Airbus Flying-V VLM model, two thrust vectors were added to the model, $T1$ for the left engine and $T2$ for the right engine when seen from behind the aircraft. For each engine, of which the locations were discussed in subsection 2.2.1, a thrust vector is modelled as being aligned with the aircraft body-frame X-axis (nose forward direction). Thus, the additional force is added to the existing X-axis body-frame force component, and the additional body-frame moments around the Y and Z body-axes are calculated based on each engine's location with respect to these axes.

The aircraft state used consists of 12 states: the earth-fixed position X_e, Y_e and Z_e, the body velocities U_b, V_b and W_b, the angular velocities p, q and r and the attitude angles φ, θ and ψ. With the aerodynamic forces X, Y, Z and and moments M_x, M_y, M_z, the derivatives of these aircraft states can be calculated. Equations 2.4, 2.5 and 2.6 show the derivative determination of $\dot{X}_e, \dot{Y}_e, \dot{Z}_e$ (assumed equal to V_N, V_E, V_D and assuming a flat earth), representing the motion of the aircraft relative to earth. Next, equations 2.7 and 2.8 show the derivative determination of $\dot{U}_b, \dot{V}_b$ and $\dot{Z}_b$, using the force equilibrium equations of motion. Furthermore, Equation 2.9 shows the derivative determination of $\dot{p}, \dot{q}$ and $\dot{r}$ using the moment equilibrium equations of motion, with I^* as shown in Equation 2.10. Finally, Equation 2.11 shows the determination of $\dot{\varphi}, \dot{\theta}$ and $\dot{\psi}$.

$$\begin{bmatrix} X_b \\ Y_b \\ Z_b \end{bmatrix} = \Gamma_{ba} \begin{bmatrix} X_a \\ Y_a \\ Z_a \end{bmatrix} \tag{2.2}$$

$$\Gamma_{ba} = \begin{bmatrix} \cos\alpha\cos\beta & -\cos\alpha\sin\beta & -\sin\alpha \\ \sin\beta & \cos\beta & 0 \\ \sin\alpha\cos\beta & -\sin\alpha\sin\beta & \cos\alpha \end{bmatrix} \tag{2.3}$$

$$\begin{bmatrix} \dot{X}_e \\ \dot{Y}_e \\ \dot{Z}_e \end{bmatrix} = \begin{bmatrix} V_N \\ V_E \\ V_D \end{bmatrix} = \mathbb{T}_{Eb} \begin{bmatrix} u \\ v \\ w \end{bmatrix} \tag{2.4}$$

$$= \begin{bmatrix} \cos\theta\cos\psi & \begin{pmatrix} \sin\varphi\sin\theta\cos\psi \\ -\cos\varphi\sin\psi \end{pmatrix} & \begin{pmatrix} \cos\varphi\sin\theta\cos\psi \\ +\sin\varphi\sin\psi \end{pmatrix} \\ \cos\theta\sin\psi & \begin{pmatrix} \sin\varphi\sin\theta\sin\psi \\ +\cos\varphi\cos\psi \end{pmatrix} & \begin{pmatrix} \cos\varphi\sin\theta\sin\psi \\ -\sin\varphi\cos\psi \end{pmatrix} \\ -\sin\theta & \sin\varphi\cos\theta & \cos\varphi\cos\theta \end{bmatrix} \begin{bmatrix} u \\ v \\ w \end{bmatrix} \tag{2.5}$$

$$= \begin{bmatrix} \begin{pmatrix} [u\cos\theta + (v\sin\varphi + w\cos\varphi)\sin\theta]\cos\psi \\ -(v\cos\varphi - w\sin\varphi)\sin\psi \end{pmatrix} \\ \begin{pmatrix} [u\cos\theta + (v\sin\varphi + w\cos\varphi)\sin\theta]\sin\psi \\ +(v\cos\varphi - w\sin\varphi)\cos\psi \end{pmatrix} \\ -u\sin\theta + (v\sin\varphi + w\cos\varphi)\cos\theta \end{bmatrix} \tag{2.6}$$

$$m \begin{bmatrix} \dot{u} + qw - rv \\ \dot{v} + ru - pw \\ \dot{w} + pv - qu \end{bmatrix} = m g_{r,0} \begin{bmatrix} -\sin\theta \\ \sin\varphi\cos\theta \\ \cos\varphi\cos\theta \end{bmatrix} + \begin{bmatrix} X \\ Y \\ Z \end{bmatrix} \tag{2.7}$$

$$\begin{bmatrix} \dot{u} \\ \dot{v} \\ \dot{w} \end{bmatrix} = \begin{bmatrix} rv - qw - g_{r,0}\sin\theta + X/m \\ pw - ru + g_{r,0}\sin\varphi\cos\theta + Y/m \\ qu - pv + g_{r,0}\cos\varphi\cos\theta + Z/m \end{bmatrix} \tag{2.8}$$

$$\begin{bmatrix} \dot{p} \\ \dot{q} \\ \dot{r} \end{bmatrix} = \begin{bmatrix} \frac{I_{zz}}{I^*}M_x + \frac{I_{xz}}{I^*}M_z + \frac{(I_{xx}-I_{yy}+I_{zz})I_{xz}}{I^*}pq + \frac{(I_{yy}-I_{zz})I_{zz}-I_{xz}^2}{I^*}qr \\ \frac{M_y}{I_{yy}} + \frac{I_{xz}}{I_{yy}}\left(r^2-p^2\right) + \frac{I_{zz}-I_{xx}}{I_{yy}}pr \\ \frac{I_{xz}}{I^*}M_x + \frac{I_{xx}}{I^*}M_z + \frac{(I_{xx}-I_{yy})I_{xx}+I_{xz}^2}{I^*}pq + \frac{(-I_{xx}+I_{yy}-I_{zz})I_{xz}}{I^*}qr \end{bmatrix} \tag{2.9}$$

$$I^* = I_{xx}I_{zz} - I_{xz}^2 \tag{2.10}$$

$$\begin{bmatrix} \dot{\varphi} \\ \dot{\theta} \\ \dot{\psi} \end{bmatrix} = \begin{bmatrix} p + \sin\varphi\tan\theta q + \cos\varphi\tan\theta r \\ \cos\varphi q - \sin\varphi r \\ \frac{\sin\varphi}{\cos\theta}q + \frac{\cos\varphi}{\cos\theta}r \end{bmatrix} \tag{2.11}$$

The equations of motion can be used to simulate the aircraft response to inputs. This can be done for each aircraft state, by first retrieving the force and moment coefficients and converting these to aerodynamic forces and moments, as elaborated upon in subsection 2.3.1, and second using the equations of moments to find the derivatives of the aircraft state vector. Next, by means of a simple Euler integration as shown in Equation 2.12, the states are updated by adding the derivative of the state times a (small) time-step to the original value of the state. By using a sufficiently small time-step, an accurate simulation of the aircraft response for each condition, state and input can be performed.

$$X(t+1) = X(t) + \dot{X}(t) \cdot dt \tag{2.12}$$

2.3.3. Model trim and linearisation

Trimming the aircraft state at a flight condition can be done by numerically optimising the equations of motion using the aerodynamic model. This optimisation follows the same procedure of determining state derivatives as the non-linear simulation, but uses it to numerically converge to a state in which all linear and angular accelerations are found to approach zero.

A numerical optimiser in MATLAB was used called *fminsearch*. It uses a trim-function with the to be trimmed states, control surfaces and engine settings as input, using the aircraft equations of motion to result in a cost function as output. The cost function is set to approach zero when all linear and angular accelerations approach zero. The numerical optimiser varies the trim-function inputs to have the cost function approach zero, showing the optimised trim-function inputs as outcome.

For different flight situations, such as a horizontal flight or a coordinated turn, different trim-functions were developed by constraining the equations of motion, such that the aircraft is trimmed in the desired flight manoeuvre.

The aircraft model can be linearised around a trimmed aircraft state. Using a linearised aircraft model for simulation yields several advantages over using a non-linear model to simulate an aircraft over time. Foremost, a linear model can be simulated considerably faster than a non-linear model. Moreover, a linear state-space model provides an uncomplicated way of assessing the eigenmode damping and frequency responses of the aircraft by assessing the eigenvalues of the state matrix (A), rapidly showing the aircraft stability. This is used often during a handling quality analysis, as discussed in Chapter 3. The (general) approach to linearising an aircraft based on its equations of motion and the appliance for the Flying-V is discussed further in Appendix B.

2.4. Flying-V Handling Qualities

As stated in the introduction of this report, flying wings are known for their limited lateral-directional stability [6] and limited handling qualities [7], due to the absence of a vertical tail surface. The preliminary winglet and rudder designs by Faggiano [5] and Palermo [14] took this stability into account, but were primarily based on the static stability of the Flying-V.

Further analysis by Cappuyns [8] showed the dynamic lateral-directional stability of the Flying-V to be insufficient. Amongst others because of this, the lateral-directional handling qualities were found limited on two aspects. First on the lateral-directional eigenmodes, which showed an unstable Dutch Roll. Second, on the lateral-directional manoeuvrability performance, for which the control authority was shown to be insufficient for multiple handling quality requirements. Cappuyns recommended further research to focus on a full investigation into the handling qualities of the Flying-V. Recommended solutions for the limited lateral-directional handling qualities were, amongst others, a redesign of the control surfaces, the use of unconventional control surfaces, optimising the control allocation and imposing a stability augmentation system. Developing a solution for the lateral-directional handling qualities and stability concerns can be of great value to the Flying-V project.

The analysis by Cappuyns [8] was performed theoretically, and no piloted experiment was performed. Hence, the found performance of the Flying-V was not validated as pilot-perceived, yielding an opportunity for further research.

2.5. Key Takeaways

The previous sections provided an overview of the Flying-V development, design, model implementation and simulation and finally on earlier research of the Flying-V handling qualities. From this, four key takeaways are most relevant for the next phase of this research.

1. Research showed the Flying-V to have a promising performance increase when compared to conventional aircraft due to its unconventional layout.
2. Due to this unconventional layout, however, the Flying-V was, in a theoretical assessment, predicted to show insufficient lateral-directional handling qualities and further research was recommended.
3. Only a theoretical assessment of the lateral-directional handling qualities of the Flying-V was performed.
4. An aerodynamic VLM model of the Flying-V as developed in previous research is available and can be used to simulate the Flying-V, thus to test the handling qualities in further research.

3

Aircraft Handling Quality Simulation and Evaluation

In this chapter, the background on aircraft handling quality simulation and evaluation is discussed. First, the handling quality assessment and requirements from literature are presented in Section 3.1. Second, theoretically assessing these requirements is elaborated upon in Section 3.2. Third, experimentally assessing the handling qualities with a pilot-in-the-loop simulation is discussed in Section 3.3. Next, the effect of flight control systems on handling qualities is elaborated upon in Section 3.4. Finally, the key takeaways from this chapter are discussed in Section 3.5.

3.1. Handling Quality Assessment and Requirements

Handling qualities are described by Cooper and Harper [17, page 2] as: *"Those qualities or characteristics of an aircraft that govern the ease and precision with which a pilot is able to perform the tasks required in support of an aircraft role"*. To evaluate the handling qualities of an aircraft, the Cooper-Harper Rating Scale was developed [17], which is still widely used to compare subjective handling quality experiences by pilots [18]. The handling quality objectives are also discussed by Roskam [19] and state four conditions. First, the airplane should have sufficient control power to maintain steady, straight flight. Second, the airplane should be able to be safely manoeuvred from one steady flight state to the other. Third, the cockpit control force levels should be acceptable during all conditions. Finally, it should be possible to trim the airplane to certain flight conditions.

Both the description by Cooper and Harper [17] as well as the objectives by Roskam [19] are qualitative. In order to objectively assess whether these are met, quantitative handling quality requirements are required. In line with Cappuyns [8], the US Department of Defence military handbook MIL-HDBK-1797 [20] and the EASA aircraft regulations of CS25 [21] were used. The military handbook specifies quantitative stability requirements on frequency and damping parameters of aircraft eigenmodes, and associated handling quality classification. The EASA regulations specify airworthiness (manoeuvrability) requirements, with quantitative constraints on amongst others the control deflections used and time to perform different manoeuvres. The military handbook and the EASA regulations both contain requirements on both the longitudinal as well as the lateral-directional handling qualities of the aircraft. Since the scope of this thesis focuses on the lateral-directional handling qualities, only these requirements will be taken into account.

To further limit the scope of the handling quality assessment, literature is used to reduce the amount of requirements and regulations to be tested. Research by Perez and Wahler [22] [23] discussed the design-constraining conditions selected from EASA CS25 and the MIL-HDBK-1797 of the US Department of Defence for, respectively, conventional and unconventional aircraft configurations. In being the design-constraining conditions, these are chosen as the most relevant conditions to test the Flying-V design on. Moreover, these requirements are in line with the research of Cappuyns [8], thus provide the opportunity for comparison with this previous research. Table 3.1 shows an overview of the requirements and regulations tested. In subsection 3.1.1 to 3.1.8, all are elaborated upon separately.

Table 3.1: Selection of handling quality requirements.

Requirement	Book	Article
Dutch Roll Stability	MIL-HDBK-1797	4.6.1.1
Spiral Stability	MIL-HDBK-1797	4.5.1.2
Lateral Control Departure Parameter	MIL-HDBK-1797	4.8.4.3.1
Coordinated Turn Capability	CS-25	25.143(h)
Time to Bank, Roll Capability	CS-25	25.147(f)
One Engine Inoperative Trim Condition	CS-25	25.161(d)
Steady Heading Sideslip	CS-25	25.177(c)
Dynamic Stability	CS-25	25.181

3.1.1. MIL-HDBK-1797 - Dutch Roll

Table 3.2 shows the MIL-HDBK-1797 requirement on the Dutch Roll eigenmode damping and frequency parameters for different handling quality levels, flight phases and aircraft classes. A lower value handling quality level indicates better handling quality performance. An elaborate definition of the different flight phases and aircraft classes discussed can be found in Appendix C. The Flying-V can be categorised in Class II or III, depending on the assumed weight. Furthermore, it will operate only in Flight Phases B and C, since the military-precision manoeuvres of Category A will not be necessary to perform (e.g., in-flight refuelling.)

Table 3.2: Dutch Roll frequency and damping parameter requirements for different handling quality levels according to MIL-HDBK-1797 [20].

Level	Flight Phase	Class	Min ζ	Min ζ ω	Min ω
1	A (CO, GA, PR, TF, RC, FF, AS)	I, II, III, IV	0.4	0.4	1
	A	I, IV	0.19	0.35	1
		II, III	0.19	0.35	0.4
	B	All	0.08	0.15	0.4
	C	I, II-C, IV	0.08	0.15	1
		II-L, III	0.08	0.1	0.4
2	All	All	0.02	0.05	0.4
3	All	All	0	-	0.4

3.1.2. MIL-HDBK-1797 - Spiral Stability

MIL-HDBK-1797 states a requirement on the spiral stability eigenmode. Although preferable, the spiral stability does not require positive damping. Requirements are set on the time to double of the amplitude of the spiral mode. Table 3.3 shows the minimum time to double (T_2) requirements of the spiral stability for each handling quality level.

Table 3.3: Spiral stability minimal time to double requirements MIL-HDBK-1797 [20].

Flight Phase Category	Level 1 T_2 [s]	Level 2 T_2 [s]	Level 3 T_2 [s]
A and C	12	8	4
B	20	8	4

3.1.3. MIL-HDBK-1797 - Lateral Control Departure Parameter

MIL-HDBK-1797 requires the Lateral Control Departure Parameter (LCDP) to be positive. The LCDP depends on the aircraft rolling and yawing moment response to a sideslip angle and aileron deflection, and is shown in Equation 3.1. C_{N_β} represents the yawing moment due to sideslip, C_{l_β} the rolling moment due to sideslip, $C_{n_{\delta_a}}$ the yawing moment due to aileron deflection and $C_{l_{\delta_a}}$ the rolling moment due to aileron deflection.

$$LCDP = C_{n_\beta} - C_{l_\beta} \cdot \frac{C_{n_{\delta_a}}}{C_{l_{\delta_a}}} > 0 \tag{3.1}$$

3.1.4. CS25.143(h) - Coordinated Turn Capability

The coordinated turn capability manoeuvre asserts that the aircraft is able to make turns at high bank angles for different flight configurations and states. Table 3.4 shows the combination of configurations, speeds, bank angles and thrust settings the aircraft should be able to achieve. This should be possible without showing the need of excessive control surface deflections. The 'asymmetric WAT-Limited Thrust Setting' indicates a Weight, Altitude and Temperature (WAT) combination, where an one engine inoperative (OEI) thrust setting should be able to provide for the minimum climb gradient as specified in CS 25.121. For, respectively, the Take-Off, En-Route and Landing configuration, the Take-Off, Cruise and Approach conditions as specified in Table 5.1 are used.

Table 3.4: Manoeuvring Bank Angle CS25.143(h) requirements [21].

Configuration	Speeds	Manoeuvring Bank Angle	Thrust/Power Setting	Minimum Climb Gradient
Take-Off	V_2	$30°$	Asymmetric WAT-Limited	2.4 %
Take-Off	$V_2 + XX$	$40°$	All Engines Operating Climb	1.2 %
En-Route	V_{FTO}	$40°$	Asymmetric WAT-Limited	1.0 %
Landing	V_{REF}	$40°$	Symmetric for $-3°$ Flight Path Angle	-

3.1.5. CS25.147(f) - Time to Bank, Roll Capability

The requirements on the roll capability of the aircraft are tested in a time to bank manoeuvre. In this manoeuvre, the aircraft should be able to roll from a 30 degree bank angle on one side to a 30 degree bank angle on the other side. This 60 degree roll manoeuvre should be finished within a specified amount of time.

For an all engine operative thrust setting, the manoeuvre should be performed in not more than 7 seconds and should be demonstrated in approach and cruise condition. For the one engine inoperative thrust setting, the manoeuvre should be performed in not more than 11 seconds and should be demonstrated in take-off condition. This thus yields three flight manoeuvres to be tested. Next to the time and angle requirements, an extra requirement on the manoeuvre has to be taken into account: the rudder may only be used to the extent necessary to minimise sideslip.

3.1.6. CS25.161(d) - One Engine Inoperative Trim Condition

In a one engine inoperative condition, the aircraft should still be able to maintain longitudinal and lateral-directional trim. For lateral trim, the angle of bank may not exceed 5°. The manoeuvre is tested in approach, take-off and cruise condition, thus yields three flight manoeuvres to be tested.

3.1.7. CS25.177(c) - Steady Heading Sideslip

In the steady heading sideslip manoeuvre, the aircraft should be able to keep a constant sideslip angle while maintaining straight flight. This should be shown for all aircraft conditions, and both for the all engine operative thrust setting and the one engine inoperative thrust setting. The sideslip angle tested follows from Equation 3.2, with β as the sideslip angle tested based on total airspeed V in km/h. However, a sideslip angle of 15 degrees is generally accepted as sufficient for most aircraft, even if the equation yields a larger sideslip angle. The manoeuvre is tested in approach, take-off and cruise condition, both for all engine operative thrust setting and the one engine inoperative, thus yields six flight manoeuvres to be tested.

$$\beta = \sin^{-1}\left(\frac{56}{V}\right) \tag{3.2}$$

3.1.8. CS25.181 - Dynamic Stability

The dynamic stability requirement states that the short period oscillations of the aircraft should be heavily damped. Besides, the lateral-directional oscillations ('Dutch Roll') should be positively damped for all flight conditions. Since this is also required in MIL-HDBK-1797, it will be discussed based on that

requirement further in this report. This CS25 article thus does not lead to additional flight manoeuvres to be tested.

3.2. Theoretical Handling Quality Simulation and Evaluation

The quantitative nature of the handling quality requirements and classifications discussed in Section 3.1 allows a theoretical assessment with an aerodynamic model of an aircraft.

As was discussed in subsection 2.3.2, the force and moment coefficients of an aerodynamic model can be used to obtain forces and moments acting on the aircraft, depending on the aircraft flight condition such as altitude, velocity and angle of attack. These forces and moments then can be used to propagate the aircraft over time based on the equations of motion, yielding a simulation over time of the aircraft dynamics. Moreover, the equations of motion and aerodynamic model implementation can be used to find the trim states of an aircraft using numerical optimisation to converge all linear and angular accelerations to zero by varying the control inputs. This simulation of the aircraft's trim states and dynamics can be used to simulate the CS-25 [21] requirement manoeuvres as discussed in Section 3.1, and check whether the quantitative requirements set on, e.g., the manoeuvre time and control surface deflections are met.

The stability requirements as stated by MIL-HDBK-1797 [20] require the eigenvalues of the aircraft to be found, in order to check the damping and frequency of the prescribed eigenmotions. As was discussed in subsection 2.3.3, to obtain these eigenvalues the equations of motion of the aircraft dynamics can be linearised around a trim point, yielding a state-space representation of the aircraft dynamics. Next, the eigenvalues of the A-matrix of this state-space representation can be found, and based on their eigenvectors be appointed to the correct eigenmotion [24]. Each eigenvalue then yields the damping and frequency parameter of each eigenmotion.

These methods were used by Cappuyns [8], who performed a first handling quality analysis on the Flying-V with them. Earlier applications can also be found, such as Voskuijl et al. [25], who performed an analysis of the controllability of a blended wing body using a flight mechanics model and linearisation of this model. Moreover, Castro used these methods to identify and evaluate flight dynamics, stability, flight controls and handling qualities of a generic blended-wing-body transport aircraft flying-wing concept [9].

3.3. Piloted Handling Quality Simulation and Evaluation

Next to the theoretical handling quality simulation and evaluation as discussed in the previous section, piloted assessments of these handling qualities are common to validate the theoretical findings and yield new insights. A piloted assessment of handling qualities can yield different results than a theoretical analysis, since experimental handling quality assessments can show pilot-subjective outcomes [10]. Moreover, in a theoretical analysis only requirement compliance is tested, while a piloted assessment can also yield qualitative feedback on the aircraft response to pilot inputs. Next, in subsection 3.3.1, performing such a pilot-in-the-loop experiment is discussed. After that, subsection 3.3.2 discusses the ground-based flight simulator available for piloted experiments at TU Delft, the SIMONA.

3.3.1. Pilot-in-the-loop experiment

In order to obtain the pilot-perceived handling qualities of an aircraft, a pilot-in-the-loop experiment needs to be performed. Since for the Flying-V currently no full-size prototype is available, the pilot-in-the-loop experiment has to be performed in a flight simulator resembling the Flying-V. Simulating a handling-quality experiment is an often used method in the conceptual design phase of an aircraft. It can be used to find the effect of an aircraft's geometry on its handling-qualities [26], but also to find, e.g., the effect of implementing a different flight control system to an existing aircraft [27].

Either a ground-based simulator can be used to simulate the aircraft dynamics [26][27], or an in-flight simulation in a simulator aircraft [28][10]. Although in-flight simulation was found to be of higher fidelity than ground-based simulation [29], the use of ground-based simulators has been validated to be useful for piloted handling quality evaluations [30].

The fidelity of a handling quality experiment in a flight simulator depends primarily on the cues presented to the pilot and whether they (would) match with in-flight cues. The cues themselves depend upon the accuracy of the models used in the simulation and the fidelity of the simulator systems [30]. State of the art ground-based flight simulators are widely used for pilot training due to their high cueing fidelity [31]. It can thus be stated that with sufficient effort put into making optimal use of a ground-based flight simulator, amongst others by using high fidelity dynamic models and cues, modern flight simulators have shown to provide an adequate alternative to in-flight piloted experiments.

3.3.2. SIMONA

The flight simulator available at the TU Delft, SIMONA, is a high fidelity, six degrees of freedom ground-based research simulator. SIMONA was initially developed for advanced research into simulation techniques, motion system control and navigation systems technologies [32]. Ever since, it has been used for a broad range of research such as piloted handling quality assessments [33] and pilot control behaviour research [34]. The SIMONA was shown to have correlated results to simulators leading in fidelity such as the Calspan Total In-Flight Simulator (TIFS) and the NASA Ames Vertical Motion Simulator (VMS) [30]. SIMONA thus is assumed to be of sufficiently high fidelity for the current development phase of the Flying-V to perform pilot-in-the-loop handling quality experiments.

The SIMONA research simulator is used in combination with DUECA (Delft University Environment for Communication and Activation). DUECA is middle-ware software, developed to facilitate the implementation of programs on a research flight simulator. Earlier architectures for real-time calculation and communication could only be used by experts in real-time programming, thus would require too much expertise from SIMONA users. DUECA simplifies the composition of a simulation or experiment using new or existing models and facilitates data access and timing of activation [35].

3.4. Flight Control Systems and Handling Qualities

The relevance of a pilot-in-the-loop experiment for the Flying-V depends on the findings of the theoretical handling quality and stability analysis. When the aerodynamic model is already theoretically found to be unstable and to have insufficient handling qualities, implementing this model into a piloted experiment is expected to yield the same subjective results. In order to take a first step in improving these handling qualities, and to obtain an aircraft which is (better) flyable in a piloted experiment, a Flight Control System was implemented. As stated in the introduction of this research, a flight control system can improve the handling qualities without the need to re-design the aircraft's control surfaces.

In a fly-by-wire control system, the flight control system converts the pilot inputs to control surface actuation. Due to the flight control system being in between the pilot and the control surfaces, indirect control surface control is possible. This yields opportunities for unconventional (i.e., not direct, mechanically linked) control. In this thesis, two of those opportunities are focused on: control allocation and stability augmentation. The first is discussed in subsection 3.4.1, the latter in subsection 3.4.2.

3.4.1. Control allocation and handling qualities

Control allocation determines which control surfaces depend on which pilot inputs. In essence, it determines which control surface contributes to the generation of which angular moments and by how much. Due to the lack of a conventional tail, the Flying-V control surfaces have a less clear pre-determined allocation than conventional wing-body-tail aircraft. Thus, a study into this control allocation can remarkably contribute to the overall control-effectiveness and controllability of the Flying-V. Earlier research on the control allocation of other flying-wings, such as the Blended-Wing-Body, showed the control allocation to have a large impact on the aircraft's command responses [36] and trim-drag [37].

The handling qualities of an aircraft are influenced by the control surface allocation. When the handling qualities prove to be limiting in the control surface sizing and design, control allocation can increase the control-effectiveness such that smaller control surfaces are required [38]. Analogous for a given

control surface design, the increase of control-effectiveness due to control allocation can improve the handling qualities at (previously) limiting aircraft manoeuvres during the handling quality assessment. This can potentially increase handling quality requirement compliance, by increasing the manoeuvrability performance at the edge of the flight-envelope. Despite, it has to be noted that a limited increase in overall control effectiveness is available with this method, since an optimal control allocation exists for each combination of control surfaces in a set manoeuvre.

3.4.2. Stability augmentation and handling qualities

Stability augmentation uses the aircraft flight-state to change the deflection of control surfaces. In this way, an aircraft can respond to condition changes without the pilot intervening. Stability augmentation can be used to increase aircraft stability, and is commonly used when the bare-airframe stability is found insufficient. As stated in Chapter 2, flying-wings are known for their limited lateral-directional stability. Research has shown stability augmentation to be suitable to improve this lateral-directional stability of flying wings [9][7][39].

When increasing the lateral-directional stability with the use of stability augmentation, the handling qualities of an aircraft can inherently be improved. Specifically the eigenmodes of an aircraft can be largely influenced by stability augmentation, by either improving an eigenmode's damping, frequency or both [9] [40]. Since the damping and frequency parameters of eigenmodes are part of the handling quality requirements as discussed in Section 3.1, implementing a stability augmentation system can considerably increase compliance to these requirements.

3.5. Key Takeaways

The previous sections provided an overview of aircraft handling quality assessment, handling quality requirements, handling quality simulation and handling quality improvement by means of a flight control system. From this, five key takeaways are most relevant for the next phase of this research.

1. For aircraft handling quality assessments, quantitative requirements on the stability and manoeuvrability are available as benchmark.
2. The handling qualities of an aircraft can be simulated both theoretically as well as experimentally, and the results can differ due to the latter being pilot-subjective.
3. A pilot-in-the-loop simulation of an aircraft model in a ground based simulator can be used to perform a pilot-subjective handling quality assessment.
4. The SIMONA research simulator at TU Delft is considered to have a sufficiently high fidelity to perform such a pilot-in-the-loop experiment.
5. A flight control system can improve the handling qualities of an aircraft without requiring a redesign of the aircraft.

4

Research Objectives & Overview

Different aspects of the thesis research are elaborated upon in this chapter. First, the research gap is discussed to show the opportunity for research in Section 4.1. Second, the goal of the research is elaborated upon in Section 4.2. Third, the associated research questions are presented in Section 4.3.

4.1. Research Gap

From the key-takeaways of Chapter 2 and 3 several research opportunities arise: the current Flying-V design requires a thorough assessment and potentially improvement of its lateral-directional handling qualities and stability. The first pilot-in-the-loop experiment of these lateral-directional handling qualities is relevant to perform, to both validate previously found theoretical handling qualities and stability by a piloted assessment, as to provide new experimental insights into these handling qualities. Modern flight simulators provide sufficient fidelity to perform a pilot-in-the-loop experiment, while eliminating the need for a prototype of a conceptual aircraft design. A pilot-in-the-loop experiment of the Flying-V is, however, specifically relevant when the used dynamical model theoretically has a minimum level of handling qualities and stability, i.e., is sufficiently flyable. Thus, the opportunity consists of three parts: first, the handling qualities and stability of the current Flying-V full scale aerodynamic model are theoretically assessed. Second, a prototype flight control system is implemented to take a first step in improving the stability and handling qualities without requiring a re-design of the aircraft. Third, the original model and improved model can be used to perform a pilot-in-the-loop handling quality experiment in a ground based flight simulator. This can provide new insights into the control and stability of the Flying-V and may bring the feasibility of the project a step further.

4.2. Research Goal

From the research gap as discussed in Section 4.1, the research goal is specified as follows.

> To investigate whether the Flying-V can meet the lateral-directional handling quality requirements of current conventional aircraft, by analytically assessing the bare airframe model of the Flying-V, developing a prototype flight control system as expected necessary for a relevant piloted experiment, and experimentally assessing the pilot perceived lateral-directional handling qualities.

The research objective contains a main goal, and three steps to attain this goal. The main goal, to assess whether the Flying-V can meet the lateral-directional handling quality requirements of current conventional aircraft, follows from the research gap, and is made measurable by taking the lateral-directional handling quality requirements of current conventional aircraft as benchmark. The three steps to attain this objective can be used to divide the objective into three sub-objectives. The **first sub-objective** is: To analytically assess the lateral-directional handling qualities of an aerodynamic model of the bare airframe Flying-V. This will provide insights into the baseline stability and handling qualities, and into the need for improving these.

From this follows the **second sub-objective**: To implement a prototype flight control system, consisting of stability augmentation systems and an improved control surface allocation, in the Flying-V model to improve the lateral-directional handling qualities. This implementation aims at yielding a theoretically (better) flyable model of the Flying-V with sufficient handling qualities for a relevant piloted experiment,

taking the handling qualities already one step further than those of the bare-airframe model.

Finally, the **third sub-objective** is: To experimentally assess the pilot-perceived lateral-directional handling qualities with a pilot-in-the-loop experiment. This pilot-in-the-loop experiment provides two research opportunities. First, the experiment is used to validate the theoretical findings on the lateral-directional handling qualities of the Flying-V, thus the method used to obtain these. Second, the experiment will be the first piloted assessment of the lateral-directional handling qualities of the Flying-V. It is thus expected to bring new insights into these handling qualities, the effect of a prototype flight control system and to show whether further design changes can be recommended to bring these handling qualities to a level sufficient for continuation of the Flying-V design program.

4.3. Research Questions

The main research question, which follows from the research goal, is as follows:

"Is the TU Delft Flying-V design capable of meeting the lateral-directional handling quality requirements of conventional commercial aircraft in a pilot-in-the-loop experiment?"

As was explained in the previous section, answering this question requires three steps. First, the lateral-directional handling qualities of the Flying-V must be theoretically (i.e., analytically) assessed, and second when necessary improved. Only then, third, a pilot-in-the-loop experiment is relevant to perform. This first step yields the following sub-question of the main research question:

> **Sub-question 1:** "When theoretically assessed, does the current bare airframe Flying-V model meet the lateral-directional handling quality requirements of conventional commercial aircraft?"

The handling quality requirements used consist of two parts: the eigen motion stability as specified in the military handbook MIL-HDBK-1797A by the USA department of defence [20] and the manoeuvrability requirements as specified in EASA CS-25 [21]. These two parts yield two further sub-questions.

> **Sub-question 1.a:** "When theoretically assessed, does the current bare airframe Flying-V model comply with the lateral-directional stability requirements of conventional commercial aircraft?"

> **Sub-question 1.b:** "When theoretically assessed, does the current bare airframe Flying-V model comply with the lateral-directional manoeuvrability requirements of conventional commercial aircraft?"

The second step in the research of the Lateral-Directional handling qualities of the Flying-V is designing a prototype flight control system, which aims at increasing the handling qualities without requiring a redesign of the Flying-V. This yields the following sub-question to the main research question:

> **Sub-question 2:** "When theoretically assessed, does the Flying-V model with a prototype flight control system implemented comply with the lateral-directional handling quality requirements of conventional commercial aircraft?"

The flight control system consists of a stability augmentation system and an adapted control allocation. Beforehand it is known that adapting the control surface allocation has no influence on the stability requirements, thus only the stability augmentation system can potentially improve the stability. The manoeuvrability requirements are influenced by both. Assessing the influence of both on the handling qualities of the Flying-V yields the following sub-questions:

> **Sub-question 2.a:** "When theoretically assessed, how does a stability augmentation system influence the current bare airframe model in complying with the lateral-directional stability requirements of conventional commercial aircraft?"

> **Sub-question 2.b:** "When theoretically assessed, how does including a stability augmentation system and adapting the control surface allocation influence the current bare airframe model in complying with the lateral-directional manoeuvrability requirements of conventional commercial aircraft?"

The third step in the research of the Lateral-Directional handling qualities of the Flying-V is assessing the pilot-perceived stability and handling qualities. This is done by a pilot-in-the-loop simulation, and yields the following sub-question to the main research question:

> **Sub-question 3:** "Are the lateral-directional handling quality requirements of conventional commercial aircraft met in a pilot-in-the-loop experiment of the Flying-V?"

Similar to the analytical part of the research question, the experimental part of the research has two aspects concerning the handling qualities: the eigenmode stability and the manoeuvrability. Following the same analogy as for Sub-questions 1.a to 2.b yields the following sub-questions 3.a to 3.d.

> **Sub-question 3.a:** "In a pilot-in-the-loop experiment, can the current bare airframe Flying-V model comply with the lateral-directional stability requirements of conventional commercial aircraft?"

> **Sub-question 3.b:** "How does a stability augmentation system influence the Flying-V model, in a pilot-in-the-loop experiment, in complying with the lateral-directional stability requirements of conventional commercial aircraft?"

> **Sub-question 3.c:** "In a pilot-in-the-loop experiment can the current bare airframe Flying-V model comply with the lateral-directional manoeuvrability requirements of conventional commercial aircraft?"

> **Sub-question 3.d:** "How do a stability augmentation system and an adapted control surface allocation influence the Flying-V model, in a pilot-in-the-loop experiment, in complying with the lateral-directional manoeuvrability requirements of conventional commercial aircraft?"

Sub-questions 1 and 2 will be answered, respectively, in Chapter 5 and 6. Next, in Chapter 7 a proposal is presented for an experiment aiming at answering sub-question 3.

5

Theoretical Handling Quality Analysis of the bare-airframe Flying-V

The theoretical handling quality evaluation discussed in Chapter 3 is used to assess the handling qualities of the bare-airframe Flying-V model, as was introduced in Chapter 2. The results of the theoretical handling quality evaluation answer sub-question 1, presented in Section 4.3. First, the application of the theoretical handling quality analysis to the Flying-V model is elaborated upon in Section 5.1. Second, the results of this analysis are presented in Section 5.2. Third, an overview of these results and the conclusions drawn from them are discussed in Section 5.3. Finally, the validation and verification performed to ensure correct results is presented in Section 5.4.

5.1. Theoretical Handling Quality Analysis Methodology

This section elaborates on the application of the theoretical aircraft handling quality analysis as discussed in Chapter 3 to the bare-airframe Flying-V. First, the assumptions on the different flight conditions tested are discussed in subsection 5.1.1. Second, the control allocation initially used in the Airbus VLM Flying-V model is discussed in subsection 5.1.2. Third, the evaluation of the handling quality requirements of MIL-HDBK-1797 [20], selected in Section 3.1, is discussed in subsection 5.1.3. Fourth the evaluation of the handling quality requirements of EASA CS-25 [21], again as selected in Section 3.1, is discussed in subsection 5.1.4.

5.1.1. Flight conditions

The flight conditions tested were chosen to be in line with earlier research [8], thus were based on the aerodynamic model as elaborated upon in subsection 2.3.1. Three different air speeds in Mach were used: Mach 0.2, 0.3 and 0.85. These are assumed to be applicable for, respectively, Approach, Take Off and Cruise condition. Table 5.1 shows an overview of these flight conditions, with their corresponding True Air Speed (TAS), altitude, air density and assumed aircraft weight (Maximum Take-Off Weight or Maximum Landing Weight).

Table 5.1: Flight condition assumptions.

Condition	TAS [Mach]	TAS [m/s]	Altitude [m]	Air Density [kg/m3]	Aircraft Weight
Approach	0.2	68.6	0	1.225	MLW
Take-Off	0.3	102.9	0	1.225	MTOW
Cruise	0.85	250.8	13000	0.2655	MTOW

5.1.2. Initial control allocation

As discussed in Section 3.4, a control allocation determines which control surfaces are deflected based on which pilot input. Since the aerodynamic model contains six control surfaces and three pilot inputs were assumed (two of the control column, one of the rudder pedals), an initial control allocation is required for simulation of the Flying-V. For this, a conventional control allocation was used, in line with previous research by Cappuyns [8]. The inboard elevons were allocated to respond to a longitudinal column input, providing a pitch moment by symmetrically deflecting these elevons. The outboard

elevons were allocated to respond to a sideway column input, providing a roll moment by asymmetrically deflecting the elevons. The rudders were allocated to respond to the rudder pedal input, providing a yaw moment by asymmetrically (but in the same body Y-direction) deflecting the rudders. Equation 5.1 represents this control allocation, and shows how the pilot inputs (pitch input δ_e, roll input δ_a and yaw input δ_r) were allocated to the control surface deflections (δ_{C1}, δ_{C2}, δ_{C3}, δ_{C4}, δ_{C5}, δ_{C6}).

$$\begin{bmatrix} \delta_{C1} \\ \delta_{C2} \\ \delta_{C3} \\ \delta_{C4} \\ \delta_{C5} \\ \delta_{C6} \end{bmatrix} = \begin{bmatrix} 0 & 0 & 1 \\ 0 & 1 & 0 \\ -1 & 0 & 0 \\ -1 & 0 & 0 \\ 0 & -1 & 0 \\ 0 & 0 & -1 \end{bmatrix} \cdot \begin{bmatrix} \delta_e \\ \delta_a \\ \delta_r \end{bmatrix} \tag{5.1}$$

5.1.3. MIL-HDBK-1797 requirements, theoretical assessment methodology

The handling quality requirements as stated by MIL-HDBK-1797 [20] are based on the damping and frequency parameters of the Flying-V's eigenmotions. As discussed in subsection 2.3.3, a straightforward procedure of obtaining these parameters is the linearisation of the equations of motion to obtain a linear state-space model. The aircraft was trimmed and linearised in all three flight conditions shown in subsection 5.1.1, and the A matrix of each state-space system was used to obtain the eigenvalues in each condition. Next, from the eigenvalues the damping and frequency parameters of each were determined, which were then paired to the corresponding eigenmotions based on their eigenvectors. [24] Finally, the damping and frequency parameters of each eigenmotion were used to check the handling quality level of the eigenmotion, described in MIL-HDBK-1797 [20] and Section 3.1.

5.1.4. EASA CS-25 requirements, theoretical assessment methodology

The handling quality requirements as stated by EASA CS-25 [21] are based on aircraft trim conditions and manoeuvre simulations in different flight conditions. It was chosen to keep all prescribed flight conditions fixed, and to find the trim state or specified time to perform a manoeuvre by varying (i.e., optimising) the control inputs and aircraft attitude. Besides, the engines were chosen to be used symmetrically when both are operative. The control surfaces were unconstrained for both trim and simulation. Next, the minimum control surface deflection required for trim or the tested manoeuvre was used to check whether the prescribed requirement can be met without excessive control surface deflections. For this, respectively, the trim and simulation methods as discussed in subsection 2.3.3 and subsection 2.3.2 were used. To determine which control surface deflections can be stated as excessive, earlier research from Cappuyns [8] and Castro [9] was used. Cappuyns uses a limit of ± 30 degrees for all control services. Castro uses different limits for different configurations of the researched blended-wing-body aircraft, however, the largest limits used were ± 37 degrees for the rudder deflection and ± 30 degrees for the elevon deflections. The latter are also deemed feasible for the Flying-V design, due to the conceptual similarity of the blended-wing-body design by Castro and the Flying-V.

5.2. Theoretical Handling Quality Analysis Results

In Section 3.1, seven requirements were selected for testing the lateral-directional handling quality of an aircraft. The results of theoretically assessing these, as elaborated upon in subsection 5.1.3 and 5.1.4, are discussed in the next seven subsections. For all requirements, the limiting cases are deemed most relevant, therefore only the results of the most forward and aft Centre of Gravity (CG) are presented. Of the results of the EASA CS-25 requirements, only the control surface deflections are presented in this section since these were used to check whether a requirement is met. The full trim-states can be found in Appendix D.

5.2.1. MIL-HDBK-1797 - Dutch Roll

Table 5.2 and Table 5.3 show the Dutch Roll damping and frequency parameters for the bare airframe Flying-V, trimmed and linearised in horizontal straight symmetric flight, for, respectively, the forward and aft CG location. The three conditions assessed were approach (APP) take-off (TO) and Cruise (CR),

using the flight conditions as elaborated upon in subsection 5.1.1. The Dutch Roll in most conditions shows a negative damping parameter, thus **does not comply** with any handling quality level requirement for Dutch Roll damping, as discussed in subsection 3.1.1. Only the Dutch Roll in cruise with the aft CG location has a positive damping, and complies with the Level 3 handling quality requirement.

Table 5.2: Bare Airframe Flying-V Dutch Roll Parameters, Forward CG.

	Damping Parameter [-]	Frequency [rad/s]
APP	-0.0698	1.05
TO	-0.0271	0.86
CR	-0.0107	0.811

Table 5.3: Bare Airframe Flying-V Dutch Roll Parameters, Aft CG.

	Damping Parameter [-]	Frequency [rad/s]
APP	-0.0758	0.899
TO	-0.0194	0.748
CR	0.00167	0.731

5.2.2. MIL-HDBK-1797 - Spiral Stability

Table 5.4 and Table 5.5 show the spiral stability time to double parameters for the bare airframe Flying-V, trimmed and linearised in horizontal straight symmetric flight, for, respectively, the forward and aft CG location. The three conditions assessed were approach (APP) take-off (TO) and cruise (CR), using the flight conditions as elaborated upon in subsection 5.1.1.

The spiral stability in cruise condition for the forward CG and for take-off and cruise condition in the aft CG were positively damped, thus have a negative time to double parameter, which represents the time to half the amplitude. The spiral stability in the other conditions have at least a time to double the amplitude of approximately 29 seconds. This is sufficient for the Level 1 handling qualities, as was shown in Table 3.3. Hence, all tested flight conditions **complies with the Level 1 requirement** of the spiral stability for all flight phase categories, as discussed in subsection 3.1.2.

Table 5.4: Bare Airframe Flying-V spiral stability time to double parameter, forward CG.

	T2 [s]
APP	27.9439
TO	447.4338
CR	-659.4537

Table 5.5: Bare Airframe Flying-V spiral stability time to double parameter, aft CG.

	T2 [s]
APP	44.3465
TO	-501.6434
CR	-379.0323

5.2.3. MIL-HDBK-1797 - Lateral Control Departure Parameter

Table 5.6 and Table 5.7 show Lateral Control Departure Parameter (LCDP) for the bare airframe Flying-V, trimmed and linearised in horizontal straight symmetric flight, for, respectively, the forward and aft CG location. The three conditions assessed were again approach (APP) take-off (TO) and cruise (CR). All three show a positive LCDP parameter, **thus complies with the requirement** as discussed in subsection 3.1.3.

Table 5.6: Lateral Control Departure Parameter for the bare airframe Flying-V, forward CG.

	LCDP [-]
APP	0.00393
TO	0.00116
CR	0.000751

Table 5.7: Lateral Control Departure Parameter for the bare airframe Flying-V, aft CG.

	LCDP [-]
APP	0.00234
TO	0.000957
CR	0.000677

5.2.4. CS25.143(h) - Coordinated Turn Capability

Table 5.8 and Table 5.9 show the trimmed input vectors for, respectively, the forward and aft CG location, for four different flight conditions trimmed in a Coordinated Turn (CTC): Take Off All Engines Operative (TO AEO), Approach All Engines Operative (APP AEO), Take Off One Engine Inoperative (TO OEI) and Cruise One Engine Inoperative (CR OEI). These conditions were elaborated upon in subsection 3.1.4, and also have constraints on the Gradient of Climb or Flight Path Angle. For the one engine inoperative conditions, the manoeuvre was performed in the most adverse direction, thus the worst cases were tested.

Although during the take-off and cruise condition the maximum acceptable control deflections were not exceeded, the approach condition differs. Here, for the inboard elevon deflection with the forward CG location, the maximum deflection found equals -52.9 degrees. This deflection is outside of the acceptable control surface deflections as stated in subsection 5.1.4, thus the aircraft **does not comply** with the requirements of the coordinated turn manoeuvre.

Table 5.8: Trimmed control input vectors in coordinated turn manoeuvre, forward CG.

	CTC TO AEO	CTC APP AEO	CTC TO OEI	CTC CR OEI
C1 [deg]	-0.4	7	6.5	3.1
C2 [deg]	-4.4	-17.3	2	0.2
C3 [deg]	-23.9	-52.9	-17.4	-19.8
C4 [deg]	-23.9	-52.9	-17.4	-19.8
C5 [deg]	4.4	17.3	-2	-0.2
C6 [deg]	0.4	-7	-6.5	-3.1
T1 [N]	55828.1	108201.1	105979.3	85447
T2 [N]	55828.1	108201.1	0	0

Table 5.9: Trimmed control input vectors in coordinated turn manoeuvre, aft CG.

	CTC TO AEO	CTC APP AEO	CTC TO OEI	CTC CR OEI
C1 [deg]	-0.7	4.9	7.4	4
C2 [deg]	-3.5	-14.2	1.2	-0.1
C3 [deg]	-5.7	-17.7	-3	-8.2
C4 [deg]	-5.7	-17.7	-3	-8.2
C5 [deg]	3.5	14.2	-1.2	0.1
C6 [deg]	0.7	-4.9	-7.4	-4
T1 [N]	60688.8	112868.6	112549.5	101849.8
T2 [N]	60688.8	112868.6	0	0

5.2.5. CS25.147(f) - Time to Bank, Roll Capability

Table 5.10 and Table 5.11 show the control surface deflections required during the time to bank (TTB) manoeuvre, respectively, for the forward and aft CG location. The manoeuvre requires rolling from a 30 degree banked horizontal turn to a 30 degree roll angle in the opposite direction, rolling a total of 60 degrees within the time specified in the last row of each table. For this manoeuvre, no servo dynamics were modelled. Hence, the real-time performance is expected to be worse due to a servo response time. As was elaborated upon in subsection 3.1.5, the maximum rudder deflection angle was limited to be equal to the maximum aileron deflection angle. It was chosen to limit the rudder deflection angle in the simulation to at most be equal in magnitude to the outboard elevons deflection angle. It was found that in this way the rudder considerably reduces the sideslip angle during a roll manoeuvre, without limiting the use of the outboard elevons.

The manoeuvre was performed for three different flight conditions: Approach All Engines Operative (APP AEO), Cruise All Engines Operative (CR AEO) and Take Off One Engine Inoperative (TO OEI). For the latter, the manoeuvre was performed in the most adverse direction, thus the worst case was tested. The maximum required control surface deflections were found by taking the sum of the trimmed control surface deflections and the minimum required deviation to perform the manoeuvre in the set time. Although during the take-off and cruise condition the maximum acceptable control deflections were not exceeded, the approach condition differs. Here, for the outboard elevon deflections, the maximum deflection found equals 99.5 degrees in approach with the aft CG location. For the inboard elevon deflections, the maximum deflection equals 51.6 degrees in approach with the forward CG location. For the rudders, the maximum deflection equals 90.6 degrees in approach with the aft CG location. All are outside of the acceptable control surface deflections as stated in subsection 5.1.4, thus the aircraft **does not comply** with the requirements of the time to bank manoeuvre.

Table 5.10: Control deflections in time to bank manoeuvre, forward CG.

	TTB APP AEO	TTB CR AEO	TTB TO OEI
C1 [deg]	23.1	10.8	20.9
C2 [deg]	-90.4	-11.3	-21.3
C3 [deg]	-51.6	-17.3	-19.9
C4 [deg]	-51.6	-17.3	-19.9
C5 [deg]	90.4	11.3	21.3
C6 [deg]	-23.1	-10.8	-20.9
T1 [N]	64075.5	26404.6	70246.9
T2 [N]	64075.5	26404.6	0
t BTB [s]	7	7	11

Table 5.11: Control deflections in time to bank manoeuvres, aft CG.

	TTB APP AEO	TTB CR AEO	TTB TO OEI
C1 [deg]	90.6	9.8	19.9
C2 [deg]	-99.5	-10.3	-19.2
C3 [deg]	-15.1	-6.9	-3.6
C4 [deg]	-15.1	-6.9	-3.6
C5 [deg]	99.5	10.3	19.2
C6 [deg]	-90.6	-9.8	-19.9
T1 [N]	79654	30900.6	75020.8
T2 [N]	79654	30900.6	0
t BTB [s]	7	7	11

5.2.6. CS25.161(d) - One Engine Inoperative Trim Condition

Table 5.12 and Table 5.13 show the control surface input vector trimmed with One Engine Inoperative (OEI) in horizontal flight, respectively, for the forward and aft CG location, for Approach (APP), Take Off (TO) and Cruise (CR) conditions.

The maximum elevon deflection found equals -41.8 degrees for the approach condition with the forward CG location, which exceeds the acceptable control surface deflection of 30 degrees as stated in subsection 5.1.4. Hence, the aircraft **does not comply** with the requirements of the One Engine Inoperative trim condition. It should be noticed, however, that both other conditions for the forward CG, and all conditions for the aft CG do meet the requirements.

Table 5.12: Trimmed control input vectors with one engine inoperative, forward CG.

	OEI TRIM APP	OEI TRIM TO	OEI TRIM CR
C1 [deg]	26.7	2.9	-0.4
C2 [deg]	5	-1	-8.8
C3 [deg]	-41.8	-15.4	-14.5
C4 [deg]	-41.8	-15.4	-14.5
C5 [deg]	-5	1	8.8
C6 [deg]	-26.7	-2.9	0.4
T1 [N]	112977.5	54963.1	45085
T2 [N]	0	0	0

Table 5.13: Trimmed control input vectors with one engine inoperative, aft CG.

	OEI TRIM APP	OEI TRIM TO	OEI TRIM CR
C1 [deg]	15.1	3.4	1.9
C2 [deg]	-11.2	-1.1	0.5
C3 [deg]	-9.3	-1.4	-5.4
C4 [deg]	-9.3	-1.4	-5.4
C5 [deg]	11.2	1.1	-0.5
C6 [deg]	-15.1	-3.4	-1.9
T1 [N]	127234.5	60240.4	47037.6
T2 [N]	0	0	0

5.2.7. CS25.177(c) - Steady Heading Sideslip

Table 5.14 and Table 5.15 show the trimmed input vector for, respectively, the forward and aft CG location, for six different flight conditions trimmed in a Steady Heading Sideslip (SHS): Take Off All Engines Operative (TO AEO), Cruise All Engines Operative (CR AEO), Approach All Engines Operative (APP AEO), Take Off One Engine Inoperative (TO OEI), Cruise One Engine Inoperative (CR OEI) and Approach One Engine Inoperative (APP OEI). For the one engine inoperative conditions, the manoeuvre was performed in the most adverse direction, thus the worst cases were tested.

The maximum elevon deflection found equals 80.9 degrees, the maximum rudder deflection found equals 66.7 degrees. Both are greatly outside of the acceptable control surface deflections as stated in subsection 5.1.4, thus the aircraft **does not comply with** the requirements of the steady heading sideslip manoeuvre.

Table 5.14: Trimmed control input vectors for different steady heading sideslip conditions, forward CG.

	SHS TO	SHS CR	SHS APP	SHS TO OEI	SHS CR OEI	SHS APP OEI
C1 [deg]	-10.9	-2.3	-66.7	-7.8	-0.8	-51.7
C2 [deg]	-33.2	-10.3	-78.5	-33.7	-10.5	-80.9
C3 [deg]	-15.4	-14.5	-36.5	-15.4	-14.5	-36.6
C4 [deg]	-15.4	-14.5	-36.5	-15.4	-14.5	-36.6
C5 [deg]	33.2	10.3	78.5	33.7	10.5	80.9
C6 [deg]	10.9	2.3	66.7	7.8	0.8	51.7
T1 [N]	27787.7	22618.1	48948.6	55565.3	45174.3	98064.3
T2 [N]	27787.7	22618.1	48948.6	0	0	0

Table 5.15: Trimmed control input vectors for different steady heading sideslip conditions, aft CG.

	SHS TO	SHS CR	SHS APP	SHS TO OEI	SHS CR OEI	SHS APP OEI
C1 [deg]	-9.4	-2.3	-41.5	-5.8	-0.5	-24.8
C2 [deg]	-29.5	-9.3	-71.3	-30.1	-9.5	-74
C3 [deg]	-1.4	-5.4	-7.5	-1.4	-5.4	-7.5
C4 [deg]	-1.4	-5.4	-7.5	-1.4	-5.4	-7.5
C5 [deg]	29.5	9.3	71.3	30.1	9.5	74
C6 [deg]	9.4	2.3	41.5	5.8	0.5	24.8
T1 [N]	30443.1	23638.1	53134.1	60863.8	47168.7	105774
T2 [N]	30443.1	23638.1	53134.1	0	0	0

5.3. Bare-Airframe Theoretical Assessment Conclusions

Table 5.16 shows an overview of the requirement compliance results, as were discussed in Section 5.2. Numerous requirements were not met. Three main findings, however, can be based on this overview. First, the Dutch Roll stability requirement was not complied with for most tested conditions and for both CG locations. It can thus be stated that a solution for this has to be found, which solves the Dutch Roll instability for all Flying-V operating conditions. Second, it can be noted that the approach (APP) condition with the forward CG location is a critical condition for most manoeuvres. This indicates a lack of control authority at low velocity since larger control deflections than feasible were found to be required to keep the aircraft trim in these conditions, or to perform the manoeuvre in the set time. Third, it can be noted that the steady heading sideslip requirement was not complied with in most conditions, indicating a lack of control authority during sideslip flight analogous to the lack of control authority at low velocity.

In summary, the theoretical handling quality analysis showed limited lateral-directional handling qualities and controllability for the bare-airframe Flying-V. This was as expected from earlier research, as discussed in Chapter 2. The theoretical compliance with the requirements simulated was of a poor level and the current bare-airframe Flying-V model is expected to have equally limited handling qualities in a piloted handling quality experiment.

Table 5.16: Overview of theoretical handling quality assessment of bare-airframe Flying-V, requirement compliance.

Requirement	Compliance	Critical Condition(s)	Critical CG(s)
Dutch Roll Stability	Failed	APP, TO, CR	Forward, Aft
Spiral Stability	Passed	-	-
Lateral Control Departure	Passed	-	-
Coordinated Turn Capability	Failed	APP AEO	Forward
Time to Bank, Roll Capability	Failed	APP AEO	Forward, Aft
One Engine Inoperative Trim	Failed	APP	Forward
Steady Heading Sideslip	Failed	APP AEO & OEI, TO AEO & OEI	Forward, Aft

5.4. Analysis Validation and Verification

The theoretical handling quality analysis performed in the previous sections was validated and verified in several steps. First, the aerodynamic model was validated by comparing the eigenmode parameters to those of a reference aircraft, shown in subsection 5.4.1. Second, the implementation of the model was verified by comparing the eigenmode parameters to those of an earlier model implementation, shown in subsection 5.4.2. Finally, the linearisation of the non-linear model implementation was verified in multiple steps, shown in subsection 5.4.3.

5.4.1. Model validation

By linearising the bare-airframe Flying-V model, as discussed in subsection 2.3.3, eigenvalues of the eigenmodes can be obtained. As a validation of the model implementation, these can be compared to

reference eigenvalues as provided by Etkin [24] for a Boeing 747 aircraft. This can show whether the model of the Flying-V shows similar behaviour to conventional aircraft. However, since the unconventional Flying-V geometry and dimensions differ considerably from a Boeing 747, the eigenvalues are also expected to differ. Moreover, the reference eigenvalues are provided for Mach 0.8 at 40,000 ft (12,192 m), which differs slightly from the Flying-V cruise condition of Mach 0.85 at 13,000 m, as was shown in Table 5.1.

Table 5.17 shows the eigenvalues of the eigenmodes in cruise as provided by Etkin [24] for a B747. Table 5.18 shows the eigenvalues of the eigenmodes in cruise for the Flying-V with the CG location aft, as determined from linearising the bare-airframe Flying-V model. When comparing these eigenmodes, it was found that in general, both aircraft behave similarly in the different eigenmodes. The phugoid mode has a similar frequency, but is less damped for the Flying-V. This can be attributed to the lack of a conventional horizontal tail surface for the Flying-V, which has less horizontal tail surface and less longitudinal stability. The short period mode has a similar damping and frequency parameter, thus shows similar behaviour for both aircraft. The spiral mode is non oscillatory for both aircraft, with the Flying-V having a lower time constant. This can be attributed to the absence of a vertical tail, yielding less roll axis stability. The roll convergence for both aircraft is similar. Finally, the Dutch Roll has a similar frequency for both aircraft, but a smaller damping for the Flying-V. This can also be attributed to the absence of a vertical tail for the Flying-V, which decreases the weather-vane stability, hence the Dutch Roll stability.

Table 5.17: B747 Reference Eigenmodes from Etkin [24].

	Eigenvalue	Damping [-]	Frequency [rad/s]
Phugoid Mode	-0.00329 $\pm$ 0.06723*i*	0.04886	0.06731
Short Period	-0.3719 $\pm$ 0.8875*i*	0.38648	0.96227
Spiral Mode	-0.00730	1	0.00730
Roll Convergence	-0.56248	1	0.56248
Dutch Roll	-0.03301 $\pm$ 0.94665*i*	0.03485	0.94722

Table 5.18: Flying-V Eigenmodes in cruise with aft CG location, from linearised model.

	Eigenvalue	Damping [-]	Frequency [rad/s]
Phugoid Mode	-0.00037 $\pm$ 0.05305*i*	0.00704	0.05305
Short Period	-0.43522 $\pm$ 1.34442*i*	0.30798	1.41312
Spiral Mode	-0.00183	1	0.00183
Roll Convergence	-0.57919	1	0.57919
Dutch Roll	-0.00122 $\pm$ 0.73149*i*	0.00167	0.73149

5.4.2. Model implementation verification

Similar to the validation of the model implementation in the previous subsection, by comparing the eigenmode parameters to Etkin's reference aircraft, the Flying-V model implementation was verified by comparing the eigenmode parameters to an earlier Flying-V model implementation. As was discussed in Section 2.4, Cappuyns performed earlier research on the handling qualities of the Flying-V. From this also followed eigenmode eigenvalues and parameters, from which the ones in cruise condition are shown in Table 5.19. Comparing these eigenvalues to the ones in Table 5.18 shows similar Short Period, Spiral and Roll Convergence behaviour, but differences in the Phugoid Mode damping and Dutch Roll damping. This difference could follow both from a difference in the analysis performed, as well as from the model being updated between the analysis of Cappuyns and the one in this report. Moreover, it is unclear which aircraft weight Cappuyns used for the determination of the eigenvalues in cruise, which influences the eigenvalues indirect but considerably. Hence, the difference was considered acceptable to continue research.

Table 5.19: Flying-V Eigenmodes as found by Cappuyns [8].

	Eigenvalue	Damping [-]	Frequency [rad/s]
Phugoid Mode	-0.0007 $\pm$ 0.026*i*	0.03	0.03
Short Period	-0.441 $\pm$ 1.28 *i*	0.33	1.36
Spiral Mode	-0.005	1	0.01
Roll Convergence	-0.7	1	0.7
Dutch Roll	0.018 $\pm$ 0.688*i*	-0.03	0.69

5.4.3. Linearisation verification

Different methods were used to verify whether the linearisation of the non-linear model was performed correctly, thus to verify if simulating the linearised model is sufficiently similar to simulating the non-linear model. First, the time responses to different control input disturbances of the linear and non-linear model were compared graphically. Second, from the non-linear time response the eigenmode frequency and decay ratio were obtained and compared to the parameters of the linear model. Finally, a numeric linearisation was performed to approximate the analytical linearisation, and the correspondence of the obtained eigenvalues was assessed. Due to the sufficiently close approximation of the linearisation to the non-linear simulation, as is shown in the following subsections, it is assumed to be sufficient for the scope of this research.

Time response comparison non-linear and linearised model

By simulating different control input disturbances on trimmed conditions in the linear and non-linear model, the output of both can be graphically compared. For this impulse (block) disturbances of one second were used, with five degrees deflection, respectively, on the inner elevons or the rudders. The impulse on the inner elevons initialises the short period and phugoid eigenmode, the impulse on the rudders initialises the roll subsidience, spiral and Dutch Roll eigenmodes. The angular time responses of the non-linear and linear model were graphically compared, and the linear approximation was evaluated. The verification was performed for all centre of gravity locations. However, in order to limit the size of this section, only the results for the forward CG location are shown and discussed. The results for the aft CG location were either better or similar.

Figure 5.1, 5.2 and 5.3, respectively, show the angular response to a five degree inner elevons impulse of one second in approach, take-off and cruise condition. It can be noted that due to the limited longitudinal-lateral cross influence of the aircraft states, only the pitch angle deviates due to the elevator input. Furthermore, the time responses show the difference in pitch angle response of the linear and non-linear model to be very similar. For approach and cruise condition, the difference is barely graphically noticeable. In take-off condition the difference can be seen more evident, but is still considerably smaller than the actual angular response.

Figure 5.4, 5.5 and 5.6, respectively, show the angular response to a five degree rudders impulse of one second in approach, take-off and cruise condition. Similar to the elevator input pitch-angle responses in approach and cruise condition shown in Figure 5.1 and 5.3, the rudder input roll and yaw angle responses in take-off and cruise condition shown in Figure 5.5 and 5.6 have a barely noticeable difference between the linear and non-linear model response. The rudder input roll and yaw angle response in approach condition as shown in 5.6 have a more evident difference between the linear and non-linear model, but this difference is again still considerably smaller than the actual angular response, and assumed sufficiently small for the scope of this research.

Comparing the time-responses graphically provides a first qualitative evaluation of the linearisation of the non-linear model. This was of good use as a first verification of the linearisation results, but further quantitative analysis was required to verify the use of the linearisation for the handling quality evaluation.

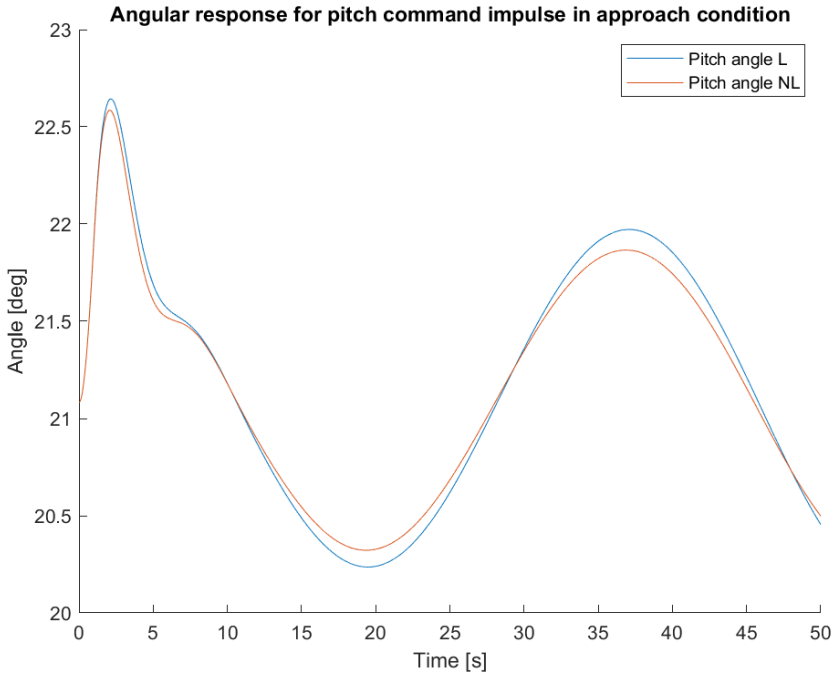

Figure 5.1: Angular time response to a five degree elevator impulse of one second in approach conditions, linearised model (L) and non-linearised model (NL).

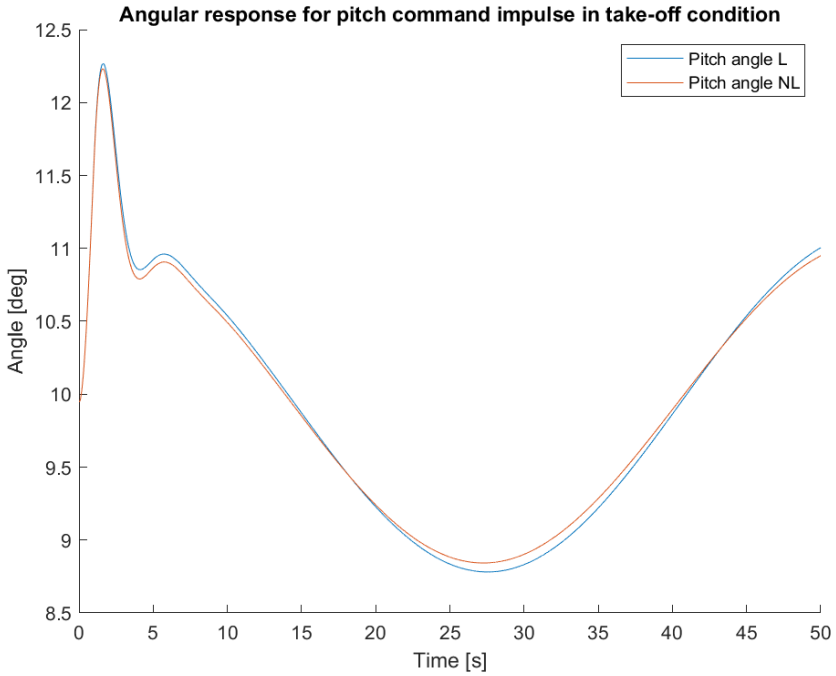

Figure 5.2: Angular time response to a five degree elevator impulse of one second in take-off conditions, linearised model (L) and non-linearised model (NL).

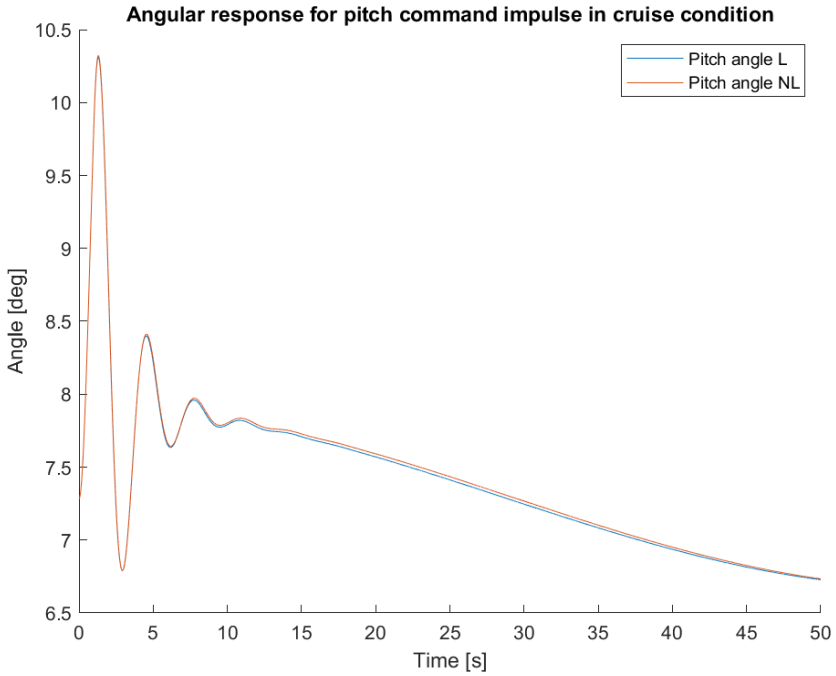

Figure 5.3: Angular time response to a five degree elevator impulse of one second in cruise conditions, linearised model (L) and non-linearised model (NL).

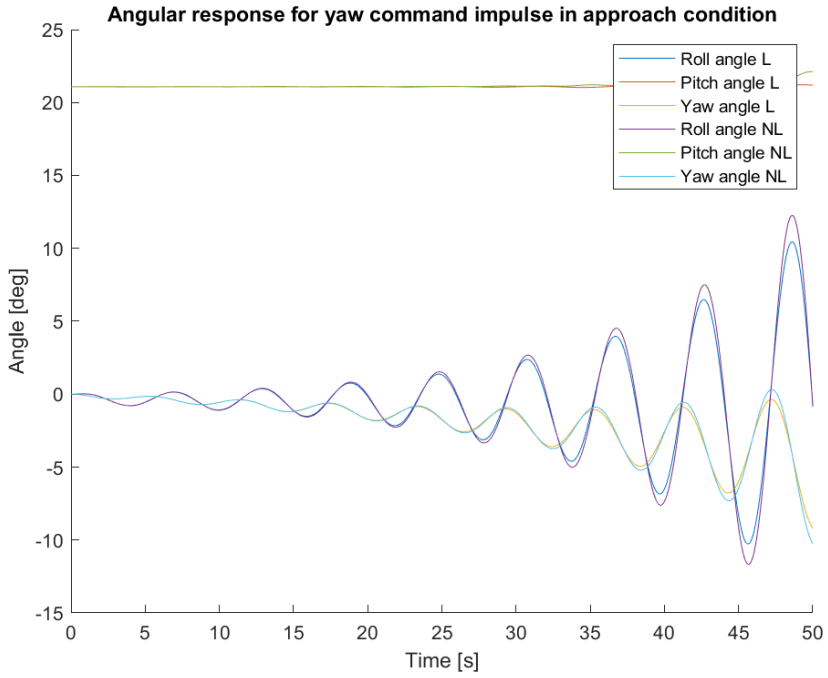

Figure 5.4: Angular time response to a five degree rudder impulse of one second in approach conditions, linearised model (L) and non-linearised model (NL).

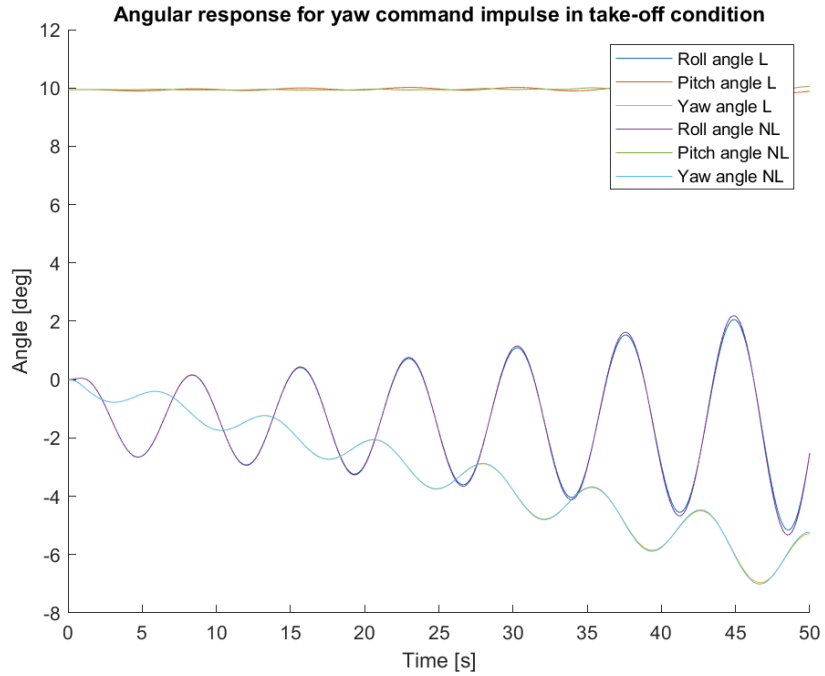

Figure 5.5: Angular time response to a five degree rudder impulse of one second in take-off conditions, linearised model (L) and non-linearised model (NL).

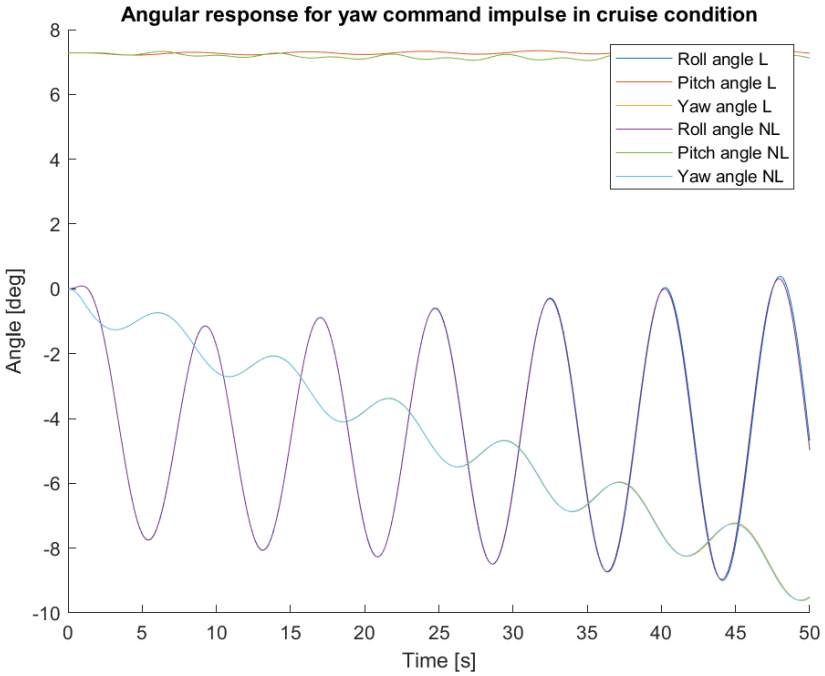

Figure 5.6: Angular time response to a five degree rudder impulse of one second in cruise conditions, linearised model (L) and non-linearised model (NL).

Dutch Roll damping and frequency parameter comparison non-linear and linearised model
Since the non-linear model is linearised to determine the different eigenmode damping and frequency parameters, a quantitative evaluation comparing these parameters of the linear and non-linear model was performed to verify this use.

Since the linearisation of the non-linear model yielded a state space system, as elaborated upon in subsection 2.3.3, the damping and frequency parameters can be directly obtained from the eigenvalues of the A matrix of the state space system. Then, based on the state contributions in the eigenvectors, each eigenvalue can be assigned to the corresponding eigenmode.

For the non-linear model, the damping and frequency parameters can't be directly obtained. However, the time responses of the non-linear model to control input disturbances, as were shown earlier in this section, can be used. First, an oscillatory angular response was used to determine the period of oscillation (P) of the response, which can later be used to compare to the frequency parameter of the linear model. The damping parameter of the response can't be directly obtained from the time response, thus the decay ratio was determined based on the change in amplitude of the response over time[1]. Figure 5.7 illustrates an oscillatory under-damped response, with the determination of amongst others the period of oscillation and Decay Ratio shown.

To be able to compare the period of oscillation and decay ratio obtained from the non-linear model time response to the frequency and damping parameter of the linear model state-space system, Equations 5.2 and 5.3 were used. Equation 5.2 determines the frequency parameter of the non-linear time response, which can be compared tot the one of the linear state-space system. Equation 5.3 determines the decay ratio of the linear state-space system damping parameter, which can be compared to the non-linear time responses decay ratio[1].

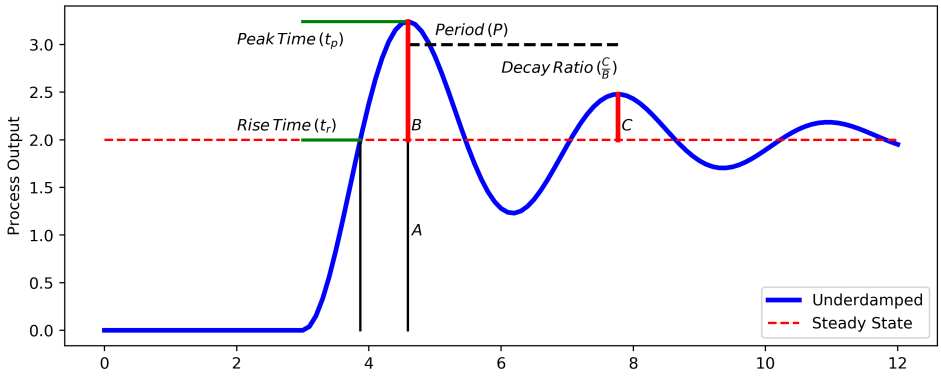

Figure 5.7: Graphical determination of period of oscillation and decay ratio[1].

$$\omega = \frac{2\pi}{P} \tag{5.2}$$

$$DR = e^{-2\pi\zeta \frac{1}{\sqrt{1-\zeta^2}}} \tag{5.3}$$

The aforementioned was implemented to verify the Dutch Roll parameters found from the linearised model in different flight conditions. The time responses shown in Figures 5.4, 5.5 and 5.6 were used to determine the Dutch Roll period, its frequency, and decay ratio from the non-linear simulation in the different flight conditions. Next, the model was linearised and the Dutch Roll frequency and damping, yielding the Decay Ratio, were obtained from the linearised model eigenvalues. Table 5.20 shows the

[1]obtained from `https://apmonitor.com/pdc/index.php/Main/SecondOrderGraphical`

results from this analysis. From the percentual difference (shown as *Diff [%]*) between the non-linear and linear decay ratio's and frequencies, it can be seen that the linear approximation of the parameters mostly deviates even less than one percent from the non-linear response. Only the decay parameter in approach condition deviates more, approximately 2 percent, which is still considered as a close approximation. It is thus concluded that the linearised system can be assumed to approximate the eigenmode parameters sufficiently.

Table 5.20: Dutch Roll decay ratio and frequency parameters obtained from the linear (L) model and non-linear (N.L.) time simulation.

	Decay N.L. [-]	Decay L. [-]	Diff [%]	ω N.L. [rad/s]	ω L. [rad/s]	Diff [%]
DR APP	1.587	1.552	2.194	1.054	1.058	-0.3503
DR TO	0.9858	0.9804	0.5468	0.8593	0.858	0.1504
DR CR	0.9098	0.9107	-0.09755	0.8298	0.8285	0.1495

Comparison analytically and numerically linearised models
Next to the analytical linearisation as was elaborated upon in subsection 2.3.3, a numerical approximation to this linearisation can be performed to verify the analytical method. As discussed in Appendix B, the state matrix A was determined by assessing the influence of each state in x on the different state derivatives in $\dot{x}$. Thus, entry (i, j) of matrix A represents the influence of state x_j on the derivative of state x_i, i.e., $\dot{x}_i$. This influence can be numerically approximated by varying each state in x, and looking at the change a small deviation in each state causes in each state derivative $\dot{x}_i$ by applying the equations of motion. Similar to the analytical linearisation, the numerical approximation was performed from a trimmed aircraft state.

Analogous to the previous subsection, the Dutch Roll eigenmode parameters are compared to assess the different results of both linearised models. The damping and frequency parameters follow directly from the eigenvalues of the state-space system A matrix of both linearised models. Table 5.21 shows these parameters for both systems, in approach, take-off and cruise conditions. It can be noted that the frequency results were similar (all with less than 0.3% difference), but a larger difference is present at the damping parameters. The maximum difference in the damping parameter is approximately -3%, which is still considered as acceptable for the scope of this thesis since it does not alter the conclusions drawn on the Dutch Roll stability.

Table 5.21: Dutch Roll damping and frequency parameters obtained from the analytically linearised model (An.) and numerically linearised model (Num.).

	ζ An. [-]	ζ Num. [-]	ζ diff [%]	ω An. [rad/s]	ω Num [rad/s]	ω diff [%]
DR APP	-0.08631	-0.08906	-3.178	1.067	1.064	0.2359
DR TO	-0.02712	-0.02768	-2.029	0.8603	0.8602	0.01362
DR CR	-0.0107	-0.01085	-1.407	0.8109	0.8109	0.0005907

5.4.4. Zero-lift drag C_{d_0}

The aerodynamic model obtained from Airbus, as was discussed in Section 2.3, was developed using the Vortex Lattice Method (VLM). This method determines the lift and induced drag based on computational fluid dynamics [41], with as input the Flying-V geometry, attitude and flow conditions. The VLM simulation has as outputs the lift estimate and lift induced drag, thus no zero-lift drag is present in the model. To assess the influence of including zero-lift drag on the handling quality assessment results, the bare-airframe theoretical handling quality assessment was re-performed while including a zero-lift drag estimate of the Flying-V by Faggiano [5]. This zero-lift drag estimate was based on semi-empirical equations for conventional aircraft, thus its fidelity is uncertain. Nevertheless, it was the only zero-lift drag estimate available for the full-size Flying-V, thus used to test the effect on the handling quality analysis.

For the re-assessment of the bare-airframe handling qualities, the zero-lift drag was implemented in the aerodynamic model by addition to the (normalised) force coefficient in the backward aerodynamic

frame X-axis. The value used for the zero lift drag, C_{d_0}, is 0.00572.

Elaborate results of the handling quality assessment with the zero-lift drag included are shown in Appendix E, but the interpretation of the results can be summarised as follows. The zero-lift drag has a primary effect on the thrust setting, since more thrust is required to compensate for the extra drag due to the zero-lift drag component. This has a limited effect on the lateral-directional eigenmodes, thus a small effect on the Dutch Roll damping and frequency and the spiral stability. Next, a larger effect was found on all trim states with a one engine inoperative condition. The higher thrust setting generates a larger moment around the yaw and pitch axis, yielding higher control surface deflections required to keep the aircraft in trim. This effect on the control surface deflections, however, did not change any of the requirement compliance outcomes. For the other trim states, with all engines operative, a small effect was present.

Since the zero-lift drag magnitude is uncertain, it was decided not to augment the VLM aerodynamic model with the zero-lift drag for further research, but to use the VLM aerodynamic model as initially obtained. In this way, the absence of the zero-lift drag in the model is known, instead of implementing a zero-lift drag with unknown error. The general effect of including a zero-lift drag, however, was found, thus can be taken into account when drawing conclusions from further analyses and from the results of the experiment proposed in Chapter 7.

5.5. Key Takeaways

From the theoretical handling quality assessment of the lateral-directional handling qualities of the bare-airframe Flying-V, four key takeaways were found most relevant.

- Compliance with the assessed handling quality stability and manoeuvrability requirements differs per requirement, centre of gravity location and flight condition.
- The Dutch Roll stability showed to be insufficient for all flight conditions and both centre of gravity locations assessed.
- Insufficient control authority was found available in approach conditions, thus at low velocity flight.
- Insufficient control authority was found available in sideslip flight.

6

Flight Control System Design

Using the results of the theoretical handling quality analysis of the bare airframe Flying-V as discussed in Chapter 5, a prototype flight control system was designed. This aims at taking the handling qualities one step further than those from the bare airframe Flying-V, yielding the opportunity for a more relevant piloted experiment. Designing a prototype flight control system follows from the second sub-objective of the thesis research, as was presented in Section 4.2. The results of the prototype flight control system implementation on the theoretical handling qualities of the Flying-V answer sub-question 2, as was shown in Section 4.3.

As stated in Section 5.3, three main findings arised from the theoretical handling quality analysis of the bare airframe Flying-V. First, the Dutch Roll instability in (almost) all conditions. Second, the insufficient control authority at low velocity. Third, the insufficient control authority at sideslip angles. The flight control system design strategy follows from these three findings. To counteract the lack of control authority, both at low velocity and at sideslip angles, the overall control effectiveness is increased with an adapted control allocation. To counteract the Dutch Roll instability, a stability augmentation system is designed. By combining the adapted control allocation with the stability augmentation system, the final flight control system prototype is obtained.

First, the adapted control allocation design and the effect on the handling qualities of this adapted control allocation is discussed in Section 6.1. Second, the stability augmentation system design and the effect on the handling qualities of this stability augmentation system is discussed in Section 6.2. Finally, an overview of the combined effect of the final flight control system prototype is shown in Section 6.3.

6.1. Control Allocation

As discussed in Section 3.4, control allocation determines which control surfaces are deflected based on which pilot input. In essence, it determines which control surface contributes to the generation of which angular moments and by how much. Due to the lack of a conventional tail, the Flying-V control surfaces have a less clear pre-determined allocation than conventional wing-body-tail aircraft. An opportunity exists of using these control surfaces more effectively than the initial allocation, which was shown in subsection 5.1.2. The adapted control allocation can increase the overall control effectiveness of the Flying-V, increasing the control authority around the different control axes. First, the design of the adapted control allocation is discussed in subsection 6.1.1. Next, the effect on the theoretical handling quality results is discussed in subsection 6.1.2.

6.1.1. Adapted control allocation design

The initial control allocation used for the bare-airframe theoretical handling quality analysis was discussed in subsection 5.1.2. This initial allocation was based on previous research [8] and is analogous to the control allocation of conventional aircraft, where an elevator controls the pitching moment, the ailerons the rolling moment and the rudder the yawing moment. This conventional allocation is called explicit ganging in literature [42], and assigns each control surface to a specific moment direction based on the designer choice. Due to the unconventional control surfaces of the tailless Flying-V, an opportunity of improving the control effectiveness with an unconventional Control Allocation exists.

The aerodynamic model contains six control surfaces, and for the new control allocation again three pilot inputs (two of the control column, one of the rudder pedals) were assumed. These pilot inputs were assumed to still control, respectively, pitch, roll and yaw control, but unconventional control of these axes using the control surfaces was researched.

Numerous control allocation methods can be found in literature [43] [36]. These allocation methods vary in linear and non-linear methods, with unconstrained allocation or numerically optimised constrained allocation. Due to the flight control system being designed as a prototype, and while accounting for regulatory compliance difficulties for conventional aircraft, it was chosen to limit the scope to linear, unconstrained control allocation methods.

From literature research, it was found that three linear unconstrained control allocation methods are most common: explicit ganging, daisy chaining and the generalized inverse [36][42]. As stated earlier this section, explicit ganging assigns each control surface to a specific moment direction based on the designer choice. Hence, this method is very dependent on the designers view on control allocation and does not take into account optimal use of the control surfaces. Daisy chaining is an analogous method to control ganging, but uses second and third allocations to assist saturated control surfaces with others. Again, this method is very dependent on the designers view on control allocation. The generalized inverse method is independent of the designers view on control allocation and takes into account the control effectiveness of each control surface for each moment axis. Because of this, it was chosen as most promising for applying to the unconventional control surfaces of the Flying-V. Moreover, the generalized inverse method can be found in literature as solution for the control allocation of aircraft with unconventional control surfaces. Amongst others Denieul [38] used the generalized inverse to design the control allocation of a blended-wing-body and Oppenheimer [44] used the generalized inverse for the control allocation of over-actuated systems.

As stated above, the generalized inverse method uses the control effectiveness of each control surface in each moment direction to distribute the roles of controlling these moments between the control surfaces. The control effectiveness matrix, as shown in Equation 6.1, is a 3 by 6 matrix holding the derivatives of the moments around the Y, X and Z body axes, respectively, m, l and n, with respect to each of the six control surfaces. This matrix can be obtained by linearising the aircraft around a trimmed state, and second obtaining the coefficients of Equation 6.1 by assessing the difference in moment output from small deviations of the control surface deflection. Second, the control effectiveness matrix is used to determine the control allocation matrix K_{alloc}. This can either be done using the unweighted pseudo-inverse of the control allocation, as shown in Equation 6.2, or using the weighted pseudo-inverse of the control allocation, as shown in Equation 6.3. The unweighted pseudo-inverse assumes no preferences of control surface use with respect to each other, where the weighted pseudo-inverse provides the opportunity to weigh the different control surfaces using a 6 by 6 matrix W, such that preferred control surfaces can be used to a larger extent than less preferred. This can for example be useful when it is found that certain control surfaces saturate more often than others, and a re-distribution of the control surface use has to be made. Finally, Equation 6.4 shows how the control allocation matrix K_{alloc} is used to convert pilot inputs to the control surface deflections. Here, $\delta_{m_{equi}}$, $\delta_{l_{equi}}$ and $\delta_{n_{equi}}$, respectively, represent an equivalent pitch, roll or yaw moment desired to obtain from one of the pilot inputs. These were used for scaling, to prevent disproportional aircraft responses to the pilot inputs.

As stated above, obtaining the control effectiveness matrix requires linearising the aircraft dynamics around a trimmed aircraft state. The aircraft state used for trimming was chosen to be the cruise condition with the aft CG position. This condition is expected to be the most occurring condition during the aircraft mission, thus optimising for this condition is expected to yield the least overall drag. This was confirmed by performing the handling quality analysis with the different control effectiveness matrices. The one trimmed in cruise condition with the aft CG position yielded the least thrust required and generally the smallest control deflections when taking into account all manoeuvres and conditions. Moreover, the control allocation matrix as trimmed in approach condition with the forward CG position, i.e., the other limit of trim conditions available, yielded a counter-intuitive control allocation. The rudder control derivatives become inconsistent at larger angles of attack, yielding the control effectiveness matrix not

being consistent with standard operations, and next yielding a counter-intuitive control allocation.

$$B = \begin{bmatrix} C_{m_{\delta c1}} & C_{m_{\delta c2}} & C_{m_{\delta c3}} & C_{m_{\delta c4}} & C_{m_{\delta c5}} & C_{m_{\delta c6}} \\ C_{l_{\delta c1}} & C_{l_{\delta c2}} & C_{l_{\delta c3}} & C_{l_{\delta c4}} & C_{l_{\delta c5}} & C_{l_{\delta c6}} \\ C_{n_{\delta c1}} & C_{n_{\delta c2}} & C_{n_{\delta c3}} & C_{n_{\delta c4}} & C_{n_{\delta c5}} & C_{n_{\delta c6}} \end{bmatrix} = \begin{bmatrix} \frac{dm}{d\delta_{c1}} & \frac{dm}{d\delta_{c2}} & \frac{dm}{d\delta_{c3}} & \frac{dm}{d\delta_{c4}} & \frac{dm}{d\delta_{c5}} & \frac{dm}{d\delta_{c6}} \\ \frac{dl}{d\delta_{c1}} & \frac{dl}{d\delta_{c2}} & \frac{dl}{d\delta_{c3}} & \frac{dl}{d\delta_{c4}} & \frac{dl}{d\delta_{c5}} & \frac{dl}{d\delta_{c6}} \\ \frac{dn}{d\delta_{c1}} & \frac{dn}{d\delta_{c2}} & \frac{dn}{d\delta_{c3}} & \frac{dn}{d\delta_{c4}} & \frac{dn}{d\delta_{c5}} & \frac{dn}{d\delta_{c6}} \end{bmatrix} \tag{6.1}$$

$$K_{alloc} = B^T(BB^T)^{-1} \tag{6.2}$$

$$K_{alloc,W} = W^{-1}B^T(BW^{-1}B^T)^{-1} \tag{6.3}$$

$$\begin{bmatrix} \delta_{C1} \\ \delta_{C2} \\ \delta_{C3} \\ \delta_{C4} \\ \delta_{C5} \\ \delta_{C6} \end{bmatrix} = K_{alloc} \cdot \begin{bmatrix} \delta_e \cdot \delta_{m_{equi}} \\ \delta_a \cdot \delta_{l_{equi}} \\ \delta_r \cdot \delta_{n_{equi}} \end{bmatrix} \tag{6.4}$$

6.1.2. Control allocation adaptation results

Altering the control allocation potentially improves the control effectiveness of an aircraft [38], thus allows a given control surface design to improve the handling qualities at (previously) limiting aircraft manoeuvres during the handling quality assessment. This performance increase can increase the handling qualities such that more requirements on aircraft trim state and manoeuvre simulation can be met. On the contrary, adapting the control allocation does not influence the stability of the eigenmodes of an aircraft. Control allocation only takes effect in translating pilot inputs to control surface deflections, while the eigenmode stability is determined without a pilot input. Hence, from the results of adapting the control allocation on the theoretical handling quality assessment, only the EASA CS-25 manoeuvrability requirements will be discussed in this section.

In order to show the effects of the adapted control allocation briefly, while not presenting all results as elaborate as already done in Section 5.2, the results shown in this section focus on the effects on the conditions found critical in the bare-airframe theoretical handling quality assessment of Chapter 5. These conditions were shown in Table 5.16 in Section 5.3.

Equation 6.5 shows the obtained control allocation matrix K_{alloc}, based on the control effectiveness matrix of the aircraft trimmed in cruise with the aft CG location. Using the equivalent moments $\delta_{m_{equi}}$, $\delta_{l_{equi}}$ and $\delta_{n_{equi}}$, each column of the control allocation matrix was scaled such that the largest magnitude equals 1, such that the relative control allocation is more apparent. This does not limit the use of the controls, since the scaling and limiting of the pilot inputs will be performed in the piloted experiment preparation. Hence, in the trim states shown further in this section, the magnitudes of each pilot input δ_e, δ_a and δ_r is less important than their sign and relative magnitude to each other.

$$\begin{bmatrix} \delta_{C1} \\ \delta_{C2} \\ \delta_{C3} \\ \delta_{C4} \\ \delta_{C5} \\ \delta_{C6} \end{bmatrix} = K_{alloc} \cdot \begin{bmatrix} \delta_e \cdot \delta_{m_{equi}} \\ \delta_a \cdot \delta_{l_{equi}} \\ \delta_r \cdot \delta_{n_{equi}} \end{bmatrix} = \begin{bmatrix} -0.046 & -0.439 & 1.000 \\ -0.601 & 0.496 & 0.150 \\ -1.000 & 1.000 & -0.179 \\ -1.000 & -1.000 & 0.179 \\ -0.601 & -0.496 & -0.150 \\ -0.046 & 0.439 & -1.000 \end{bmatrix} \cdot \begin{bmatrix} \delta_e \\ \delta_a \\ \delta_r \end{bmatrix} \tag{6.5}$$

Table 6.1 shows the effect of adapting the initial (conventional) control allocation on the critical condition of the coordinated turn capability requirement, of which the previous results were shown in subsection 5.2.4. A clear re-distribution of the use of the control surfaces can be seen. The total control servo

use was spread over more control surfaces, and the maximum deflection used is decreased from 52.9 degrees to 46.0 degrees. Although this is a substantial decrease in maximum deflection, the actuator limit set of 30 degrees for the inner elevons was still not attained, thus the condition remains critical. This implicates that a redesign of the inner elevons is required to comply with the requirement.

Table 6.1: Control Allocation effect on critical Coordinated Turn trim condition.

Manoeuvre	Coordinated Turn	
Condition	APP AEO	
CG	Forward	
CA	Conventional	Adapted
δ_e [-]	52.9	37.2
δ_a [-]	-17.3	-8.4
δ_r [-]	7.0	2.0
C1 [deg]	7.0	4.0
C2 [deg]	-17.3	-26.2
C3 [deg]	-52.9	-46.0
C4 [deg]	-52.9	-28.4
C5 [deg]	17.3	-18.5
C6 [deg]	-7.0	-7.4
T1 [N]	108000	113000
T2 [N]	108000	113000

Table 6.2 shows the effect of adapting the initial (conventional) control allocation on the critical conditions of the time to bank manoeuvre, of which the previous results were shown in subsection 5.2.5. A clear re-distribution of the use of the control surfaces can be seen. For the forward CG location, the maximum deflection was decreased to 83.0 degrees. For the aft CG, the maximum deflection was decreased from 99.5 degrees to 76.4 degrees. Despite these decreases, the actuator limit set of 30 degrees for the inner and outer elevons was still not attained for both conditions, thus both conditions remain critical. This implicates that a redesign of both the inner and outer elevons is required to comply with the requirement.

Table 6.2: Control Allocation effect on critical Time to Bank condition.

Manoeuvre	Time To Bank			
Condition	APP AEO			
CG	Forward		Aft	
CA	Conventional	Adapted	Conventional	Adapted
δ_e [-]	51.6	36.1	15.1	10.6
δ_a [-]	-90.4	-47	-99.5	-66
δ_r [-]	23.1	-0.9	90.6	-1.2
C1 [deg]	23.1	18.1	90.6	27.3
C2 [deg]	-90.4	-45.1	-99.5	-39.2
C3 [deg]	-51.6	-83.0	-15.1	-76.4
C4 [deg]	-51.6	10.7	-15.1	55.2
C5 [deg]	90.4	1.8	99.5	26.5
C6 [deg]	-23.1	-21.4	-90.6	-28.3
T1 [N]	64100	71000	79600	81000
T2 [N]	64100	71000	79600	81000

Table 6.3 shows the effect of adapting the initial (conventional) control allocation on the critical condition of the one engine inoperative trim manoeuvre, of which the previous results were shown in subsection 5.2.6. A clear re-distribution of the use of the control surfaces can be seen. The total control servo use is spread over more control surfaces, and the maximum deflection used is decreased from 41.8 degrees to 37.2 degrees. Although this is a substantial decrease in maximum deflection, the actuator

limit set of 30 degrees for the inner elevons was still not attained. Thus, the condition remains critical, and again a redesign of the control surfaces is required to comply with the requirement.

Table 6.3: Control Allocation effect on critical One Engine Inoperative trim condition.

Manoeuvre	OEI trim	
Condition	APP OEI	
CG	Forward	
CA	Conventional	Adapted
δ_e [-]	41.8	29.5
δ_a [-]	5	-7.1
δ_r [-]	26.7	3.1
C1 [deg]	26.7	4.9
C2 [deg]	5	-20.8
C3 [deg]	-41.8	-37.2
C4 [deg]	-41.8	-21.8
C5 [deg]	-5	-14.6
C6 [deg]	-26.7	-7.6
T1 [N]	113000	122000
T2 [N]	0	0

Table 6.4 shows the effect of adapting the initial (conventional) control allocation on the critical forward CG conditions of the steady heading sideslip manoeuvre, of which the previous results were shown in subsection 5.2.7. The aft CG conditions were analogous, thus are not shown to limit the size of the table. A clear re-distribution of the use of the control surfaces can be seen for all conditions. For both approach conditions the maximum deflection was substantially decreased, respectively, from 78.5 to 68.3 for the all engines operative approach condition and from 80.9 to 57.1 for the one engine inoperative approach condition. Despite this decrease, the actuator limits set of 30 degrees for the inner and outer elevons and 37 degrees for the rudder were still not attained for both conditions. Thus, both conditions remain critical, and a redesign of the rudders, inner and outer elevons is required to comply with the requirement. Also for both take-off conditions the maximum deflection is substantially decreased, respectively, from 33.2 to 24.3 for the all engines operative take-off condition and from 33.7 to 24.9 for the one engine inoperative take-off condition. Here, the adapted control surface allocation decreases the maximum control surface deflections sufficiently to comply with all actuator limits. Hence, both take-off conditions were no longer critical for compliance with the steady heading sideslip manoeuvre requirements.

Table 6.4: Control Allocation effect on critical Steady Heading Sideslip trim conditions, comparison between conventional (Conv.) control allocation and adapted control allocation..

Manoeuvre	Steady Heading Sideslip							
CG	Forward							
Condition	APP AEO		APP OEI		TO AEO		TO OEI	
CA	Conv.	Adapted	Conv.	Adapted	Conv.	Adapted	Conv.	Adapted
δ_e [-]	36.5	25.8	36.6	25.8	15.4	11.1	15.4	11.1
δ_a [-]	-78.5	-43.6	-80.9	-44	-33.2	-17.1	-33.7	-17.1
δ_r [-]	-66.7	-86.2	-51.7	-71	-10.9	-21.3	-7.8	-18.2
C1 [deg]	-66.7	-68.3	-51.7	-52.8	-10.9	-14.3	-7.8	-11.1
C2 [deg]	-78.5	-50	-80.9	-47.9	-33.2	-18.3	-33.7	-17.9
C3 [deg]	-36.5	-54	-36.6	-57.1	-15.4	-24.3	-15.4	-24.9
C4 [deg]	-36.5	2.4	-36.6	5.4	-15.4	2.2	-15.4	2.8
C5 [deg]	78.5	19	80.9	16.9	33.2	5.0	33.7	4.6
C6 [deg]	66.7	65.9	51.7	50.5	10.9	13.3	7.8	10.1
T1 [N]	48900	52300	98100	105000	27800	29500	55600	59100
T2 [N]	48900	52300	0	0	27800	29500	0	0

In summary, the adapted control allocation as developed in the previous subsection influences the control deflections in favour of the trim and manoeuvre requirements compliance. Nevertheless, its influence was insufficient to improve the handling qualities to a level compliant with all requirements in all conditions. Further fine-tuning of the control allocation matrix is possible using the weighted generalized inverse, as was shown in Equation 6.3. This, however, is not expected to yield requirement compliance for all conditions, due to the excessively large control deflections still required for most critical conditions after the already adapted control allocation implication. Hence, redesigning the control surfaces is expected to be required to comply with all requirements set.

6.2. Stability Augmentation System

Stability augmentation systems can be used to improve the stability of an aircraft. As discussed in Section 3.4, research has shown stability augmentation to be suitable to improve lateral-directional stability of flying wings [7][9]. Castro discusses the use of three stability augmentation systems: sideslip feedback, yaw damping and roll damping. Moreover, the combination of these stability augmentation systems was found to substantially improve the lateral-directional handling qualities compared to the bare airframe dynamics of the designed flying wing. These improved handling qualities were validated both theoretically and experimentally in a ground-based simulator [9]. Hence, they are expected to also substantially improve the lateral-directional handling qualities of the Flying-V.

First, the design process of the stability augmentation system is discussed in subsection 6.2.1, with the final stability augmentation system design obtained presented in subsection 6.2.2. Next, the control servo dynamics, linearisation of the new Flying-V model and the gain tuning of the stability augmentation system are discussed in, respectively, subsection 6.2.3, 6.2.4 and 6.2.5. Finally, the effect of implementing the stability augmentation system on the handling quality results, and the effect of excluding the roll damper are discussed in, respectively, subsection 6.2.6 and 6.2.7.

6.2.1. Stability augmentation system design

As stated in the introduction of this section, the stability augmentation system design was based on the research of Castro [9]. Analogous to the approach in that research, each stability augmentation system element will be discussed separately, after which the final stability augmentation system combining all three is discussed.

Yaw damper

A yaw damper counteracts the yaw rate of an aircraft by feeding back the yaw rate proportionally to the yaw angle control input. In this way, a yaw rate yields a control surface deflection opposing it, preventing the yaw rate to become excessive. Since an unstable Dutch Roll eigenmode yields excessive roll and yaw rates, a yaw damper stabilises this eigenmode.

A proportional yaw rate feedback prevents a yaw rate to increase, even if the pilot desires a yaw rate in for example a coordinated turn. To enable the pilot to perform these manoeuvres, a washout filter was used to decrease the effect of the yaw damper in time. In this way, disturbances on the yaw rate are counteracted by the yaw damper, but a constant desired yaw rate is not. The general transfer function of a yaw damper is shown in Equation 6.6. Here, time constant τ determines the time in which the effect of the yaw damper decreases to zero. A very small time constant would limit the effect of the yaw damper, where a very large time constant would fight against the pilot setting up a turn [45]. For the yaw damper of the stability augmentation system developed in this section, a time constant of 10 seconds was chosen based on the time responses for different time constants tested. Figure 6.1 shows the implementation of a yaw damper with washout filter in a system diagram.

Yaw dampers are widely used as components of stability augmentation systems [24], and can be certified to improve the Dutch Roll stability to the required level when their reliability is sufficient [21].

$$H_{washout}(s) = \frac{\tau s}{\tau s + 1} \tag{6.6}$$

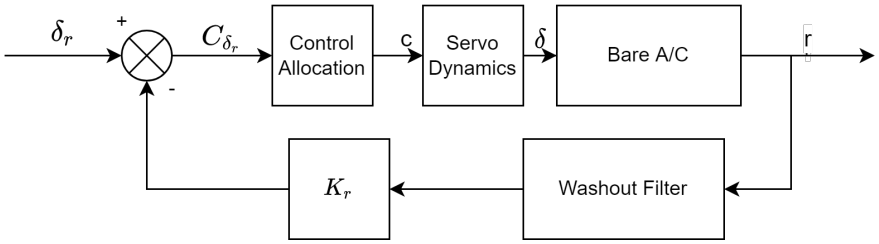

Figure 6.1: Yaw damper system diagram.

Sideslip angle feedback and reference command

Sideslip angle feedback is used to augment directional stability by opposing sideslip angles with an opposing yaw angle control input. In this way, a sideslip angle due to a disturbance is counteracted and decreased to zero. As an unstable Dutch Roll moment yields the sideslip angle's magnitude to increase oscillatory, counteracting the sideslip angle stabilises the Dutch Roll eigenmode. As the sideslip angle β is not directly available as aircraft state in the developed models of the Flying-V, the sideways body velocity V_b is used for proportional feedback to the rudder input. Equation 6.7 shows the relation between the sideslip angle β and the body velocities in X, Y and Z direction, U_b, V_b and W_b. Since the sideslip angle β is proportional to the body velocity V_b, and β equals zero when V_b equals zero, the body velocity can be used for the feedback system instead of the sideslip angle.
Figure 6.2 shows the implementation of Sideslip Angle Feedback in a system diagram, by using the sideways body velocity V_b for feedback to the yaw control input.

$$\beta = \sin^{-1}\left(\frac{V_b}{\sqrt{U_b^2 + V_b^2 + W_b^2}}\right) \tag{6.7}$$

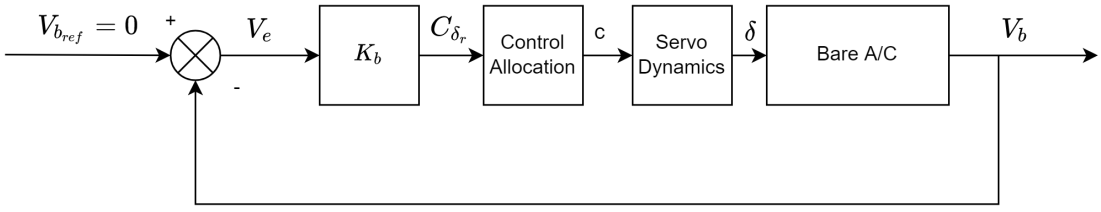

Figure 6.2: Sideslip feedback, system diagram.

Since the sideslip angle feedback reduces the sideslip angle to zero, a pilot-desired sideslip can't be achieved. This can harm the aircraft operations in e.g. side-wind landings and decrab manoeuvres. To allow for a pilot-desired sideslip, the rudder-pedal controls of the pilot can be used as sideslip reference input, to which the sideslip feedback converges. The rudder-pedal input is proportionally converted to a desired sideslip angle, which is fed into the system as reference command. Figure 6.3 shows the system diagram of the sideslip angle feedback with reference command from the rudder-pedals.

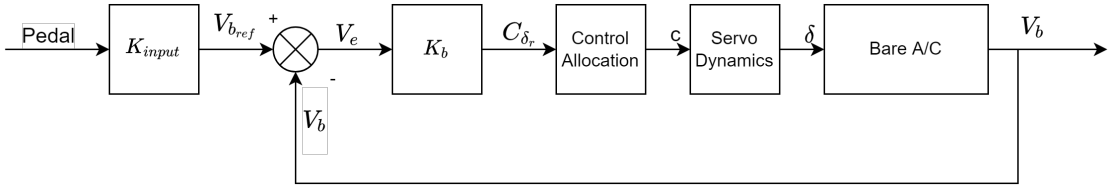

Figure 6.3: Sideslip feedback with reference input, system diagram.

Roll damper
A roll damper counteracts the roll rate of an aircraft by feeding back the roll rate proportionally to the roll angle control input. In this way, a roll rate yields an aileron deflection opposing it, preventing the roll rate to become excessive. As an unstable Dutch Roll moment yields the roll angle's magnitude to increase oscillatorily, counteracting the roll rate stabilizes the Dutch Roll eigenmode. In order to still control the roll angle of the aircraft, the sideways stick input of the pilot is used as reference roll rate. Figure 6.4 shows a system diagram of the roll damper.

The roll damper introduces a trade-off between stability and manoeuvrability around the roll axis. Earlier research found this trade-off to be pilot subjective after both assessing the stability augmentation system experimentally with and without roll-damper [9], and receiving inconsistent favourable pilot comments. For the stability augmentation system implementation and results shown next the roll damper was included, with the theoretical effect of excluding the roll damper discussed further in subsection 6.2.7.

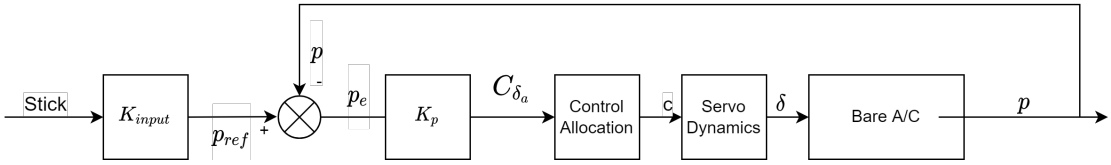

Figure 6.4: Roll damper with reference input, system diagram.

6.2.2. Final stability augmentation system design

By combining the yaw damper, roll damper and the sideslip angle feedback with reference command, the final stability augmentation system proposed is obtained. In order to provide aircraft trim options in the stability augmentation system, a sideslip and roll rate trim input were added to the input signal from the pilot. Figure 6.5 shows an overview of the final stability augmentation system by means of a system diagram.

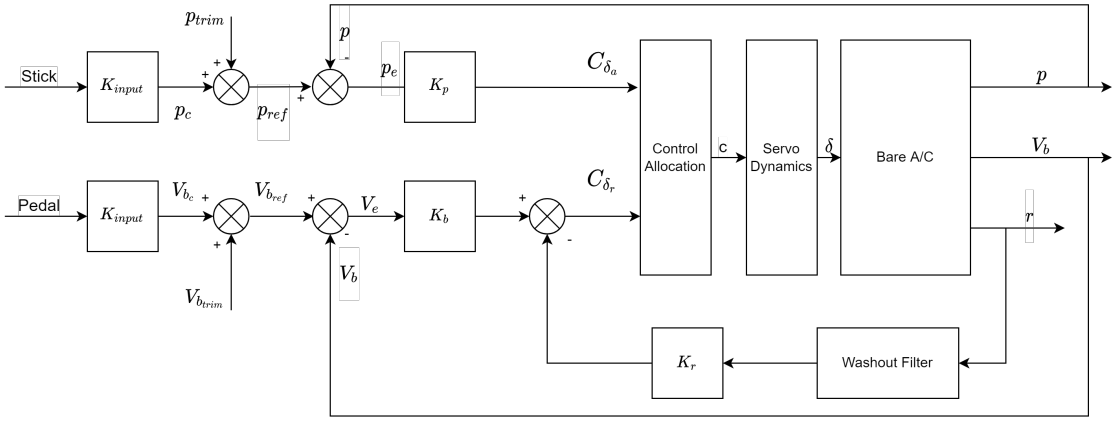

Figure 6.5: Final stability augmentation system, system diagram

6.2.3. Control servo dynamics

In the previous subsections the servo dynamics were shown as part of each stability augmentation system diagram, which is in contrast with the bare-airframe handling quality analysis where the servo dynamics were not included. The servo dynamics were excluded from the bare-airframe handling quality analysis since they are not needed to find a trim state and omitting them significantly simplifies the linearisation process. Moreover, due to the lack of a state feedback, the servo dynamics did not in-

fluence the eigenmodes of the bare-airframe aircraft. In order to assess the influence of a stability augmentation system with state feedback, however, modelling the servo dynamics is essential and assumptions on the servo dynamics need to be made.

Control surfaces can be modelled as a first order lag, in which the time constant dictates the servo response speed to an input signal. Equation 6.8 shows the assumed transfer function for all control surfaces of the Flying-V. K_{servo} is assumed equal to 1, to prevent an overreaction to a control input. T_{servo} is assumed $0.05s$, representing a fast hydraulic actuator [45]. Next to the first order lag response, a servo-deflection rate limit was imposed which limits the angular velocity of the servo response. Different rate limits were considered from earlier research [46][47][48][49], ranging from 28 degrees per second to 60 degrees per second. In collaboration with Airbus, it was decided to rate-limit all servos at 40 degrees per second.

$$H_{servo}(s) = \frac{K_{servo}}{1 + T_{servo}s} \tag{6.8}$$

6.2.4. Linearisation with stability augmentation system

Obtaining the eigenmode damping and frequency parameters requires linearising the aircraft dynamics, as was previously discussed in subsection 2.3.3 and subsection 5.1.3. The complexity of the stability augmentation system design provides a challenge in linearising this system. Hence, MATLAB was used to extend the linearised system as developed for the bare-airframe handling quality analysis of Chapter 5 with the control surface dynamics and stability augmentation system. Each input of the 6 control surface inputs of the linearised system was multiplied by its transfer function, yielding an extra state for each in the A matrix. This state contains the actual deflection of the control surface, while the input to the model now is the demanded deflection. The A matrix then becomes an 18x18 matrix due to the extra 6 states of the 6 control surfaces. The B matrix was updated to be in line with this new structure.

Next, the yaw, roll and sideslip feedback were implemented by creating a feedback matrix containing all feedback gains and the yaw-damper washout filter. This feedback matrix is connected to the three pilot inputs, which next were converted to control surface inputs using the control allocation matrix and the MATLAB *feedback* command. The washout filter as discussed in subsection 6.2.1 is a first order lead function thus also introduces an aircraft state to keep track of the washout filter status, yielding the A matrix to become a 19x19 matrix. Finally, the state-space system obtained by these operations can be used to obtain the eigenvalues of the aircraft with stability augmentation implemented, using the *eig* and *damp* MATLAB commands.

It should be noted that imposing the servo deflection rate-limit, as discussed in the previous subsection, introduced a non-linearity in the aircraft response to inputs. This non-linearity can't be linearised, thus introduced a discrepancy between the non-linear and linearised system. The rate-limit, however, only has an effect on the eigenmode damping and frequency parameters in edge of the envelope load cases. Thus, the discrepancy was assumed to be acceptable for the scope of the research.

6.2.5. Gain tuning stability augmentation

The linearised system discussed in the previous subsection was used to tune the different gains in the stability augmentation system. First, by varying the feedback gains of the yaw damper and sideslip feedback, the Dutch Roll damping and frequency parameter were tuned to a desired state. Next, the roll damper gain was tuned based on the time-responses of impulse and step inputs on both the sideslip reference and roll reference command. A trade-off between tuning based on the latter two exists, since a larger roll damping yields better constant sideslip performance, but a more oscillatorily response to a pilot roll-input. Since the roll damping had a positive effect on the Dutch Roll damping and frequency parameter, the yaw damper and sideslip feedback gains could afterwards be reduced while taking the roll damping into account and keeping equal Dutch Roll damping performance.

Gain tuning was performed at all three flight conditions as were specified in subsection 5.1.1. Due to

the different flight speeds and air density parameters at each condition, different gains are required at each condition for satisfactory performance [45]. Table 6.5 shows the gains used for the stability augmentation system implementation.

Table 6.5: Gain variables of stability augmentation system for different flight conditions.

	Approach	Take-Off	Cruise
K_r	-400	-200	-150
K_b	4	2	1
$K_{v_{in}}$	0.666	0.666	0.666
K_p	1300	900	400
$K_{p_{in}}$	0.01	0.01	0.01

6.2.6. Stability augmentation system implementation results

As discussed in Section 3.4, research has shown stability augmentation to be suitable to improve the lateral-directional stability of flying wings [7][39][9]. This increase in lateral-directional stability can inherently improve the handling qualities of an aircraft. Specifically the eigenmodes of an aircraft can be positively influenced by stability augmentation, by either improving an eigenmode's damping, frequency or both [9] [40]. Of the handling quality requirements as discussed in Section 3.1 and Section 5.2, the Dutch Roll and spiral stability requirements of MIL-HDBK-1797 [20] are based on these damping and frequency parameters, thus are influenced by implementing a stability augmentation system.

The stability augmentation system was developed such that the trim conditions as required for the EASA CS-25 requirements do not require re-assessment: the same trim control deflections as without the stability augmentation system are still attainable by the use of the trim inputs as shown in Figure 6.5. Nonetheless the stability augmentation system does influence the time to bank requirement of EASA CS-25, since this requirement does not only involve a trim condition but also performing a manoeuvre within a set time. The stability augmentation system influences the aircraft's response on pilot inputs, hence influences whether this manoeuvre can be performed successfully.

In summary, the implementation of the stability augmentation system influences three requirements as were tested in Section 5.2: the MIL-HDBK-1797 Dutch Roll damping and frequency requirement, the MIL-HDBK-1797 spiral stability damping requirement and the EASA CS-25 time to bank manoeuvre requirement. The results of the stability augmentation system implementation on the theoretical handling quality analysis are discussed separately below. The adapted control allocation as discussed in the previous subsection was already implemented, since then the final flight control system is directly obtained and assessed for these requirements. The MIL-HDBK-1797 requirements were not influenced by implementing the control allocation, as was discussed before, nevertheless the time to bank manoeuvre was influenced.

Table 6.6 shows the effect of implementing the stability augmentation system on the Dutch Roll damping and frequency parameter for different CG locations and flight conditions. The damping parameter improves for all conditions. When comparing these results to Table 3.2 in subsection 3.1.1, the damping and frequency parameters for the aircraft with stability augmentation comply with the Level-1 requirements in Flight Phase B for all aircraft classes. Further gain tuning can be performed when the stability augmentation system is experienced too invasive, since a small margin still exists with respect to the minimal Dutch Roll parameter requirements for Level-1 performance.

Table 6.7 shows the effect of implementing the stability augmentation system on the spiral stability time to double parameter ($T2$) for different CG locations and flight conditions. The time to double parameter decreases in magnitude for all conditions. When comparing these results to Table 3.3 in subsection 3.1.2, the $T2$ parameters for the aircraft with stability augmentation comply with the Level-1 requirements in take-off and cruise. In approach Level-2 is met for Flight Phase Categories A and C, and Level-1 for Flight Phase Category B. Further gain tuning can increase this performance, this, however, decreases the Dutch Roll performance. Due to the aircraft mainly operating in Flight Phase Category B, the spiral stability is still assumed as sufficient.

Table 6.6: Stability augmentation system implementation effect on Dutch Roll parameters.

Requirement		Dutch Roll			
CG		Forward		Aft	
Configuration		Bare A/C	SAS	Bare A/C	SAS
APP	ζ [-]	-0.070	0.405	-0.076	0.385
	ω [rad/s]	1.058	0.694	0.899	0.615
TO	ζ [-]	-0.027	0.332	-0.019	0.321
	ω [rad/s]	0.860	0.759	0.748	0.715
CR	ζ [-]	-0.011	0.257	0.002	0.247
	ω [rad/s]	0.811	0.977	0.731	0.931

Table 6.7: Stability augmentation system implementation effect on Spiral Stability parameter.

Requirement		Spiral Stability			
CG		Forward		Aft	
Configuration		Bare A/C	SAS	Bare A/C	SAS
APP	T2	27.94	15.02	44.35	18.11
TO	T2	447.43	43.98	-501.64	52.06
CR	T2	-659.45	137.00	-379.03	160.52

Table 6.8 shows the effect of implementing the stability augmentation system (together with the adapted control allocation) on the maximum control deflection of each control surface for the critical conditions of the time to bank manoeuvre. Since the stability augmentation system increases the lateral-directional stability, the roll-ability of the aircraft decreases. This yields a slower initial response to the control input, and therefore requires a larger maximum control deflection to still meet the time set for the manoeuvre. Moreover, the sideslip feedback of the stability augmentation system drastically increases the rudder use, while the rudder use was constrained in the bare-airframe simulation of the time to bank manoeuvre. The adapted control allocation, however, damps this effect, by increasing the overall control surface effectiveness.

As shown in Table 6.8, the previously found critical conditions (Approach All Engines Operative, forward and aft CG location) still do not comply with the maximum control deflection requirement for both the rudders and elevons. Moreover a new critical condition arises, the Take Off One Engine Inoperative condition with a forward CG. It exceeds the control deflection limit of the left inner elevon (C3) with a difference of 4.0 degrees.

Table 6.8: Stability augmentation system implementation effect on critical Time to Bank manoeuvre control surface deflections.

Manoeuvre	Time To Bank					
Condition	APP AEO				TO OEI	
CG	Forward		Aft		Forward	
Configuration	Bare A/C	SAS	Bare A/C	SAS	Bare A/C	SAS
C1 [deg]	23.1	70.0	90.6	76.4	20.9	19.8
C2 [deg]	-90.4	-54.2	-99.5	-40.6	-21.3	-24.5
C3 [deg]	-51.6	-104.5	-15.1	-80.8	-19.9	-34.0
C4 [deg]	-51.6	39.9	-15.1	62.5	-19.9	-14.1
C5 [deg]	90.4	-16.1	99.5	29.6	21.3	-12.3
C6 [deg]	-23.1	-73.0	90.6	-77.2	-20.9	-21.2
T1 [N]	64100	61000	79600	67000	70200	74900
T2 [N]	64100	61000	79600	67000	0	0

6.2.7. Roll damper effect

As stated in subsection 6.2.1, the use of a roll damper did not consistently yield favourable pilot comments in earlier research. To first theoretically assess the effect of excluding the roll damper, the same assessment as performed for the stability augmentation system with roll damper was performed without roll damper. The roll damper exclusion effect can be tested experimentally in further research, as will be elaborated upon in Chapter 7.

Re-assessing the handling qualities of the aircraft with the stability augmentation system prototype without roll damper required new gain tuning for similar performance. The tuning was based on the eigenmode damping and frequency parameters, since these are desired to have similar performance as with a roll damper. Table 6.9 shows the tuned control gains for the yaw damper and sideslip angle feedback. When compared to the gains of the stability augmentation system with a roll damper, as shown in Table 6.5, it stands out that larger (mostly yaw damper) gains are required for similar theoretical performance.

Table 6.9: Gain variables of stability augmentation system without roll damper.

	Approach	Take-Off	Cruise
K_r	-1000	-400	-200
K_b	10	2	1
$K_{v_{in}}$	0.666	0.666	0.666

The Dutch Roll stability damping and frequency parameters after tuning the stability augmentation system without roll damper are show in Table 6.10. Similar parameters were obtained as for the stability augmentation system with roll damper.

Table 6.10: Dutch Roll parameters stability augmentation without roll damper.

Requirement	Dutch Roll		
Configuration	SAS without Roll Damper		
CG		Forward	Aft
APP	ζ [-]	0.153	0.168
	ω [rad/s]	1.220	1.070
TO	ζ [-]	0.215	0.236
	ω [rad/s]	0.984	0.880
CR	ζ [-]	0.195	0.205
	ω [rad/s]	1.120	1.040

Next to the Dutch Roll stability the time to bank manoeuvre is of special interest when assessing the roll damper effect, since this manoeuvre tests the roll capability. Excluding the roll damper from the stability augmentation system is expected to decrease roll stability, thus increase roll manoeuvrability. The theoretical handling quality assessment, however, showed a different result. Table 6.11 shows the (maximum) control deflections occurring during the time to bank manoeuvre. When compared to the results from the assessment with roll damping included, as shown in Table 6.8, the results without roll damping do not show improved roll manoeuvrability. It was found that the increased yaw damper control gains influence the aircraft response more significantly than the exclusion of the roll damper.

The exclusion of the roll damper from the stability augmentation system yields the following conclusions. First, for similar Dutch Roll performance, larger yaw damper control gains were required without roll damper. This increase led to a decrease in time to bank performance, although still similar to the results with roll damping. Thus, the decision on whether to include or exclude the roll damper in the stability augmentation system is not based on theoretical analysis, but proposed to be based on the piloted assessment discussed in Chapter 7.

Table 6.11: Critical Time to Bank manoeuvre control deflections without roll damper.

Manoeuvre	Time To Bank		
Configuration	SAS without Roll Damper		
Condition	APP AEO		TO OEI
CG	Forward	Aft	Forward
C1 [deg]	123.7	161.3	27.7
C2 [deg]	-69.7	-70.4	-17.5
C3 [deg]	-100.6	-96.2	-34.5
C4 [deg]	36.0	77.9	-12.2
C5 [deg]	30.9	59.4	-8.1
C6 [deg]	126.6	-162.1	-29.0
T1 [N]	61000	67000	74900
T2 [N]	61000	67000	0

6.3. Flight Control System Prototype Implementation Conclusions

By combining the adapted control allocation as discussed in subsection 6.1.1 with the stability augmentation system in subsection 6.2.1, the final prototype flight control system was obtained. Combining the results of the influence of the adapted control allocation and the stability augmentation system on the handling quality requirements yields a new compliance with these requirements. Table 6.12 shows an overview of this compliance, as was shown for the bare-airframe handling quality analysis in Table 5.16. It can be noted that more requirements were complied with, and the amount of critical conditions was reduced for most requirements. Only the compliance with the coordinated turn capability requirement was not increased, since the compliance in the take-off condition was adversely influenced by the stability augmentation system.

Table 6.12: Overview of the requirement compliance with the theoretical handling quality assessment of bare-airframe Flying-V after FCS implementation. The condition indicated with * is newly critical with respect to the bare-airframe analysis.

Requirement	Compliance	Critical Condition(s)	Critical CG
Dutch Roll Stability	Passed	-	-
Spiral Stability	Passed	-	-
Lateral Control Departure	Passed	-	-
Coordinated Turn Capability	Failed	APP AEO	Forward
Time to Bank, Roll Capability	Failed	APP, TO*	Forward, Aft
One Engine Inoperative Trim	Failed	APP AEO	Forward
Steady Heading Sideslip	Failed	APP AEO, APP OEI	Forward, Aft

Implementing the flight control system prototype showed both its opportunities as well as its limitations on improving the handling qualities of the Flying-V. It was shown that a stability augmentation system is a suitable method for improving the stability concerns, but manoeuvrability has to be taken into account when designing this system. The trade-off between the stability and manoeuvrability yields room for further flight control system improvement, since current research yields more complex stability augmentation system designs [7], which can possibly account better for both.

Moreover, it was also shown that the overall control effectiveness can indeed be improved by adapting the control allocation, but only up to a certain extent. It was found that the control allocation adaptation proposed was insufficient to solve all lack of requirement compliance. Further control allocation improvement is expected to be still possible, but is not expected to yield full requirement compliance. The control deflections required for amongst others the time to bank manoeuvre are expected to be too excessive to be decreased within limits just by using the control servo´s differently distributed or for example dynamically. Hence, further research into the control surface sizing and functioning is expected to be required to achieve theoretical compliance to all handling quality requirements set.

6.4. Key Takeaways

From the theoretical assessment of the design and implementation of the prototype flight control system, five key takeaways were found most relevant.

- The implementation of a roll-, yaw- and sideslip-feedback stability augmentation system increased the Dutch Roll stability of the Flying-V, but reduced the roll manoeuvrability, thus introduced a trade-off.
- Adapting the control allocation increased the overall control effectiveness of the Flying-V and reduced the maximum control surface deflection needed for each requirement assessed.
- Implementing the prototype flight control system increased the handling qualities with respect to the bare-airframe Flying-V and improved the overall requirement compliance.
- The implementation of the prototype flight control system, however, increased the handling qualities insufficient to comply with all requirements tested.
- Further research into control surface sizing and (re-)design is expected to be required to comply with all requirements.

7

Experiment Proposal

The results of the bare-airframe handling quality analysis and flight control system implementation analysis as shown in Chapters 5 and 6 are used to develop a piloted experiment. This chapter presents the experiment proposal for this piloted experiment, and marks the start of the next phase of the thesis research. First, the experiment goals are discussed in Section 7.1. Next, the associated research questions and expected results are elaborated upon in Section 7.2. Finally, the experiment design proposed to answer these research questions is presented in Section 7.3.

7.1. Experiment Goals

The experiment aims both at experimentally validating the theoretical assessments as shown in the previous two chapters, as well as at answering the final thesis research question as was discussed in Section 4.3: *Are the Lateral-Directional Handling Quality requirements of conventional commercial aircraft met in a pilot-in-the-loop experiment of the Flying-V?*. This yields three experiment goals, as shown below.

1. Validate the theoretical handling quality analysis of the bare-airframe Flying-V.
2. Validate the theoretically found influence of the prototype flight control system on the handling qualities of the Flying-V.
3. Assess whether the lateral-directional handling quality requirements of conventional commercial aircraft can be met in a pilot-in-the-loop experiment of the Flying-V.

7.2. Experiment Research Questions and Expected Results

From the three experiment goals as presented in the previous section, three research questions follow. For each research question, an expected result was set. The expected result of Research Question 3 led to a fourth research question, which is elaborated upon at the end of this section. Below, the research questions and the set expected results are shown.

1. Are the theoretically found handling qualities of the bare-airframe Flying-V equal to those found in a pilot-in-the-loop experiment?

E: Yes, since the requirements and metrics used in the theoretical analysis are expected to represent pilot-experienced handling qualities.

2. Does the prototype flight control system increase the pilot-perceived handling qualities of the Flying-V as found in the theoretical analysis?

E: Yes, since literature shows flight control systems improve aircraft handling qualities both theoretically and experimentally.

3. Are the lateral-directional handling quality requirements of conventional commercial aircraft met in a pilot-in-the-loop experiment of the Flying-V with the prototype flight control system?

E: No, since theoretical analysis showed excessively large control surface deflections are required to comply with all requirements.

4. Are the lateral-directional handling quality requirements of conventional commercial aircraft met in a pilot-in-the-loop experiment of the Flying-V with the prototype flight control system, when extending the control servo limits to the extent theoretically found required?

E: Yes, since a lack of control authority is expected to be the main cause of the theoretically found lack of requirement compliance.

As stated in the introduction of this section the expected result of research question 3 yielded a fourth research question and expected result. If this final expected result can be experimentally confirmed, it can be shown that increasing the control authority solves the lateral-directional handling quality concerns for the Flying-V. This would yield a useful design recommendation for further research.

7.3. Experiment Design

From the research goals, questions and expected results as shown in the previous sections, an experiment was developed. This section elaborates on the proposed experiment design. First, the different aircraft configurations, flight conditions and requirements to be simulated are discussed and selected in subsection 7.3.1. Second, simulating the requirements in a piloted experiment is discussed in subsection 7.3.2. Third, a two-phase approach to perform the experiment is presented in subsection 7.3.3. Finally, the experiment variables, hypotheses and use of the results are discussed in subsection 7.3.4.

7.3.1. Aircraft configurations and conditions selection

In order to answer the four research questions listed in Section 7.2, three aircraft configurations are simulated as shown below in Simulations A to C.

A. Bare-airframe Flying-V

B. Flying-V with prototype flight control system

C. Flying-V with prototype flight control system and extended control surface deflection limits

Each simulation of an aircraft configuration aims at answering one or multiple research questions as discussed in Section 7.2. Simulation A tests Research Question 1, validating the theoretically found handling qualities of the bare-airframe Flying-V. Simulation B tests both Research Question 2 and 3, by validating the prototype flight control system influence on the handling quality results, and by assessing whether the set requirements are met when the flight control system is applied. Finally, Simulation C tests Research Question 4, by assessing whether all requirements set can be complied to when extending the control surface deflection limits sufficiently.

Simulating these three aircraft configurations in all requirements and flight conditions with both centre of gravity locations, as tested in the theoretical handling quality analysis, would yield over 150 simulation runs. This is an unfeasible amount for pilot testing, thus a selection of combinations of requirements, centre of gravity locations and flight conditions had to be made.

The selection was performed in four steps. First, it was decided to exclude the spiral stability and lateral control departure parameter from testing, since theoretical analysis showed these requirements to be marginally influenced by changes in aircraft configurations and conditions. Next for the remaining requirements, it was decided to validate the theoretical analyses by experimentally testing the best and worst case scenarios. These scenarios were found to be, respectively, the cruise condition with aft limit centre of gravity and approach condition with forward limit centre of gravity. For each scenario the engine setting, all engines operative or one engine inoperative, was chosen from the available settings as tested in the theoretical analysis. One engine inoperative was set as worst case, all engines operative as best case. Finally, it was decided that a proper validation of the flight control system implementation required extra conditions to be tested, and the conditions on which the flight control system effect is expected largest were selected: the forward centre of gravity conditions of the Dutch Roll and Steady Heading Sideslip requirement. This yields 14 selected combinations of requirement, flight condition and centre of gravity as shown in Table 7.1. By simulating these 14 conditions with all 3 aircraft configurations as discussed at the start of this subsection, a total of 42 simulation runs are required for the

Table 7.1: Selected centre of gravity and flight condition combinations for the piloted simulation of different requirements.

	CG Forward	CG Aft
Dutch Roll	APP, TO, CR (AEO)	CR (AEO)
Steady Heading Sideslip	APP, TO, CR (OEI)	CR (AEO)
Time to Bank	APP (AEO)	CR (AEO)
Coordinated Turn Capability	APP (AEO)	CR (OEI)
One Engine Inoperative trim	APP (OEI)	CR (OEI)

piloted handling quality assessment.

As discussed in both subsection 6.2.1 and subsection 6.2.7, within the stability augmentation system the use of a roll damper did not consistently yield favourable pilot comments in earlier research. Moreover, no conclusion was drawn based on the theoretical results of excluding the roll damper from the stability augmentation system. Hence, the experiment is extended to also assess the pilot-subjective influence of excluding or including the roll damper on the handling qualities. For this, the Dutch Roll, Steady Heading Sideslip and Time to Bank requirement for the forward centre of gravity and all three flight conditions are selected, as these are expected to be influenced most by the roll damper. Hence, to assess the roll damper effect, these requirements are simulated for the Flying-V with flight control system prototype while both including and excluding the roll damper. Table 7.2 shows an overview of the selected combinations of requirement, flight condition and centre of gravity location for the roll damper experiment.

Table 7.2: Selected centre of gravity and flight condition combinations for the piloted simulation of different requirements in the roll damper experiment.

	CG Forward
Dutch Roll	APP, TO, CR (AEO)
Steady Heading Sideslip	APP, TO, CR (OEI)
Time to Bank	APP, CR (AEO), TO (OEI)

7.3.2. Requirement simulation

To simulate the different stability and manoeuvrability requirements, the manoeuvre performed in the simulator needs to be determined for each. For this, a US Federal Aviation Administration flight test guide for certification of transport category airplanes is used. Advisory Circular (AC) 25-7D is used [50], which includes flight test methods and procedures to show compliance with regulations as presented in EASA CS25. For each of the CS25 requirements tested, AC 25-7D discusses a manoeuvre which can be performed in flight (or flight simulation) and the allowed state limits to prove requirement compliance.

7.3.3. Experiment phases

As discussed in subsection 7.3.1, the piloted experiment offers the opportunity to assess the effect of including or excluding a roll damper from the stability augmentation system. By testing this first, the flight control system can be adapted based on the results and the pilot-in-the-loop experiment can be performed using the stability augmentation system yielding the best subjective handling qualities. Hence, a two-phase experiment structure is proposed.

In the first phase of the experiment, the roll damper effect is tested and all tests planned for the pilot-in-the-loop handling quality experiment are tested to be flyable. The latter requires testing the 42 runs as discussed in subsection 7.3.1. The roll damper experiment requires the 9 conditions shown in Table 7.2 to be simulated for both the stability augmentation system with and without a roll damper, yielding 18 extra simulation runs. 7 of these, however, were already performed in the previously mentioned 42 runs to ensure fly-ability, thus 11 extra runs remain to test the roll damper experiment in the first phase of the experiment. This yields a total of **53 runs** for each pilot performing the **first phase** of the experiment.

In the second phase of the experiment, the pilot-in-the-loop handling quality experiment is performed, after using the results of the first phase to perform a final iteration on the flight control system design. Hence, the second phase requires simulating the 14 conditions as shown in Table 7.1 for all 3 aircraft configurations, yielding a total of **42 runs** for each pilot performing the **second phase** of the experiment.

7.3.4. Experiment hypotheses and outcome

The experiment planned makes use of different independent variables as input and yields several dependent variables as output. Based on the expected results of the research questions, the expected effect of the independent variables on the dependent variables was used to formulate hypotheses answering the experiment research questions. The independent variables influencing the tests of each requirement are summarised as follows:

- Aircraft Configuration — bare-A/C, FCS, FCS with extended servo limits
- Centre of Gravity location — forward, aft
- Flight Condition — approach, take-off, cruise
- Engine Setting — AEO, OEI

The independent variables are expected to have an influence on (amongst others) the following dependent variables:

- Cooper-Harper rating for each aircraft configuration and condition — scale 1-10
- Compliance with requirement state limits during each manoeuvre — pass / fail
- Qualitative feedback on each aircraft configuration — -

The expected outcomes of the research questions yield the following hypotheses:

I. For the bare-airframe aircraft configuration, the experimental requirement compliance to the state limits in each manoeuvre in each condition tested is equal to the theoretical requirement compliance of that manoeuvre in that condition.

II. For the aircraft with the flight control system implemented, each flight condition tested yields a better (i.e., lower) Cooper-Harper rating than that condition tested in the bare-airframe aircraft configuration.

III. For the aircraft with the flight control system implemented, the experimental requirement compliance to the state limits in each manoeuvre in each condition tested is equal to the theoretical requirement compliance of that manoeuvre in that condition.

IV. For the aircraft with the flight control system implemented and extended control surface limits, in every manoeuvre tested the requirements on the state limits are complied with.

From these, testing hypothesis I answers (Experiment) Research Question 1, as presented in Section 7.2. Next, testing both Hypotheses II and III answers Research Question 2. Testing Hypothesis III answers Research Question 3. Finally, testing Hypothesis IV answers Research Question 4. With this, the contribution to the Flying-V project can be summarised as follows:

First of all, the experimental validation of the theoretical handling quality assessment method and results will show whether future Flying-V designs can rely on a the shown theoretical assessment method only, or whether a different (possibly piloted) assessment is required after each design iteration. Second, the assessment of the prototype flight control system influence on the pilot-experienced handling qualities shows the opportunities and limitations regarding the used type of flight control system. Finally, the handling quality requirement compliance tested in the piloted simulation is expected to yield useful insights into the Flying-V design and its control surface design, showing opportunities for future research and re-design.

8

Conclusion

This preliminary thesis aimed at presenting the research on the lateral-directional handling qualities of the Flying-V performed so far, which is used as basis for a proposed piloted assessment of these handling qualities. The research was presented and proposed in three phases: first, the theoretical analysis of the lateral-directional handling qualities of the bare-airframe Flying-V was presented. Second, the design of a prototype flight control system improving these handling qualities and the theoretical assessment of this improvement was presented. Third, the proposed pilot-in-the-loop experiment design for experimental validation of the theoretical results was shown.

The theoretical analysis showed limited lateral-directional stability and handling qualities. The main conclusions were threefold. First, insufficient Dutch Roll stability was found for all flight conditions and at both centre of gravity limits. Second, insufficient yaw and roll control authority was found in approach condition, predominantly for the forward centre of gravity location. Third insufficient yaw and roll control authority was found during sideslip flight in the approach and take-off condition.

To counteract the deficiencies found in the theoretical analysis of the handling qualities of the bare-airframe Flying-V, a prototype flight control system was designed. In this flight control system, an adapted control allocation was implemented to increase the overall control effectiveness, and the Dutch Roll instability was counteracted by implementing a stability augmentation system. A theoretical assessment of their influence showed both flight control system elements to positively influence the lateral-directional handling qualities, but the effect was insufficient to increase the handling qualities to comply with all set requirements in all conditions. First due to excessively large control surface deflections required to keep the aircraft in the required trim conditions, predominantly for approach and sideslip flight with the forward centre of gravity limit. Second, due to insufficient roll control authority to comply with the roll manoeuvrability requirement in approach and take-off conditions.

Using the results of the theoretical handling quality assessment and prototype flight control system implementation, a piloted-experiment was proposed. The experiment plans on validating the theoretical results experimentally, by testing a selection of the requirements as theoretically assessed by simulating manoeuvres in a pilot-in-the-loop experiment. Second, the experiment plans at showing that increased control authority will yield full requirement compliance by performing these manoeuvres with extended control surface deflection limits. The results of the experiment can be used to show the theoretical assessment performed is applicable for further research. Second, the results can experimentally validate the positive influence of the prototype flight control system, and show further opportunities and limitations regarding this type of flight control system. Third, the results will bring new insights into the effect of the Flying-V design and control surface design on the lateral-directional handling qualities, yielding opportunities for further research.

To conclude, the first two phases of the research have been completed. Based on the results from these phases, an experiment was proposed to complete the final phase of the research. The experiment proposed is expected to fulfil the research goal of the MSc. thesis of the author.

A

Mass Moment of Inertia in Landing

From Cappuyns [8], the mass moments of inertia at maximum take-off weight were obtained. Moreover, the maximum take-off weight and maximum landing weight were given. The mass moments of inertia at maximum landing weight, however, were not available in the thesis of Cappuyns, hence an approximation of these is required to simulate the aircraft properties at landing.

First of all, the weight different between the maximum take-off weight and maximum landing weight is assumed to occur due to fuel use. The mass moments of inertia at maximum landing weight thus can be obtained by subtracting the mass moment of inertia of this fuel used from the mass moments of inertia at maximum take-off weight. Since the mass of the fuel used can be determined, an assumption on the (point force assumed) acting location of this fuel is sufficient to determine the mass moments of inertia of the fuel used.

Cappuyns approximated the mass moments of inertia by dividing the (half-model of) the Flying-V in 6 sections, as indicated in Figure A.1. Next, for each element of the mass breakdown of the Flying-V, one or multiple sections were assumed to contain this element of mass. For the fuel, section three was assumed to contain all. Hence, the fuel used is assumed to have its point force acting location inside section three.

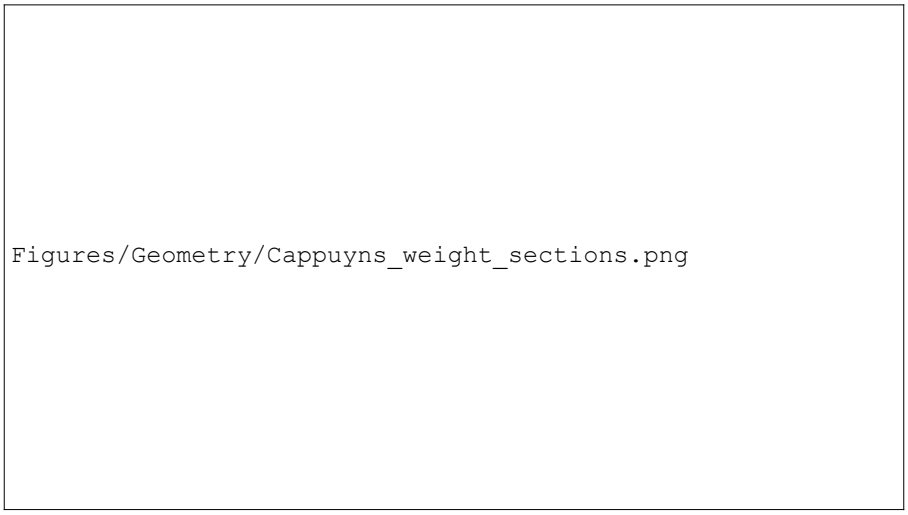

Figure A.1: Flying-V planform section breakdown for inertia estimation [8].

Next, the point force acting location of the fuel used was graphically determined. This was done by assuming a triangular fuel location area inside section 3, and taking the centroid of this triangle as point force acting location. Figure A.2 shows this graphical determination.
Equations A.1, A.2 and A.3 next were used to determine the mass moments of inertia of the fuel used. As reference location for X, the aft limit centre of gravity was taken. As reference location of Y and Z,

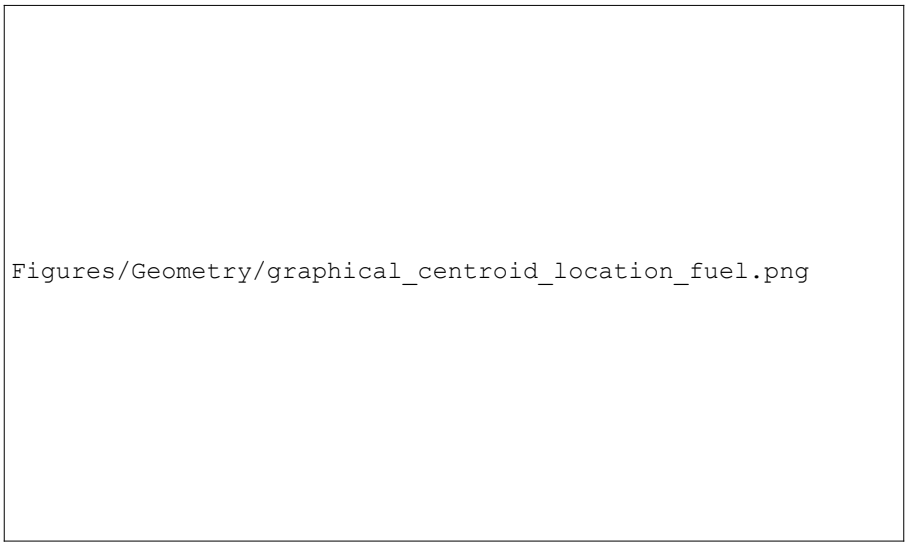

Figure A.2: Graphical determination of fuel assumed point-force acting location.

zero was used. Table A.1 shows the variables finally used and obtained for the fuel used mass moments of inertia determination, and the resulting mass moments of inertia at maximum landing weight.

$$I_{xx_{used-fuel}} = m_{used-fuel}\left[\left(Y_{fuel} - Y_{\text{ref}}\right)^2 + \left(Z_{fuel} - Z_{\text{ref}}\right)^2\right] \tag{A.1}$$

$$I_{yy_{used-fuel}} = m_{used-fuel}\left[\left(Z_{fuel} - Z_{\text{ref}}\right)^2 + \left(X_{fuel} - X_{\text{ref}}\right)^2\right] \tag{A.2}$$

$$I_{zz_{used-fuel}} = m_{used-fuel}\left[\left(X_{fuel} - X_{\text{ref}}\right)^2 + \left(Y_{fuel} - Y_{\text{ref}}\right)^2\right] \tag{A.3}$$

Table A.1: Variable overview of mass moments of inertia approximation in maximum landing weight.

Variable	Description	Value	Unit
MTOW	Maximum take-off weight	X	kg
MLW	Maximum landing weight	X	kg
Fuel used	Difference MTOW MLW	X	kg
X_{fuel}	X location fuel point force acting point	X	m
Y_{fuel}	Y location fuel point force acting point	X	m
Z_{fuel}	Z location fuel point force acting point	X	m
$I_{xx_{fuel-used}}$	Mass Moment of Inertia around X axis fuel used	X	$10^7 kgm^2$
$I_{yy_{fuel-used}}$	Mass Moment of Inertia around Y axis fuel used	X	$10^7 kgm^2$
$I_{zz_{fuel-used}}$	Mass Moment of Inertia around Z axis fuel used	X	$10^7 kgm^2$
$I_{xx_{MLW}}$	Mass Moment of Inertia around X axis MLW	X	$10^7 kgm^2$
$I_{yy_{MLW}}$	Mass Moment of Inertia around Y axis MLW	X	$10^7 kgm^2$
$I_{zz_{MLW}}$	Mass Moment of Inertia around Z axis MLW	X	$10^7 kgm^2$

B

Model linearisation

As discussed in subsection 2.3.3, using a linearised aircraft model for simulation yields several advantages over using a non-linear model to simulate an aircraft over time. With the linearisation of the aircraft model, a linear state-space system is developed. Equation B.1 shows the state equation of a state space system. Here, x is the state vector of the aircraft, holding all variables necessary to have a complete overview of the aircraft state. $\dot{x}$ is the derivative of the state vector with respect to time. State matrix A determines the influence of each state in vector x, on each of the different state derivatives in $\dot{x}$. Next, input vector u holds the input variables, and input matrix B determines the influence of each of these input variables on each of the state derivatives in $\dot{x}$.

$$\dot{x} = Ax + Bu \tag{B.1}$$

For the aircraft state, a state vector containing 12 variables is used, based on the equations of motion as discussed in subsection 2.3.2:

- Earth location: X_e, Y_e, Z_e
- Body velocities: U_b, V_b, W_b
- Angular velocities: p, q, r
- Euler angles: φ, θ, ψ

The state matrix A is determined by assessing the influence of each state in x on the different state derivatives in $\dot{x}$. Thus, entry (i, j) of matrix A represents the influence of state x_j on the derivative of state x_i, i.e., $\dot{x}_i$. This influence is analytically approximated by taking the first derivative of the equation of motion of $\dot{x}_i$, with respect to x_j. Equation B.2 shows an example of determining the influence of pitching velocity q on the derivative of rolling angle φ: $\dot{\varphi}$. Equation B.3 shows the full A matrix in the state equation. The B matrix is found analogous, by determining the influence of each control input in u on each state derivative in $\dot{x}$.

$$\begin{aligned} \dot{\varphi} &= p + \sin(\phi)\tan(\theta)q + \cos(\phi)tan(\theta)r \\ \frac{d\dot{\varphi}}{dq} &= \sin(\phi)\tan(\theta) \\ A(10,8) &= \frac{d\dot{\varphi}}{dq} = \sin(\phi)\tan(\theta) \end{aligned} \tag{B.2}$$

$$\dot{x} = \begin{bmatrix} \frac{d\dot{X}_e}{dX_e} & \frac{d\dot{X}_e}{dY_e} & \frac{d\dot{X}_e}{dZ_e} & \frac{d\dot{X}_e}{dU_b} & \frac{d\dot{X}_e}{dV_b} & \frac{d\dot{X}_e}{dW_b} & \frac{d\dot{X}_e}{dp} & \frac{d\dot{X}_e}{dq} & \frac{d\dot{X}_e}{dr} & \frac{d\dot{X}_e}{d\varphi} & \frac{d\dot{X}_e}{d\theta} & \frac{d\dot{X}_e}{d\psi} \\ \frac{d\dot{Y}_e}{dX_e} & \frac{d\dot{Y}_e}{dY_e} & \frac{d\dot{Y}_e}{dZ_e} & \frac{d\dot{Y}_e}{dU_b} & \frac{d\dot{Y}_e}{dV_b} & \frac{d\dot{Y}_e}{dW_b} & \frac{d\dot{Y}_e}{dp} & \frac{d\dot{Y}_e}{dq} & \frac{d\dot{Y}_e}{dr} & \frac{d\dot{Y}_e}{d\varphi} & \frac{d\dot{Y}_e}{d\theta} & \frac{d\dot{Y}_e}{d\psi} \\ \frac{d\dot{Z}_e}{dX_e} & \frac{d\dot{Z}_e}{dY_e} & \frac{d\dot{Z}_e}{dZ_e} & \frac{d\dot{Z}_e}{dU_b} & \frac{d\dot{Z}_e}{dV_b} & \frac{d\dot{Z}_e}{dW_b} & \frac{d\dot{Z}_e}{dp} & \frac{d\dot{Z}_e}{dq} & \frac{d\dot{Z}_e}{dr} & \frac{d\dot{Z}_e}{d\varphi} & \frac{d\dot{Z}_e}{d\theta} & \frac{d\dot{Z}_e}{d\psi} \\ \frac{d\dot{U}_b}{dX_e} & \frac{d\dot{U}_b}{dY_e} & \frac{d\dot{U}_b}{dZ_e} & \frac{d\dot{U}_b}{dU_b} & \frac{d\dot{U}_b}{dV_b} & \frac{d\dot{U}_b}{dW_b} & \frac{d\dot{U}_b}{dp} & \frac{d\dot{U}_b}{dq} & \frac{d\dot{U}_b}{dr} & \frac{d\dot{U}_b}{d\varphi} & \frac{d\dot{U}_b}{d\theta} & \frac{d\dot{U}_b}{d\psi} \\ \frac{d\dot{V}_b}{dX_e} & \frac{d\dot{V}_b}{dY_e} & \frac{d\dot{V}_b}{dZ_e} & \frac{d\dot{V}_b}{dU_b} & \frac{d\dot{V}_b}{dV_b} & \frac{d\dot{V}_b}{dW_b} & \frac{d\dot{V}_b}{dp} & \frac{d\dot{V}_b}{dq} & \frac{d\dot{V}_b}{dr} & \frac{d\dot{V}_b}{d\varphi} & \frac{d\dot{V}_b}{d\theta} & \frac{d\dot{V}_b}{d\psi} \\ \frac{d\dot{W}_b}{dX_e} & \frac{d\dot{W}_b}{dY_e} & \frac{d\dot{W}_b}{dZ_e} & \frac{d\dot{W}_b}{dU_b} & \frac{d\dot{W}_b}{dV_b} & \frac{d\dot{W}_b}{dW_b} & \frac{d\dot{W}_b}{dp} & \frac{d\dot{W}_b}{dq} & \frac{d\dot{W}_b}{dr} & \frac{d\dot{W}_b}{d\varphi} & \frac{d\dot{W}_b}{d\theta} & \frac{d\dot{W}_b}{d\psi} \\ \frac{d\dot{p}}{dX_e} & \frac{d\dot{p}}{dY_e} & \frac{d\dot{p}}{dZ_e} & \frac{d\dot{p}}{dU_b} & \frac{d\dot{p}}{dV_b} & \frac{d\dot{p}}{dW_b} & \frac{d\dot{p}}{dp} & \frac{d\dot{p}}{dq} & \frac{d\dot{p}}{dr} & \frac{d\dot{p}}{d\varphi} & \frac{d\dot{p}}{d\theta} & \frac{d\dot{p}}{d\psi} \\ \frac{d\dot{q}}{dX_e} & \frac{d\dot{q}}{dY_e} & \frac{d\dot{q}}{dZ_e} & \frac{d\dot{q}}{dU_b} & \frac{d\dot{q}}{dV_b} & \frac{d\dot{q}}{dW_b} & \frac{d\dot{q}}{dp} & \frac{d\dot{q}}{dq} & \frac{d\dot{q}}{dr} & \frac{d\dot{q}}{d\varphi} & \frac{d\dot{q}}{d\theta} & \frac{d\dot{q}}{d\psi} \\ \frac{d\dot{r}}{dX_e} & \frac{d\dot{r}}{dY_e} & \frac{d\dot{r}}{dZ_e} & \frac{d\dot{r}}{dU_b} & \frac{d\dot{r}}{dV_b} & \frac{d\dot{r}}{dW_b} & \frac{d\dot{r}}{dp} & \frac{d\dot{r}}{dq} & \frac{d\dot{r}}{dr} & \frac{d\dot{r}}{d\varphi} & \frac{d\dot{r}}{d\theta} & \frac{d\dot{r}}{d\psi} \\ \frac{d\dot{\varphi}}{dX_e} & \frac{d\dot{\varphi}}{dY_e} & \frac{d\dot{\varphi}}{dZ_e} & \frac{d\dot{\varphi}}{dU_b} & \frac{d\dot{\varphi}}{dV_b} & \frac{d\dot{\varphi}}{dW_b} & \frac{d\dot{\varphi}}{dp} & \frac{d\dot{\varphi}}{dq} & \frac{d\dot{\varphi}}{dr} & \frac{d\dot{\varphi}}{d\varphi} & \frac{d\dot{\varphi}}{d\theta} & \frac{d\dot{\varphi}}{d\psi} \\ \frac{d\dot{\theta}}{dX_e} & \frac{d\dot{\theta}}{dY_e} & \frac{d\dot{\theta}}{dZ_e} & \frac{d\dot{\theta}}{dU_b} & \frac{d\dot{\theta}}{dV_b} & \frac{d\dot{\theta}}{dW_b} & \frac{d\dot{\theta}}{dp} & \frac{d\dot{\theta}}{dq} & \frac{d\dot{\theta}}{dr} & \frac{d\dot{\theta}}{d\varphi} & \frac{d\dot{\theta}}{d\theta} & \frac{d\dot{\theta}}{d\psi} \\ \frac{d\dot{\psi}}{dX_e} & \frac{d\dot{\psi}}{dY_e} & \frac{d\dot{\psi}}{dZ_e} & \frac{d\dot{\psi}}{dU_b} & \frac{d\dot{\psi}}{dV_b} & \frac{d\dot{\psi}}{dW_b} & \frac{d\dot{\psi}}{dp} & \frac{d\dot{\psi}}{dq} & \frac{d\dot{\psi}}{dr} & \frac{d\dot{\psi}}{d\varphi} & \frac{d\dot{\psi}}{d\theta} & \frac{d\dot{\psi}}{d\psi} \end{bmatrix} x + Bu \quad \text{(B.3)}$$

For small deviations around a trimmed (i.e. constant) aircraft state, the linearised state-space system can accurately approximate deviations as in the non-linear system. Since a state-space system can only respond to inputs, it only yields a deviation from the original state when an input is given. Thus, the state-space system can only approximate an aircraft condition which was trimmed in the non-linear model.

C

Aircraft Classes and Flight Phases

The regulations discussed in US Department of Defense MIL-HDBK-1797 [20] uses four different aircraft classes (I to IV) and three different flight phases (A to C). Table C.1 shows the definition of the different aircraft classes. Table C.2 shows the definition of the different flight phases.

Table C.1: Aircraft classes definition and examples [20].

Class	Aircraft type	Examples
I	Small light aircraft	Light utility Primary trainer Light observation
II	Medium weight, low-to-medium manoeuvrability aircraft	Heavy/utility search and rescue Light or medium transport / cargo Antisubmarine Assault transport Reconnaissance Tactical bomber
III	Large, heavy, low-to-medium manoeuvrability aircraft	Heavy attack Heavy transport/cargo/tanker Heavy bomber
IV	High-manoeuvrability aircraft	Fighter-interceptor Attack

Table C.2: Flight phases definitions and examples [20].

Flight phase	Description	Examples
A	Nonterminal Flight Phases that require manoeuvring, precision tracking or precise flight-path control	Air-to-air combat (CO) Ground attack (GA) Weapon delivery/launch (WD) Aerial recovery (AR) Reconnaissance (RC) In-flight refueling (receiver) (RR) Terrain following (RF) Antisubmarine search (AS) Close formation flying (FF)
B	Nonterminal Flight Phases that are normally accomplished using gradual manoeuvres and without precision tracking, although accurate flight-path control may be required.	Climb (CL) Cruise (CR) Loiter (LO) In-flight refueling (tanker) (RT) Descent (D) Emergency descent (ED) Emergency deceleration (DE) Aerial delivery (AD)
C	Terminal Flight Phases that are normally accomplished using gradual manoeuvres and usually require accurate flight-path control.	Takeoff (TO) Catapult takeoff (CT) Approach (PA) Waveoff/go-around (WO) Landing (L)

D

Full Trim States Bare-Airframe Handling Quality Analysis

This appendix shows the full trim states obtained during the bare-airframe handling quality analysis shown in Chapter 5. First, the trim states for straight symmetric horizontal flight in approach, take-off and cruise are shown, since these were used to check the Dutch Roll, spiral stability and lateral control departure parameter requirements. Next, the trim states obtained for each other requirement are shown separately. It should be noted that the angular rates (P, Q, R) are only shown in the trim states when they are non-zero.

Straight, Symmetric Horizontal Flight Trim States

Table D.1 and D.2 show the full trim states during straight symmetric horizontal flight in approach, take-off and cruise, respectively, for the forward and aft CG location.

Coordinated Turn Trim States

Table D.3 and D.4 show the full trim states for the different coordinated turn capability requirement conditions tested, respectively, for the forward and aft CG location.

Time to Bank Trim States

Table D.5 and D.6 show the full trim states for the different time to bank requirement conditions tested, respectively, for the forward and aft CG location.

One Engine Inoperative Trim States

Table D.7 and D.8 show the full trim states for the different one engine inoperative trim conditions tested, respectively, for the forward and aft CG location.

Steady Heading Sideslip Trim States

Table D.9 and D.10 show the full trim states for the different steady heading sideslip conditions tested, respectively, for the forward and aft CG location.

Table D.1: Trim states Flying-V in straight symmetric horizontal flight, forward CG.

	APP	TO	CR
U [m/s]	64.008	101.354	248.727
V [m/s]	0	0	0
W [m/s]	24.676	17.771	31.786
ϕ [deg]	0	0	0
θ [deg]	21.082	9.945	7.283
ψ [deg]	0	0	0
α [deg]	21.082	9.945	7.283
β [deg]	0	0	0
C1 [deg]	0	0	0
C2 [deg]	0	0	0
C3 [deg]	-36.813	-15.41	-14.461
C4 [deg]	-36.813	-15.41	-14.461
C5 [deg]	0	0	0
C6 [deg]	0	0	0
T1 [N]	48095.534	27481.978	22370.12
T2 [N]	48095.534	27481.978	22370.12

Table D.2: Trim states Flying-V in straight symmetric horizontal flight, aft CG.

	APP	TO	CR
U [m/s]	65.437	101.826	249.298
V [m/s]	0	0	0
W [m/s]	20.592	14.828	26.947
ϕ [deg]	0	0	0
θ [deg]	17.468	8.285	6.169
ψ [deg]	0	0	0
α [deg]	17.468	8.285	6.169
β [deg]	0	0	0
C1 [deg]	0	0	0
C2 [deg]	0	0	0
C3 [deg]	-7.475	-1.364	-5.374
C4 [deg]	-7.475	-1.364	-5.374
C5 [deg]	0	0	0
C6 [deg]	0	0	0
T1 [N]	51262.103	30121.266	23460.026
T2 [N]	51262.103	30121.266	23460.026

Table D.3: Trim states Flying-V in coordinated turn, forward CG.

	CTC TO AEO	CTC APP AEO	CTC TO OEI	CTC CR OEI
U [m/s]	100	61.5	101	247
V [m/s]	0	0	0	0
W [m/s]	23.2	30.3	18.3	41.3
P [rad/s]	-0.0145	-0.0408	0.00941	0.00442
Q [rad/s]	0.049	0.0612	0.0259	0.0203
R [rad/s]	0.0584	0.0729	-0.0449	-0.0242
ϕ [deg]	40	40	-30	-40
θ [deg]	10.8	23.2	10.3	7.97
ψ [deg]	0	0	0	0
α [deg]	13.1	26.2	10.3	9.47
β [deg]	0	0	0	0
C1 [deg]	-0.4	7	6.5	3.1
C2 [deg]	-4.4	-17.3	2	0.2
C3 [deg]	-23.9	-52.9	-17.4	-19.8
C4 [deg]	-23.9	-52.9	-17.4	-19.8
C5 [deg]	4.4	17.3	-2	-0.2
C6 [deg]	0.4	-7	-6.5	-3.1
T1 [N]	55828.1	108201.1	105979.3	85447
T2 [N]	55828.1	108201.1	0	0

Table D.4: Trim states Flying-V in coordinated turn, aft CG.

	CTC TO AEO	CTC APP AEO	CTC TO OEI	CTC CR OEI
U [m/s]	101	63.4	102	248
V [m/s]	0	0	0	0
W [m/s]	19.6	26.2	15.4	35.1
P [rad/s]	-0.0125	-0.036	0.00812	0.00382
Q [rad/s]	0.0497	0.0656	0.0261	0.0204
R [rad/s]	0.0592	0.0782	-0.0452	-0.0243
ϕ [deg]	40	40	-30	-40
θ [deg]	9.15	19.5	8.84	6.88
ψ [deg]	0	0	0	0
α [deg]	11	22.5	8.6	8.05
β [deg]	0	0	0	0
C1 [deg]	-0.7	4.9	7.4	4
C2 [deg]	-3.5	-14.2	1.2	-0.1
C3 [deg]	-5.7	-17.7	-3	-8.2
C4 [deg]	-5.7	-17.7	-3	-8.2
C5 [deg]	3.5	14.2	-1.2	0.1
C6 [deg]	0.7	-4.9	-7.4	-4
T1 [N]	60688.8	112868.6	112549.5	101849.8
T2 [N]	60688.8	112868.6	0	0

Table D.5: Trim states Flying-V before time to bank manoeuvre, forward CG.

	TTB APP AEO	TTB CR AEO	TTB TO OEI
U [m/s]	61.2	248	101
V [m/s]	0	0	0
W [m/s]	30.9	36.8	20.7
P [rad/s]	-0.0292	-0.00285	-0.00957
Q [rad/s]	0.0333	0.0111	0.0269
R [rad/s]	0.0578	0.0192	0.0466
ϕ [deg]	30	30	30
θ [deg]	23.6	7.32	10.1
ψ [deg]	0	0	0
α [deg]	26.8	8.43	11.6
β [deg]	0	0	0
C1 [deg]	2.8	-0.1	3.4
C2 [deg]	-13.3	-0.4	-3.8
C3 [deg]	-51.6	-17.3	-19.9
C4 [deg]	-51.6	-17.3	-19.9
C5 [deg]	13.3	0.4	3.8
C6 [deg]	-2.8	0.1	-3.4
T1 [N]	64075.5	26404.6	70246.9
T2 [N]	64075.5	26404.6	0

Table D.6: Trim states Flying-V before time to bank manoeuvre, aft CG.

	TTB APP AEO	TTB CR AEO	TTB TO OEI
U [m/s]	63.4	249	101
V [m/s]	0	0	0
W [m/s]	26.3	31.3	17.3
P [rad/s]	-0.0256	-0.00243	-0.00808
Q [rad/s]	0.0356	0.0111	0.0273
R [rad/s]	0.0617	0.0193	0.0472
ϕ [deg]	30	30	30
θ [deg]	19.8	6.21	8.43
ψ [deg]	0	0	0
α [deg]	22.5	7.16	9.71
β [deg]	0	0	0
C1 [deg]	2	-0.1	3.8
C2 [deg]	-10.9	-0.3	-3.2
C3 [deg]	-15.1	-6.9	-3.6
C4 [deg]	-15.1	-6.9	-3.6
C5 [deg]	10.9	0.3	3.2
C6 [deg]	-2	0.1	-3.8
T1 [N]	79654	30900.6	75020.8
T2 [N]	79654	30900.6	0

Table D.7: Trim states Flying-V with one engine inoperative, forward CG.

	OEI TRIM APP	OEI TRIM TO	OEI TRIM CR
U [m/s]	62.9	101	248
V [m/s]	1.51	-0.225	-13
W [m/s]	27.4	17.8	31.7
ϕ [deg]	-0.811	-0.328	-1.18
θ [deg]	23.5	9.95	7.34
ψ [deg]	-1.58	0.0688	2.83
α [deg]	23.6	9.94	7.28
β [deg]	1.26	-0.126	-2.98
C1 [deg]	26.7	2.9	-0.4
C2 [deg]	5	-1	-8.8
C3 [deg]	-41.8	-15.4	-14.5
C4 [deg]	-41.8	-15.4	-14.5
C5 [deg]	-5	1	8.8
C6 [deg]	-26.7	-2.9	0.4
T1 [N]	112977.5	54963.1	45085
T2 [N]	0	0	0

Table D.8: Trim states Flying-V with one engine inoperative, aft CG.

	OEI TRIM APP	OEI TRIM TO	OEI TRIM CR
U [m/s]	64.6	102	249
V [m/s]	-1.63	-0.284	1.21
W [m/s]	23	14.8	26.9
ϕ [deg]	-0.888	-0.395	-0.183
θ [deg]	19.6	8.29	6.17
ψ [deg]	1.07	0.101	-0.296
α [deg]	19.6	8.28	6.17
β [deg]	-1.36	-0.158	0.277
C1 [deg]	15.1	3.4	1.9
C2 [deg]	-11.2	-1.1	0.5
C3 [deg]	-9.3	-1.4	-5.4
C4 [deg]	-9.3	-1.4	-5.4
C5 [deg]	11.2	1.1	-0.5
C6 [deg]	-15.1	-3.4	-1.9
T1 [N]	127234.5	60240.4	47037.6
T2 [N]	0	0	0

Table D.9: Trim states Flying-V in steady heading sideslip, forward CG.

	SHS TO	SHS CR	SHS APP	SHS TO OEI	SHS CR OEI	SHS APP OEI
U [m/s]	100	248	62.4	100	248	62.4
V [m/s]	-15.6	-15.6	-15.6	-15.6	-15.6	-15.6
W [m/s]	17.6	31.7	24	17.6	31.7	24
ϕ [deg]	-1.57	-1.12	0.253	-1.88	-1.36	-0.406
θ [deg]	10.2	7.35	21	10.2	7.37	21.1
ψ [deg]	8.42	3.41	13.2	8.37	3.38	13
α [deg]	9.94	7.28	21	9.94	7.28	21
β [deg]	-8.69	-3.56	-13.1	-8.69	-3.56	-13.1
C1 [deg]	-10.9	-2.3	-66.7	-7.8	-0.8	-51.7
C2 [deg]	-33.2	-10.3	-78.5	-33.7	-10.5	-80.9
C3 [deg]	-15.4	-14.5	-36.5	-15.4	-14.5	-36.6
C4 [deg]	-15.4	-14.5	-36.5	-15.4	-14.5	-36.6
C5 [deg]	33.2	10.3	78.5	33.7	10.5	80.9
C6 [deg]	10.9	2.3	66.7	7.8	0.8	51.7
T1 [N]	27787.7	22618.1	48948.6	55565.3	45174.3	98064.3
T2 [N]	27787.7	22618.1	48948.6	0	0	0

Table D.10: Trim states Flying-V in steady heading sideslip, aft CG.

	SHS TO	SHS CR	SHS APP	SHS TO OEI	SHS CR OEI	SHS APP OEI
U [m/s]	101	249	63.7	101	249	63.7
V [m/s]	-15.6	-15.6	-15.6	-15.6	-15.6	-15.6
W [m/s]	14.6	26.9	20	14.6	26.9	20
ϕ [deg]	-1.85	-1.22	-0.686	-2.21	-1.5	-1.44
θ [deg]	8.56	6.24	17.6	8.61	6.26	17.8
ψ [deg]	8.42	3.42	12.9	8.37	3.39	12.7
α [deg]	8.28	6.17	17.5	8.28	6.17	17.5
β [deg]	-8.69	-3.56	-13.1	-8.69	-3.56	-13.1
C1 [deg]	-9.4	-2.3	-41.5	-5.8	-0.5	-24.8
C2 [deg]	-29.5	-9.3	-71.3	-30.1	-9.5	-74
C3 [deg]	-1.4	-5.4	-7.5	-1.4	-5.4	-7.5
C4 [deg]	-1.4	-5.4	-7.5	-1.4	-5.4	-7.5
C5 [deg]	29.5	9.3	71.3	30.1	9.5	74
C6 [deg]	9.4	2.3	41.5	5.8	0.5	24.8
T1 [N]	30443.1	23638.1	53134.1	60863.8	47168.7	105774
T2 [N]	30443.1	23638.1	53134.1	0	0	0

E

Zero-lift drag, Theoretical Handling Quality Re-Analysis Results

This appendix shows the results of the theoretical handling quality re-analysis, including the zero-lift drag of Faggiano as discussed in subsection 5.4.4 of Chapter 5. The results are presented for each requirement tested.

MIL-HDBK-1797 - Dutch Roll

Table E.1 and Table E.2 show the Dutch Roll damping and frequency parameters for the bare airframe Flying-V, trimmed and linearised in horizontal straight symmetric flight, for, respectively, the forward and aft CG location. The three conditions assessed were approach (APP) take-off (TO) and Cruise (CR), using the flight conditions as elaborated upon in subsection 5.1.1. In both tables, first the results when including zero-lift drag are shown, second the (earlier) results of excluding the zero-lift drag.

MIL-HDBK-1797 - Spiral Stability

Table E.3 and Table E.4 show the spiral stability time to double parameters for the bare airframe Flying-V, trimmed and linearised in horizontal straight symmetric flight, for, respectively, the forward and aft CG location. The three conditions assessed were approach (APP) take-off (TO) and cruise (CR), using the flight conditions as elaborated upon in subsection 5.1.1. In both tables, first the results when including zero-lift drag are shown, second the (earlier) results of excluding the zero-lift drag.

MIL-HDBK-1797 - Lateral Control Departure Parameter

Table E.5 and Table E.6 show Lateral Control Departure Parameter (LCDP) for the bare airframe Flying-V, trimmed and linearised in horizontal straight symmetric flight, for, respectively, the forward and aft CG location. The three conditions assessed were again approach (APP) take-off (TO) and cruise (CR). In both tables, first the results when including zero-lift drag are shown, second the (earlier) results of excluding the zero-lift drag.

CS25.143(h) - Coordinated Turn Capability

Table E.7 and Table E.8 show the trimmed input vectors for, respectively, the forward and aft CG location, for four different flight conditions trimmed in a Coordinated Turn (CTC): Take Off All Engines Operative (TO AEO), Approach All Engines Operative (APP AEO), Take Off One Engine Inoperative (TO OEI) and Cruise One Engine Inoperative (CR OEI). These conditions were elaborated upon in subsection 3.1.4, and also have constraints on the Gradient of Climb or Flight Path Angle. In both tables, first the results when including zero-lift drag are shown, second the (earlier) results of excluding the zero-lift drag.

CS25.147(f) - Time to Bank, Roll Capability

Table E.9 and Table E.10 show the control surface deflections required during the time to bank (TTB) manoeuvre, respectively, for the forward and aft CG location. The manoeuvre was performed for three different flight conditions: Approach All Engines Operative (APP AEO), Cruise All Engines Operative (CR AEO) and Take Off One Engine Inoperative (TO OEI). The maximum required control surface deflections were found by taking the sum of the trimmed control surface deflections and the minimum required deviation to perform the manoeuvre in the set time. In both tables, first the results when including zero-lift drag are shown, second the (earlier) results of excluding the zero-lift drag.

CS25.161(d) - One Engine Inoperative Trim Condition

Table E.11 and Table E.12 show the control surface input vector trimmed with One Engine Inoperative (OEI) in horizontal flight, respectively, for the forward and aft CG location, for Approach (APP), Take Off (TO) and Cruise (CR) conditions. In both tables, first the results when including zero-lift drag are shown, second the (earlier) results of excluding the zero-lift drag.

CS25.177(c) - Steady Heading Sideslip

Table E.13 and Table E.14 show the trimmed input vector for, respectively, the forward and aft CG location, for six different flight conditions trimmed in a Steady Heading Sideslip (SHS): Take Off All Engines Operative (TO AEO), Cruise All Engines Operative (CR AEO), Approach All Engines Operative (APP AEO), Take Off One Engine Inoperative (TO OEI), Cruise One Engine Inoperative (CR OEI) and Approach One Engine Inoperative (APP OEI). In both tables, first the results when including zero-lift drag are shown, second the (earlier) results of excluding the zero-lift drag.

Table E.1: Bare Airframe Flying-V Dutch Roll Parameters, Forward CG.

	C_{d_0} included		C_{d_0} excluded	
	Damping Parameter [-]	Frequency [rad/s]	Damping Parameter [-]	Frequency [rad/s]
APP	-0.0695	1.05	-0.0698	1.05
TO	-0.0263	0.86	-0.0271	0.86
CR	-0.0101	0.811	-0.0107	0.811

Table E.2: Bare Airframe Flying-V Dutch Roll Parameters, Aft CG.

	C_{d_0} included		C_{d_0} excluded	
	Damping Parameter [-]	Frequency [rad/s]	Damping Parameter [-]	Frequency [rad/s]
APP	-0.0754	0.898	-0.0758	0.899
TO	-0.0185	0.748	-0.0194	0.748
CR	0.00223	0.731	0.00167	0.731

Table E.3: Bare Airframe Flying-V spiral stability time to double parameter, forward CG.

	C_{d_0} included	C_{d_0} excluded
	T2 [s]	T2 [s]
APP	28.0855	27.9439
TO	454.3357	447.4338
CR	-657.2026	-659.4537

Table E.4: Bare Airframe Flying-V spiral stability time to double parameter, aft CG.

	C_{d_0} included T2 [s]	C_{d_0} excluded T2 [s]
APP	44.5556	44.3465
TO	-497.6221	-501.6434
CR	-378.7571	-379.0323

Table E.5: Lateral Control Departure Parameter for the bare airframe Flying-V, forward CG.

	C_{d_0} included LCDP [-]	C_{d_0} excluded LCDP [-]
APP	0.00391	0.00393
TO	0.00116	0.00116
CR	0.000754	0.000751

Table E.6: Lateral Control Departure Parameter for the bare airframe Flying-V, aft CG.

	C_{d_0} included LCDP [-]	C_{d_0} excluded LCDP [-]
APP	0.00233	0.00234
TO	0.000957	0.000957
CR	0.000679	0.000677

Table E.7: Trimmed control input vectors in coordinated turn manoeuvre, forward CG.

	C_{d_0} included			
	CTC TO AEO	CTC APP AEO	CTC TO OEI	CTC CR OEI
C1 [deg]	-0.4	6.9	8.3	4.6
C2 [deg]	-4.4	-17.3	1.6	0
C3 [deg]	-23.9	-52.8	-17.3	-19.8
C4 [deg]	-23.9	-52.8	-17.3	-19.8
C5 [deg]	4.4	17.3	-1.6	0
C6 [deg]	0.4	-6.9	-8.3	-4.6
T1 [N]	72409.6	115871.7	138760.4	127891.3
T2 [N]	72409.6	115871.7	0	0

	C_{d_0} excluded			
	CTC TO AEO	CTC APP AEO	CTC TO OEI	CTC CR OEI
C1 [deg]	-0.4	7	6.5	3.1
C2 [deg]	-4.4	-17.3	2	0.2
C3 [deg]	-23.9	-52.9	-17.4	-19.8
C4 [deg]	-23.9	-52.9	-17.4	-19.8
C5 [deg]	4.4	17.3	-2	-0.2
C6 [deg]	0.4	-7	-6.5	-3.1
T1 [N]	55828.1	108201.1	105979.3	85447
T2 [N]	55828.1	108201.1	0	0

Table E.8: Trimmed control input vectors in coordinated turn manoeuvre, aft CG.

	C_{d_0} included			
	CTC TO AEO	CTC APP AEO	CTC TO OEI	CTC CR OEI
C1 [deg]	-0.7	4.8	9.4	5.6
C2 [deg]	-3.5	-14.2	0.9	-0.3
C3 [deg]	-5.7	-17.8	-3	-8.2
C4 [deg]	-5.7	-17.8	-3	-8.2
C5 [deg]	3.5	14.2	-0.9	0.3
C6 [deg]	0.7	-4.8	-9.4	-5.6
T1 [N]	77177.8	120294.2	145283.1	143914.1
T2 [N]	77177.8	120294.2	0	0

	C_{d_0} excluded			
	CTC TO AEO	CTC APP AEO	CTC TO OEI	CTC CR OEI
C1 [deg]	-0.7	4.9	7.4	4
C2 [deg]	-3.5	-14.2	1.2	-0.1
C3 [deg]	-5.7	-17.7	-3	-8.2
C4 [deg]	-5.7	-17.7	-3	-8.2
C5 [deg]	3.5	14.2	-1.2	0.1
C6 [deg]	0.7	-4.9	-7.4	-4
T1 [N]	60688.8	112868.6	112549.5	101849.8
T2 [N]	60688.8	112868.6	0	0

Table E.9: Control deflections in time to bank manoeuvre, forward CG.

	C_{d_0} included		
	TTB APP AEO	TTB CR AEO	TTB TO OEI
C1 [deg]	23.3	10.8	22.8
C2 [deg]	-90.7	-11.3	-21.6
C3 [deg]	-51.5	-17.3	-20
C4 [deg]	-51.5	-17.3	-20
C5 [deg]	90.7	11.3	21.6
C6 [deg]	-23.3	-10.8	-22.8
T1 [N]	71958.9	47614.1	103535.9
T2 [N]	71958.9	47614.1	0
t BTB [s]	7	7	11

	C_{d_0} excluded		
	TTB APP AEO	TTB CR AEO	TTB TO OEI
C1 [deg]	23.1	10.8	20.9
C2 [deg]	-90.4	-11.3	-21.3
C3 [deg]	-51.6	-17.3	-19.9
C4 [deg]	-51.6	-17.3	-19.9
C5 [deg]	90.4	11.3	21.3
C6 [deg]	-23.1	-10.8	-20.9
T1 [N]	64075.5	26404.6	70246.9
T2 [N]	64075.5	26404.6	0
t BTB [s]	7	7	11

Table E.10: Control deflections in time to bank manoeuvres, aft CG.

	TTB APP AEO	TTB CR AEO	TTB TO OEI
		C_{d_0} included	
C1 [deg]	90.7	9.8	21.9
C2 [deg]	-99.7	-10.3	-19.6
C3 [deg]	-15.1	-6.9	-3.7
C4 [deg]	-15.1	-6.9	-3.7
C5 [deg]	99.7	10.3	19.6
C6 [deg]	-90.7	-9.8	-21.9
T1 [N]	79654	30900.6	75020.8
T2 [N]	79654	30900.6	0
t BTB [s]	7	7	11

		C_{d_0} excluded	
	TTB APP AEO	TTB CR AEO	TTB TO OEI
C1 [deg]	90.6	9.8	19.9
C2 [deg]	-99.5	-10.3	-19.2
C3 [deg]	-15.1	-6.9	-3.6
C4 [deg]	-15.1	-6.9	-3.6
C5 [deg]	99.5	10.3	19.2
C6 [deg]	-90.6	-9.8	-19.9
T1 [N]	79654	30900.6	75020.8
T2 [N]	79654	30900.6	0
t BTB [s]	7	7	11

Table E.11: Trimmed control input vectors with one engine inoperative, forward CG.

		C_{d_0} included	
	OEI TRIM APP	OEI TRIM TO	OEI TRIM CR
C1 [deg]	26	4.7	2.1
C2 [deg]	1.8	-1.5	-4.3
C3 [deg]	-41.7	-15.4	-14.5
C4 [deg]	-41.7	-15.4	-14.5
C5 [deg]	-1.8	1.5	4.3
C6 [deg]	-26	-4.7	-2.1
T1 [N]	128349.7	88019.4	87296.3
T2 [N]	0	0	0

		C_{d_0} excluded	
	OEI TRIM APP	OEI TRIM TO	OEI TRIM CR
C1 [deg]	26.7	2.9	-0.4
C2 [deg]	5	-1	-8.8
C3 [deg]	-41.8	-15.4	-14.5
C4 [deg]	-41.8	-15.4	-14.5
C5 [deg]	-5	1	8.8
C6 [deg]	-26.7	-2.9	0.4
T1 [N]	112977.5	54963.1	45085
T2 [N]	0	0	0

Table E.12: Trimmed control input vectors with one engine inoperative, aft CG.

	C_{d_0} included		
	OEI TRIM APP	OEI TRIM TO	OEI TRIM CR
C1 [deg]	23.8	5.3	3.1
C2 [deg]	-3	-1.7	-1.4
C3 [deg]	-9.4	-1.4	-5.4
C4 [deg]	-9.4	-1.4	-5.4
C5 [deg]	3	1.7	1.4
C6 [deg]	-23.8	-5.3	-3.1
T1 [N]	142131.5	93141	89342.8
T2 [N]	0	0	0

	C_{d_0} excluded		
	OEI TRIM APP	OEI TRIM TO	OEI TRIM CR
C1 [deg]	15.1	3.4	1.9
C2 [deg]	-11.2	-1.1	0.5
C3 [deg]	-9.3	-1.4	-5.4
C4 [deg]	-9.3	-1.4	-5.4
C5 [deg]	11.2	1.1	-0.5
C6 [deg]	-15.1	-3.4	-1.9
T1 [N]	127234.5	60240.4	47037.6
T2 [N]	0	0	0

Table E.13: Trimmed control input vectors for different steady heading sideslip conditions, forward CG.

	C_{d_0} included					
	SHS TO	SHS CR	SHS APP	SHS TO OEI	SHS CR OEI	SHS APP OEI
C1 [deg]	-10.9	-2.3	-66.2	-6	0.7	-49
C2 [deg]	-33.2	-10.2	-78.4	-33.9	-10.6	-81.2
C3 [deg]	-15.4	-14.5	-36.5	-15.4	-14.5	-36.5
C4 [deg]	-15.4	-14.5	-36.5	-15.4	-14.5	-36.5
C5 [deg]	33.2	10.2	78.4	33.9	10.6	81.2
C6 [deg]	10.9	2.3	66.2	6	-0.7	49
T1 [N]	44505.2	43815.5	56718.5	88991.7	87564.7	113614.9
T2 [N]	44505.2	43815.5	56718.5	0	0	0

	C_{d_0} excluded					
	SHS TO	SHS CR	SHS APP	SHS TO OEI	SHS CR OEI	SHS APP OEI
C1 [deg]	-10.9	-2.3	-66.7	-7.8	-0.8	-51.7
C2 [deg]	-33.2	-10.3	-78.5	-33.7	-10.5	-80.9
C3 [deg]	-15.4	-14.5	-36.5	-15.4	-14.5	-36.6
C4 [deg]	-15.4	-14.5	-36.5	-15.4	-14.5	-36.6
C5 [deg]	33.2	10.3	78.5	33.7	10.5	80.9
C6 [deg]	10.9	2.3	66.7	7.8	0.8	51.7
T1 [N]	27787.7	22618.1	48948.6	55565.3	45174.3	98064.3
T2 [N]	27787.7	22618.1	48948.6	0	0	0

Table E.14: Trimmed control input vectors for different steady heading sideslip conditions, aft CG.

	C_{d_0} included					
	SHS TO	SHS CR	SHS APP	SHS TO OEI	SHS CR OEI	SHS APP OEI
C1 [deg]	-9.4	-2.3	-41.3	-3.8	1.1	-22.2
C2 [deg]	-29.5	-9.3	-71.3	-30.3	-9.7	-74.3
C3 [deg]	-1.4	-5.4	-7.5	-1.4	-5.4	-7.5
C4 [deg]	-1.4	-5.4	-7.5	-1.4	-5.4	-7.5
C5 [deg]	29.5	9.3	71.3	30.3	9.7	74.3
C6 [deg]	9.4	2.3	41.3	3.8	-1.1	22.2
T1 [N]	47081	44791.1	60720	94123.3	89496.3	120867.2
T2 [N]	47081	44791.1	60720	0	0	0

	C_{d_0} excluded					
	SHS TO	SHS CR	SHS APP	SHS TO OEI	SHS CR OEI	SHS APP OEI
C1 [deg]	-9.4	-2.3	-41.5	-5.8	-0.5	-24.8
C2 [deg]	-29.5	-9.3	-71.3	-30.1	-9.5	-74
C3 [deg]	-1.4	-5.4	-7.5	-1.4	-5.4	-7.5
C4 [deg]	-1.4	-5.4	-7.5	-1.4	-5.4	-7.5
C5 [deg]	29.5	9.3	71.3	30.1	9.5	74
C6 [deg]	9.4	2.3	41.5	5.8	0.5	24.8
T1 [N]	30443.1	23638.1	53134.1	60863.8	47168.7	105774
T2 [N]	30443.1	23638.1	53134.1	0	0	0

Bibliography

[1] R. Martinez-Val. “Flying Wings. A New Paradigm for Civil Aviation?” In: *Acta Polytechnica* 47 (2007). DOI: 10.14311/914. URL: https://www.semanticscholar.org/paper/Flying-Wings.-A-New-Paradigm-for-Civil-Aviation-Mart%5C%C3%5C%ADnez-Val/0f4587635e7d2bff414d971019aea526f639ff08.

[2] R. H. Liebeck. “Design of the Blended Wing Body Subsonic Transport”. In: *Journal of Aircraft* 41 (2004), pages 10–25. ISSN: 15333868. DOI: 10.2514/1.9084.

[3] M. Brown and R. Vos. “Conceptual design and evaluation of blended-wing-body aircraft”. In: *AIAA Aerospace Sciences Meeting, 2018* (2018). DOI: 10.2514/6.2018-0522.

[4] J. Benad. “The Flying V-A new Aircraft Configuration for Commercial Passenger Transport”. In: *Deutscher Luft- und Raumfahrtkongress 2015, Rostock* (2015). DOI: 10.25967/370094. URL: https://www.researchgate.net/publication/324150114.

[5] F. Faggiano. “Aerodynamic Design Optimization of a Flying V Aircraft”. Master’s thesis. TU Delft, 2016. URL: http://resolver.tudelft.nl/uuid:0b1472a5-3aad-433c-9a64-242c84b114fd.

[6] A. L. Bolsunovsky et al. “Flying wing - Problems and decisions”. In: *Aircraft Design* 4 (2001), pages 193–219. ISSN: 13698869. DOI: 10.1016/S1369-8869(01)00005-2.

[7] Y. Pan and J. Huang. “Research on lateral-directional stability augmentation system of flying wing aircraft based on reliability model”. In: *Proceedings of the Institution of Mechanical Engineers, Part G: Journal of Aerospace Engineering* 233 (2019), pages 4214–4221. ISSN: 20413025. DOI: 10.1177/0954410018817449.

[8] T. Cappuyns. “Handling Qualities of a Flying-V configuration”. Master’s thesis. TU Delft, 2019. URL: http://resolver.tudelft.nl/uuid:69b56494-0731-487a-8e57-cec397452002.

[9] H. V. D. Castro. “Flying and handling Qualities of a Fly-by-Wire Blended-Wing-Body Civil Transport Aircraft”. 2003. URL: https://dspace.lib.cranfield.ac.uk/handle/1826/119.

[10] J. Ehlers, D. Niedermeier, and D. Leißling. “Verification of a flying wing handling qualities analysis by means of in-flight simulation”. In: *AIAA Atmospheric Flight Mechanics Conference 2011* (2011). DOI: 10.2514/6.2011-6540.

[11] M. Claeys. “Flying V and Reference Aircraft Structural Analysis and Mass Comparison”. Master’s thesis. TU Delft, 2018. URL: http://resolver.tudelft.nl/uuid:ee7f2ecb-cdb6-46de-8b57-d55b89f8c7e6.

[12] R. A. Viet. “Analysis of the flight characteristics of a highly swept cranked flying wing by means of an experimental test”. Master’s thesis. TU Delft, 2019. URL: http://resolver.tudelft.nl/uuid:90de4d9e-70ae-4efc-bd0a-7426a0a669c3.

[13] A. R. Garcia. “Aerodynamic Model Identification of the Flying V Using Wind Tunnel Data”. Master’s thesis. TU Delft, 2019. URL: http://resolver.tudelft.nl/uuid:79e01f29-1789-4501-8556-ca2bcf06f3ab.

[14] M. Palermo and R. Vos. “Experimental aerodynamic analysis of a 4.6%-scale flying-v subsonic transport”. In: *AIAA Scitech 2020 Forum* 1 PartF (2020). DOI: 10.2514/6.2020-2228.

[15] B. R. Pascual. “Engine-Airframe Integration for the Flying”. Master’s thesis. 2018. URL: http://resolver.tudelft.nl/uuid:75be27a7-6fd4-4112-a600-45df2999758f.

[16] J. A. Mulder et al. *Flight Dynamics Lecture Notes*. Delft University of Technology, 2013.

[17] G. E. Cooper and R. P. Harper. “The Use of Pilot Rating in the Evaluation of Aircraft Handling Qualities”. In: (1969). URL: https://ntrs.nasa.gov/citations/19690013177.

[18] D. G. Mitchell. “Fifty years of the cooper-harper scale”. In: *AIAA Scitech 2019 Forum* (2019). DOI: 10.2514/6.2019-0563.

[19] J. Roskam. *Airplane design. Pt. 7. Determination of stability, control and performance characteristics : far and military requirements.* Roskam Aviation and Engineering, 1988.

[20] US Department Of Defence. *Handbook MIL-HDBK-1797a Flying Qualities of Piloted Aircraft*. 1997, pages 2–18. URL: http://everyspec.com/MIL-HDBK/MIL-HDBK-1500-1799/MIL-HDBK-1797_NOTICE-1_39380/.

[21] EASA. *Certification Specifications for Large Aeroplanes CS-25 - Amendment 23*. European Union Aviation Safety Agency, 2019. URL: https://www.easa.europa.eu/document-library/certification-specifications/cs-25-amendment-23.

[22] R. E. Perez, H. H. Liu, and K. Behdinan. "Multidisciplinary optimization framework for control-configuration integration in aircraft conceptual design". In: *Journal of Aircraft* 43 (2006), pages 1937–1948. ISSN: 15333868. DOI: 10.2514/1.22263.

[23] N. F. M. Wahler. "The Impact of Control Allocation on Optimal Control Surface Positioning and Sizing A comparative study for a PrandtlPlane". Master's thesis. 2021. URL: http://resolver.tudelft.nl/uuid:5e9baf63-8a8f-4c1b-98cd-5aa993938027.

[24] B. Etkin and L. D. Reid. *Dynamics of Flight Stability and Control*. John Wiley & Sons, inc, 1996. URL: https://www.worldcat.org/title/dynamics-of-flight-stability-and-control/oclc/849073275.

[25] M. Voskuijl, G. L. Rocca, and F. Dircken. "Controllability of Blended Wing Body Aircraft". In: *Proceedings of the 26th International Congress of the Aronautical Sciences, ICAS 2008, including the 8th AIAA Aviation Technology, Integration and Operations (AIO) Conference, Anchorage, Alaska* (2008). URL: http://resolver.tudelft.nl/uuid:feb50bf7-6f4c-4292-aed7-5700e8e4beeb.

[26] V. Portapas and A. Cooke. "Simulated pilot-in-the-loop testing of handling qualities of the flexible wing aircraft". In: *Aviation* 24 (2020), pages 1–9. ISSN: 18224180. DOI: 10.3846/aviation.2020.12175.

[27] T. Berger, M. B. Tischlery, and S. G. Hagerottz. "Piloted simulation handling qualities assessment of a business jet fly-by-wire flight control system". In: *AIAA Atmospheric Flight Mechanics Conference, 2015* (2015). DOI: 10.2514/6.2015-0019.

[28] T. Berger et al. "Handling qualities flight test assessment of a business jet NzU P-β fly-by-wire control system". In: American Institute of Aeronautics and Astronautics Inc, AIAA, 2017. ISBN: 9781624104480. DOI: 10.2514/6.2017-1398.

[29] E. J. Field et al. "Comparison of in-flight and ground based simulations of large aircraft flying qualities". In: American Institute of Aeronautics and Astronautics Inc., 2002. ISBN: 9781563479458. DOI: 10.2514/6.2002-4800.

[30] E. J. Field et al. "Validation of simulation models for piloted handling qualities evaluations". In: *Collection of Technical Papers - AIAA Modeling and Simulation Technologies Conference* 2 (2004), pages 815–828. DOI: 10.2514/6.2004-5268.

[31] J. Vidakovic and M. Lazarevic. "Flight Simulation Training Devices: Application, Classification, and Research". In: *International Journal of Aeronautical and Space Sciences* (2021). ISSN: 20932480. DOI: 10.1007/s42405-021-00358-y.

[32] S. K. Advani. "The development of SIMONA: A simulator facility for advanced research into simulation techniques, motion system control and navigation systems technologies". In: American Institute of Aeronautics and Astronautics Inc, AIAA, 1993, pages 156–166. DOI: 10.2514/6.1993-3574.

[33] O. Stroosma et al. "A handling qualities assessment of a business jet augmented with an L1 adaptive controller". In: 2011. ISBN: 9781600869525. URL: https://www.scopus.com/record/display.uri?eid=2-s2.0-84880597033&origin=inward.

[34] M. Pieters et al. "A simulator comparison study into the effects of motion filter order on pilot control behavior". In: cited By 2. American Institute of Aeronautics and Astronautics Inc, AIAA, 2019. ISBN: 9781624105784. DOI: 10.2514/6.2019-0712.

[35] M. van Paassen, O. Stroosma, and J. Delatour. “DUECA - Data-driven activation in distributed real-time computation”. In: cited By 36. American Institute of Aeronautics and Astronautics Inc., 2000. DOI: 10.2514/6.2000-4503.

[36] N. Zhang, F. Li, and L. Wang. “Control allocation approach study for BWB aircraft”. In: volume 459. Springer Verlag, 2019, pages 2099–2115. DOI: 10.1007/978-981-13-3305-7_168.

[37] C. Huijts and M. Voskuijl. “The impact of control allocation on trim drag of blended wing body aircraft”. In: *Aerospace Science and Technology* 46 (2015), pages 72–81. ISSN: 12709638. DOI: 10.1016/j.ast.2015.07.001.

[38] Y. Denieul et al. “Multicontrol surface optimization for blended wing-body under handling quality constraints”. In: volume 55. American Institute of Aeronautics and Astronautics Inc., 2018, pages 638–651. DOI: 10.2514/1.C034268.

[39] N. U. Rahman and J. F. Whidborne. *A Lateral Directional Flight Control System for the MOB Blended Wing Body Planform*. 2008. URL: https://www.researchgate.net/publication/237087377.

[40] Y. Denieul et al. “Integrated design of flight control surfaces and laws for new aircraft configurations”. In: *IFAC-PapersOnLine* 50 (2017), pages 14180–14187. ISSN: 24058963. DOI: 10.1016/j.ifacol.2017.08.2085.

[41] V. Falkner. “The Solution of Lifting-Plane Problems by Vortex-Lattice Theory”. In: *Aeronautical Research Council Reports and Memoranda* 2591 (1943). URL: http://resolver.tudelft.nl/uuid:dbb5c03a-afb5-4067-a5f4-97d9f8195a0a.

[42] T. A. Johansen and T. I. Fossen. “Control allocation - A survey”. In: *Automatica* 49 (2013), pages 1087–1103. ISSN: 00051098. DOI: 10.1016/j.automatica.2013.01.035.

[43] M. W. Oppenheimer, D. B. Doman, and M. A. Bolender. *Control Allocation*. Edited by W. S. Levine. 2010. URL: https://nl1lib.org/book/899141/e56e71?id=899141&secret=e56e71&dsource=recommend.

[44] M. W. Oppenheimer, D. B. Doman, and M. A. Bolender. “Control allocation for over-actuated systems”. In: 2006. ISBN: 0978672003. DOI: 10.1109/MED.2006.328750.

[45] B. L. Stevens, F. L. Lewis, and E. N. Johnson. *Aircraft Control and Simulation - Dynamics, Controls Design, and Autonomous Systems (3rd Edition)*. John Wiley & Sons, 2016. ISBN: 978-1-118-87098-3. URL: https://app.knovel.com/hotlink/toc/id:kpACSDCDAU/aircraft-control-simulation/aircraft-control-simulation.

[46] E. Johansson. “Implications of Designing Unstable Aircraft from a Flight Control Perspective”. Master’s thesis. 2018. URL: https://kth.diva-portal.org/smash/get/diva2:1380845/FULLTEXT01.pdf.

[47] National Research Council (U.S.). Committee on the Effects of Aircraft-Pilot Coupling on Flight Safety. *Aviation safety and pilot control: understanding and preventing unfavorable pilot-vehicle interactions*. National Academy Press, 1997, page 208. ISBN: 0309056888. URL: https://skybrary.aero/sites/default/files/bookshelf/4045.pdf.

[48] Y. Yildiz and I. V. Kolmanovsky. “A Control Allocation Technique to Recover From Pilot-Induced Oscillations (CAPIO) due to Actuator Rate Limiting”. In: 2010. URL: https://ntrs.nasa.gov/citations/20100033693.

[49] G. D. Hanson and R. F. Stengel. “Effects of displacement and rate saturation on the control of statically unstable aircraft”. In: *Journal of Guidance, Control, and Dynamics* 7 (2 1984), pages 197–205. DOI: 10.2514/3.8567. URL: https://doi.org/10.2514/3.8567.

[50] M. Johnson and M. C. Romanowski. *Advisory Circular Subject: Flight Test Guide for Certification of Transport Category Airplanes*. 2018. URL: https://www.faa.gov/documentLibrary/media/Advisory_Circular/AC_25-7D.pdf.